Hydrogel Artificial Ionic Skins for Wearable Electronics and Soft Robotics

by

Binbin Ying

Department of Mechanical Engineering

McGill University

Montreal, Quebec, Canada

August 2020

A thesis submitted to McGill University in partial fulfillment of the requirements for a doctoral degree

Dedication

To my lovely parents, my parents-in-laws, my lovely son **Marc Ying** *and my beloved wife* **Zhen Yang** *for their love and support.*

To all the lives gone due to COVID-19

Table of Contents

List of Figures

List of Tables

Abstract

Hydrogel as a biomimic soft material has been studied intensively for the use of ionic devices or iontronics. Due to their superior softness, wetness, responsiveness and biocompatibility, hydrogel materials have been utilized as an alternative to fabricate stretchable skin-like electronics for applications such as personalized healthcare monitoring, human-machine interaction and soft robotics. Herein the thesis first reviews the recent advances of hydrogel skin-like ionic devices for wearables, soft robotics and beyond. As issues like limited functionality, low stability, and high-power consumption and poor adhesive still hinder the further development of hydrogel iontronics, I thereafter introduce three of my research projects subsequently to address certain emergent issues to empower hydrogel ionotronics with more practicality.

Skin serves as physical and hygroscopic barriers to protect the inner body, and also contains sensory receptors to perceive environmental and mechanical stimuli. Inspired by these features, in the first part of my research a novel artificial ionic skin (AIskin)—an analog of the diode based on controlled ion mobility—is demonstrated with high toughness, stretchability, ambient stability and transparency. The AIskin consists of a bilayer of oppositely-charged, double-network hydrogel, and converts mechanical stimuli and humidity into signals of resistance, capacitance, open-circuit voltage (OCV), and short-circuit current (SCC), among which the OCV- and SCC-based sensing signals are self-generated. Its multimodal sensation can be maintained in a wide range of relative humidity (13%~85%). It is demonstrated for wearable strain-humidity sensing, human-machine interaction and walking energy harvesting.

On the other hand, natural living systems such as wood frogs develop tissues composed of active hydrogels with cryoprotectants to survive in cold environments. However, existing synthetic hydrogels are inevitably frozen at the sub-zero temperature; most hydrogel materials do not have strong surface adhesion. In the second part of my research, a hydrogel-based ionic skin (iSkin) is developed with a unique combination of merits, including high toughness and stretchability, good ionic conductivity, excellent ambient stability, anti-freezing capability and strong diverse surface adhesion. The iSkin-based strain sensor provides high flexibility for integration with different wearable and soft robotic systems made from different materials. It is demonstrated for applications including strain sensing on both human body and winter coat, human-machine interaction, soft bending gripper, and soft robot at various environmental conditions.

The fast development of stretchable electronics and soft robotics, including hydrogel ionic devices, requires a sustainable power source that can match their mechanical stretchability in various working environment. In the third part of my research, a low-cost ionic triboelectric nanogenerator (iTENG) is developed with a unique combination of merits, including highly stretchability, anti-freezing capability, and mechanical reliability. Biomechanical motion energies can be harvested by the iTENG for powering electronics in real time and for charging energy storage devices in both regular environment and the extremely cold temperature. The stretchable iTENG overcomes the strain-induced performance degradation using percolated electrical conductors and water frozen-induced degradation using ionic conductive hydrogel.

The presented research focuses on overcoming several challenges of hydrogel skin-like ionic devices to endow them with multimodality, multifunction, stability, adhesive, and energy harvesting. These works will open new avenues toward next-generation artificial skins for wearable sensing and soft robotics and energy harvesting.

Resume

L'hydrogel en tant que matériau mou biomimique a été étudié de manière intensive pour des dispositifs ioniques ou iontroniques. Grâce à leur douceur, humidité, réactivité et biocompatibilité supérieures, des matériaux d'hydrogel ont été utilisés comme alternative pour fabriquer des composants électroniques extensibles « comme la peau » pour des applications telles que la surveillance médicale personnalisée, l'interaction homme-machine et la robotique douce. La thèse passe d'abord en revue les progrès récents des dispositifs ioniques d'hydrogel « comme la peau » pour les appareils portables, la robotique douce, etc. Vu des problèmes tels que la fonctionnalité limitée, la faible stabilité, la consommation d'énergie élevée et la mauvaise adhérence qui entravent le développement de l'hydrogel iontronique, j'introduis ensuite trois de mes projets de recherche pour résoudre certains problèmes émergents pour rendre plus pratique l'hydrogel ionotronique.

La peau sert de barrières physiques et hygroscopiques pour protéger l'intérieur du corps, et contient des récepteurs sensoriels pour percevoir des stimulis environnementaux et mécaniques. Inspiré par ces caractéristiques, j'introduis dans la première partie de mes recherches AIskin, une nouvelle peau ionique artificielle, qui est caractérisée par une excellente ténacité, extensibilité, stabilité ambiante et transparence. L'AIskin se compose d'une bicouche d'hydrogel à double réseau de charge opposée qui convertit les stimulis mécaniques et l'humidité en signaux de résistance, de capacité, de tension en circuit ouvert (OCV) et de courant de court-circuit (SCC), parmi lesquels les signaux de l'OCV et SCC sont auto-générés. Sa sensation multimodale peut être maintenue dans une large plage d'humidité relative (13%~85%). Il est démontré pour la détection portable de la déformation-humidité, l'interaction homme-machine et la récolte d'énergie.

D'autre part, les systèmes vivants naturels tels que les grenouilles des bois développent des tissus composés d'hydrogels actifs avec des cryoprotecteurs pour survivre dans des environnements

froids. Cependant, les hydrogels synthétiques existants sont congelés à la température inférieure à zéro; la plupart des matériaux d'hydrogel n'ont pas une forte adhérence à la surface. Dans la deuxième partie de mes recherches, une peau ionique à base d'hydrogel (iSkin) est développée, montrant une bonne résistance, extensibilité, conductivité ionique et stabilité ambiante, une capacité antigel et une forte adhérence aux surfaces diversifiée. Le capteur de contrainte basé sur iSkin offre une flexibilité pour l'intégration avec différents systèmes robotiques portables et souples de différents matériaux. Il est démontré pour la détection de contrainte sur le corps humain et le manteau d'hiver, l'interaction homme-machine, la pince souple et le robot souple dans diverses conditions.

Le développement rapide de l'électronique extensible et de la robotique douce, y compris les dispositifs ioniques d'hydrogel, nécessite une source d'énergie durable dans diverses conditions de travail. Dans la troisième partie de ma recherche, un nanogénérateur triboélectrique ionique à faible coût (iTENG) est développé avec une bonne extensibilité, capacité antigel et fiabilité mécanique. L'énergie biomécanique peut être récupérée par l'iTENG pour alimenter or charger des dispositifs dans un environnement normal ou extrêmement froid. L'iTENG extensible surmonte la dégradation des performances induite par la déformation et la congélation à l'aide de conducteurs électriques percolés et d'hydrogel conducteur ionique.

La recherche présentée se concentre sur la résolution de plusieurs défis des dispositifs d'hydrogel « comme la peau » pour les doter de multimodalité, multifonction, stabilité, adhérence et récupération d'énergie. Ces travaux ouvriront de nouvelles voies vers les peaux artificielles de nouvelle génération pour la détection portable, la robotique douce et la récolte d'énergie.

Acknowledgment

First, I would like to thank my supervisor Professor Xinyu Liu for his kind support both in academic and financial aspects, for his guidance and encouragement throughout my studies both at McGill University and my exchanging period at the University of Toronto. His enthusiasm both for research and life will inspire me in my future career. Besides, I would like to thank my co-supervisor Professor Jianyu Li for his strong academic training on my thesis, especially the experimental design, and academic writing on our first collaboration at McGill University. His altitude for research will inspire me in my future career as well.

Besides my supervisors, I would like to thank my Ph.D. thesis committee members Prof. Allen Ehrlicher and Prof. Srikar Vengallatore, for their insightful suggestions, comments and encouragement on my Ph.D. study. My research could not be finished without the strong supports from the collaborators. Especially, I want to express my thanks to Prof. Edmond W. K. Young at the University of Toronto for his kind help of cell culture and Prof. Mitch Winnik at the University of Toronto for his help of hydrogel material characterization, Dr. David Liu at McGill University for his help of nanomaterial characterization.

I appreciate the financial supports from the Faculty of Engineering at McGill University, the Faculty of Engineering at University of Toronto and the Natural Sciences and Engineering Research Council of Canada.

I would like to express my great appreciation to my colleagues in Biomedical Microsystem Laboratory: Dr. Longyan Chen, Dr. Ran Peng, Dr. Xiao Li, Dr. Weize Zhang, Dr. Pengfei Song, Dr. Xianke Dong, Dr. Chen Zhao, Dr. Juntian Qu, Dr. Qiyang Wu, Dr. Hao Fu, Dr. Qigao Fan, Dr. Xin Wang, Dr. Elina Kolker Baravik, Yu-Hsuan Wang, Pan Peng, Sina Kheiri, Zhen Qin, Yueyue Pan, Pengfei Xu, Zhaoyi Xu, Yuxiao Zhou, Dante Filice, Ryan Chen, Runze Zuo, Yilun Wan, Yitong Zhang, Junyu Chen, Yichao Shi; my colleagues in the Lab of Biomaterials Engineering: Guangyu Bao and Zhenwei Ma, Zhen Yang and Huo Ran; and other friends who are always ready to help: Siwan Park, Dr. Yang Liu, Dr. Hang Zhou, Dr.Teng Cui, Wenkun Dou, Dr.Xian Wang.

In addition, I’d like to express the special thank to my best Ph.D. friend, Dr. Zhen Yin. He assistants me a lot on my research, including protocol development, schematic figure presenting, and sample photo taking, etc. He also brings me so much happiness during my whole doctoral studies at Canada.

Finally, I owe the deepest thanks to my parents, my parents-in-law for their love and support. To my lovely wife Zhen Yang, thank you for standing with me throughout my academic journey during the past five years, providing me with both financial and emotional support during the challenging moments, as well as raising our lovely son Marc Ying.

Contributions of Authors

This is a manuscript-based thesis consisting of three journal articles. The titles of the articles, names of the authors, and their contributions are listed below.

1. Recent Advances of Hydrogel Skin-like Devices for Wearables, Soft Robotics and Beyond

Binbin Ying[1,2], Xinyu Liu[1,2,3]*

[1]Department of Mechanical Engineering, McGill University, 817 Sherbrooke Street West, Montreal, QC H3A 0C3, Canada.

[2]Department of Mechanical and Industrial Engineering, University of Toronto, 5 King's College Road, Toronto, Ontario, M5S 3G8, Canada.

[3]Institute of Biomaterials and Biomedical Engineering, University of Toronto, 164 College Street, Toronto, ON M5S 3G9, Canada

To be submitted.

Author contributions:

B. Ying: Wrote the manuscript, organized the literature information, and suggested the presentation items.

X. Liu: Wrote the manuscript.

2. An ambient-stable, stretchable and self-powered ionic skin with multimodal sensation

Binbin Ying[1,2], Qiyang Wu[1,2], Jianyu Li[1,3]*, Xinyu Liu[1,2,4]*

[1]Department of Mechanical Engineering, McGill University, 817 Sherbrooke Street West, Montreal, QC H3A 0C3, Canada.

[2]Department of Mechanical and Industrial Engineering, University of Toronto, 5 King's College Road, Toronto, Ontario, M5S 3G8, Canada.

[3]Department of Biomedical Engineering, McGill University, 3775 rue University, Montreal, QC H3A 2B4, Canada

[4]Institute of Biomaterials and Biomedical Engineering, University of Toronto, 164 College Street, Toronto, ON M5S 3G9, Canada

Materials Horizons, Royal Society of Chemistry, 2020,7, 477-488

DOI: 10.1039/c9mh00715f.

Author contributions:

B. Ying: Conceived the idea, designed the experiment, fabricated the devices, performed measurements, analyzed the experimental data and prepared the manuscript.

Q. Wu: Developed the data acquisition and game interface in the part of human-machine interface demonstration.

J. Li: Conceived the idea, designed the experiment, guided the project, analyzed the experimental data and prepared the manuscript.

X. Liu: Conceived the idea, designed the experiment, guided the project, analyzed the experimental data and prepared the manuscript.

3. An anti-freezing, ambient-stable and highly stretchable ionic skin with strong surface adhesion capability for wearable sensing and soft robotics

Binbin Ying[1,2], Runze Zuo[2], Ryan Chen[2], Jianyu Li[1,3], Xinyu Liu[1,2,4]*

[1]Department of Mechanical Engineering, McGill University, 817 Sherbrooke Street West, Montreal, QC H3A 0C3, Canada.

[2]Department of Mechanical and Industrial Engineering, University of Toronto, 5 King’s College Road, Toronto, Ontario, M5S 3G8, Canada.

[3]Department of Biomedical Engineering, McGill University, 3775 rue University, Montreal, QC H3A 2B4, Canada

[4]Institute of Biomaterials and Biomedical Engineering, University of Toronto, 164 College Street, Toronto, ON M5S 3G9, Canada

In submission

Author contributions:

B. Ying: Conceived the idea, designed the experiment, carried out material preparation, characterization, the experiments of strain sensing, human machine interaction and soft robotics, performed data analysis, and wrote the manuscript with input from all the other authors.

R. Zuo: Carried out the experiments of strain sensing, human machine interaction and soft robotics, performed data analysis and movie editing.

R. Chen: carried out material preparation and characterization, the experiments of strain sensing, human machine interaction and soft robotics, performed data analysis and movie editing.

J. Li: Conceived the idea and designed experiments.

X. Liu: Conceived the idea, designed the experiment, guided the project, analyzed the experimental data and prepared the manuscript.

4. An anti-freezing, and stretchable ionic hydrogel triboelectric nanogenerator for mechanical energy harvesting and self-powering sensing

Binbin Ying[1,2], Yilun Wan[2], Runze Zuo[2], Xinyu Liu[2, 3]*

[1]Department of Mechanical Engineering, McGill University, 817 Sherbrooke Street West, Montreal, QC H3A 0C3, Canada.

[2]Department of Mechanical and Industrial Engineering, University of Toronto, 5 King's College Road, Toronto, Ontario, M5S 3G8, Canada.

[3]Institute of Biomedical Engineering, University of Toronto, 164 College Street, Toronto, ON M5S 3G9, Canada

To be submitted.

Author contributions:

B. Ying: Conceived the idea, designed the experiment, fabricated the devices, performed measurements, analyzed the experimental data and prepared the manuscript

Y. Wan: Fabricated the devices, set up the electrical characterization instrument, performed measurements.

R. Zuo: Set up the electrical circuit for demonstration, performed the demonstration measurements, edited movie.

X. Liu: Guided the project, provide the funding, analyzed the experimental data and prepared the manuscript.

Chapter 1

Introduction

1. Chapter 1: Introduction

As the fast development of personalize healthcare, implantable monitoring, human-machine interaction, soft and wearable robotic gait measurement and soft prosthetic sensing, there is an increasing demanding of suitable wearable electronics to better meet these application scenarios. Currently, traditional electronics are brittle and rigid, not compatible to soft tissues and other soft substrates in regarding to the mechanical property, i.e., the mismatch between the young's moduli of biological tissues and common materials for machines and electronics (*1*). On the other aspect, unlike conventional electronics where electrons serve as carriers of information, our human body uses ions as the carrier to realize bioelectronic activities, such as the propagation of action potentials originated from the transmembrane ion flow within neurons (*2*). Both mechanical and electrical mismatches generally arise issues like long-term wearing uncomfortability, inflammation, large interface impedance and low signal-to-noise ratio.

To bridge the gap between biological tissues and electronics, hydrogel-based electronics or hydrogel iontronics are emerging as a promising alternative to conventional electronics. For example, hydrogel skin-like sensors better mimic the human tissues in terms of tunable and comparable mechanical moduli and sensing principles (i.e., sensing signals are transmitted through ions rather than electrons) (*3*). Currently, varies of hydrogel skin-like ionic devices, such as ionic cables (*4*), epidermal touch panel (*5*), strain/ pressure/ humidity/ temperature sensors (*2, 6*-*9*), energy harvester (*10*-*12*) and soft robotic sensing (*13, 14*), have been developed for personalized healthcare, human-machine interaction, soft and wearable robotics, and rehabilitations. Despite the significant efforts and progress, the development of hydrogel iontronics is still in the infancy, issues such as limited functionality, low stability, external power consumption and poor adhesive still hinder their further development.

1.1. Thesis objectives

The overall objective of this thesis is to develop hydrogel skins-like ionic devices to meet the real-world requirements particularly for wearable electronics and soft robotics. The specific objectives are to:

- Develop an artificial ionic hydrogel skin with high toughness, stretchability, ambient stability, and transparency for strain and humidity sensing, including self-powering sensing mode due to its diode-like electrical characteristic.
- Develop an artificial ionic skin with extremely stretchability, ambient stability, anti-freezing and strong adhesion capability to diverse surfaces for wearable sensing and soft robotics.
- Develop an ionic hydrogel triboelectric nanogenerator with high stretchability, anti-freezing and strong interfacial hydrogel-elastomer bonding for energy harvesting and self-powering wearable sensing.

1.2. Thesis organization

This is a manuscript-based thesis composed of six chapters. The current chapter (Chapter 1) of this thesis briefly introduces the general concepts and challenges in the field of hydrogel skin-like ionic devices, followed by the objective and the organization of this thesis.

Chapter 2 contains a more detailed overview and review of the subject. I start with a brief introduction of hydrogel concept, current hydrogel toughening mechanisms, common approaches to endow hydrogels with ionic conductivity and their combination. The strategies to design bioinspired hydrogel matrix with enhanced merits including the ambient stability, antifreezing capability and adhesive are reviewed thereafter. Next, I summarize hydrogel skin-like ionic devices for several popular yet important applications including wearables, soft robotics and energy harvesting. In the end, several challenges for the applications of wearable electronics and soft robotics are highlighted so that this thesis will tackle in the following chapters. Briefly, chapter 3 endows hydrogels with multifunctionality, capable of self-powering multimodal sensing with ambient stability; chapter 4 endows hydrogels with anti-freezing capability and strong surface adhesive; chapter 5 endows hydrogels with the capability of unprecedented energy harvesting and self-powering sensing in a wide range of temperature.

Specifically, Chapter 3 introduces an ambient-stable ionic hydrogel material (AIskin), made from a bilayer of oppositely-charged ionic DN hydrogels, with features resembling the human skin. The facile structural design of the material realizes a high stretchability of more than 400%, fully satisfying the mechanical requirement of skin-like wearable sensors. Experimental results show that our AIskin is an analog of semiconductor diode due to controlled movements of oppositely-charged ions at the interface of its bilayer structure. By incorporating EG, our AIskin maintains its high optical transparency and electronic characteristics under ambient environment for more than a week. Based on its ionic diode structure, the AIskin converts mechanical stimuli into changes in resistance, capacitance, open-circuit voltage (OCV), and short-circuit current (SCC), among which the OCV- and SCCD-based sensing modes are self-powered. The AIskin is calibrated, in its four types of sensing modes (e.g., resistance, capacitance, OCV, and SCCD), under different levels of compressive strain and environment humidity, confirming its use for strain and humidity sensing. Thanks to the unique combination of mechanical, physical and electrical properties, the AIskin enables numerous applications such as strain/humidity sensing, human-machine interaction, and energy harvesting, respectively.

In Chapter 4, a novel hydrogel-based ionic skin (iSkin) capable of strain sensing is demonstrated with high toughness, high stretchability, excellent ambient stability, superior anti-freezing capability, and strong surface adhesion. The iSkin consists of a layer of tough ionic hydrogel containing both ionically and covalently cross-linked polymers and a thin layer of bioadhesive coating. With the addition of biocompatible cryoprotectants and electrolyte, the iSkin shows good electrical conductivity in a wide range of relative humidity (15~90%) and temperature (−95~25 °C) levels. In addition, with the bioadhesive layer, the hydrogel matrix can adhere firmly to diverse material surfaces under different conditions, including cloth fabric, human skin and elastomers, in both dry and wet conditions and at subzero temperature with dynamic movement. We demonstrate iSkin for applications including strain sensing on both the human body and winter coat, human-machine interaction, soft bending gripper, and soft robot at −22 °C.

Chapter 5 introduces a low-cost, highly stretchable and anti-freezing ionic triboelectric nanogenerator (iTENG) for self-powering sensing and mechanical energy harvesting. The iTENG consists tough double network hydrogel and Ecoflex as the soft ionic electrode and electrification layer, respectively. With the incorporation of glycerol and NaCl into the tough hydrogel as well as the robust bonding between the hydrogel and elastomer, this iTENG shows an extremely anti-freezing capability of −53 ^{o}C and a stretchability of 300%. Due to the reliable interfacial bonding, the iTENG shows no delamination and good self-powering durability under both initial and stretched status at both room and subzero temperatures. We demonstrate the application of biomechanical energy harvesting for powering electronics in real time and for charging energy storage devices in both regular environment and the extremely cold temperature.

Finally, Chapter 6 highlights the accomplishments and the main contributions of this research. At the end, a few guidelines for future works are also recommended.

1.3. References

1. X. Liu, J. Liu, S. Lin, X. Zhao, Hydrogel machines. *Materials Today*, (2020).
2. B. Ying, Q. Wu, J. Li, X. Liu, An ambient-stable and stretchable ionic skin with multimodal sensation. *Materials Horizons* **7**, 477-488 (2020).
3. C. Yang, Z. Suo, Hydrogel ionotronics. *Nature Reviews Materials* **3**, 125 (2018).
4. C. H. Yang *et al.*, Ionic cable. *Extreme Mechanics Letters* **3**, 59-65 (2015).
5. C.-C. Kim, H.-H. Lee, K. H. Oh, J.-Y. Sun, Highly stretchable, transparent ionic touch panel. *Science* **353**, 682-687 (2016).
6. K. Tian *et al.*, 3D printing of transparent and conductive heterogeneous hydrogel–elastomer systems. *Advanced Materials* **29**, 1604827 (2017).
7. J. Wu *et al.*, An intrinsically stretchable humidity sensor based on anti-drying, self-healing and transparent organohydrogels. *Materials Horizons* **6**, 595-603 (2019).
8. A. Choe *et al.*, Stretchable and wearable colorimetric patches based on thermoresponsive plasmonic microgels embedded in a hydrogel film. *NPG Asia Materials* **10**, 912-922 (2018).
9. J. Y. Sun, C. Keplinger, G. M. Whitesides, Z. Suo, Ionic skin. *Advanced Materials* **26**, 7608-7614 (2014).
10. X. Pu *et al.*, Ultrastretchable, transparent triboelectric nanogenerator as electronic skin for biomechanical energy harvesting and tactile sensing. *Science advances* **3**, e1700015 (2017).
11. T. Liu *et al.*, Triboelectric-nanogenerator-based soft energy-harvesting skin enabled by toughly bonded elastomer/hydrogel hybrids. *ACS nano* **12**, 2818-2826 (2018).
12. K. Parida *et al.*, Highly transparent, stretchable, and self‐healing ionic‐skin triboelectric nanogenerators for energy harvesting and touch applications. *Advanced Materials* **29**, 1702181 (2017).
13. C. Larson *et al.*, Highly stretchable electroluminescent skin for optical signaling and tactile sensing. *science* **351**, 1071-1074 (2016).
14. S. Cheng, Y. S. Narang, C. Yang, Z. Suo, R. D. Howe, Stick‐On Large‐Strain Sensors for Soft Robots. *Advanced Materials Interfaces* **6**, 1900985 (2019).

Chapter 2

Recent Advances of Hydrogel Skin-like Devices for Wearable Biomedicals and Soft Robotics and Beyond

2. Chapter 2. Recent Advances of Hydrogel Skin-like Devices for Wearables, Soft Robotics and Beyond

Binbin Ying and Xinyu Liu

2.1. Abstract

Nowadays, numerous novel types of skin-like electronics are being rapidly developed to satisfy various applications including wearable electronics and soft robotics. Among them, hydrogels as biomaterials have recently been studied intensively for electronic utilities due to their superior softness, wetness, responsiveness, biocompatibility and unique ionic sensing nature. Those features could potentially blur the gap between the soft body (e.g. human being) and hard electronics and machines. However, the current development of hydrogel skin-like devices is still in the infant stage and facing many important challenges including limited functionality, low stability, poor adhesion and power consumption. The present review aims to summarize current strategies to address these challenges. We first introduce the overview of hydrogels and existing strategies to increase their toughness and conductivity. Next, we describe current bioinspired approaches to advance hydrogel devices with enhanced merits, in particular, their anti-dehydration, anti-freezing and adhesion. Thereafter, we highlight the state-of-the-art applications of hydrogel skin-like devices, particularly for wearable electronics, soft robotics and energy harvestings. Last but not least, we conclude and propose the future perspectives for this field.

2.1. Introduction

Skin is the largest organ of the human body and serves as the first physical, thermal and hygroscopic barrier between the external environment and its internal components. Importantly, the skin contains the largest sensing receptors to perceive various environmental stimuli that humans encounter, such as pressure, strain, humidity, temperature and pain (**Figure 2.1**A**).** Today, many flexible and stretchable electronic counterparts (i.e., artificial skins) get inspired and have been engineered by understanding biological sensing functions of the human skin (*1–16*). These progresses have revolutionized wearable electronics and other related fields. Current wearable devices have already been used for personal health monitoring [e.g., glucose, uric acid, lactose, heart rate, blood pressure, ions level, stress level, strain, tactile, temperature, humidity (*17–19*)], for the communication between humans and devices [e.g., human–machine interfaces (*20*))], and for wearable robotic assistance [e.g., exosuit, artificial prosthetics (*21*, *22*)]. On the other hand, next-generation soft robotics require a variety of embedded soft, wearable and stretchable sensors to sense, plan, and act by interacting with the surroundings, in which the sensing capability of skin-like electronics would be incredibly useful to improve the design of soft robotics (*23*). Noticeably, because of the inherent material match and functional complementarity between artificial skins and soft robotics, there have been significant research efforts spent on developing skin-like stretchable and wearable sensors for the integration with various soft robotic systems. Biological, optical, strain, tactile sensing capabilities have been embedded into soft bodies to interact with their users and environments more intelligently (*21*, *24–28*).

Among the materials for artificial skins, hydrated and ionic materials such as deformable and tough hydrogels are one of the most suitable candidates and have recently got a lot of attention to bridge the gap between human and electrical counterparts promisingly. Hydrogels as biomaterials can mimic the multiple functions of biological systems, such as their superior softness, wetness, responsiveness, excellent material biocompatibility and uniquely skin-like ionic sensing nature (*29–31*). In addition, their tunable mechanical properties with on-demand design of toughness, stretchability and elasticity can accommodate the diverse mechanical properties of to-be-mounted substrates (e.g., cloth, skin, elastomer and organ). Those features could potentially blur the gap between the soft body and hard machine. So far, a variety of hydrogel artificial skin devices have been developed for applications including wearable sensors, smart soft robotics and energy harvesting (**Figure 2.1**B**).** These devices are capable of transducing applied touch, pressure, deformation, humidity or temperature into changes of electrical signals (e.g., capacitance or resistance, open circuit voltage and short circuit current), mimicking the sensing functions of natural skins.

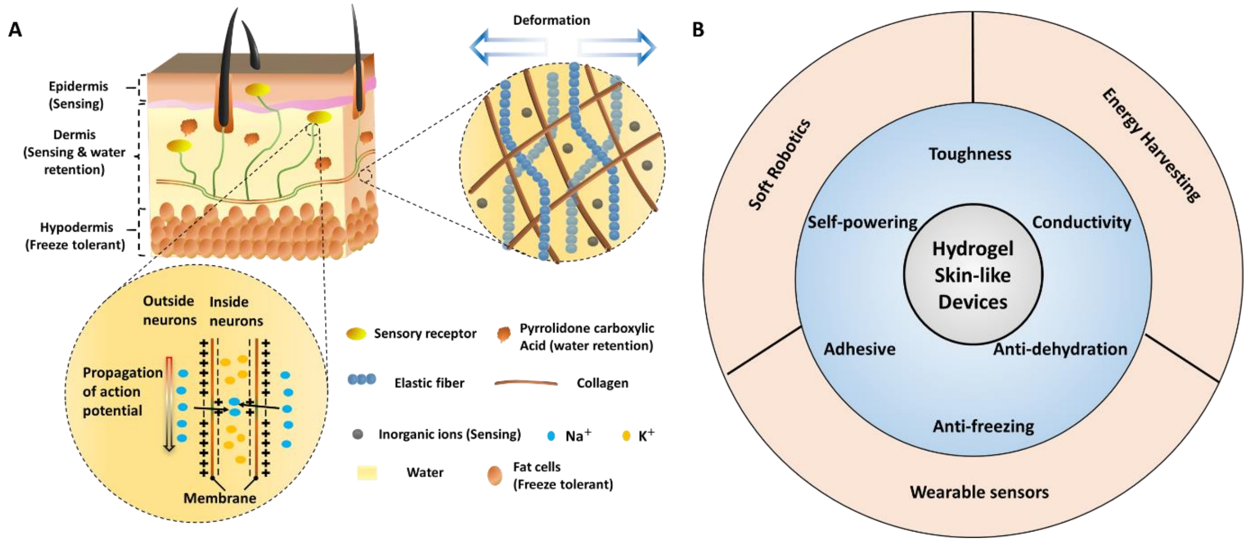

Figure 2.1. Hydrogel skin-like devices. (A). Schematic of the human skin that resists physical deformation due to the elastin fibre and collagen in the dermis layer, maintains the body temperature due to the fat cells in hypodermis layer, holds water due to the hygroscopic substance (i.e., pyrrolidone carboxylic acid), and transports ionic signal directionally within sensory neurons. (**B**). Enhanced features of hydrogels (e.g., toughness, ionic conductivity, anti-dehydration, anti-freezing, adhesive, and self-powering) desired during their practical use as wearable sensors, soft robotics and energy harvesting.

However, the development of hydrogel devices is still in the very early stage and is facing certain challenges. For example, many hydrogel skins have limited functionality to sense only one stimulus. As a sensing component, hydrogels usually require external power supplies. In addition, hydrogel-based devices are not stable during open-air operation, and cannot maintain mechanical deformability and electrical conductivity in cold environments. Moreover, conventional hydrogels usually have poor adhesion capability and therefore can only adhere to substrates with the assistance of additional commercial adhesives (*14*, *32*). This poor adhesive cannot ensure the firm adherence to substrates of different materials (e.g., human skins, fabric clothes, and elastomers), reducing the fidelity of signals acquisition during wearable and soft robotic sensing under various conditions (e.g., dry and wet surfaces, sweaty skin, subzero temperature, and dynamic deformation and movement). Therefore, in this review we primarily aim to summarize the current strategies to address these challenges for real-world applications.

There have been several hydrogel-related reviews published about their toughening mechanism (*33*–*36*), enhanced environment adaptability (*37*), adhesive mechanism (*34*, *38*), bioelectronics (*39*), ionotronics (*31*) and machines (*40*). This review will put an emphasis on the state-of-the-art ionic conductive hydrogel skin-like devices with specific yet important features for the emergent application areas such as wearable electronics, soft robotics and their infusions. We start with a brief introduction on the fundamental concept of hydrogel and strategies to increase its toughness and conductivity. Thereafter, the recent advances of ionic conductive hydrogel devices with enhanced merits, particularly, their anti-dehydration, anti-freezing and adhesion, will be reviewed. Then we summarize some state-of-the-art applications of hydrogel skin-like devices for wearable electronics, soft robotics and some other important applications such as energy harvesting. Finally, we conclude with a perspective discussion on the remaining opportunities and challenges. We hope this review will bring new insights into seamless merging between human, wearables and robotics.

2.2. Brief overview of hydrogel

Hydrogel is defined as a class of three-dimensional (3D) hydrophilic polymer networks infiltrated with high water content. Natural hydrogels exist in most soft tissues of animals and plants in biology. With hundreds of millions of years of evolution, soft tissues have achieved many key features to enable sophisticated functions in nature due to their water-containing and elaborate structure (*41*). For example, in our human bodies there are a variety of soft tissues made of natural hydrogels containing 60–90 wt% water, ranging from tendons, muscles, cartilages and skin (tough and strong) to mucosa, extracellular matrix, axon and brain (brittle and weak) (*36*, *40*–*42*). On the other hand, inspired by nature, people have kept exploring the artificial counterparts of natural hydrogel to mimic both their structures and functions since the birth of synthetic hydrogel in 1960 (*41*, *43*).

Currently, synthetic hydrogel (here called as hydrogel directly) can possess tunable chemical, mechanical, and electrical properties and behaves uniquely like both solids and fluids (*44*). Due to these versatility, hydrogels have been widely explored for diverse applications including drug delivery (*45*), ophthalmology (*46*, *47*), wound dressings (*45*, *48*), tissue engineering (*45*, *49*, *50*). In addition, hydrogels can responsive (mainly in the form of volume swelling and shrinking) under different stimuli (e.g., light, temperature, pH, ionic strength, chemicals) (*51*–*56*), which has been utilized for sensing and actuating study (*57*–*61*). However, conventional hydrogels (e.g., single-network polymers) typically are soft, weak and brittle with limited stretchability (<100%), low elastic moduli (~10 kPa) and small fracture energy (0.1-10 J/m^2) (*33*, *35*, *44*). They are prone to permanently break, hindering their potential applications that require high mechanical toughness or stretchability (e.g., artificial load-bearing bio-tissues, wearable electronics and soft robotics). Therefore, novel hydrogels with enhanced mechanical properties need to be designed. In addition, most pristine synthetic hydrogels are electrically insulating while natural hydrogels in our bio-tissues are conductive due to the existing mobile charge ions. Therefore, empowering hydrogels with conductivity is necessary for applications such as wearable and soft robotic sensing. In this section, fundamentals to toughen hydrogel are briefly introduced first. We then introduce several general strategies for the design of ionically conductive hydrogels.

2.2.1. Tough hydrogel and its DN format

Over the last few decades, many efforts have been made to improve the mechanical strength and fracture toughness of conventional hydrogels to broaden their biomedical applications. The fracture toughness is defined as the energy per unit area required to make a notched crack propagate, which is an ability to absorb mechanical energy and deform without fracturing (*62*). Typical existing toughening strategies include but not limited to: topological hydrogels with slide-ring cross-linking points (*63–67*), hydrogels cross-linked with nanocomposite or macromolecular microsphere composite (*68–78*), double-network (DN) hydrogels (*16*, *79–81*), tetra-arm PEG hydrogels (*82*, *83*), hydrogels cross-linked by strong cooperative hydrogen bonding (*84*), hydrogels enhanced with physical interaction (*85–88*), hydrogels with hybrid chemical and physical cross-linkers (*80*, *81*, *89–92*), hydrogels with crystalline or transformable domains (*49*, *93*, *94*). A number of recent review articles have summarized the progress of various tough hydrogels that readers can refer to, including their preparation, mechanical properties, toughening mechanisms and applications (*33–36*, *44*, *95*, *96*). In this section, we focus on one specific tough hydrogel (i.e., DN hydrogel), due to its popularity of been studied (more than 60,000 related literatures since its first publication in 2003 and more than 40,000 related literatures in the past decades, according to the search of “Double Network hydrogel” in google scholar) and one of highest mechanical performance (e.g., fracture toughness) so far (*97*).

DN hydrogel has received tremendous attention since it was first developed by Gong and co-workers in 2003 (*79*), in which monomers are subsequently polymerized into two networks in the presence of cross-linkers via a two-step synthesis method. By the classical definition, DN hydrogel consists of two polymer networks with strong asymmetric structure and contrasting mechanical properties such as network density, rigidity, molecular weight, cross-linking density etc. (*79*, *95*, *97*). In general, materials of two networks can be selected from two same or different polymer systems (*95*, *97*). In the aspect of structure, DN hydrogel is a type of gel that has a very specific structure of interpenetrating polymer network (IPN): densely cross-linked first network is stiff, rigid yet brittle; sparsely cross-linked second network is soft, stretchable and ductile. The molar concentration of the second network is usually tens of times the first network (*79*, *95*, *97*–*99*).

While in a broader view, any hydrogels possessing IPN structure can be regarded as the DN type principally; however, DN gels with the contrasting network structure and mechanical properties make them quite different from the conventional IPN system (*97*). Compared with the SN hydrogel, the DN ones are much tougher due to a synergistic effect of the binary structure rather than a linear combination of two SN components (*100*). Currently, the widely acceptable explanation of this high mechanical fracture toughness is that the first network serves as sacrificial bonds by breaking into small clusters during deformation, which can efficiently disperse the stress around the crack tip into the surrounding damage zone, while the second polymer chains act as hidden length, which effectively absorbs the crack energy by large deformation of the network (*97*). In other words, the strong mechanical toughness is largely attributed to the effective relaxation of locally applied stress and dissipation of the crack energy through combinations of two networks with different structure and densities (*79*). In addition, strong network entanglement and chain interaction could contribute to the increasing toughness of DN hydrogel as well (*35*). The toughness can be tuned by adjusting the parameters including the molar ratio between the first and the second network, their crosslinking density (*79*), and the length of the polymer chains (*101*). Accordingly, DN hydrogels show excellent mechanical properties, as summarized into **Table 2.1** from the previous review papers (*33*, *35*, *44*, *95*, *100*). For example, while containing high water content (~90 wt%), they possess 0.1–10 MPa in elastic modulus, 1000%–2000% in tensile fracture strain, 20–60 MPa in failure compressive fracture stress, 90%–95% in compressive fracture stain, and 100–16000 J/m^2 in fracture energy, which are comparable to that of rubbers and soft load-bearing bio-tissues (*33*, *100*).

Table 2.1. Mechanical property of existing DN hydrogel

Water content	~90%
Tensile fracture strain	1000–2000%
Elastic modulus	0.1–10 MP
Fracture toughness	100-16000 J/m^2
Failure compressive nominal stress	20–60 MPa
Compressive fracture stain	90–95%

DN hydrogels can be mainly categorized into two types regarding their network structures: chemically-chemically cross-linked networks and physically-chemically cross-linked networks. DN hydrogels such as poly(2-acrylamido-2-methylpropanesulfonic acid)-poly(acrylamide) (PAMPS-PAAm) (*79*), poly(ethylene glycol)-poly(acrylic acid) (PEG-PAA) (*102*) and most of synthesized hydrogels by the molecular stent methods (*103*, *104*) belong to chemically-chemically cross-linked DN hydrogel. For example, PAMPS-PAAm DN hydrogel was formed by covalently cross-linking strong polyelectrolytes (i.e., PAMPS) as the first network and subsequently covalently cross-linking the second-network monomers (AAm) diffused from the precursor solution into the first-network gel **(Figure 2.2**A and B**)** (*79*)**.**

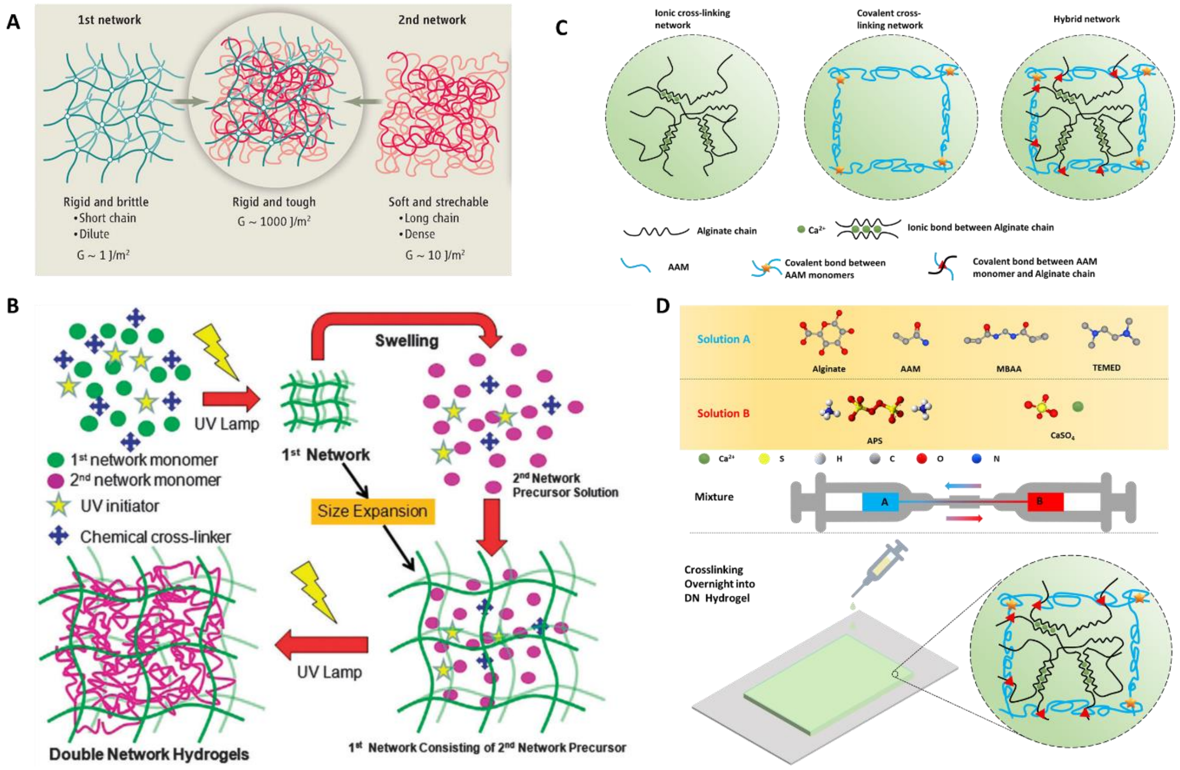

Figure 2.2. **Two typical DN hydrogel structures and their synthesis strategies.** (**A**). By combining different hydrogel network materials, tough DN hydrogels can be created. Reprinted and adapted with permission from Ref. (62), 2014 American Association for the Advancement of Science. (**B**). Classical two-step polymerization method to prepare chemically–chemically cross-linked DN hydrogels. Reprinted and adapted with permission from Ref. (35), Royal Society of Chemistry. (**C**). The composition of a typical physically-chemically cross-linked DN hydrogel,

i.e., alginate-PAAm hydrogel. (**D**). Preparation of physically–chemically cross-linked alginate-PAAm DN hydrogel.

While the recently developed DN hydrogels such as carrageenan-epoxy-amines (*105*), polysaccharides-epoxy-amines (*105*), agarose–PAAm (*16*, *106*), and alginate-PAAm (*80*) belong to physically-chemically crosslinked DN type, in which the 1st network is usually physically cross-linked while the 2nd network is chemically cross-linked. For example, the alginate-PAAm DN hydrogel was formed by ionically cross-linking alginate chains as the first network and covalently cross-linking the second-network monomers (AAm) into PAAm (**Figure 2.2**C and D). During polymerization, there were also hybrid cross-links between the first network and the second network, which is the origin of network entanglement and chain interaction mentioned before.

Since chemically–chemically crosslinked DN hydrogel has been studied for almost ten years earlier than physically-chemically crosslinked one, the mechanism understanding is relatively much more in depth. Whereas, increasing attention has recently been paid on physically-chemically cross-linked hydrogels because of its less additional cross-linking agents which are often toxic for biomedical applications. In addition, the irreversible failure of covalent bonds in the first network of chemically–chemically cross-linked DN hydrogels could be a limitation for the application scenarios where self-healing function is needed (*33*), which can be achieved by constructing physically-chemically DN hydrogel (*33*, *35*).

Currently, there are several methods to prepare DN hydrogels, including classical two-step polymerization (*79*), one-pot methods (*80*, *106*), molecular stent methods (*103*, *104*) and their combination with other technologies such as 3D printing (*107*, *108*) in which molecular stent methods can be categorized into the two-step scopes as well according to its schematic reported before (*103*). Here we will mainly discuss the difference between two-step and one-pot methods.

The classical two-step method is extremely popular because it is well developed, robust, and easy to operate (*79*). Taking the free-radical synthesis of PAMPS-PAAm DN hydrogel as an example (**Figure 2.2**B), in the first step, strong polyelectrolyte (PAMPS) was free-radically polymerized to form a covalently cross-linked, rigid and brittle first network, which thereafter immersed and swelled in a precursor solution containing neutral second-network monomers (AAm), initiators, and cross-linkers for a while to equivalent status (e.g., 24 h). In the second step, AAm was polymerized to form a loosely cross-linked yet stretchable second network (PAAm) inside the first brittle gel (*79*). The final DN hydrogel belongs to chemically–chemically cross-linked DN type. Whereas, the two-step method can also be adapted to synthesize physically–chemically crosslinked DN hydrogels [e.g., agarose-PAAm hydrogel (*16*)], which could construct the DN tough hydrogel with reversible bindings in the first network.

On the other hand, Suo *et al.* developed a simple one-pot method to synthesize a new type of hybrid physically–chemically cross-linked alginate-PAAm DN hydrogels (**Figure 2.2**D) (*80*). Briefly, sodium alginate, $CaSO_4$, AAm, N,N'-methylenebis(acrylamide) (MBAA), tetramethyl-ethylenediamine (TEMED), ammonium persulfate (APS) were mixed and cured in a sealed chamber for overnight, during which ionic cross-linking took place to form the first alginate network while free radical polymerization of AAm and covalent cross-linking took place to form the second PAAm network (**Figure 2.2**D).

Overall, both methods can easily tune the mechanical properties through simply adjusting the concentration of monomers, initiators and cross-linkers (*79, 80, 106*). The one-spot method is more advantageous in regarding of constructing the DN gels with complex shapes, saving experimental synthesis time, and saving the monomer solution of the second network (*35*), while the two-step method shows better stability due to its less swelling ratio in aqueous environment (*16*) as well as the suitability for the synthesis of both physically–chemically and chemically-chemically cross-linked DN hydrogel (*16*, *79*).

2.2.2. Conductive hydrogels and their ionic types

The main composition of our human body is hydrogel and neuron signals are delivered in the hydrogel-like human body through ions transporting including the transmembrane movement of sodium, potassium, calcium, and chloride ions along ion channels on neuron cells (**Figure 2.1**A) (*16*, *30*). While significant efforts have been made on engineering flexible electrical components to interface the human body with machines and devices, the gap/mismatch still exists in terms of their mechanical young's modulus and their signal charge carriers (electrons versus ions) (*16*, *30*).

Recent progress of the hydrogel could make it become a promising biocompatible medium to bridge the gap between human and machines. Hydrogels possess tunable mechanical properties with on-demand design of toughness, stretchability and elasticity to accommodate the diverse mechanical properties of our human tissue (*40*, *109*). Pristine hydrogels are generally considered as electrical insulators due to the absence of mobile charge carriers (*39*, *40*). Currently, there are several strategies to empower hydrogels with conductivity, including nanocomposite-based conductive hydrogels (CHs) (e.g., CNT, graphene, metal nanomaterials), conducting-polymer-based CHs, electrolyte/polyelectrolyte-based CHs and other novel CHs formats (e.g., ionic-liquid-based conductive gels) (*30*, *31*, *39*, *40*, *96*, *110–112*). Except nanomaterial-based CH, most CHs use ions to transmit signals within the conductor, which better mimic the biology and have the potential to offer unconventional yet improved interface between human beings and electronics.

In this section, we mainly introduce the ionically CHs: (i) electrolyte/polyelectrolyte-based CHs; (ii) conducting-polymer-based CHs; and (iii) other novel ionically conductive gels**.**

2.2.2.1. Electrolyte/polyelectrolyte-based conductive hydrogels.

Electrolyte-based conductive hydrogels: Aqueous solutions with salts (electrolytes) have been utilized for many applications including the daily use of alkaline batteries and ionically stimulating electrodes (*113*). However, solution-based electrolyte devices have issues such as potential liquid leakage, limiting their further applications on biomedical applications (e.g., wearables). Electrolytes-based CHs are promising alternatives due to both solid- and fluid-like behaviours of hydrogels. While porous structures of the polymeric skeleton make CHs behave as solid electrolytes, the presence of polar solvent (H_2O) enables liquid-like ionically conductive performance. Ionic current occurs under electric fields due to the conduction of ions. When the applied potential is above the voltage threshold of water electrolysis (i.e., 1.23 V), the ionic current is mainly faradic; in contrast, the ionic current is mainly capacitive (transient) once the applied potential is below 1.23V. Currently, salts such as NaCl, LiCl, and KCl have been incorporated into hydrogel matrices (e.g., the PAAm hydrogel) to achieve ionically CHs. By adjusting the concentration of salts, CHs can reach a conductivity in the order of magnitude of 10 S/m, which can be regarded as comparable charge conductors (*30*). Those CHs have been demonstrated as artificial muscle, skin, axon and energy harvesting (*12*, *14*, *31*, *114–116*). Among those salts, LiCl is the most frequently-used salt incorporated into hydrogels (*12*, *14*, *31*, *114*, *115*) due to their excellent conductivity plus their hygroscopic and anti-freezing features. Those features are important for the practical applications of wearable and soft robotic sensing.

Polyelectrolyte-based conductive hydrogels: Polyelectrolyte has been incorporated into hydrogels for constructing CHs as well (*30*). Polyelectrolyte is a type of polymer with dissociating electrolyte groups in their repeat units. Depending on the electricity of mobile counterions fixed to the polymeric backbone chains, polyelectrolytes can be divided into polycations and polyanions. They can dissociate in aqueous solutions similar to ordinary electrolytes while their solutions are usually viscous. Polyelectrolytes such as polypeptides, glycosaminoglycans, and DNA are natural ones; polyelectrolytes such as PAMPS, poly (diallyldimethylammonium chloride) (PDAC), poly (sodium styrene sulfonate) (PSS), polyacrylic acid (PAA) are synthetic ones. Different from the ionic conduction within regular hydrogels with electrolytes, polyelectrolyte-incorporated CHs possess selective ionic conduction because the charged functional groups on polymeric backbone chains only allow the free transportation of oppositely charged ions. This feature has been explored for the construction of ion-selective membranes and for applications such as seawater desalination (*30*), hydrogel ionic diodes (*16*, *117*, *118*) and energy harvesting (*16*, *119*).

In summary, while this method is relatively facile and straightforward to enable hydrogels with ionic conductivity, electrolyte-based CHs currently are mainly applied in non-invasive scenarios such as epidermal sensing (*12*, *16*). Those CHs face challenges for implantable applications due to their potential biocompatibility. The salt concentration in those CHs is usually more than 1 M, much higher than the electrolyte concentration in body fluids (0.15 M~0.3 M), leading to the ions diffusing from CHs to human bodies. The ionic diffusion from hydrogels to the extracellular fluid usually causes disorders of water and salt metabolism as well as the conductivity instability of CHs (*39*, *40*).

2.2.2.2. Conducting-polymer-based hydrogels

The conductivity of conventional CHs typically is very limited, typically 6–9 orders of magnitude smaller than that of metals (*114*), which could further hinder their biomedical applications (e.g., hydrogel bioelectronics such as implantable neural signal recording, nerve stimulation and deep brain stimulation). In contrast, the recent advance of conducting-polymer-based hydrogel offers much higher conductivity, promising for the emerging field of hydrogel bioelectronics (e.g., increased signal-to-noise ratio and enhanced stimulation capability) (*39*, *120*, *121*). Conducting polymers [e.g., Polypyrrole (PPy) (*122*), polyaniline (PAni) (*121*, *123*, *124*), and poly(3,4-ethylenedioxythiophene) doped with polystyrene sulfonate (PEDOT:PSS) (*125–130*)] are synthetic ones able to conduct electrons through π-conjugated structures. Many conducting polymers swell in wet environments and become electrically conductive hydrogels with soft mechanical properties and high-water contents, similar to soft biological tissues. Recently, conducting polymers have gained increasing attention for hydrogel bioelectronics due to their advantages such as tunable mechanical and electrical properties, biocompatibility, flexibility, electrochemical stability and processability for chemical modification (*40*, *131*). In addition, the co-presence of ionic and electronic conduction makes conducting-polymer-based hydrogels particularly charming for bioelectronic application due to their excellent conductivity and lower interfacial impedance (*130*, *132*). Conducting polymer hydrogels can be prepared by two strategies: 1. forming interpenetrating polymer networks (IPNs) between conducting polymers and non-conducting hydrogel networks. 2. forming pure conducting polymer hydrogels (*39*, *40*, *130*, *132*).

Here we compare the fabrication difference using PEDOT: PSS hydrogel as a model example due to their excellent biocompatibility, exceptional electrochemical stability, and favourable cytocompatibility as a bioelectronic material (*127*, *134*). The commercially available PEDOT:PSS usually possesses poor solubility in water (a universal solvent for bioelectronic applications) (*135*). Therefore, chemical solvents such as glycerol, sorbitol, dimethyl sulfoxide (DMSO), ethylene glycol (EG), acids and ionic liquid are usually adopted as secondary dopants to increase their solubility and conductivity by reinforcing the intermolecular interactions (*125*, *126*, *128*, *132*, *135*).

For example, IPNs can be formed between conducting polymers (i.e., PEDOT:PSS) and non-conducting hydrogel networks (i.e., PAAm) during PEDOT:PSS-PAAm hydrogel synthesis in the EG aqueous solution, possessing a 200% stretchability (*126*). On the other hand, a mechanically tunable and conductive IPN hydrogel is formed by the ionic-liquid-induced gelation of loosely-cross-linked PEDOT: PSS hydrogel and a subsequentially interpenetrated polymerization of a soft and stretchable network [i.e., polyacrylic acid (PAAc)] (**Figure 2.3**A and B) (*133*). The as-made gels possess ultra-soft and tunable moduli over three biologically relevant orders of magnitude (8–374 kPa) without compromising conductivity (> 10 S/m) or stretchability (>100%), which is promising to compliantly interface with a wider range of bio-tissues such as the brain (0.5–1 kPa) to stiffer tissues such as the skin and certain regions of the heart (100–500 kPa) (*133*).

However, existing IPN-based conducting polymer hydrogels mostly blend PEDOT:PSS with other compositions such as non-conductive polymers, sacrificing their electrical conductivity and/or electrochemical performances since the non-conductive hydrogel network acts as an electrical insulator (e.g., their electrical conductivity is typically below 100 S/m in deionized water) (*40*, *130*). A recent work has achieved the highest electrical conductivity (880 S/m) by forming a pure PEDOT: PSS hydrogel with over 95% water (*125*). Whereas, this pure conductive hydrogel requires concentrated sulfuric acid for fabrication and the extraordinary conductivity is tested in an acidic solution (pH=1), unsuitable for most implementable biomedical applications (*125*).

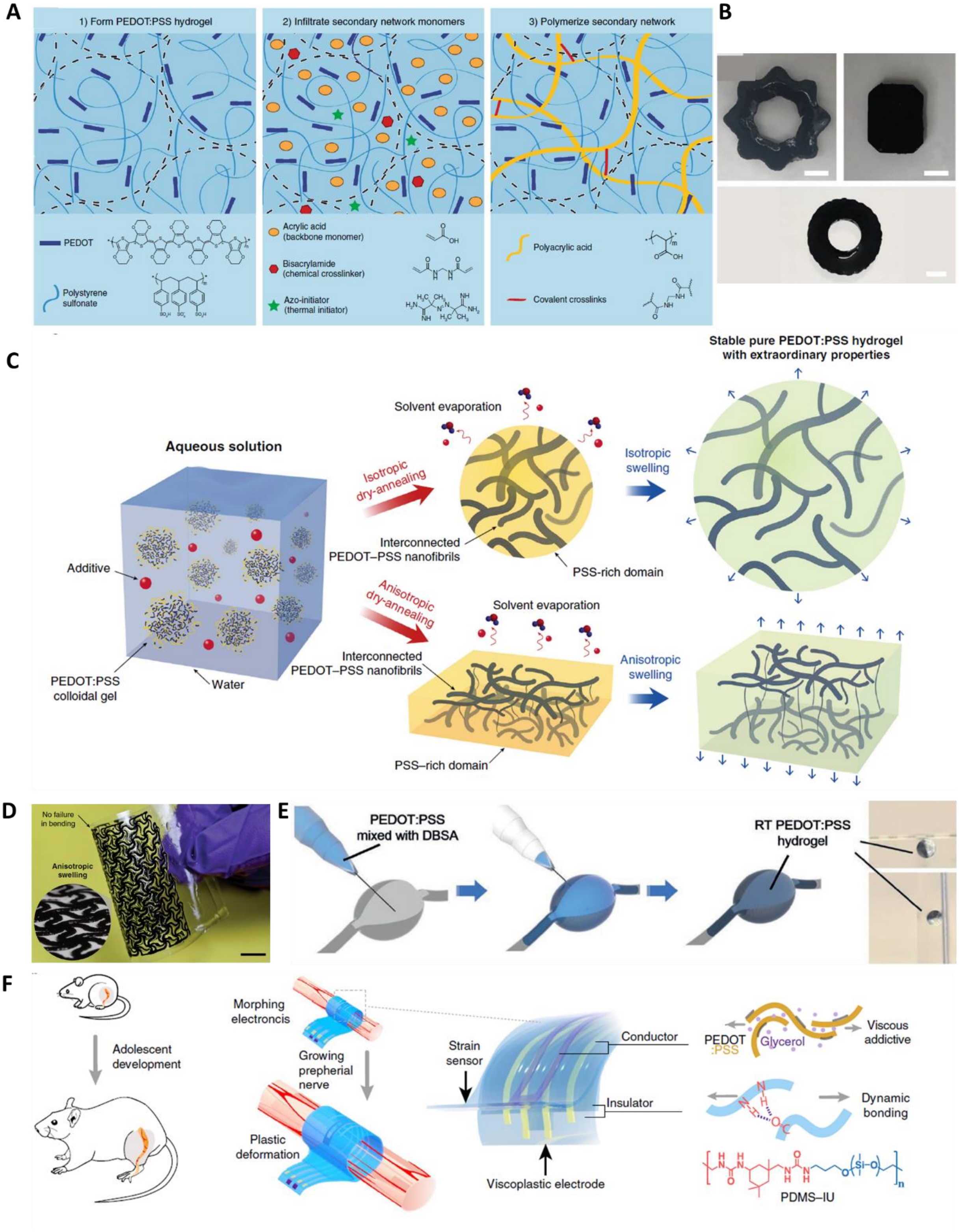

Figure 2.3. Conducting-polymer-based hydrogels. (**A**) Process for fabricating conductive PEDOT:PSS-based IPN hydrogels. (**B**). PEDOT:PSS/acrylic acid mixture casted into different

silicone soap molds. Reprinted and adapted with permission from Ref. (133). (**C**). Dry-annealing and swelling processes of pure PEDOT:PSS with DMSO as the additive. (**D**). Robust laminate of pure PEDOT:PSS hydrogel pattern. Reprinted and adapted with permission from Ref. (130). (**E**) Schematic of injectable RT-PEDOT:PSS hydrogels. Reprinted and adapted with permission from Ref. (127). (**F**) Schematics of Mmorphing electronics enable neuromodulation in growing tissue Reprinted and adapted with permission from Ref. (128).

Recently, Lu et al. designed pure PEDOT: PSS hydrogels with the addition of volatile DMSO into aqueous PEDOT: PSS solutions followed by controlled dry-annealing and rehydration procedures. The resultant hydrogels yield a set of properties highly desirable for bioelectronic applications, including high electrical conductivity (~2000 S/m in PBS, ~4000 S/m in deionized water), high stretchability (> 35% strain), low Young's modulus (~2 MPa), superior mechanical, electrical and electrochemical stability, and tunable isotropic/anisotropic swelling in wet physiological environments (**Figure 2.3**C and D) (*130*)**.** While most pure PEDOT: PSS hydrogels are fabricated at elevated temperatures, they are unsuitable to in-situ synthesize and are difficult to be conformed seamlessly on the unregular biological tissue surfaces. Recently, Zhang et al. designed a room-temperature-formed PEDOT:PSS (RT-PEDOT:PSS) conductive hydrogel that is injectable, soft, and healable (*127*). Spontaneous gelation occurred at the room temperature by simply mixing PEDOT:PSS suspension with 4-dodecylbenzenesulfonic acid [DBSA, a widely used secondary dopant (surfactant)] without any additional treatments (**Figure 2.3**E)(*127*). Organic electrochemical transistors (OECTs) with injected RT-PEDOT:PSS hydrogel fibre was demonstrated and this technology can promote PEDOT:PSS hydrogels toward biomedical applications, along with the already demonstrated applications such as soft and elastic microelectronics for localized low-voltage neuromodulation (*132*) and morphing electronics enable neuromodulation in growing tissue (*128*) (**Figure 2.3**F).

Overall, although the development of conducting-polymer-based hydrogels is extremely fast, there is still a persisting challenge as well as trade-off of their maximum stretchability, conductivity, processability, and transparency, which is worth to be further explored in the future for their practical biomedical applications. More examples and detailed mechanisms of conducting-polymer-based hydrogels can be found in recent reviews (*39, 110, 111, 136*).

2.2.2.3. Other novel conductive gels

Currently, several other ionic conductive gels have been explored as well, providing great potential for diverse applications. Among them, polymeric ionic liquids (PILs) and ionogels that are made from ionic liquids (ILs) are getting increasing attention due to their both polymeric and ionically conductive features. PILs and ionogels are usually nonvolatile and do not dry out in both ambient and extremely hot environments, and do not freeze at the low temperature, which could be good compensation candidates to broaden the biomedical application scenarios of ionically conductive hydrogels.

Polymeric Ionic Liquids (PILs): Before the introduction of PILs**,** ILs will be described first here. ILs are defined as molten organic salts that are composed of organic cations and organic/inorganic anions with melting temperature below 100 °C. ILs have many interesting physicochemical properties such as ionic conductivity (10^{-2} to 1 S/m), negligible vapour pressure, thermal stability and non-flammability, wide electrochemical stability window (~5.7V), wide tolerant temperature range (up to 200-300 °C) and tunable physical and chemical properties (numerous combinations of cations and anions) (*137–140*). ILs have been widely applied to research areas such as synthetic chemistry, catalysis, energy storage, and recent sensors and actuators (*60*, *137*, *140–144*). However, the liquid feature of ILs could induce complexity such as leakage, difficulty of handling, non-portability, and impossibility of miniaturization (*137*, *145*, *146*) when applied for wearable/biomedical applications and soft robotics.

The most straightforward strategy is the polymerization of ILs into PILs (or called ionic polymers or novel polyelectrolytes). PILs can be prepared by either chemical cross-linking of IL monomers (*147*) or physical assembly of block polymers (*148*). PILs retain most unique properties of ILs along with the intrinsic polymeric feature without leakage issue. Similar to conventional polyelectrolytes, PILs can be categorized as polycations that bear cations, polyanions that bear anions, and unique polyzwitterions that bear both anions and cations in the polymeric backbone. Contrary to conventional polyelectrolytes that are water soluble, most PILs are only soluble in polar organic solvents since the typical counter-anions [e.g., tetrafluoroborate (BF_4^-), hexafluorophosphate (PF_6^-), bis(trifluoromethanesulfonyl)amide ($TFSI^-$), bis(fluorosulfonyl)imide (FSI^-), trifluoroacetic ($CF_3CO_2^-$), and dicyanamide (DCA^-)] of PILs are hydrophobic while the counter-anions (e.g., Cl^-, Br^- and I^-) of conventional cationic polyelectrolytes are hydrophilic; on the other hand, conventional polyelectrolytes commons consists metallic counter-cations (e.g., Li^+, Na^+ and K^+), while typical counter-cations [1-Butyl-3-methylimidazolium ($BMIM^+$), 1-Ethyl-3-methylimidazolium ($EMIM^+$) and 1-methyl-3-octylimidazolium ($OMIM^+$)] of PILs are organic. Interestingly, polyzwitterions as a type of unique PILs are water soluble, consisting of zwitterionic moieties as monomers. Polyzwitterions have recently been explored for many applications. For example, a soft PIL-based anti-freezing ionic skin for a soft robotic gripper has been developed based on a type of zwitterionic PIL. This zwitterionic PIL gel exhibits a stretchability of 900%, self-healing ability, anti-freezing capability and high ionic conductivity (1.1 S/ m) at low temperature (-20 °C) (**Figure 2.4**A) (*149*).

Ionogels: Another strategy is to introduce ILs into physically or chemically cross-linked networks of polymer matrices to form ionogels (or call ionoelastomers). Ionogels keep most properties of ILs without the leakage and exhibit an elastomeric feature. Therefore, ionogels have been applied as lithium-ion batteries, fuel cells, solar cells, electrochemical sensors and biosensors, wearable biophysical sensors, actuators, ionic diodes and energy harvesting (*137*, *140*, *150–156*). For example, IL–based ionogel was prepared by the thiol-ene click chemistry, in which solution A [poly(ethylene glycol) diacrylate (PEGDA), pentaerythritol tetraacrylate (PETA; cross-linker for covalent network), and anionic BTCA (cross-linker for the ionic bond network) dissolved in methanol] was mixed with solution B [mixture containing PIL-BF_4, triethylamine (TEA; a catalyst for the thiol-ene click reaction), and 1,2-ethanedithiol (ED) dissolved in methanol] at room temperature to form gel and then a room temperature IL, 1-propyl-3-methylimidazolium fluoborate (IL-BF_4) was introduced into the formed gel at 80°C under vacuum for 24 hours. This ionogel exhibits excellent mechanical properties, resilience after 10,000 fatigue cycles, high ionic conductivity, transparency, and nonflammability performance over a wide temperature range (−75° to 340 °C). A demonstrated click-ionogel based triboelectric nanogenerator exhibits excellent mechanical, freeze-thaw, and heat stability thereafter (**Figure 2.4**B) (*150*).

Overall, both PILs and ionogels have shown huge potential for flexible electronic applications such as flexible sensors, energy storage, and electronic skin. Whereas, the complexity of synthesis and relatively high still limit their further and broader applications. In addition, the currently reported biomedical applications are mostly non-invasive, their in-vivo biocompatibility should be examined in the future to broaden their application. The relatively low conductivity of ionogel and PILs compared to the conducting-polymer-based hydrogel may hinder their further application for wearable bioelectronics such as implantable neural signal recording, nerve stimulation and deep brain stimulation.

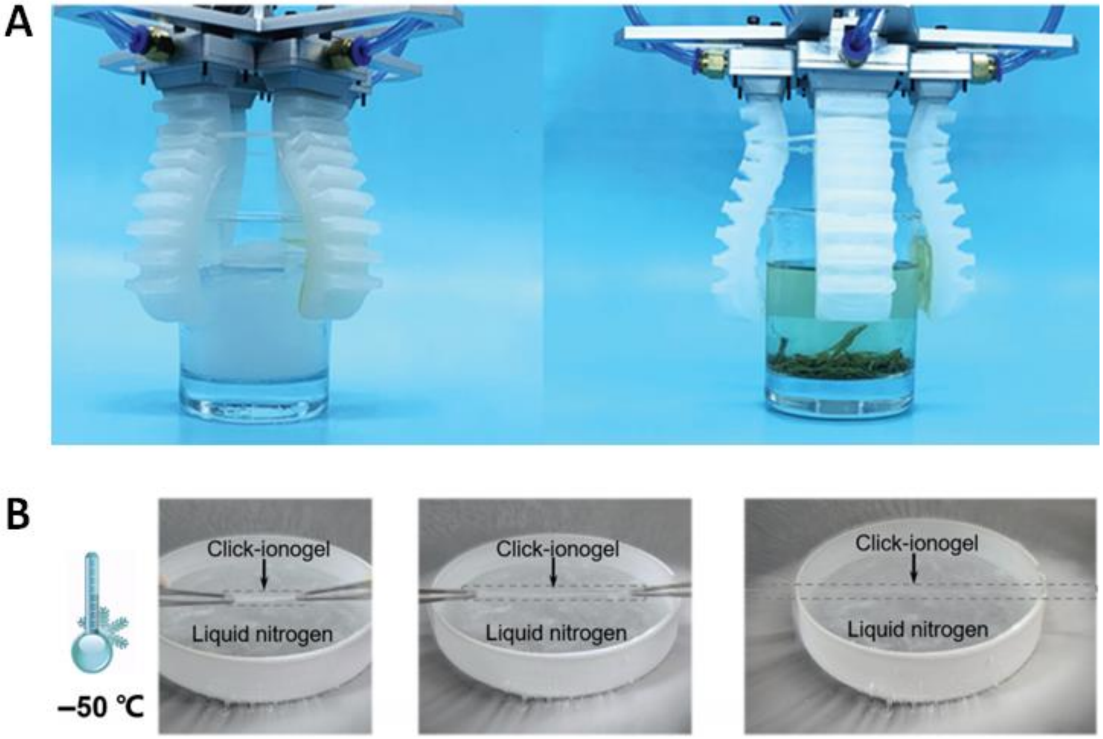

Figure 2.4. Other novel conductive gels. (A). Photos of the soft gripper holding a cup of ice water and a hot tea. Reprinted and adapted with permission from Ref. (149), Royal Society of Chemistry. **(B).** Photos of a click-ionogel stretched above liquid nitrogen (about −50°C). Reprinted and adapted with permission from Ref. (150), 2019 American Association for the Advancement of Science.

2.2.3. The combination of conductivity and toughness

Tough and conducting hydrogels made from double networks are very attractive for developing artificial muscles, robotics, flexible electronics and soft actuators. Nowadays, some wearable, bioelectronic and soft robotic applications appreciate the enhanced electrical performance together with the mechanical toughness. Recently, several efforts have been made to construct conductive tough hydrogels. The simplest way is to incorporate electrolytes or polyelectrolytes into an existing neutral tough hydrogel matrix. For example, NaCl has been introduced into a poly(vinyl alcohol)/poly(acrylic amide) (PVA/PAAm) DN hydrogel to prepare PVA/PAAM/NaCl conductive tough hydrogel via a one-pot method (*157*). On the other hand, two oppositely-charged polyelectrolytes can be incorporated into an agarose-PAAm DN hydrogel, which shows an ionic diode tough hydrogel (*16*).

While the incorporation of monovalent ions could impair the mechanical performance of some non-neutral tough hydrogels such as the most popular alginate-PAAm tough hydrogel (*101*, *158*), the addition of neutral hygroscopic chemicals (e.g., glycerol) could suppress this negative influence and maintain both the conductivity and toughness *(320)*. This is due to noncovalent interactions between the hydrogel polymer chains and the neutral hygroscopic chemicals (*159*). The reduced competition of the monovalent ions for binding sites on the alginate chains could protect the ionic cross-links *(320)*.

In addition, inspired by IPN formation of DN hydrogel synthesis, conducive monomers could be polymerized into a first/second-network hydrogel matrix to form IPN hydrogels with both conductivity and mechanical toughness (*160–163*).

2.3. Bioinspired and advanced hydrogel with enhanced merits.

Natural living systems display complex tissue and organ structures composed of active hydrogels to survive in complicated and diverse environments. For example, properties such as freeze tolerance, dehydration resistance, self-healing, biodegradability are commonly found in certain mammals, fishes, frogs, insects and bacteria. In addition, certain animals (e.g., mussels) can form adhesion in wet environments.

Inspired by these examples in nature, conductive hydrogel-based biomimetic materials have been intensively studied to develop stretchable electronics for various applications including wearable physical/biosensing, human-machine interaction and soft robotics. Many bioinspired hydrogel devices consist of enhanced merits such as anti-freezing, anti-dehydration, self-healing, biodegradability and diverse adhesive (*31*, *39*, *44*, *164*). Those advanced features will further feature hydrogels as a more reliable material for the practical use. In this section, we point out several key issues of current hydrogel devices and highlight recent advances of strategies to empower hydrogels with enhanced merits including anti-freezing, anti-dehydration, and adhesive capability.

2.3.1. Anti-dehydration and Anti-freezing

The water content inside the hydrogel and the state of the water molecules will seriously affect the properties of hydrogels. There are three different states of water in a hydrogel, namely "free water" (fast exchange), "intermediate water" (slow exchange), and "unfrozen bound water". Regular hydrogels will easily lose water in the open air and inevitably freeze at subzero temperature due to the large existence of free water, losing their mechanical stretchability and electrical conductivity and severely hindering their practical applications for wearables and robotics.

In order to enhance the long-term ambient stability and anti-freezing capability of hydrogels, it is necessary to change the free water into the other two states as much as possible. Inspired by nature, hygroscopic substances (e.g., salts, organic solvents and combinations thereof) have been added into regular hydrogels to sustain its ambient stability; in addition, an epithelium-like elastomer layer can be coated on hydrogel to reduce the evaporation rate as well. On the other hand, most hygroscopic substances are cryoprotective. Therefore, in this section, we plan to discuss different strategies to enhance the anti-dehydration and anti-freezing capability of hydrogels; moreover, some novel nonvolatile gels will be briefly presented in the end.

Salts-incorporated hydrogels: Pure salts in high concentration (> 1 M) such as sodium chloride (NaCl), lithium chloride (LiCl), potassium acetate (KAc), magnesium chloride ($MgCl_2$), calcium chloride ($CaCl_2$) and their combination thereof have been incorporated into both regular and tough hydrogels (*165*, *166*) to enhance their water retention capacity as well as their freezing tolerance. For example, LiCl salt is more hydrable compared with other salt species and PAAm hydrogel containing high content of LiCl (12 M) can retain over 70% of its initial water even in extremely dried environments (RH = 10%) for 5 days. This high water retention capacity and low water evaporation of LiCl-incorporated PAAm hydrogel is due to the stronger bond strength between dissolved cation/anion and the water molecule pairs (*165*, *166*). The freezing point of this LiCl-PAAm was accordingly reduced to -80 °C as their conductivity is relatively high in such a low temperature. Whereas, most monovalent ions (e.g., Li^+, Na^+ and Cl^-) could impair the mechanical performance of some tough hydrogels with ionic crosslinking (e.g., alginate-PAAm hydrogel) (*158*). In order to protect their toughness, multivalent-ionic salts such as $CaCl_2$ were incorporated into the regular alginate-PAAm tough hydrogel to increase its anti-freezing capability. Without reporting its ambient stability, the freezing point of this resulting hydrogel (30 wt% $CaCl_2$) can be as low as −57 °C. Although the toughness of this hydrogel reduces to 2000 J/m^2 from the original 9000 J/m^2 due to its reduced stretchability (λ=4.5), it can still be stretched more than four times their initial length and have a fracture toughness of 5000 J/m^2 at −57 °C (*166*).

Organic-solvent-incorporated hydrogel: Alternatively, organic solvents such as glycerol (*159*, *167–171*), EG (*172–175*), and DMSO (*176*), sorbitol (*168*) and the combination thereof (*168*) have been incorporated into both regular and tough hydrogels to enhance the water retention capacity and depress the freeze point of water-based devices for applications such as battery (*176*), flexible solid-state supercapacitors (*173*), flexible wearable devices (*170*, *174*, *175*) in the extreme environment. In addition, the anti-freezing and anti-dehydration capability of hydrogels as well as their mechanical and electrical properties can be altered by adjusting the concentration of organic contents. For example, our group found that the incorporation the glycerol solution with an optimal concentration of 66.5 wt.% into alginate-PAAm tough hydrogel, it can maintain 75% of its original mass even after 30 days in an extremely dry environment (RH = 15%) and the freezing point can reach down to -97 °C, which is due to the glycerol's strong water-retaining capability and its effective freezing inhibiting effect by altering the water states in hydrogels. In addition, different from salts-incorporated strategy, the elastic modulus and mechanical toughness of glycerol-incorporated hydrogels can be enhanced due to the noncovalent interactions (hydrogen bonds) between the hydroxyl groups on glycerol chains and carboxyl groups and amino groups on alginate and PAAm chains *(320)***.**

Currently, there are mainly two strategies (one-spot synthesis and two-step solvent exchange method) to add organic solvents into hydrogels. For example, during one-spot synthesis, binary solvent-water systems can be mixed into polymer (*172*) or monomer (*159*) solutions before network crosslinking; while during two-step solvent exchanging, the as-fabricated hydrogel can be soaked into the binary solvent-water system for a while (e.g., 3 h) to reach the equivalent status (*168*). One-spot synthesis is usually regarded as a more regent-saving and environmental friendly method while the two-step solvent exchange method can avoid the complicated synthesize optimization steps because the binary solvent is introduced after polymerization and cross-linking of hydrogels (e.g., ionic cross-linking of alginate network, polymerization of AAm and covalent cross-linking of PAAm network for alginate-PAAm tough hydrogel) (*168*). In addition, two-step solvent exchange methods can be conveniently expanded to fabricate tough hydrogels with various cryoprotective solutions, concentrations to realize different anti-freezing, conductivity and mechanical performances (e.g., toughness and stretchability) as on-demand *(320).*

The combination: Some pure nontoxic salts (e.g., NaCl and KCl) have limited water retention capacity and limited freezing inhibiting capability, although they are very popular for wearable hydrogel sensors application. For example, hydrogels laden with 5.4M NaCl remain only 35% of the original mass after 15 days at RH= 15% due to the evaporation of water and loss its high transparency because of the salt precipitation once RH is below 63%; in addition, its freezing point is -22 °C *(320)*. While most organic-solvents-incorporated hydrogels can achieve both good ambient stability and antifreezing capability, these hydrogels (or called organohydrogels) suffer from low conductivity, which is not suitable for wearable and robotic applications. Recently, more studies focus on the incorporation of salts (*170*, *171*, *173*, *175*, *177*, *178*), conductive polymers (*172*) or conductive fillers (*159*, *174*) with organic solvents into hydrogels to increase their conductivity, ambient stability and anti-freezing capacity. As one of the most popular methods, incorporating monovalent salts and binary solvents into hydrogels is facile through solvent exchange *(320)*. Surprisingly, our group found that the common nontoxic monovalent ions (e.g., Na^+ and Cl^-) at high concentration did not impair the mechanical performance of tough hydrogels with ionic cross-links (e.g., alginate-PAAm tough hydrogel) *(320)*. This mechanical maintenance is probably due to the incorporation of the binary solvent system. Solvents like glycerol introduces noncovalent interactions within the hydrogel polymer chains (*159*), and increases the polymer network density due to a slight hydrogel shrinkage (~10% in length) during solvent exchange (*168*). In addition, the incorporation of glycerol reduces the sodium ions competition with calcium ions for the binding sites on the alginate chains, protecting the ionic cross-links *(320)*.

On the other hand, conductive polymers (e.g., PEDOT:PSS) have already been added into the hydrogel matrix for bioelectronic applications (*39*). In order to increase the solubility of PEDOT:PSS and its conductivity, chemical solvents such as glycerol, sorbitol, DMSO and EG were usually adopted as secondary dopants (*126*, *128*, *132*, *135*). Although their ambient stability and anti-freezing capability are usually not reported due to their specific implantable bioelectronic applications, those conductive hydrogels usually consist of good electrical and mechanical performance (*126*, *172*) as well as ambient stability and anti-freezing capability (*172*).

In addition, inspired by the robustly laminated hybrids of elastomer-like epidermis and hydrogel-like dermis within mammalian skins, water can be retained for at least 2 days by encapsulating the hydrogel into a layer of elastomer (*179*). Although coating with an elastomer can only slow down and cannot stop long-term dehydration entirely due to their relatively large permeability of water (*31*), this hydrophobic coating strategy can be combined with the salt addition (*180*) and even salt-solvent addition (*177*) to further prevent the fluctuation of water content in the hydrogel as well as maintain its anti-freezing ability and conductivity. Moreover, hydrophobic coating can prevent naked hydrogels from many potential issues such as swelling, ions leakage in the aqueous environment, and can broaden their potential application scenarios such as stability in the acid environment and high temperature (*181*). Hydrophobic coating can also broaden the selection scopes of hygroscopic/cryoprotective chemicals with no need to constrain on those nontoxic chemicals (*182*) if applied for wearable ionotronics.

Novel nonvolatile gel: As we mentioned in *section 2.2.2.3*, conductive gels such as PILs (*147–149*) and ionogels (*137*, *138*, *140*, *150–156*) originating from ILs are usually nonvolatile and do not dry out in both ambient and extremely hot environments and do not freeze at the low temperature. To our best knowledge, the best anti-freezing capability of these nonvolatile gel can reach at least -75 °C (*150*) and no weight changes are observed in ambient conditions (*151*), high vacuum (6×10^{-4} Pa) or high humidity (RH=99%) (*138*). Further improvement of their relatively small rupturing stretch, low conductivity, high cost, difficulty of fabrication will further broaden their applications as an alternative to hydrogels.

2.3.2. Hydrogel Adhesive

Hydrogel as a biocompatible material has gained a lot of attention for wearable sensors (*12*, *14*, *16*, *115*, *183*), implantable bioelectronics (*128*, *129*, *132*, *184*) and soft robotics (*15*, *23*, *24*). However, hydrogel devices typically consist of poor surface adhesion and do not adhere strongly to any materials, losing the fidelity of sensing signal acquisition and bringing motion-induced signal artifacts in the as-mentioned application scenarios. Previous years have witnessed the rapid progress of hydrogel adhesion, which will be briefly reviewed in this section.

Hydrogel-solid materials bonding: Solid materials including metal, glass, ceramics, silicone and plastic are commonly used for actuators, biomedicals, robotics, soft electronics (*46*, *57*, *114*, *129*). Strong hydrogel bonding to diverse solid surfaces remained a challenge due to the nature of hydrogels that contain significant amounts of water. In 2016, Yuk et at., designed a strategy, in which the precursors of long-chain polymer networks of tough hydrogels (e.g., alginate-PAAm, PAAm-hyaluronan, PAAm-chitosan, PEGDA-alginate, PEGDA-hyaluronan) were cast on the non-porous 3-(Trimethoxysilyl)propyl methacrylate (TMSPMA)-silanalized solid surfaces including glass, silicon, ceramics, titanium and aluminium (*185*). During the curing of tough hydrogels, methacrylate groups on the functionalized surface covalently grafted PAAm or PEGDA networks (**Figure 2.5**A and B**)**. Compared with other physical interactions and non-tough hydrogel chemical bonding, this design results in an interfacial toughness value over 1,000 J/m^2 due to simultaneous chemical anchorage and significant energy dissipation of bulk tough hydrogel during detachment (*185*). This interfacial toughness is comparable with the toughest bonding found between a tendon and a bone in humans (800 J/m^2) (*186*).

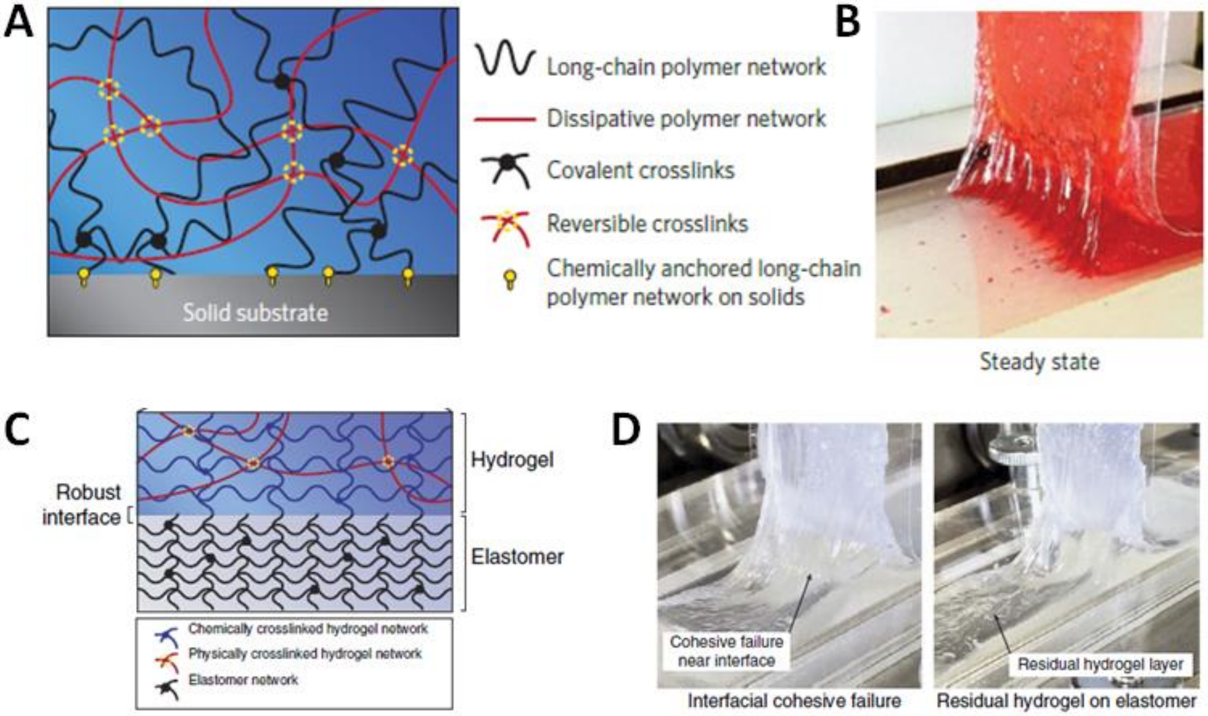

Figure 2.5. Hydrogel adhesive. (A). The tough bonding between hydrogel and solid surfaces. **(B).** Photos of the peeling process of a tough hydrogel with its long-chain network chemically anchored on a glass substrate. Reprinted and adapted with permission from Ref. (185), Nature publish group. **(C).** The tough bonding between hydrogel and soft materials (**D**). Photos of the hydrogel–elastomer interface during peeling test. Reprinted and adapted with permission from Ref. (179), Nature publish group.

Hydrogel-soft materials bonding: Soft elastomers such as PDMS, Ecoflex, VHB are commonly used for soft robotics and soft electronics (*15*, *44*). The delamination issues occurs due to no hydrogel-elastomer bonding in the previous works including soft actuators, soft energy harvesting, wearable sensor (*12*, *14*, *114*, *183*). Strongly bonding hydrogels to elastomers could empower soft robotics with novel functions such as intelligent sensing capability. Yet, hydrogel-elastomer assembly is another challenge due to their huge contrast of hydrophilicity and hydrophobicity. In addition, the adhesion should withstand large deformation (at least over 100% stretchability) for soft robotic applications, in which the connection between the hydrogel and the elastomer must be strong and sparse (*38*). The previous strategy of strongly bonding hydrogels to rigid solids is generally inapplicable in forming hydrogel–elastomer hybrids with robust interfaces. This bonding failure is due to the fact that oxygen permeable elastomers could inhibit the free radical polymerization of the hydrogel polymers (*187*, *188*) and hydrophobic recovery of saline-functionalized elastomer surfaces could significantly lower the effectiveness of hydrogel bonding on elastomers (*189*, *190*). Again, Yuk et al. described a method, in which the precursors of tough hydrogels (e.g., alginate-PAAm, PAAm-hyaluronan, PAAm-chitosan, PEGDA-alginate, PEGDA-hyaluronan) with physically crosslinked first network were gently mounted on the freshly benzophenone-treated elastomer surfaces including PDMS, Ecoflex, polyurethane, latex and VHB. During photo-curing of the second network of tough hydrogel, PAAm or PEGDA networks were covalently grafted to the methacrylate groups on the active elastomer surfaces (**Figure 2.5**C and D) (*179*). This method achieves an adhesion energy above 1000 J/m^2 as well as an elastomer-hydrogel hybrid with 700% stretchability. This strategy has been utilized to coat a thin layer of hydrogel skin on a wide range of common polymers with arbitrary geometries and shapes including medical tubing, foley catheters, cardiac pacemaker leads with low friction, anti-fouling properties (*191*). Soft and stretchable nanogenerators with this robust hydrogel-elastomer interfacial bonding have been demonstrated recently with enhanced mechanical reliability and ambient stability (*182*, *192*).

Whereas, the above-mentioned strategy is not suitable to construct soft devices with microstructures patterned on cured elastomers (or hydrogels) due to the infiltration of pre-gel solutions (or pre-elastomer resins). In addition, the elastomer cannot be coated on a preformed hydrogel of arbitrary shape. Recently, Suo et al. designed a strategy to coat and print various hydrogels and elastomers of arbitrary shapes, in arbitrary sequences, with strong adhesion, in which silanes can be incorporated as coupling agents into the precursors of both the hydrogel and elastomer to form strong bonding independent of the sequence of network formation (*181*). This hydrophobic coating can enhance the hydrogel stability even at high temperatures (*181*). Later on, an ionic hydrogel skin sensor was adhered on a soft gripper through this strategy for smart soft robotics (*15*).

Hydrogel-tissue bonding: Hydrogel as a biocompatible material has recently been applied for biomedical applications including wearable electronics, implantable electronics and wound healing. However, bonding between hydrogel and tissue is usually poor due to the complex environment of biological tissue (bloody, wet, dynamic etc.), limiting the application of hydrogel. Existing commercially available tissue adhesives such as Cyanoacrylate adhesive (Super Glue), albumin-based adhesives (BioGlue), fibrin glue (TISSEEL, Baxter), polyethylene glycol–based adhesives (COSEAL, Baxter and DURASEAL, Confluent Surgical) (*193–196*) are either cytotoxic, brittle or non-wet-adherable (*195*, *196*). On the other hand, all the above-mentioned chemical modifications are not suitable for tissue adhesion due to the toxic chemical and long adhesion time during multiple steps of reaction. In 2017, Li et al. described a method to empower tough hydrogel surface (e.g., alginate-PAAm) with the strong adhesive by employing a bridging polymer that bears positively charged primary amine groups to achieve strong tissue–hydrogel adhesion (*196*). Such a bridging polymer can be absorbed to a surface through both electrostatic attraction and covalent bonding. In term of covalent bonding, specifically, amide bond (-COO−NH-) can be formed in the presence of two common coupling reagents [1-ethyl-3-(3-dimethylaminopropyl)carbodiimide (EDC) and N-hydroxysulfosuccinimide (NHS)] between 1. primary amine groups on bridging polymers and carboxylic acid groups on both the tough hydrogel matrix and to-be-adhered tissue substrates (e.g., skin). 2. carboxylic acid groups on the tough hydrogel matrix (mainly the alginate network) and primary amine groups on the to-be-adhered tissue substrates. In addition, the bridging polymer can penetrate into the permeable tissue surfaces to form physical entanglements and chemical anchors (**Figure 2.6**A and B). Suitable bridging polymers include chitosan, polyallylamine, and polyethylenimine. During peeling, strong adhesion energy of more than 1,000 J/m^2 can be achieved due to the electrostatic interactions, covalent bonds, and physical interpenetration between tissues and hydrogels and energy dissipation of the tough hydrogel matrix (*196*). Such adhesive strategy was further applied on a PNIPAM-alginate DN hydrogel to realize a thermal active adhesive dressing to accelerate wound closure (*197*). However, strategy to enable strong tissue adhesion takes time (more than 30 min), which is undesirable during surgery. More recently, Yuk et al. further reported an alternative tissue adhesive in the form of a dry double-sided tape (DST) made from a combination of a biopolymer (gelatin or chitosan) and crosslinked poly(acrylic acid) (PAAc) grafted with N-hydrosuccinimide ester (**Figure 2.6**C-E) (*198*). By removing interfacial water from the tissue surface, the dry DST becomes wet and can form a fast temporary crosslinking to the wet tissue surface within 5s. The

NHS ester groups grafted on the PAAc also couple covalently with primary amine groups on various tissues within a few minutes to provide tough, and long-term stable adhesion (*198*).

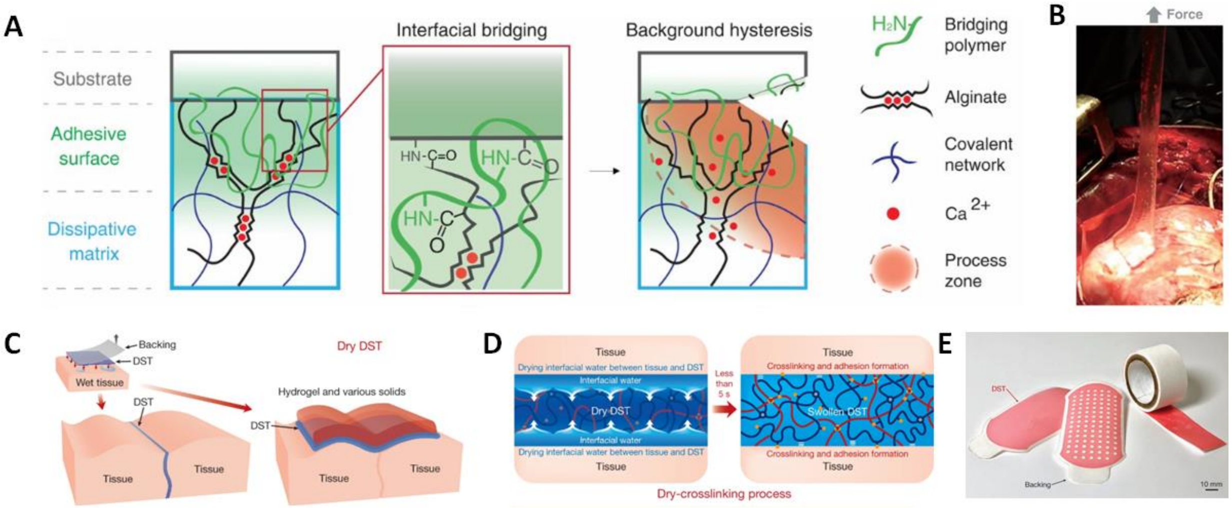

Figure 2.6. **Hydrogel bioadhesive.** (**A**) Design of hydrogel tough adhesives (**B**) In vivo test on a beating porcine heart with blood exposure. (A-B) Reprinted and adapted with permission from Ref. (196)**,** 2017 American Association for the Advancement of Science. **(C**). Tissue adhesive takes the form of a dry DST. (**D**). The dry-crosslinking mechanism for the DST integrates the drying of interfacial water by hydration and swelling of the dry DST, temporary crosslinking, and covalent cross-linking. (**E**). The DST can take on various shapes owing to its high flexibility in fabrication. (C-E) Reprinted and adapted with permission from Ref. (198), Nature publish group.

In summary, in this section we mainly introduce several strategies to realize tough and strong adhesion between hydrogel and substrates including metal, plastics, glass, ceramics, PDMS, Ecoflex, VHB and tissues. The readers can refer to other literature reviews for deeper mechanisms and more examples (*31*, *38*, *40*). While most current hydrogel adhesives are permanent, novel adhesives designed with various functions such as ambient stability, anti-freeze, anti-swell, conductivity, reversibility, degradability, and on-demand detachability are needed in many practical applications including wearables, implantable and robotics. For example, our group reported an ambient stability and anti-freezing conductive tough hydrogel with diverse adhesions for wearables and soft robotics *(320)*. Yang et al. reported a PH triggered on-demand detachable adhesive recently (*199*); Chen et al. reported a saline solution (glutathione and sodium bicarbonate) triggered benign detachable tissue adhesive (*200*); Kim et al. reported a low-voltage (1 V) reversible electroadhesion based on an ionoelastomer diode (*201*).

2.4. Applications of hydrogel artificial skin devices

Hydrogel devices such as artificial skins have been shown to have tremendous potential to blur the boundary between humans and robots/machines. In a human–robot interaction loop, wearable hydrogel skin/sensors can empower the robot with human-like sensation capability to sense the mechanical, thermal and other biochemical stimuli from the environment; while hydrogel-based or hydrogel-integrated soft robotics can take human-like mechanical actions following the control signals. This section will summarize the recent progress of hydrogel wearable sensors and hydrogel soft robotics in the human–robot sensing–acting loop. In addition, compliant hydrogel–based energy harvesters for wearables and soft robotics as a special topic will be discussed thereafter.

2.4.1. Hydrogel wearable sensors

Sensing receptors in our human skin can perceive various environmental stimuli including pressure, strain, deformation, humidity, temperature and pain. So far, numerous skin-inspired flexible and stretchable wearable electronics have been demonstrated. Among them, hydrogel artificial skins or wearable sensors have been attracting notable attention in the past decade due to their softness, skin-like ionic sensing nature, biocompatibility and tunable mechanical properties.

Herein we will go in further detail about these hydrogel wearable iontronics including wearable biophysical and biochemical sensors and touch a little bit about the current challenges simultaneously.

2.4.1.1. Hydrogel wearable biophysical sensors

Hydrogel wearables have been designed to monitor various biophysical stimuli such as strain, stress and temperature, mimicking the function of human skins. Currently, hydrogel based wearable biophysical sensors are mainly monitoring the external stimuli using electrical signals including resistance, capacitance, and some self-powering signals such as open circuit voltage and short circuit current.

2.4.1.1.1. Hydrogel-based biomechanical sensor

Hydrogel-based wearable sensors have been developed to monitor the cardiovascular status (blood pressure, heart/pulse rate), and body movements (skin strain during daily activity) that indicate a person’s health condition. Therefore, hydrogel-based pressure and strain sensors will be discussed here.

Pressure sensor

The development of hydrogel based pressure sensors with human-skin sensitivity have been demonstrated in recent years, with capabilities ranging from the low-pressure regime (<10 kPa, generated by the gentle touch, intraocular pressure and intracranial pressure) to the medium-pressure regime (10–100 kPa, generated by the heart rate, blood pressure wave, respiration rate and normal object manipulation, blood pressure) and to high-pressure regime (>100 kPa, generated by the body weight) (*12*, *17*, *115*, *202–204*). The sensing mechanisms of hydrogel pressure sensors have been based primarily on changes in capacitance (*12*, *177*, *203*, *204*), triboelectricity (*115*, *182*, *192*), and piezoresistivity (*202*, *205*, *206*). While the piezoresistive sensing is mainly based on hydrogels containing conductive fillers that do not belong to the scope of ionic conductive hydrogel, therefore, in the following we will focus on capacitance-based and triboelectricity-based hydrogel pressure sensors.

Capacitance-based ionic hydrogel pressure sensors: Capacitors are usually constructed by sandwiching a dielectric layer between two conductors. The capacitance C is given by the equation $C = \varepsilon_0\varepsilon_r(A/d)$, where ε_0 is the electric constant, ε_r is the relative static permittivity of the dielectric, A is the area of the overlap of the two conductors plates, and d is the thickness of the dielectric. For capacitive pressure sensors, the parameters of the dielectric layers (ε_r, A, and d) can be sensitive to changes in pressure and the change of thickness d is commonly used to for the detection of applied pressure. Various elastomers including PDMS, Ecoflex, and VHB with small modulus values are usually used as the dielectric layer on soft and stretchable capacitive pressure sensors. Upon pressing to λ times its original thickness, both the width and the thickness of the dielectric changed by a factor $1/\sqrt{\lambda}$ due to incompressibility. As a result, the ratio of the capacitance of the stretched strain sensor (C) to that of the unstretched (C_0) is as shown in **Eq. 2.1**.

$$C/C0 = \{\varepsilon_0\varepsilon r[(1/\lambda)\, l*(1/\lambda)\, w]/(\lambda\cdot d)\}/[\varepsilon_0\varepsilon_r(l\cdot w/d)] = \lambda^{-2} \qquad \textbf{Eq. 2.1}$$

Accordingly, the gauge factor (GF) of the capacitance-based ionic hydrogel pressure sensors is

$GF = \frac{C-C_0}{(1-\lambda)C_0} = (1+\lambda)/\lambda^2$, where λ is equal to $(1-\varepsilon)$, here ε is the pressure-induced strain.

For example, Sun et al. developed a transparent, stretchable hydrogel-based wearable pressure sensor by sandwiching an elastomer between two PAAm hydrogels containing NaCl salts with two metallic electrodes connecting to a capacitive meter (**Figure 2.7**A) (12). The whole sensor is encapsulated by two additional layers of VHB for electrical insulation and water retention. The equivalent series capacitance is dominated by the hydrogel-elastomer-hydrogel capacitance other than the capacitance of the EDL in the hydrogel-metal interface because the latter one is much larger. The thickness of the elastomer is decreased as well as the area increased if there is any pressure applied, leading to the increase of capacitance. This hydrogel-based pressure sensor showed high resolution in the range of 1 kPa, sensitive enough to detect a gentle touch of a finger (<10 kPa) (12). Later on, a hydrogel-based sensor array was developed and can sense multiple gentle finger touches even in bending and stretch status (207). In addition, based on the capacitive sensing mechanism, a pure PAAm hydrogel containing lithium chloride salts with metallic electrodes at both ends was designed into a soft, stretchable and transparent touchpad for human–machine interfaces with negligible delay (~10^{-3} s) (14).

Current hydrogel-based capacitive pressure sensors usually suffer from low-response speed, low sensitivity and limited or saturated response under high pressures (>100kPa), while applications such as robotic manipulation and pressure monitoring in the human body demand both high sensitivity and high-pressure resolution at pressures over 100 kPa. Bai et al. developed a hydrogel based capacitive pressure sensor with ultra-broad pressure sensing range with high sensitivity as well as fast response (*204*). By engineering graded intrafillable microstructures on the ionic hydrogel, a mechanically dynamic EDL was formed between hydrogels and the metal. This flexible capacitive pressure sensor exhibits an unprecedentedly high sensitivity ($S_{min} > 220\ kPa^{-1}$) over a broad pressure regime (0.08 Pa-360 kPa), and an ultrahigh pressure resolution (18 Pa or 0.0056%) over the full pressure range, and a fast response time (<20 ms at 1 kHz for the loading of 5 kPa) (**Figure 2.7**B**)** (*204*)**.**

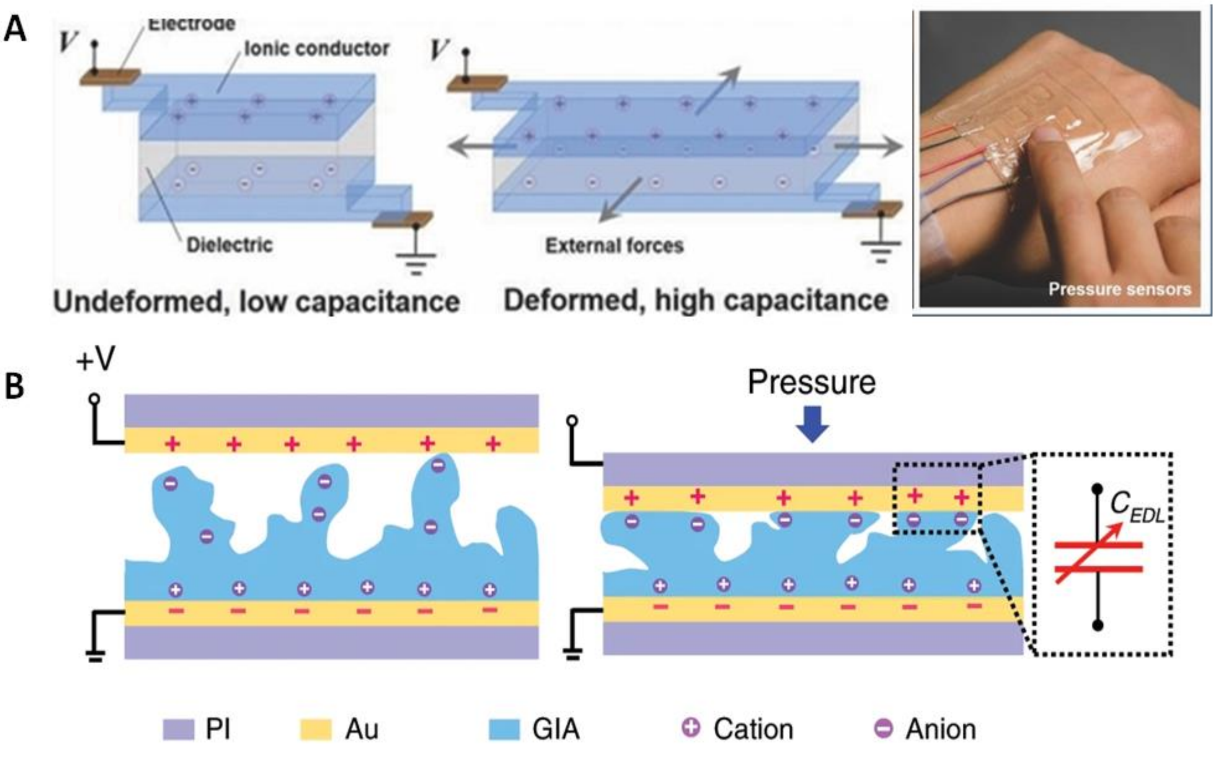

Figure 2.7. **Capacitance-based ionic hydrogel pressure sensors**. (**A**). Ionic skin, Reprinted and adapted with permission from Ref. (12)**. (B**). Schematic illustration for the functioning of the iontronic pressure sensor before and after applying pressure. Reprinted and adapted with permission from Ref. (204).

Triboelectricity-based ionic hydrogel pressure sensors: Most above-mentioned flexible and stretchable capacitive or resistive based pressure sensors required a continuous power supply with comparable stretchability and flexibility. On the other side, the recently developed triboelectric nanogenerator (TENG) could use the self-powered current and voltage signals to monitor the applied pressure without external power. For the first time, Pu et al. reported a soft skin-like triboelectric nanogenerator (STENG) that enables both biomechanical energy harvesting and tactile sensing by hybridizing elastomer and ionic hydrogel as the electrification layer and electrode, respectively (*115*). A STENG-based artificial electronic skin with 3 × 3 sensor arrays is pressure sensitive, enabling its application for wearable touch/pressure perception using the self-powered open circuit voltage (OCV) with a comparable sensitivity of 0.013 kPa^{-1} and limit of detection of 1.3 kPa **(Figure 2.8)** (*115*). This work provides new opportunities for multifunctional power sources and potential applications in soft/wearable electronics.

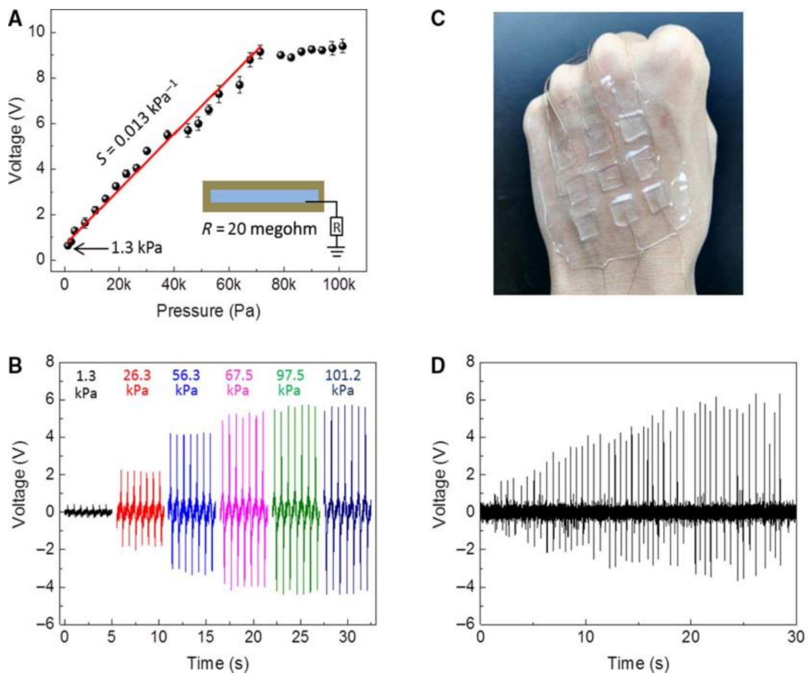

Figure 2.8. Tactile sensing by the STENG. Reprinted and adapted with permission from Ref. (115).

Strain sensor

The strain signal on the human body can be measured for healthcare application such as diagnosis, rehabilitation assistance and activity monitoring. Hydrogel-based strain sensors have been demonstrated in recent years, with capabilities ranging from the detection of small (e.g., breath, wrist pulse, vibration of the vocal cords, heartbeat) to large body deformations (e.g., the body joint movements) (*208*). The sensing mechanisms of ionic hydrogel strain sensors have been based primarily on changes in resistance (*15*, *128*, *209–211*) and capacitance (*12*, *13*, *212*), which will be introduced as follows together with their sensing performances include stretchability, sensitivity (gauge factor), hysteresis, and linearity.

Resistance-based ionic hydrogel strain sensors: The resistance R is given by the equation R = ρ·l/A, where ρ is resistivity, l is length, and A is the cross-sectional area of the material. Note that the deformation of an ionic hydrogel only changes the configuration of its polymer network and water molecules with negligible effect on its ionic conductivity (*15*). Upon stretching to λ times its original length, the cross-sectional area of ionic hydrogel is reduced by a factor of λ due to incompressibility. As a result, the ratio of the resistance of the stretched hydrogel (R) to that of the unstretched hydrogel (R_0) is R/R_0=λ^2 (*15*). Accordingly, the gauge factor (GF) of the resistance-based ionic hydrogel strain sensors is

$$GF = \frac{R-R_0}{(\lambda-1)R_0} = \lambda+1$$

As GF is increased with the applied strain, which makes stretchable ionic hydrogels ideal as large-strain sensors. For example, an ionic PAAm hydrogel was adhered to the elastomeric soft robot for robotic sensing (**Figure 2.9**A) (*15*). GF of the hydrogel-based robotic skin increases from 2 to 6 within the whole large strain range (0~400%). Additionally, Tian et al. developed a strategy for the 3D Printing of Transparent and Conductive Hydrogel. With sub-millimeter printing resolution, resistance-based LiCl/PAAm hydrogel strain sensors can be printed for human-machine interaction and soft robotics applications (*209*). This 3D Printing technology may enhance the GF of resistive hydrogel strain sensors by accurately printing wavy-shape hydrogels to better monitor small strains such as vocal vibration.*Capacitance-based ionic hydrogel strain sensors:* Capacitance-based ionic hydrogel sensor is another common type of device for strain monitoring. The mechanism of capacitance-based pressure sensing has been introduced in the section *of*

Capacitance-based ionic hydrogel pressure sensors. Similarly, the parameters of the dielectric layers (length l, width w and thickness d) can be sensitive to the applied strain. Upon uniaxially stretching to λ times its original length, both the width and the thickness of the dielectric reduce by a factor $\sqrt{\lambda}$ due to incompressibility. As a result, the ratio of the capacitance of the stretched strain sensor (C) to that of the unstretched (C_0) is shown in **Eq.** 2.2:

$$C/C_0 = \{\varepsilon_0\varepsilon_r[(1+\lambda)l*(1-\sqrt{\lambda})w]/[(1-\sqrt{\lambda})d)]\}/[\varepsilon_0\varepsilon_r(l\cdot w/d)]=\lambda \qquad \textbf{Eq. } 2.2$$

Accordingly, the gauge factor (GF) of the capacitance-based ionic hydrogel strain sensors is

$$GF = \frac{C-C_0}{(\lambda-1)C_0} =1$$

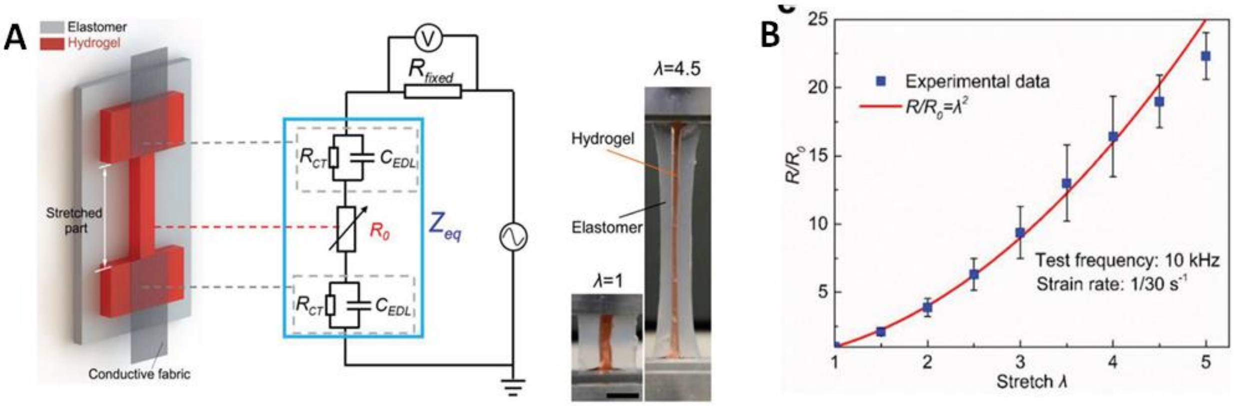

Figure 2.9. Resistance-based ionic hydrogel strain sensors. (A) Schematic of hydrogel strain sensing. (**B**). The change of resistance is stretched. Reprinted and adapted with permission from Ref. *(*15*)*.

The capacitance of capacitance-based ionic hydrogel strain sensors is increased linearly as the applied strain. Therefore, capacitance-based ionic hydrogel strain sensors have a better linearity than the resistance-based. In addition, capacitance-based has less hysteresis and is usually temperature independent (*13*). However, this linear regime is limited to a certain strain range because of the reducing permittivity of the dielectric at large strain (*213*). For example, the ionic skin developed by Sun et al. can monitor the strain change with maximum stretchability around 500% (*12*). At large stretches near rupture, the measured capacitance is slightly lower than that of the theoretical prediction (*12*). Therefore, capacitance-based ionic hydrogel strain sensors are not suitable for large strain sensing applications.

The above-mentioned stretchable capacitive or resistive based pressure sensors usually required an external power supply with comparable stretchability and flexibility, several recently developed hydrogel based soft ionic diodes could realize the self-powering strain sensing (*16*, *151*, *214*). For example, our group developed a hydrogel ionic diode with a stretchability of 400% which consists of a bilayer double-network hydrogel with positively- and negatively-charged polyelectrolytes (PSS and PDAC) in its two separate layers (*16*, *151*, *214*) By forming a depletion layer (or call ionic double layer) in the interface, the build-in potential can change according to any mechanical deformation (pressure, compressive strain and stretching strain)-induced geometry change and the re-diffusion of mobile ions within the depletion layer. Larger deformation results in a larger change of the built-in potential (*16*, *151*, *214*).

2.4.1.1.2. Hydrogel-based temperature sensor:

Temperature sensing is another critical functionality of human skin and plays a significant role for our human health. Several types of hydrogels are able to respond to the varying of temperature, including the commonly used thermoresponsive poly(N-isopropylacrylamide) (PNIPAM) hydrogels and other cross-linkable polymers such as N,N-dimethylacrylamide (DMAAm) and 2-(dimethyl maleimide)-N-ethyl-acrylamide (DMIAAm) (*215*). For example, the polymeric structure of PNIPAM switches between hydrophilic and hydrophobic status at the lower critical solution temperature (LCST, 30~35°C) (*216*), leading to the abrupt changes in the volume and shape of the polymeric hydrogels (*56*). This feature has been utilized for the design of adaptive microlenses (*46*) and smart windows (217).

However, traditional thermoresponsive hydrogels are generally electrically non-conductive, while conductive hydrogels are promising for more accurate and quantitative sensing applications. In addition, traditional thermoresponsive hydrogels usually do not consist of good mechanical performance due to their single-network structure. Therefore, Shi et al. recently introduced the conductive polymer hydrogels (PANI or PPy) into PNIPAM hydrogels through in situ formation of continuous network of conductive polymer hydrogels cross-linked by phytic acid in the PNIPAM matrix (**Figure 2.10**A) (*122*). This unique interpenetrating binary network structure empowers the hybrid hydrogels high electrical conductivity (0.84 ± 0.02 S/m), high thermoresponsive sensitivity (significant volume change as well as corresponding resistance change within 10 s) and enhanced mechanical properties. The significant and rapid electrical signal (e.g., resistance) change in a cooling-heating cycle (between 25 and 50 °C) of these hybrid hydrogels may find bioelectronic potential as wearable temperature sensors (*122*).

Alternatively, gold nanoparticles were decorated on PNIPAM to form raspberry-shaped plasmonic microgels that were thereafter embedded in stretchable PAAm hydrogels to construct a smart colorimetric thermometer patch **(Figure 2.10**B) (*217*). This as-fabricated hydrogel film achieved a fast (1 s) and efficient thermoresponsive colour change visualization with a temperature-sensing resolution of 0.2 °C **(**higher than that obtained for previous colorimetric temperature sensors based on plasmonic coupling**).** This thermoresponsive smart colorimetric patch enabled high sensitivity and repeatable temperature monitoring without external power source over a wider temperature range of 29–40 °C. By encapsulating the hydrogel film with polydimethylsiloxane (PDMS) film, it can be stretched film, it can be stretched by up to 90% without showing a colour change (*217*). This robust and sensitive yet stretch-insensitive smart colorimetric temperature sensing patch can be potentially applicable in smart, wearable sensors and soft robotics.

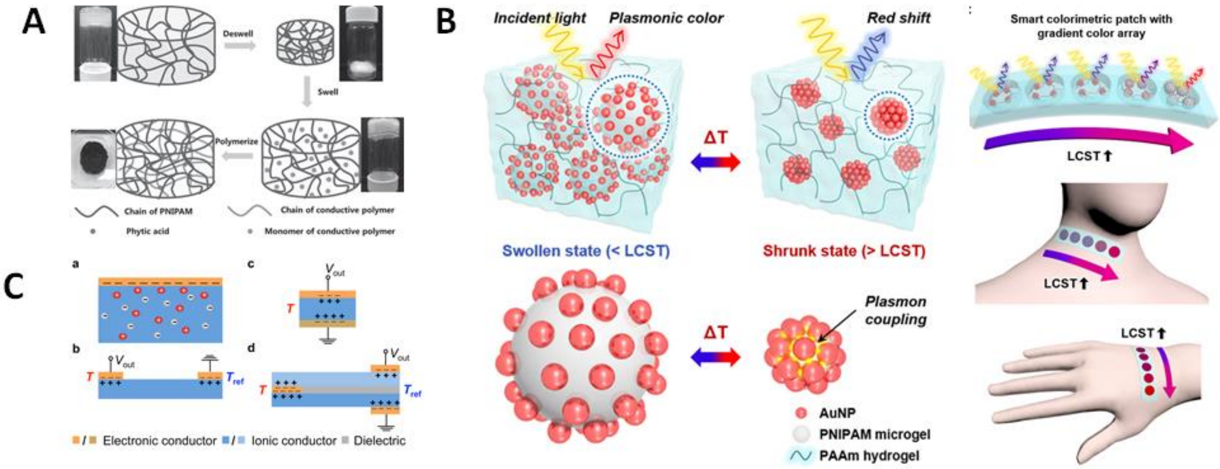

Figure 2.10. (A). Schematic illustration of synthesis process of hybrid hydrogel composed of PNIPAM and conductive polymers. Reprinted and adapted with permission from Ref. (122). **(B**). Schematic illustration of the plasmonic microgels in the PAAm hydrogel under swollen and shrunk states and Schemes of the sensor array patches attached to human skin at different positions (neck and hand). Reprinted and adapted with permission from Ref. (217). **(C**). Three principle of stretchable elastomeric thermocouple. Reprinted and adapted with permission from Ref. (218).

On the other hand, an ionic hydrogel conductor (NaCl-PAAm gel) was demonstrated as a novel soft, transparent and stretchable wearable temperature sensor (*218*). The voltage across the EDL at the electrode-hydrogel interface is sensitive to temperature. Therefore, based on three unique designs of electrode-hydrogel junctions **(Figure 2.10**C**)**, this hydrogel sensor can use the self-generated voltage difference according to the change of temperature. This temperature sensor shows a much higher sensitivity and faster thermal response than the traditional thermocouples. In addition, the generated voltage is only sensitive to temperature but insensitive to stretch (*218*). The mechanically stretchable yet stretch-insensitive temperature sensing ability enables this hydrogel thermocouple perfectly useful for the conformal temperature monitoring in applications such as healthcare and soft robots.

The measuring temperature of the above-mentioned hydrogel-based sensors mainly range from room temperature to 50 °C because common hydrogels are intrinsically volatile at high temperature and freeze at sub-zero temperature. In order to broaden their temperature sensing range to the extremely hot or cold environment, strategies such as adding glycerol, EG and $CaCl_2$ (*219*) or using nonvolatile PILs (*149*) are applicable.

2.4.1.2. Hydrogel wearable biochemical sensors

Wearable biochemical sensing has attracted academic and industrial attention for huge potential for healthcare analytics due to their portability, low cost, noninvasiveness, and ease of operation. Current biochemical sensors have already been demonstrated for personal health monitoring and fitness tracking by detecting various analytes including glucose, uric acid, lactate, ions level, stress level, humidity and PH (*220–222*). Hydrogel, as a biocompatible material, has been widely applied as a sensing material for those wearable and skin-attachable biochemical monitoring and point-of-care detection (*40*, *215*, *223*, *224*).

Hydrogel-based humid sensor

Humidity level is one of the most important indicators in our daily life. The moisture level of our skin contains substantial and valuable physiological and metabolic information. On the other hand, moisture monitoring of the wound site would also provide information on the healing state of the wound (*225*, *226*). Hydrogel as a biocompatible material is promising for the development of epidermal wearable and stretchable humidity sensors. In order to broaden the working range of ionic hydrogel humidity sensors, hygroscopic materials such EG and glycerol are usually incorporated into the hydrogel matrix to enhance its ambient stability. For example, our group developed an ambient-stable and stretchable ionic skin with humidity sensation (*16*). By incorporating EG, the hydrated double network can absorb, or release water based on the ambient humidity and won't dry out and can still be highly stretchable even in the extremely dried environment. Due to humidity-included geometric and ion concentration change, this diode-like stretchable hydrogel sensor can monitor the humidity change (13%-85%) by four electrical signals: resistance, capacitance, SCC and OCV, in which, the latter two are self-powering signals (*16*).

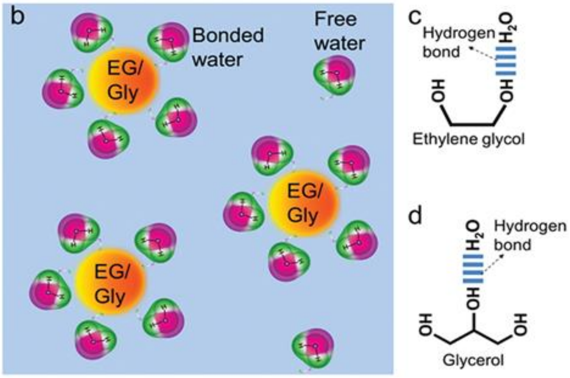

Figure 2.11. Schematics of hydrogel-based humid sensor due to hygroscopic EG/Gly molecules can adsorb water molecules via forming hydrogen bonds with them, improving both the water-holding and humidity sensing capabilities of the organohydrogels. Reprinted and adapted with permission from Ref. *(*227*)*.

In another demonstration, Wu et al., reported EG/glycerol (Gly) modified carrageenan/PAAm organohydrogels for humidity sensing (**Figure 2.11**) (*227*). Due to the ready formation of strong hydrogen bonds between H_2O molecules and enormous hydrophilic groups in the binary solvent and DN polymer chains, this extremely stretchable (1225% strain), self-healing and transparent ion conductive hydrogel displayed high humidity sensitivity with a wide humidity detection range (4–90%), stability, linearity and ultrafast response (0.27 s) and recovery (0.3 s) for human respiration monitoring (*227*). The family of hygroscopic-chemical-incorporated ionic hydrogels as new humidity responsive materials is promising for the emerging wearable applications.

Hydrogel-based glucose sensor

Metabolic molecules such as the glucose, lactate acid and uric acid level are several important indicators of human health condition. Therefore, the continuous sensing of these essential indicators is important for personal healthcare, diagnostics and exercise tracking. For example, diabetes-a chronic disease that often leads to severe secondary complications-affects over 425 million people around the world (*228*), therefore, the continuous real-time monitoring of glucose level of diabete patients is necessary. Currently, several epidermal wearable biosensors have been developed to noninvasive monitor the glucose level in sweat (*229*), tears (*230*, *231*), saliva (*232*, *233*), and interstitial fluid (ISF) (*222*, *234*). Among them, hydrogel as a biocompatible material has been utilized for the development of wearable glucose sensors (*230*, *235*). Currently, the mechanisms of hydrogel based glucose sensors are mainly based on electrochemical (*236–241*), optical (*242–246*), colorimetric (*247–249*), geometric (*250–254*), electrical (*255*, *256*). Some mechanisms such as geometric changes have been utilized to design the glucose-responsive wearable insulin patch for the regulation of blood glucose (*257–259*). Whereas its popularity for glucose biosensing, currently, hydrogels are mainly used as binding matrix of enzymes (e.g., glucose oxidase)-based electrochemical detection. The integration of ionic hydrogel for wearable glucose sensing is still largely lacking. In the future, the shape and structure change of ionic conductive hydrogels (e.g. doped with boronic acid) in responding to the various glucose levels as well as their corresponding change of electrical and optical parameters can be further taken advantage of for the designing of novel wearable hydrogel glucose sensors (*230*, *255*)**.**

Hydrogel-based PH sensor

PH is a significant physical indicator of human health. Any disturbances and variations in pH can be either the cause or effect of disease (e.g., cancer, wound healing and skin disorders) and dysfunction within a biological system (*260*). Therefore, the continuous sensing of this essential parameter is important for personal healthcare. Today, conductive polymers such as the polyaniline (PANI) have been widely used for PH sensing because of their high conductivity, stability, ion-exchanging ability and biocompatibility (*260–262*). On the other hand, hydrogel as a stimuli-responsive polymeric biomaterial can be used for PH sensing based on the change of geometric/optical/electrical/mechanical during volume swelling/shrinking at different PHs (*224*, *261*, *263–268*). Among various hydrogels, poly(acrylic acid) (PAA), an ionic hydrogel with the high density of carboxylic acids as well as the superior biocompatibility, perfect water absorptivity and good thin-film formability, has attracted remarkable interests for PH sensor design (*268*). Currently, PAA and its copolymerization with other hydrogels has been developed for PH sensing (*266*, *268–271*).

For instance, The poly(vinyl alcohol)-poly(acrylic acid) (PVA−PAA) hydrogel swell due to pH value changes, leading to the mechanical deformation of the attached metal plate and a corresponding change of capacitive or resistive signals (*266*). Richter et al. showed that swelling for a PVA−PAA-coated quartz crystal microbalance pH sensor had a short response time of 500 ms, a shrinking time of 800 ms, and sensitivity of 13.2 kHz/ pH, in the 3−10 pH range (*271*). In addition, PVA−PAA hydrogel usually is highly stretchable (*272*), which could be potentially applied as wearable and stretchable PH sensors although little has been reported so far.

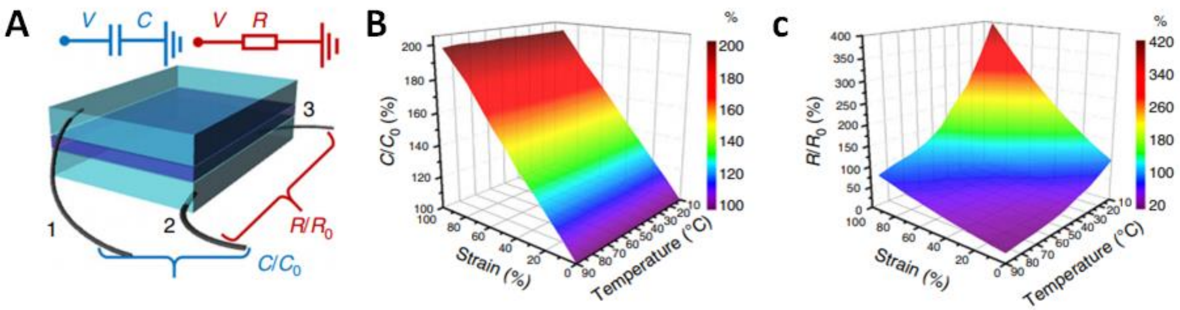

Figure 2.12. Strain and temperature sensations of the biomimetic skin. (A) Schematic design and two simplified equivalent electrical circuits of the biomimetic skin. (**B**). The capacitive response of the biomimetic skin upon mutual effect of strain and temperature. **(C)** The resistive response of the biomimetic skin upon mutual effect of strain and temperature. Reprinted and adapted with permission from Ref. (13).

2.4.1.3. Section conclusion

In this section, various skin-inspired hydrogel based wearable sensors have been reviewed. Biophysical stimuli sensing (e.g., pressure, strain, and temperature) as well as biochemical stimuli sensing (e.g., humidity, glucose and PH) were summarized here along with their sensing mechanisms and performance including sensitivity, linearity, range, hysteresis, resolution, response time etc. In addition, today's ionic hydrogel as electrodes or coating have also been applied for the measurement of electrophysiology signals such as ECG and EEG (*129*, *184*, *273*). On the other hand, human skin can perceive multiple environmental stimuli simultaneously with negligible mutual interference. This feature has inspired the development of many multifunctional/multiplexed wearable sensors for sensing strain, pressure, temperature, humidity, glucose, ions (*229*, *274–278*), including some ionic-hydrogel-based (*13*, *16*, *279*). Ionic hydrogel is a polymeric biomaterial that can simultaneously respond to multiple stimuli such as PH, ions, strain, pressure, temperature, humidity (*40*), which is a potential drawback for the application of multiplexed sensing. To decouple those multiple interferences, there have been several strategies developed. For example, the previously-mentioned stretchable and wearable colorimetric patches can decouple temperature from strain using simple color signals (*217*). Also, different electrical signals have different degrees of correlation with those external stimuli. Our previous ionic diode based artificial skin found that the resistance and SCCD signals show more obvious changing trends with the RH change than the capacitance and OCV signals in the full RH range; the OCV outputs showed little correlation with the RH change, the SCCD mode is more suitable for humidity sensing (*16*). In addition, to better decouple multiple interference, integrating multiple pieces of sensor on one patch through microfabrication and 3-D printing technologies as well elastomer encapsulation on strain sensor could reduce the coupling effect between strain and humidity (*16*). In a recent literature, Lei et al. developed a type of biomimetic iontronics to imitate natural skins using supramolecular polyelectrolyte hydrogels with multiple sensory capabilities (**Figure 2.12)** (*13*)**.** The sandwiched configuration between two ionic–conductive hydrogel layers and a VHB dielectric are connected with three metal electrodes, in which a parallel-plate capacitive sensor (between electrodes 1 and 2) and an ionic resistive sensor (between electrodes 2 and 3) were formed to mimic different stimuli-receptors in natural skins**.** The parallel-plate capacitance is insensitive to temperature variations and is increased linearly with the tensile strain; while resistive signals are both thermal-sensitive and strain-sensitive. Consequently, in a complex environment with both strain and temperature stimuli, the capacitive sensor (“mechanoreceptor”) can distinguish the strain stimuli and meanwhile the temperature variation can be derived from the resistive hyperplane (*13*). This work promotes the development of biomimetic skins with sophisticated intelligence similar to natural skins.

2.4.2. Ionic hydrogel integrated soft robotics

Soft robots, the nature-inspired machines, are a type of robots that can deform and actuate continuously. As a complement to the rigid-bodied robots used extensively in manufacturing , soft robots have been developed to bridge the gap between the hard machines and soft humans due to their unprecedented adaptability to unstructured environments (*280*). Constructed from intrinsically soft and/or stretchable materials, soft robots hold great potential for many application scenarios, including human-machine interaction, safely manipulation (e.g., grasping fragile objects), navigation in space-restricted, rough and/or harsh environments with good resilience, and human rehabilitation and assistance (*23*, *280*, *281*). Currently, soft materials such as silicone rubbers, Ecoflex, PDMS, VHB, paper and their combinations have been used for the design of traditional soft robotic bodies (*24*, *281–285*).

Today**,** hydrogels as biocompatible and biodegradable materials have gained much attention for the designing of soft robots on biomedical applications (*31*, *40*, *215*). Through a facile modification of hydrogels with other functional groups/additives/nanofillers, hydrogel based soft robots can response (e.g., change shapes and/or structures) to the external stimuli including heat, light, pH, humidity, electrical fields, ions, magnetic signals, biomolecules, and their combinations, and passive driven force such as pneumatic and hydraulic pressure (*257*, *265*, *286–295*). Readers can refer to several previous review papers for more information (*40*, *296*, *297*). On the other hand, ionic conductive hydrogels that can respond to stimuli including electrical fields and mechanical deformation have been integrated into soft bodies of traditional soft robotics as robotic sensing skins and/or as solid electrolytes of soft dielectric actuators.

2.4.2.1. Robotic skins based on ionic hydrogel

Stretchable artificial skins capable of physical and chemical sensation are critical for human-like robots and smart rehabilitative devices. Due to the combination of highly optical transparency, electrical conductivity and mechanical stretchability, ionic hydrogel is a good candidate for robotic skins.

For example, inspired from octopuses that have a combination of a stretchable skin and color-tuning organs to control both posture and color for visual communication and disguise, Larson et al. presented a hyperplastic light emitting capacitor (HLEC) skin (*24*). By sandwiching a dielectric Ecoflex layer doped with electroluminescent ZnS phosphors between two ionic hydrogel (LiCl-PAAm) electrodes, the whole setup was encapsulated between two layers of Ecoflex film to form the HLEC skin (**Figure 2.13**). This artificial skin can change illuminance and capacitance simultaneously under deformation (stretches to >480% strain). Arrays of individually controllable pixels in thin rubber sheets were fabricated using replica molding and were subjected to stretching, folding, and rolling to demonstrate their use as stretchable displays with spatial resolution. After integrating into a soft robot, the HLEC skin provides robots with the ability to sense their actuated state, sense the environmental pressure and communicate optically (**Figure 2.13**) (*24*). Thereafter, organic liquid crystal devices and luminescent devices were developed based on ionic hydrogel by taking advantage of its optical transparency (*298, 299*).

While the previous fabrication strategies were mainly used for empowering soft robotics with single sensing capability, those are not suitable for the next-generation soft robots that require multiplex skin-like somatosensory feedback to realize their full potential due to the higher complexity. Truby et. al. recently used embedded 3D printing technology to print conductive ionogel soft sensors into a soft robotic finger (*300*). By embedding multiple sensor networks, this soft robotic finger consists of haptic, proprioceptive, and thermoreceptive sensing capabilities **(Figure 2.14**). This approach is promising for soft robotic, wearable, and haptic devices requiring embedded soft sensing for closed-loop and machine learning based control (*300*). IL-based ionogel sensors can endow soft robots with sensing capability at subzero temperature (*149*). Furthermore, by endowing a strong adhesion of ionic hydrogel to the elastomeric soft robotic body, the soft robots can potentially sense a larger strain and bending angle (*15*).

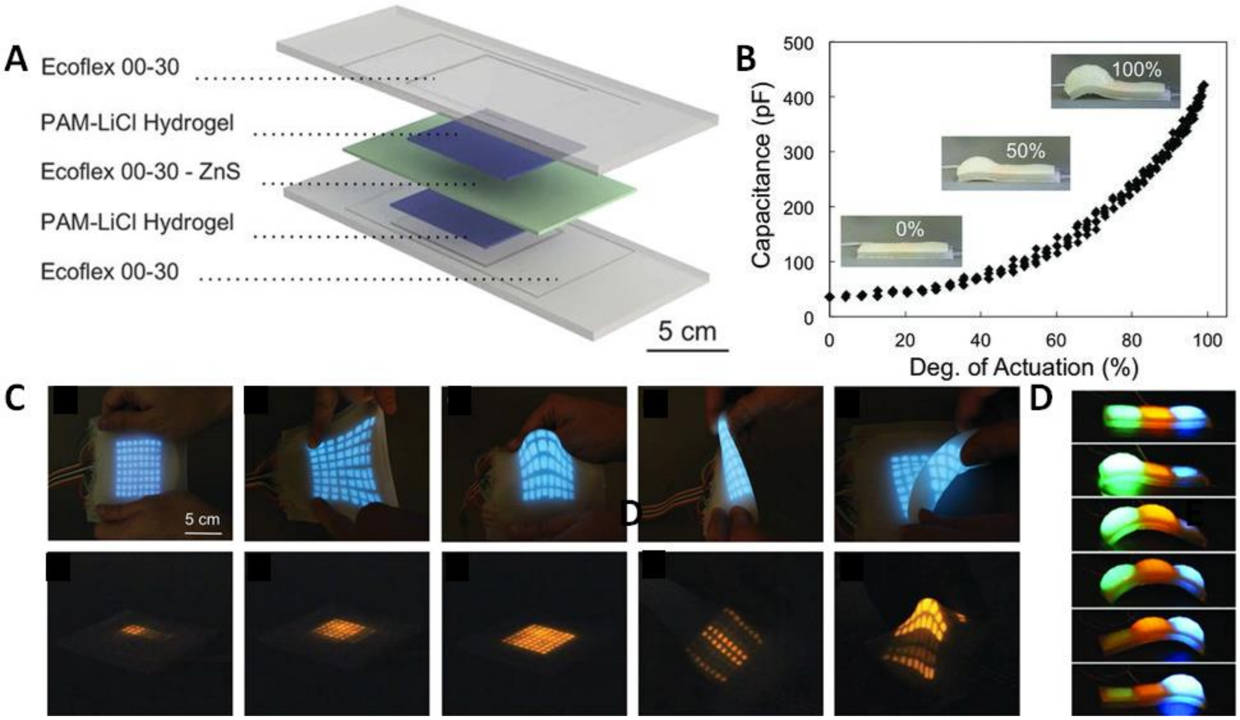

Figure 2.13. Highly stretchable electroluminescent skin for optical signaling and tactile sensing. (**A**). Schematic illustrations (**B**). Capacitance plotted versus the actuation amplitude. (C). Multipixel electroluminescent displays. (**D**). A soft crawler under undulating gait and outer

electroluminescent skin is stretched with the luminescence increasing. Reprinted and adapted with permission from Ref. *(*24*)*.

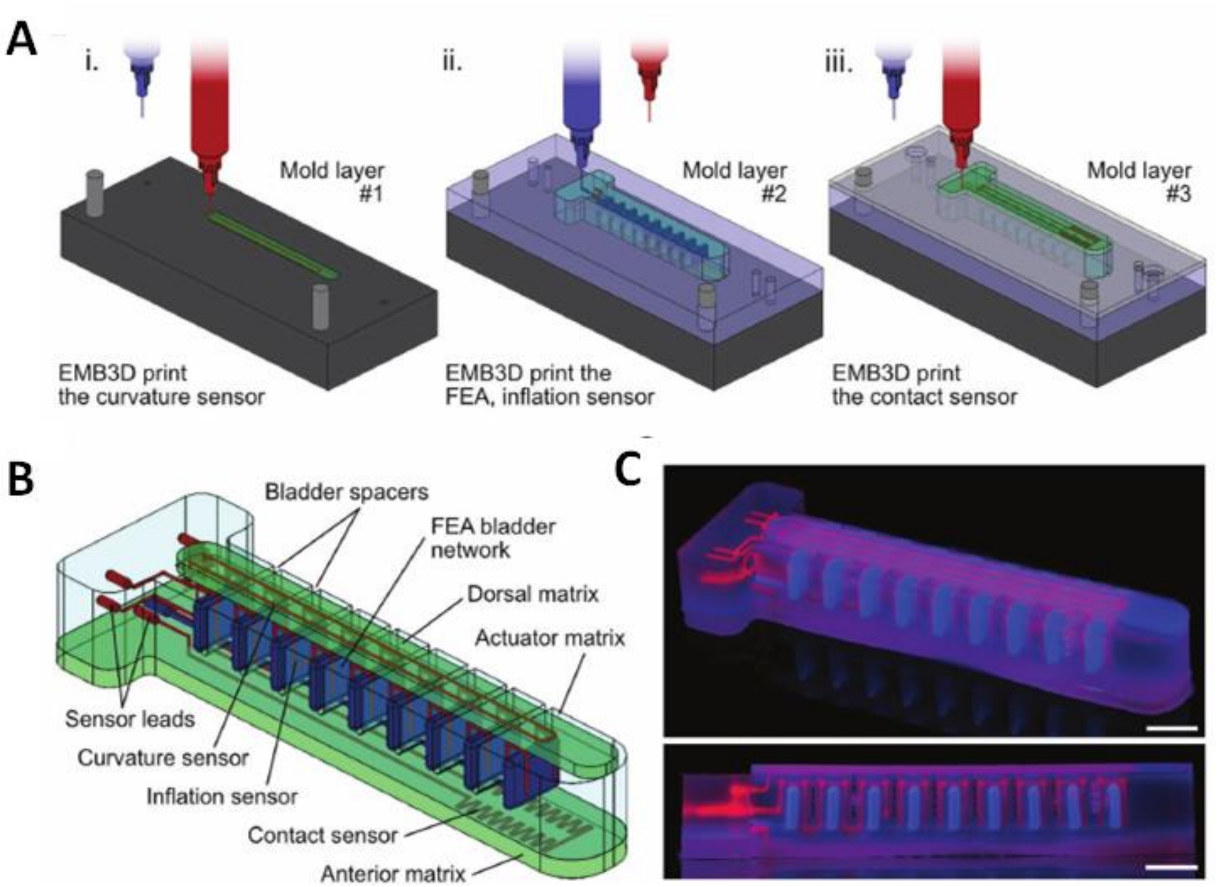

Figure 2.14. Fabrication of soft somatosensitive actuator (SSA) innervated with multiple soft sensors. (A) 3D printing of the curvature sensor, the inflation sensor and the contact sensor within the SSA. (**B**) Schematic illustrations and (**C**) images of the final SSA. Reprinted and adapted with permission from Ref. (300).

2.4.2.2. Ionic hydrogel based stretchable electrodes for soft actuators

Electrically powered muscle-mimetic actuators [e.g., dielectric elastomer actuator (DEA)] that offer high actuation strain (>100%) and potentially high efficiency (80%) and are self-sensing (*301*) have undergone substantial development to enable a broad range of applications, including soft robots prosthetic devices (*31*). Within the DEA structure, stretchable conductors are needed to realize the electromechanical transduction. Currently, many stretchable conductors exist, including carbon grease, serpentine-shaped metallic wires, carbon nanotubes, graphene sheets, silver nanowires and liquid metals, and saline solutions. However, these conductors are limited by their optical transparency, maximum stretchability, or liquid status, which will potentially hinder the further broader applications of DEA.

Whereas, ionic hydrogel as a transparent, solid, highly stretchable and conductive material showed great potential for DEA. For example, Keplinger et. al. built a transparent, high-speed, large-strain soft actuator enabled by sandwiched a layer of dielectric elastomer between two layers of highly stretchable and fully transparent ionic hydrogel (NaCl-PAAm). Due to the short response time (10^{-3} s) of free ions in ionic hydrogels in response to external electric fields (*40*), and the large capacitance within the hydrogel-electrode electrical double layer, this assembled hydrogel-elastomer-hydrogel DEA is capable of operation at frequencies beyond 10 kilohertz and voltages above 10 kilovolts. When a high voltage (e.g. 10 kV) is applied between the hydrogel ionic conductors, the main voltage drop is across the dielectric on the order of ~ 10 kV, leading to a large amount of ions of different charge polarities collecting on the two surfaces of the dielectric elastomer. The electrical attraction between the oppositely charged ions can reduce the thickness and increase the area of dielectric, leading to the electromechanical transduction (*114*). In addition, the electromechanical transduction is achieved without electrochemical reaction between the metal electrodes and hydrogels due to small voltage drop (< 1V) across the electrical double layer (**Figure 2.15**).

Similarly, an ionically conductive hydrogel (LiCl-PAAm) served as an electrode sandwiched between two dielectric elastomers to fabricate the fins of a soft fish. When a voltage was applied between the encapsulated hydrogel conductor and the surrounding tap water, opposite charges accumulated on either side of the dielectric elastomer, inducing Maxwell stress that deformed the soft fin to a lower-curvature structure. This design enabled the fish body and fins flapped between the actuated and the rest states, leading to the exceptionally fast propulsion motions of a soft fish robot with swimming speed of 6.4 cm/s (i.e. 0.69 body length per second) (*285*).

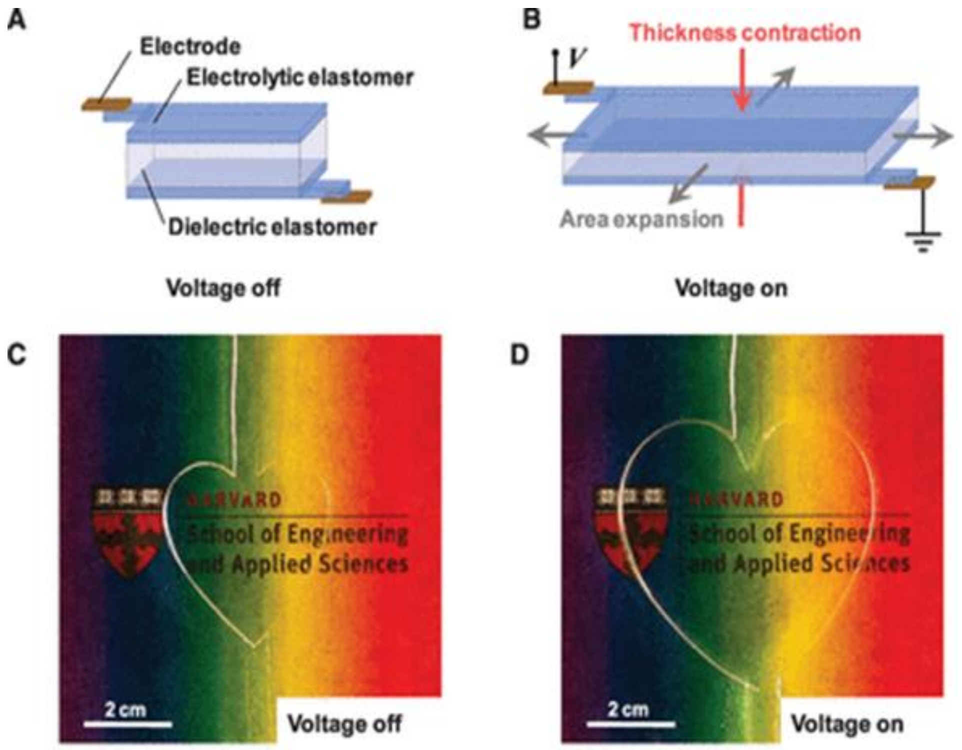

Figure 2.15. **Ionic hydrogel integrated stretchable electrodes for soft actuators.** A dielectric elastomer is sandwiched between two layers of an electrolytic elastomer (**A**) before and (**B**) after subject to voltage. The actuator is transparent **(C**) before and (**D**) after subject to voltage. Reprinted and adapted with permission from Ref. (114).

2.4.3. Hydrogel-based energy harvesting

The rapid growth of wearable electronics and soft robotics relies on power sources that are mechanically flexible, stretchable and even biocompatible. So far, flexible energy storage devices [e.g., supercapacitors (*302–304*) and batteries (*304*, *305*)] have been developed to reduce the constraint on our human body and the soft robotic body. On the other side, energy harvesting devices such as solar cells and nanogenerators have been made into flexible types in the past decade (*306–309*). In particular, recently developed triboelectric nanogenerator (TENG), by converting mechanical energy into electricity based on the coupling effect of contact electrification and electrostatic induction, has gained tremendous attention due to the advantages of high voltage output, simple structure, easy availability, environmental friendliness, and low costs (*310–313*). Recently, several stretchable TENGs have been reported based on the conductive materials including carbon nanotubes, graphene, carbon paste, silver nanowires (*314–318*) and more recently ionic hydrogel (*115*).

Due to the water-based yet solid, soft, stretchable, transparent and biocompatible features of hydrogel, ionic-hydrogel-based TENG can enable many potential applications for soft robotics and wearable biomedicals. For example, in 2017, Wang et al. the first time reported a soft skin-like TENG (STENG) for both biomechanical energy harvesting and tactile sensing by hybridizing elastomer and ionic hydrogel as the electrification layer and electrode, respectively. With ultrahigh stretchability (1160%) and transparency (96.2%), this STENG achieved an instantaneous peak power density of 35 mW/m^{-2} (**Figure 2.16**) (*115*). Thereafter, Wang et al. further enhanced the bonding between the conductive hydrogel and electrification elastomer by the interface modification with benzophenone (BP) upon ultraviolet (UV) irradiation. With better mechanical reliability, the novel STENG achieved a significantly reduced dehydration rate compared with the unmodified STENG, enabling its potential application in harsh environments (*192*). In addition, other important features such as self-healing and anti-contamination have been further realized on hydrogel-based TENG to open up new opportunities for applications including human-machine interaction, health monitoring, wearable and implantable electronics, and smart robotics (*182*, *183*).

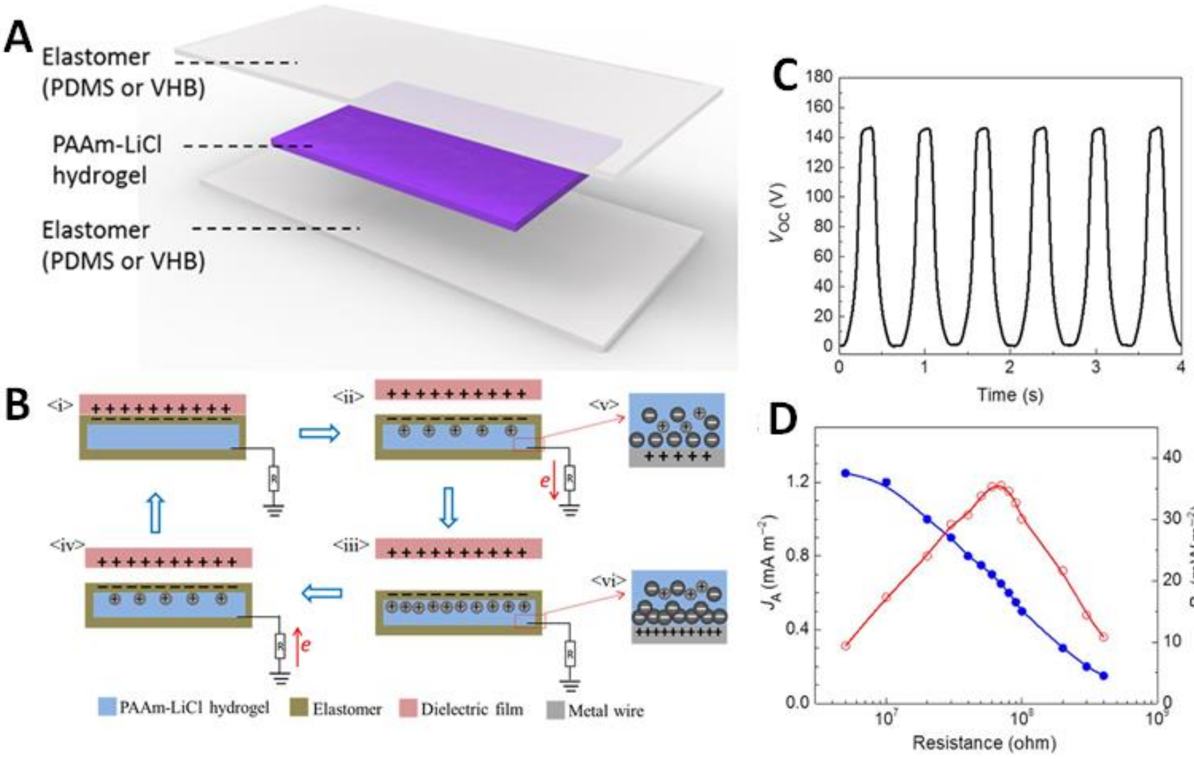

Figure 2.16. Biomechanical energy harvesting by the STENG. (A) Scheme of the STENG with sandwich structure. ((**B**) the working mechanism of the STENG. (**C**) OCV of a PDMS-STENG. (**D**) Variation of the output current density and power density with the external loading resistance. Reprinted and adapted with permission from Ref. *(115)***.**

Later on, several novel materials such as PILs and ionogels were utilized as the conductive gels for TENG as well. The as-fabricated devices consist of practically useful features such as ambient stable, and anti-freezing capability and can realize mechanical energy harvesting over a wide temperature range due to the intrinsically nonvolatile performance of ionic liquids (*149*, *150*, *319*). Those novel stretchable TENGs could broad their soft robotic and wearable applications under the harsh environment.

TENG has been demonstrated for harvesting various mechanical energies with effective frequency typically at >10 Hz (*16*). However, their performance in the low frequency range (e.g. less than 1 Hz of human motions) decay dramatically (*119*). Alternatively, a recently developed hydrogel ionic diode has been proved to harvest low frequency mechanical energy with a high output current of 13.5 μA/cm^2. Further stacking five units with parallel structure, the hydrogel diode device can generate an output current of 64.3 μA/cm^2 and power density of 0.48 μW/cm^2 (*119*). While the previous hydrogel-based ionic diodes are usually not stretchable (*117*, *119*), and sometimes not transparent (*119*, *214*), our group recently for the first time demonstrated a novel artificial ionic skin (AIskin) with high toughness, stretchability, ambient stability and transparency. The AIskin consists of a bilayer double-network hydrogel with hygroscopic substances and positively- and negatively-charged polyelectrolytes (PSS and PDAC) in its two separate layers. Due to its excellent mechanical performance (e.g. stretchability: 400%; fracture toughness: 1826 J/m^2), the AIskin can reach an energy output per stimulus at 3200 μJ/m^2 and generate a peak output current of 128 μA/cm^2 at the low frequency (0.02-0.5 Hz) (*16*).

Again, two layers of liquid-free PILs with oppositely charged mobile ionic species can form a diode-like junction, yielding an ionic double layer. Similarly, the deformable ionic diode junctions enabled the transduction of mechanical movements into electrical signals for sensing and energy harvesting while showing good ambient stability (*151*).

2.5. Conclusion

Hydrogels represent an important class of materials possessing a watery environment and broadly tunable physicochemical properties. Efforts devoted to engineering hydrogel devices with skin-like enhanced properties have expanded their opportunities in numerous applications, including biomedical wearables, soft electronics, sensors, and actuators. Over the past decade, substantial progress has been made to develop hydrogels with high mechanical toughness, stretchability and/or conductivity. In addition, designing of nature-inspired hydrogel systems with enhanced merits (e.g., anti-dehydration, anti-freezing and bio-adhesion) for better real-world practical usage have been reviewed here.

Despite the promising progress of the applications for wearables, soft robotics and beyond, hydrogel skin-like development is still in its infancy, several challenges still need to be addressed. As issues like limited functionality, low stability, and high-power consumption and poor adhesive still hinder the further development of hydrogel iontronics, which could be addressed in my thesis to empower hydrogel ionotronic more practicality.

2.6. Reference

1. Y. Sun, W. M. Choi, H. Jiang, Y. Y. Huang, J. A. Rogers, Controlled buckling of semiconductor nanoribbons for stretchable electronics. Nature Nanotechnology. 1 (2006), pp. 201–207.
2. D.-H. Kim, N. Lu, R. Ma, Y.-S. Kim, R.-H. Kim, S. Wang, J. Wu, S. M. Won, H. Tao, A. Islam, K. J. Yu, T.-I. Kim, R. Chowdhury, M. Ying, L. Xu, M. Li, H.-J. Chung, H. Keum, M. McCormick, P. Liu, Y.-W. Zhang, F. G. Omenetto, Y. Huang, T. Coleman, J. A. Rogers, Epidermal Electronics. Science. 333 (2011), pp. 838–843.
3. D.-H. Kim, N. Lu, R. Ghaffari, Y.-S. Kim, S. P. Lee, L. Xu, J. Wu, R.-H. Kim, J. Song, Z. Liu, J. Viventi, B. de Graff, B. Elolampi, M. Mansour, M. J. Slepian, S. Hwang, J. D. Moss, S.-M. Won, Y. Huang, B. Litt, J. A. Rogers, Materials for multifunctional balloon catheters with capabilities in cardiac electrophysiological mapping and ablation therapy. Nature Materials. 10 (2011), pp. 316–323.
4. T. Sekitani, H. Nakajima, H. Maeda, T. Fukushima, T. Aida, K. Hata, T. Someya, Stretchable active-matrix organic light-emitting diode display using printable elastic conductors. Nature Materials. 8 (2009), pp. 494–499.
5. T. Sekitani, Y. Noguchi, K. Hata, T. Fukushima, T. Aida, T. Someya, A Rubberlike Stretchable Active Matrix Using Elastic Conductors. Science. 321 (2008), pp. 1468–1472.

6. S. J. Benight, C. Wang, J. B. H. Tok, Z. Bao, Stretchable and self-healing polymers and devices for electronic skin. Progress in Polymer Science. 38 (2013), pp. 1961–1977.
7. J. Y. Oh, S. Rondeau-Gagné, Y.-C. Chiu, A. Chortos, F. Lissel, G.-J. N. Wang, B. C. Schroeder, T. Kurosawa, J. Lopez, T. Katsumata, J. Xu, C. Zhu, X. Gu, W.-G. Bae, Y. Kim, L. Jin, J. W. Chung, J. B. -H. Tok, Z. Bao, Intrinsically stretchable and healable semiconducting polymer for organic transistors. Nature. 539 (2016), pp. 411–415.
8. R. Pelrine, R. Kornbluh, J. Joseph, R. Heydt, Q. Pei, S. Chiba, High-field deformation of elastomeric dielectrics for actuators. Materials Science and Engineering: C. 11 (2000), pp. 89–100.
9. J. Zang, S. Ryu, N. Pugno, Q. Wang, Q. Tu, M. J. Buehler, X. Zhao, Multifunctionality and control of the crumpling and unfolding of large-area graphene. Nature Materials. 12 (2013), pp. 321–325.
10. D. J. Lipomi, M. Vosgueritchian, B. C.-K. Tee, S. L. Hellstrom, J. A. Lee, C. H. Fox, Z. Bao, Skin-like pressure and strain sensors based on transparent elastic films of carbon nanotubes. Nature Nanotechnology. 6 (2011), pp. 788–792.
11. J. Liang, L. Li, X. Niu, Z. Yu, Q. Pei, Elastomeric polymer light-emitting devices and displays. Nature Photonics. 7 (2013), pp. 817–824.
12. J.-Y. Sun, C. Keplinger, G. M. Whitesides, Z. Suo, Ionic skin. Advanced Materials. 26 (2014), pp. 7608–7614.
13. Z. Lei, P. Wu, A supramolecular biomimetic skin combining a wide spectrum of mechanical properties and multiple sensory capabilities. Nature Communications. 9 (2018), , doi:10.1038/s41467-018-03456-w.
14. C.-C. Kim, H.-H. Lee, K. H. Oh, J.-Y. Sun, Highly stretchable, transparent ionic touch panel. Science. 353, 682–687 (2016).
15. S. Cheng, Y. S. Narang, C. Yang, Z. Suo, R. D. Howe, Stick-On Large-Strain Sensors for Soft Robots. Advanced Materials Interfaces. 6 (2019), p. 1900985.
16. B. Ying, Q. Wu, J. Li, X. Liu, An ambient-stable and stretchable ionic skin with multimodal sensation. Materials Horizons. 7 (2020), pp. 477–488.
17. T. Q. Trung, N.-E. Lee, Flexible and Stretchable Physical Sensor Integrated Platforms for Wearable Human-Activity Monitoringand Personal Healthcare. Advanced Materials. 28 (2016), pp. 4338–4372.
18. C. Xu, Y. Yang, W. Gao, Skin-interfaced sensors in digital medicine: from materials to applications. Matter. 2, 1414–1445 (2020).
19. Y. Yu, H. Y. Y. Nyein, W. Gao, A. Javey, Flexible Electrochemical Bioelectronics: The Rise of In Situ Bioanalysis. Adv. Mater. 32, e1902083 (2020).
20. J. Wang, M.-F. Lin, S. Park, P. S. Lee, Deformable conductors for human–machine interface. Materials Today. 21 (2018), pp. 508–526.
21. H. Zhao, K. O'Brien, S. Li, R. F. Shepherd, Optoelectronically innervated soft prosthetic hand via stretchable optical waveguides. Science Robotics. 1 (2016), p. eaai7529.
22. Y. Mengüç, Y.-L. Park, H. Pei, D. Vogt, P. M. Aubin, E. Winchell, L. Fluke, L. Stirling, R. J. Wood, C. J. Walsh, Wearable soft sensing suit for human gait measurement. The International Journal of Robotics Research. 33 (2014), pp. 1748–1764.
23. B. Shih, D. Shah, J. Li, T. G. Thuruthel, Y.-L. Park, F. Iida, Z. Bao, R. Kramer-Bottiglio, M. T. Tolley, Electronic skins and machine learning for intelligent soft robots. Science Robotics. 5 (2020), p. eaaz9239.

24. C. Larson, B. Peele, S. Li, S. Robinson, M. Totaro, L. Beccai, B. Mazzolai, R. Shepherd, Highly stretchable electroluminescent skin for optical signaling and tactile sensing. Science. 351, 1071–1074 (2016).
25. J. W. Booth, D. Shah, J. C. Case, E. L. White, M. C. Yuen, O. Cyr-Choiniere, R. Kramer-Bottiglio, OmniSkins: Robotic skins that turn inanimate objects into multifunctional robots. Science Robotics. 3 (2018), p. eaat1853.
26. S. Y. Kim, Y. Choo, R. Adam Bilodeau, M. C. Yuen, G. Kaufman, D. S. Shah, C. O. Osuji, R. Kramer-Bottiglio, Sustainable manufacturing of sensors onto soft systems using self-coagulating conductive Pickering emulsions. Science Robotics. 5 (2020), p. eaay3604.
27. T. G. Thuruthel, B. Shih, C. Laschi, M. T. Tolley, Soft robot perception using embedded soft sensors and recurrent neural networks. Science Robotics. 4 (2019), p. eaav1488.
28. K. B. Justus, T. Hellebrekers, D. D. Lewis, A. Wood, C. Ingham, C. Majidi, P. R. LeDuc, C. Tan, A biosensing soft robot: Autonomous parsing of chemical signals through integrated organic and inorganic interfaces. Science Robotics. 4 (2019), p. eaax0765.
29. H. Sheng, X. Wang, N. Kong, W. Xi, H. Yang, X. Wu, K. Wu, C. Li, J. Hu, J. Tang, J. Zhou, S. Duan, H. Wang, Z. Suo, Neural interfaces by hydrogels. Extreme Mechanics Letters. 30 (2019), p. 100510.
30. H.-R. Lee, C.-C. Kim, J.-Y. Sun, Stretchable Ionics - A Promising Candidate for Upcoming Wearable Devices. Adv. Mater. 30, e1704403 (2018).
31. C. Yang, Z. Suo, Hydrogel ionotronics. Nature Reviews Materials. 3 (2018), pp. 125–142.
32. J. Ge, L. Sun, F.-R. Zhang, Y. Zhang, L.-A. Shi, H.-Y. Zhao, H.-W. Zhu, H.-L. Jiang, S.-H. Yu, A Stretchable Electronic Fabric Artificial Skin with Pressure-, Lateral Strain-, and Flexion-Sensitive Properties. Advanced Materials. 28 (2016), pp. 722–728.
33. J. P. Gong, Why are double network hydrogels so tough? Soft Matter. 6 (2010), p. 2583.
34. C. W. Peak, J. J. Wilker, G. Schmidt, A review on tough and sticky hydrogels. Colloid and Polymer Science. 291 (2013), pp. 2031–2047.
35. Q. Chen, H. Chen, L. Zhu, J. Zheng, Fundamentals of double network hydrogels. J. Mater. Chem. B Mater. Biol. Med. 3, 3654–3676 (2015).
36. X. Zhao, Multi-scale multi-mechanism design of tough hydrogels: building dissipation into stretchy networks. Soft Matter. 10, 672–687 (2014).
37. D. Zhou, F. Chen, S. Handschuh-Wang, T. Gan, X. Zhou, X. Zhou, Biomimetic Extreme-Temperature- and Environment-Adaptable Hydrogels. ChemPhysChem. 20 (2019), pp. 2139–2154.
38. J. Yang, R. Bai, B. Chen, Z. Suo, Hydrogel Adhesion: A Supramolecular Synergy of Chemistry, Topology, and Mechanics. Adv. Funct. Mater. 30, 1901693 (2020).
39. H. Yuk, B. Lu, X. Zhao, Hydrogel bioelectronics. Chem. Soc. Rev. 48, 1642–1667 (2019).
40. Hydrogel machines. Mater. Today (2020), doi:10.1016/j.mattod.2019.12.026.
41. H. Fan, J. P. Gong, Fabrication of Bioinspired Hydrogels: Challenges and Opportunities. Macromolecules (2020), , doi:10.1021/acs.macromol.0c00238.
42. S. McGurk, Junqueira’s Basic Histology Text and Atlas – 13th edition Mescher Anthony L Junqueira’s Basic Histology Text and Atlas – 13th edition 544pp CD-ROM £45.99 McGraw-Hill Professional 978 1 2590 7232 1 1259072320. Nursing Standard. 28 (2013), pp. 34–34.
43. O. Wichterle, D. Lím, Hydrophilic Gels for Biological Use. Nature. 185 (1960), pp. 117–118.

44. Y. S. Zhang, A. Khademhosseini, Advances in engineering hydrogels. Science. 356 (2017), p. eaaf3627.
45. J. L. Drury, D. J. Mooney, Hydrogels for tissue engineering: scaffold design variables and applications. Biomaterials. 24, 4337–4351 (2003).
46. L. Dong, A. K. Agarwal, D. J. Beebe, H. Jiang, Adaptive liquid microlenses activated by stimuli-responsive hydrogels. Nature. 442 (2006), pp. 551–554.
47. J. Kopeček, HYDROGELS FROM SOFT CONTACT LENSES AND IMPLANTS TO SELF-ASSEMBLED NANOMATERIALS. J. Polym. Sci. A Polym. Chem. 47, 5929–5946 (2009).
48. T. Hakkarainen, R. Koivuniemi, M. Kosonen, C. Escobedo-Lucea, A. Sanz-Garcia, J. Vuola, J. Valtonen, P. Tammela, A. Mäkitie, K. Luukko, M. Yliperttula, H. Kavola, Nanofibrillar cellulose wound dressing in skin graft donor site treatment. J. Control. Release. 244, 292–301 (2016).
49. N. A. Peppas, E. W. Merrill, Development of semicrystalline poly(vinyl alcohol) hydrogels for biomedical applications. J. Biomed. Mater. Res. 11, 423–434 (1977).
50. K. Y. Lee, D. J. Mooney, Hydrogels for Tissue Engineering. Chemical Reviews. 101 (2001), pp. 1869–1880.
51. J. P. Gong, N. Hirota, A. Kakugo, T. Narita, Y. Osada, Effect of Aspect Ratio on Protein Diffusion in Hydrogels. The Journal of Physical Chemistry B. 104 (2000), pp. 9904–9908.
52. Y. Osada, M. Hasebe, ELECTRICALLY ACTIVATED MECHANOCHEMICAL DEVICES USING POLYELECTROLYTE GELS. Chemistry Letters. 14 (1985), pp. 1285–1288.
53. T. Tanaka, E. Sato, Y. Hirokawa, S. Hirotsu, J. Peetermans, Critical Kinetics of Volume Phase Transition of Gels. Physical Review Letters. 55 (1985), pp. 2455–2458.
54. Y. Osada, H. Okuzaki, H. Hori, A polymer gel with electrically driven motility. Nature. 355 (1992), pp. 242–244.
55. T. Hirai, H. Nemoto, T. Suzuki, S. Hayashi, M. Hirai, Actuation of Poly(vinyl alcohol) Gel by Electric Field. Journal of Intelligent Material Systems and Structures. 4 (1993), pp. 277–279.
56. R. Yoshida, K. Uchida, Y. Kaneko, K. Sakai, A. Kikuchi, Y. Sakurai, T. Okano, Comb-type grafted hydrogels with rapid deswelling response to temperature changes. Nature. 374 (1995), pp. 240–242.
57. N. A. Peppas, J. Z. Hilt, A. Khademhosseini, R. Langer, Hydrogels in Biology and Medicine: From Molecular Principles to Bionanotechnology. Advanced Materials. 18 (2006), pp. 1345–1360.
58. Y. Osada, J.-P. Gong, Soft and Wet Materials: Polymer Gels. Advanced Materials. 10 (1998), pp. 827–837.
59. J. P. Gong, Friction and lubrication of hydrogels—its richness and complexity. Soft Matter. 2 (2006), pp. 544–552.
60. P. Calvert, Gel Sensors and Actuators. MRS Bulletin. 33 (2008), pp. 207–212.
61. P. Calvert, Hydrogels for Soft Machines. Advanced Materials. 21 (2009), pp. 743–756.
62. J. P. Gong, Materials science. Materials both tough and soft. Science. 344 (2014), pp. 161–162.
63. N. A. Peppas, E. W. Merrill, Determination of interaction parameter $\chi 1$, for poly(vinyl alcohol) and water in gels crosslinked from solutions. Journal of Polymer Science: Polymer Chemistry Edition. 14 (1976), pp. 459–464.

64. Y. Okumura, K. Ito, The Polyrotaxane Gel: A Topological Gel by Figure-of-Eight Cross-links. Advanced Materials. 13 (2001), pp. 485–487.
65. K. Ito, Novel Cross-Linking Concept of Polymer Network: Synthesis, Structure, and Properties of Slide-Ring Gels with Freely Movable Junctions. Polymer Journal. 39 (2007), pp. 489–499.
66. K. Ito, Slide-ring materials using topological supramolecular architecture. Current Opinion in Solid State and Materials Science. 14 (2010), pp. 28–34.
67. G. Fleury, G. Schlatter, C. Brochon, C. Travelet, A. Lapp, P. Lindner, G. Hadziioannou, Topological Polymer Networks with Sliding Cross-Link Points: The “Sliding Gels”. Relationship between Their Molecular Structure and the Viscoelastic as Well as the Swelling Properties. Macromolecules. 40 (2007), pp. 535–543.
68. K. Haraguchi, T. Takehisa, Nanocomposite Hydrogels: A Unique Organic–Inorganic Network Structure with Extraordinary Mechanical, Optical, and Swelling/De-swelling Properties. Advanced Materials. 14 (2002), p. 1120.
69. K. Haraguchi, H.-J. Li, Control of the Coil-to-Globule Transition and Ultrahigh Mechanical Properties of PNIPA in Nanocomposite Hydrogels. Angewandte Chemie International Edition. 44 (2005), pp. 6500–6504.
70. Q. Wang, J. L. Mynar, M. Yoshida, E. Lee, M. Lee, K. Okuro, K. Kinbara, T. Aida, High-water-content mouldable hydrogels by mixing clay and a dendritic molecular binder. Nature. 463 (2010), pp. 339–343.
71. T. Huang, H. G. Xu, K. X. Jiao, L. P. Zhu, H. R. Brown, H. L. Wang, A Novel Hydrogel with High Mechanical Strength: A Macromolecular Microsphere Composite Hydrogel. Advanced Materials. 19 (2007), pp. 1622–1626.
72. K. Haraguchi, T. Takehisa, S. Fan, Effects of Clay Content on the Properties of Nanocomposite Hydrogels Composed of Poly(N-isopropylacrylamide) and Clay. Macromolecules. 35 (2002), pp. 10162–10171.
73. F. A. Aouada, M. R. de Moura, W. J. Orts, L. H. C. Mattoso, Preparation and Characterization of Novel Micro- and Nanocomposite Hydrogels Containing Cellulosic Fibrils. Journal of Agricultural and Food Chemistry. 59 (2011), pp. 9433–9442.
74. S. Miyazaki, H. Endo, T. Karino, K. Haraguchi, M. Shibayama, Gelation Mechanism of Poly(N-isopropylacrylamide)−Clay Nanocomposite Gels. Macromolecules. 40 (2007), pp. 4287–4295.
75. K. Haraguchi, Nanocomposite hydrogels. Current Opinion in Solid State and Materials Science. 11 (2007), pp. 47–54.
76. R. Liu, S. Liang, X.-Z. Tang, D. Yan, X. Li, Z.-Z. Yu, Tough and highly stretchable graphene oxide/polyacrylamide nanocomposite hydrogels. Journal of Materials Chemistry. 22 (2012), p. 14160.
77. G. Gao, G. Du, Y. Cheng, J. Fu, Tough nanocomposite double network hydrogels reinforced with clay nanorods through covalent bonding and reversible chain adsorption. Journal of Materials Chemistry B. 2 (2014), p. 1539.
78. K. Haraguchi, H.-J. Li, Mechanical Properties and Structure of Polymer−Clay Nanocomposite Gels with High Clay Content. Macromolecules. 39 (2006), pp. 1898–1905.
79. J. P. Gong, Y. Katsuyama, T. Kurokawa, Y. Osada, Double-Network Hydrogels with Extremely High Mechanical Strength. Advanced Materials. 15 (2003), pp. 1155–1158.
80. J.-Y. Sun, X. Zhao, W. R. K. Illeperuma, O. Chaudhuri, K. H. Oh, D. J. Mooney, J. J. Vlassak, Z. Suo, Highly stretchable and tough hydrogels. Nature. 489, 133–136 (2012).

81. J. Berger, M. Reist, J. M. Mayer, O. Felt, N. A. Peppas, R. Gurny, Structure and interactions in covalently and ionically crosslinked chitosan hydrogels for biomedical applications. European Journal of Pharmaceutics and Biopharmaceutics. 57 (2004), pp. 19–34.
82. T. Sakai, Y. Akagi, T. Matsunaga, M. Kurakazu, U.-I. Chung, M. Shibayama, Highly Elastic and Deformable Hydrogel Formed from Tetra-arm Polymers. Macromol. Rapid Commun. 31, 1954–1959 (2010).
83. T. Sakai, T. Matsunaga, Y. Yamamoto, C. Ito, R. Yoshida, S. Suzuki, N. Sasaki, M. Shibayama, U.-I. Chung, Design and Fabrication of a High-Strength Hydrogel with Ideally Homogeneous Network Structure from Tetrahedron-like Macromonomers. Macromolecules. 41 (2008), pp. 5379–5384.
84. G. Song, L. Zhang, C. He, D.-C. Fang, P. G. Whitten, H. Wang, Facile Fabrication of Tough Hydrogels Physically Cross-Linked by Strong Cooperative Hydrogen Bonding. Macromolecules. 46 (2013), pp. 7423–7435.
85. T. Bai, P. Zhang, Y. Han, Y. Liu, W. Liu, X. Zhao, W. Lu, Construction of an ultrahigh strength hydrogel with excellent fatigue resistance based on strong dipole–dipole interaction. Soft Matter. 7 (2011), p. 2825.
86. Y. Zhang, Y. Li, W. Liu, Dipole-Dipole and H-Bonding Interactions Significantly Enhance the Multifaceted Mechanical Properties of Thermoresponsive Shape Memory Hydrogels. Advanced Functional Materials. 25 (2015), pp. 471–480.
87. W. Li, H. An, Y. Tan, C. Lu, C. Liu, P. Li, K. Xu, P. Wang, Hydrophobically associated hydrogels based on acrylamide and anionic surface active monomer with high mechanical strength. Soft Matter. 8 (2012), p. 5078.
88. D. C. Tuncaboylu, A. Argun, M. Sahin, M. Sari, O. Okay, Structure optimization of self-healing hydrogels formed via hydrophobic interactions. Polymer. 53 (2012), pp. 5513–5522.
89. K. J. Henderson, T. C. Zhou, K. J. Otim, K. R. Shull, Ionically Cross-Linked Triblock Copolymer Hydrogels with High Strength. Macromolecules. 43 (2010), pp. 6193–6201.
90. F. R. Kersey, D. M. Loveless, S. L. Craig, A hybrid polymer gel with controlled rates of cross-link rupture and self-repair. Journal of The Royal Society Interface. 4 (2007), pp. 373–380.
91. H. J. Kong, E. Wong, D. J. Mooney, Independent Control of Rigidity and Toughness of Polymeric Hydrogels. Macromolecules. 36 (2003), pp. 4582–4588.
92. T. L. Sun, T. Kurokawa, S. Kuroda, A. B. Ihsan, T. Akasaki, K. Sato, M. A. Haque, T. Nakajima, J. P. Gong, Physical hydrogels composed of polyampholytes demonstrate high toughness and viscoelasticity. Nature Materials. 12 (2013), pp. 932–937.
93. S. R. Stauffer, N. A. Peppast, Poly(vinyl alcohol) hydrogels prepared by freezing-thawing cyclic processing. Polymer. 33 (1992), pp. 3932–3936.
94. A. E. X. Brown, R. I. Litvinov, D. E. Discher, P. K. Purohit, J. W. Weisel, Multiscale Mechanics of Fibrin Polymer: Gel Stretching with Protein Unfolding and Loss of Water. Science. 325 (2009), pp. 741–744.
95. T. Nonoyama, J. P. Gong, Double-network hydrogel and its potential biomedical application: A review. Proc. Inst. Mech. Eng. H. 229, 853–863 (2015).
96. Z. Wang, Y. Cong, J. Fu, Stretchable and Tough Conductive Hydrogels for Flexible Pressure and Strain Sensors. Journal of Materials Chemistry B (2020), , doi:10.1039/c9tb02570g.
97. M. A. Haque, T. Kurokawa, J. P. Gong, Super tough double network hydrogels and their application as biomaterials. Polymer. 53 (2012), pp. 1805–1822.

98. S. Ahmed, T. Nakajima, T. Kurokawa, M. A. Haque, J. P. Gong, Brittle–ductile transition of double network hydrogels: Mechanical balance of two networks as the key factor. Polymer. 55 (2014), pp. 914–923.
99. T. Matsuda, T. Nakajima, J. P. Gong, Fabrication of Tough and Stretchable Hybrid Double-Network Elastomers Using Ionic Dissociation of Polyelectrolyte in Nonaqueous Media. Chemistry of Materials. 31 (2019), pp. 3766–3776.
100. O. E. Philippova, R. Rulkens, B. I. Kovtunenko, S. S. Abramchuk, A. R. Khokhlov, G. Wegner, Polyacrylamide Hydrogels with Trapped Polyelectrolyte Rods. Macromolecules. 31 (1998), pp. 1168–1179.
101. J. Li, Z. Suo, J. J. Vlassak, Stiff, strong, and tough hydrogels with good chemical stability. J. Mater. Chem. B. 2 (2014), pp. 6708–6713.
102. D. Myung, W. Koh, J. Ko, Y. Hu, M. Carrasco, J. Noolandi, C. N. Ta, C. W. Frank, Biomimetic strain hardening in interpenetrating polymer network hydrogels. Polymer. 48 (2007), pp. 5376–5387.
103. T. Nakajima, H. Sato, Y. Zhao, S. Kawahara, T. Kurokawa, K. Sugahara, J. P. Gong, A Universal Molecular Stent Method to Toughen any Hydrogels Based on Double Network Concept. Advanced Functional Materials. 22 (2012), pp. 4426–4432.
104. T. Nakajima, Y. Fukuda, T. Kurokawa, T. Sakai, U.-I. Chung, J. P. Gong, Synthesis and Fracture Process Analysis of Double Network Hydrogels with a Well-Defined First Network. ACS Macro Letters. 2 (2013), pp. 518–521.
105. L. Stevens, P. Calvert, G. G. Wallace, M. in H. Panhuis, Ionic-covalent entanglement hydrogels from gellan gum, carrageenan and an epoxy-amine. Soft Matter. 9 (2013), p. 3009.
106. Q. Chen, L. Zhu, C. Zhao, Q. Wang, J. Zheng, A Robust, One-Pot Synthesis of Highly Mechanical and Recoverable Double Network Hydrogels Using Thermoreversible Sol-Gel Polysaccharide. Advanced Materials. 25 (2013), pp. 4171–4176.
107. H. Muroi, R. Hidema, J. Gong, H. Furukawa, Development of Optical 3D Gel Printer for Fabricating Free-Form Soft ^|^amp; Wet Industrial Materials and Evaluation of Printed Double-Network Gels. Journal of Solid Mechanics and Materials Engineering. 7 (2013), pp. 163–168.
108. S. E. Bakarich, R. Gorkin, M. in H. Panhuis, G. M. Spinks, Three-Dimensional Printing Fiber Reinforced Hydrogel Composites. ACS Applied Materials & Interfaces. 6 (2014), pp. 15998–16006.
109. M. Zhu, X. Wang, H. Tang, J. Wang, Q. Hao, L. Liu, Y. Li, K. Zhang, O. G. Schmidt, Antifreezing Hydrogel with High Zinc Reversibility for Flexible and Durable Aqueous Batteries by Cooperative Hydrated Cations. Advanced Functional Materials. 30 (2020), p. 1907218.
110. Q. Peng, J. Chen, T. Wang, X. Peng, J. Liu, X. Wang, J. Wang, H. Zeng, Recent advances in designing conductive hydrogels for flexible electronics. InfoMat (2020), , doi:10.1002/inf2.12113.
111. Q. Rong, W. Lei, M. Liu, Conductive Hydrogels as Smart Materials for Flexible Electronic Devices. Chemistry. 24, 16930–16943 (2018).
112. V. Amoli, J. S. Kim, S. Y. Kim, J. Koo, Y. S. Chung, H. Choi, K. Do Hwan, Ionic Tactile Sensors for Emerging Human-Interactive Technologies: A Review of Recent Progress. Advanced Functional Materials (2019), p. 1904532.
113. S. Zhao, P. Tseng, J. Grasman, Y. Wang, W. Li, B. Napier, B. Yavuz, Y. Chen, L. Howell, J. Rincon, F. G. Omenetto, D. L. Kaplan, Programmable Hydrogel Ionic Circuits for Biologically Matched Electronic Interfaces. Advanced Materials. 30 (2018), p. 1800598.

114. C. Keplinger, J.-Y. Sun, C. C. Foo, P. Rothemund, G. M. Whitesides, Z. Suo, Stretchable, Transparent, Ionic Conductors. Science. 341 (2013), pp. 984–987.
115. X. Pu, M. Liu, X. Chen, J. Sun, C. Du, Y. Zhang, J. Zhai, W. Hu, Z. L. Wang, Ultrastretchable, transparent triboelectric nanogenerator as electronic skin for biomechanical energy harvesting and tactile sensing. Sci Adv. 3, e1700015 (2017).
116. C. H. Yang, B. Chen, J. J. Lu, J. H. Yang, J. Zhou, Y. M. Chen, Z. Suo, Ionic cable. Extreme Mechanics Letters. 3 (2015), pp. 59–65.
117. O. J. Cayre, S. T. Chang, O. D. Velev, Polyelectrolyte Diode: Nonlinear Current Response of a Junction between Aqueous Ionic Gels. Journal of the American Chemical Society. 129 (2007), pp. 10801–10806.
118. H.-R. Lee, J. Woo, S. H. Han, S.-M. Lim, S. Lim, Y.-W. Kang, W. J. Song, J.-M. Park, T. D. Chung, Y.-C. Joo, J.-Y. Sun, A Stretchable Ionic Diode from Copolyelectrolyte Hydrogels with Methacrylated Polysaccharides. Advanced Functional Materials. 29 (2019), p. 1806909.
119. Y. Zhou, Y. Hou, Q. Li, L. Yang, Y. Cao, K. H. Choi, Q. Wang, Q. M. Zhang, Biocompatible and Flexible Hydrogel Diode-Based Mechanical Energy Harvesting. Advanced Materials Technologies. 2 (2017), p. 1700118.
120. J. Rivnay, H. Wang, L. Fenno, K. Deisseroth, G. G. Malliaras, Next-generation probes, particles, and proteins for neural interfacing. Sci Adv. 3, e1601649 (2017).
121. D. Mawad, C. Mansfield, A. Lauto, F. Perbellini, G. W. Nelson, J. Tonkin, S. O. Bello, D. J. Carrad, A. P. Micolich, M. M. Mahat, J. Furman, D. Payne, A. R. Lyon, J. J. Gooding, S. E. Harding, C. M. Terracciano, M. M. Stevens, A conducting polymer with enhanced electronic stability applied in cardiac models. Sci Adv. 2, e1601007 (2016).
122. Y. Shi, C. Ma, L. Peng, G. Yu, Conductive “Smart” Hybrid Hydrogels with PNIPAM and Nanostructured Conductive Polymers. Advanced Functional Materials. 25 (2015), pp. 1219–1225.
123. L. Pan, G. Yu, D. Zhai, H. R. Lee, W. Zhao, N. Liu, H. Wang, B. C.-K. Tee, Y. Shi, Y. Cui, Z. Bao, Hierarchical nanostructured conducting polymer hydrogel with high electrochemical activity. Proc. Natl. Acad. Sci. U. S. A. 109, 9287–9292 (2012).
124. J. Stejskal, I. Sapurina, M. Trchová, J. Prokeš, I. Křivka, E. Tobolková, Solid-State Protonation and Electrical Conductivity of Polyaniline. Macromolecules. 31 (1998), pp. 2218–2222.
125. B. Yao, H. Wang, Q. Zhou, M. Wu, M. Zhang, C. Li, G. Shi, Ultrahigh-Conductivity Polymer Hydrogels with Arbitrary Structures. Adv. Mater. 29 (2017), doi:10.1002/adma.201700974.
126. Y.-Y. Lee, H.-Y. Kang, S. H. Gwon, G. M. Choi, S.-M. Lim, J.-Y. Sun, Y.-C. Joo, A Strain-Insensitive Stretchable Electronic Conductor: PEDOT:PSS/Acrylamide Organogels. Adv. Mater. 28, 1636–1643 (2016).
127. S. Zhang, Y. Chen, H. Liu, Z. Wang, H. Ling, C. Wang, J. Ni, B. Çelebi-Saltik, X. Wang, X. Meng, H.-J. Kim, A. Baidya, S. Ahadian, N. Ashammakhi, M. R. Dokmeci, J. Travas-Sejdic, A. Khademhosseini, Room-Temperature-Formed PEDOT:PSS Hydrogels Enable Injectable, Soft, and Healable Organic Bioelectronics. Adv. Mater. 32, e1904752 (2020).
128. Y. Liu, J. Li, S. Song, J. Kang, Y. Tsao, S. Chen, V. Mottini, K. McConnell, W. Xu, Y.-Q. Zheng, J. B.-H. Tok, P. M. George, Z. Bao, Morphing electronics enable neuromodulation in growing tissue. Nat. Biotechnol. (2020), doi:10.1038/s41587-020-0495-2.
129. H. Yuk, B. Lu, S. Lin, K. Qu, J. Xu, J. Luo, X. Zhao, 3D printing of conducting polymers. Nat. Commun. 11, 1604 (2020).

130. B. Lu, H. Yuk, S. Lin, N. Jian, K. Qu, J. Xu, X. Zhao, Pure PEDOT:PSS hydrogels. Nat. Commun. 10, 1–10 (2019).
131. F. Zhao, Y. Shi, L. Pan, G. Yu, Multifunctional Nanostructured Conductive Polymer Gels: Synthesis, Properties, and Applications. Accounts of Chemical Research. 50 (2017), pp. 1734–1743.
132. Y. Liu, J. Liu, S. Chen, T. Lei, Y. Kim, S. Niu, H. Wang, X. Wang, A. M. Foudeh, J. B. -H. Tok, Z. Bao, Soft and elastic hydrogel-based microelectronics for localized low-voltage neuromodulation. Nature Biomedical Engineering. 3 (2019), pp. 58–68.
133. V. R. Feig, H. Tran, M. Lee, Z. Bao, Mechanically tunable conductive interpenetrating network hydrogels that mimic the elastic moduli of biological tissue. Nat. Commun. 9, 2740 (2018).
134. M. Berggren, A. Richter-Dahlfors, Organic Bioelectronics. Advanced Materials. 19 (2007), pp. 3201–3213.
135. S. Zhang, P. Kumar, A. S. Nouas, L. Fontaine, H. Tang, F. Cicoira, Solvent-induced changes in PEDOT:PSS films for organic electrochemical transistors. APL Materials. 3 (2015), p. 014911.
136. R. Green, M. R. Abidian, Conducting Polymers for Neural Prosthetic and Neural Interface Applications. Adv. Mater. 27, 7620–7637 (2015).
137. S. Zhang, G. Deng, F. Liu, B. Peng, Y. Bao, F. Du, A. T. Chen, J. Liu, Z. Chen, J. Ma, X. Tang, Q. Chen, J. Zhou, Autocatalytic Delivery of Brain Tumor-targeting, Size-shrinkable Nanoparticles for Treatment of Breast Cancer Brain Metastases. Adv. Funct. Mater. 30 (2020), doi:10.1002/adfm.201910651.
138. Z. Cao, H. Liu, L. Jiang, Transparent, mechanically robust, and ultrastable ionogels enabled by hydrogen bonding between elastomers and ionic liquids. Mater. Horiz. (2019), doi:10.1039/C9MH01699F.
139. N. Sun, X. Gao, A. Wu, F. Lu, L. Zheng, Mechanically strong ionogels formed by immobilizing ionic liquid in polyzwitterion networks. Journal of Molecular Liquids. 248 (2017), pp. 759–766.
140. J. Le Bideau, L. Viau, A. Vioux, Ionogels, ionic liquid based hybrid materials. Chem. Soc. Rev. 40, 907–925 (2011).
141. M. C. Buzzeo, R. G. Evans, R. G. Compton, Non-Haloaluminate Room-Temperature Ionic Liquids in Electrochemistry—A Review. ChemPhysChem. 5 (2004), pp. 1106–1120.
142. N. V. Plechkova, K. R. Seddon, Applications of ionic liquids in the chemical industry. Chem. Soc. Rev. 37 (2008), pp. 123–150.
143. M. Watanabe, M. L. Thomas, S. Zhang, K. Ueno, T. Yasuda, K. Dokko, Application of Ionic Liquids to Energy Storage and Conversion Materials and Devices. Chemical Reviews. 117 (2017), pp. 7190–7239.
144. D. R. MacFarlane, N. Tachikawa, M. Forsyth, J. M. Pringle, P. C. Howlett, G. D. Elliott, J. H. Davis, M. Watanabe, P. Simon, C. Austen Angell, Energy applications of ionic liquids. Energy Environ. Sci. 7 (2014), pp. 232–250.
145. Y.-S. Ye, J. Rick, B.-J. Hwang, Ionic liquid polymer electrolytes. J. Mater. Chem. A. 1 (2013), pp. 2719–2743.
146. S. Z. Bisri, S. Shimizu, M. Nakano, Y. Iwasa, Endeavor of Iontronics: From Fundamentals to Applications of Ion-Controlled Electronics. Advanced Materials. 29 (2017), p. 1607054.

147. J. W. Steed, Supramolecular gel chemistry: developments over the last decade. Chem. Commun. 47 (2011), pp. 1379–1383.
148. D. F. Miranda, C. Versek, M. T. Tuominen, T. P. Russell, J. J. Watkins, Cross-Linked Block Copolymer/Ionic Liquid Self-Assembled Blends for Polymer Gel Electrolytes with High Ionic Conductivity and Mechanical Strength. Macromolecules. 46 (2013), pp. 9313–9323.
149. Z. Liu, Y. Wang, Y. Ren, G. Jin, C. Zhang, W. Chen, F. Yan, Poly(ionic liquid) hydrogel-based anti-freezing ionic skin for a soft robotic gripper. Materials Horizons (2020), , doi:10.1039/c9mh01688k.
150. Y. Ren, J. Guo, Z. Liu, Z. Sun, Y. Wu, L. Liu, F. Yan, Ionic liquid–based click-ionogels. Science Advances. 5 (2019), p. eaax0648.
151. H. J. Kim, B. Chen, Z. Suo, R. C. Hayward, Ionoelastomer junctions between polymer networks of fixed anions and cations. Science. 367, 773–776 (2020).
152. S.-Y. Lee, T. Yasuda, M. Watanabe, Fabrication of protic ionic liquid/sulfonated polyimide composite membranes for non-humidified fuel cells. Journal of Power Sources. 195 (2010), pp. 5909–5914.
153. M. Armand, F. Endres, D. R. MacFarlane, H. Ohno, B. Scrosati, Ionic-liquid materials for the electrochemical challenges of the future. Nature Materials. 8 (2009), pp. 621–629.
154. P. Wang, S. M. Zakeeruddin, P. Comte, I. Exnar, M. Grätzel, Gelation of Ionic Liquid-Based Electrolytes with Silica Nanoparticles for Quasi-Solid-State Dye-Sensitized Solar Cells. Journal of the American Chemical Society. 125 (2003), pp. 1166–1167.
155. G.-C. Zhao, M.-Q. Xu, J. Ma, X.-W. Wei, Direct electrochemistry of hemoglobin on a room temperature ionic liquid modified electrode and its electrocatalytic activity for the reduction of oxygen. Electrochemistry Communications. 9 (2007), pp. 920–924.
156. T. Fukushima, K. Asaka, A. Kosaka, T. Aida, Fully Plastic Actuator through Layer-by-Layer Casting with Ionic-Liquid-Based Bucky Gel. Angewandte Chemie International Edition. 44 (2005), pp. 2410–2413.
157. G. Chen, J. Huang, J. Gu, S. Peng, X. Xiang, K. Chen, X. Yang, L. Guan, X. Jiang, L. Hou, Highly tough supramolecular double network hydrogel electrolytes for an artificial flexible and low-temperature tolerant sensor. Journal of Materials Chemistry A. 8 (2020), pp. 6776–6784.
158. C. H. Yang, M. X. Wang, H. Haider, J. H. Yang, J.-Y. Sun, Y. M. Chen, J. Zhou, Z. Suo, Strengthening Alginate/Polyacrylamide Hydrogels Using Various Multivalent Cations. ACS Applied Materials & Interfaces. 5 (2013), pp. 10418–10422.
159. L. Han, K. Liu, M. Wang, K. Wang, L. Fang, H. Chen, J. Zhou, X. Lu, Mussel-Inspired Adhesive and Conductive Hydrogel with Long-Lasting Moisture and Extreme Temperature Tolerance. Advanced Functional Materials. 28 (2018), p. 1704195.
160. Z. Wang, J. Chen, Y. Cong, H. Zhang, T. Xu, L. Nie, J. Fu, Ultrastretchable Strain Sensors and Arrays with High Sensitivity and Linearity Based on Super Tough Conductive Hydrogels. Chemistry of Materials. 30 (2018), pp. 8062–8069.
161. T. Dai, X. Qing, H. Zhou, C. Shen, J. Wang, Y. Lu, Mechanically strong conducting hydrogels with special double-network structure. Synthetic Metals. 160 (2010), pp. 791–796.
162. W. Li, F. Gao, X. Wang, N. Zhang, M. Ma, Strong and Robust Polyaniline-Based Supramolecular Hydrogels for Flexible Supercapacitors. Angewandte Chemie. 128 (2016), pp. 9342–9347.

163. F. Zhu, J. Lin, Z. L. Wu, S. Qu, J. Yin, J. Qian, Q. Zheng, Tough and Conductive Hybrid Hydrogels Enabling Facile Patterning. ACS Applied Materials & Interfaces. 10 (2018), pp. 13685–13692.
164. S. Wang, M. W. Urban, Self-healing polymers. Nature Reviews Materials (2020), , doi:10.1038/s41578-020-0202-4.
165. Y. Bai, B. Chen, F. Xiang, J. Zhou, H. Wang, Z. Suo, Transparent hydrogel with enhanced water retention capacity by introducing highly hydratable salt. Applied Physics Letters. 105 (2014), p. 151903.
166. X. P. Morelle, W. R. Illeperuma, K. Tian, R. Bai, Z. Suo, J. J. Vlassak, Highly Stretchable and Tough Hydrogels below Water Freezing Temperature. Advanced Materials. 30 (2018), p. 1801541.
167. H. Liu, W. Zhao, G. Gao, X. Ren, Tough, anti-freezing and non-drying double network organohydrogels. Materials Today Communications. 21 (2019), p. 100609.
168. F. Chen, D. Zhou, J. Wang, T. Li, X. Zhou, T. Gan, S. Handschuh-Wang, X. Zhou, Rational Fabrication of Anti-Freezing, Non-Drying Tough Organohydrogels by One-Pot Solvent Displacement. Angew. Chem. Int. Ed Engl. 57, 6568–6571 (2018).
169. M. Ju, B. Wu, S. Sun, P. Wu, Redox-Active Iron-Citrate Complex Regulated Robust Coating-Free Hydrogel Microfiber Net with High Environmental Tolerance and Sensitivity. Advanced Functional Materials (2020), p. 1910387.
170. Y. Yang, L. Guan, X. Li, Z. Gao, X. Ren, G. Gao, Conductive Organohydrogels with Ultrastretchability, Antifreezing, Self-Healing, and Adhesive Properties for Motion Detection and Signal Transmission. ACS Applied Materials & Interfaces. 11 (2019), pp. 3428–3437.
171. Z. Qin, D. Dong, M. Yao, Q. Yu, X. Sun, Q. Guo, H. Zhang, F. Yao, J. Li, Freezing-Tolerant Supramolecular Organohydrogel with High Toughness, Thermoplasticity, and Healable and Adhesive Properties. ACS Applied Materials & Interfaces. 11 (2019), pp. 21184–21193.
172. Q. Rong, W. Lei, L. Chen, Y. Yin, J. Zhou, M. Liu, Anti-freezing, Conductive Self-healing Organohydrogels with Stable Strain-Sensitivity at Subzero Temperatures. Angewandte Chemie International Edition. 56 (2017), pp. 14159–14163.
173. Q. Rong, W. Lei, J. Huang, M. Liu, Low Temperature Tolerant Organohydrogel Electrolytes for Flexible Solid-State Supercapacitors. Advanced Energy Materials. 8 (2018), p. 1801967.
174. H. Liao, X. Guo, P. Wan, G. Yu, Conductive MXene Nanocomposite Organohydrogel for Flexible, Healable, Low-Temperature Tolerant Strain Sensors. Advanced Functional Materials. 29 (2019), p. 1904507.
175. H. Chen, X. Ren, G. Gao, Skin-Inspired Gels with Toughness, Antifreezing, Conductivity, and Remoldability. ACS Applied Materials & Interfaces. 11 (2019), pp. 28336–28344.
176. Q. Nian, J. Wang, S. Liu, T. Sun, S. Zheng, Y. Zhang, Z. Tao, J. Chen, Aqueous Batteries Operated at -50 °C. Angew. Chem. Int. Ed Engl. 58, 16994–16999 (2019).
177. W. Xie, J. Duan, H. Wang, J. Li, R. Liu, B. Yu, S. Liu, J. Zhou, Ultra-stretchable, bio-inspired ionic skins that work stably in various harsh environments. Journal of Materials Chemistry A. 6 (2018), pp. 24114–24119.
178. J. Song, S. Chen, L. Sun, Y. Guo, L. Zhang, S. Wang, H. Xuan, Q. Guan, Z. You, Mechanically and Electronically Robust Transparent Organohydrogel Fibers. Adv. Mater. 32, e1906994 (2020).

179. H. Yuk, T. Zhang, G. A. Parada, X. Liu, X. Zhao, Skin-inspired hydrogel–elastomer hybrids with robust interfaces and functional microstructures. Nature Communications. 7 (2016), , doi:10.1038/ncomms12028.
180. P. Le Floch, X. Yao, Q. Liu, Z. Wang, G. Nian, Y. Sun, L. Jia, Z. Suo, Wearable and Washable Conductors for Active Textiles. ACS Appl. Mater. Interfaces. 9, 25542–25552 (2017).
181. Q. Liu, G. Nian, C. Yang, S. Qu, Z. Suo, Bonding dissimilar polymer networks in various manufacturing processes. Nat. Commun. 9, 846 (2018).
182. Y. Lee, S. H. Cha, Y.-W. Kim, D. Choi, J.-Y. Sun, Transparent and attachable ionic communicators based on self-cleanable triboelectric nanogenerators. Nature Communications. 9 (2018), , doi:10.1038/s41467-018-03954-x.
183. K. Parida, V. Kumar, W. Jiangxin, V. Bhavanasi, R. Bendi, P. S. Lee, Highly Transparent, Stretchable, and Self-Healing Ionic-Skin Triboelectric Nanogenerators for Energy Harvesting and Touch Applications. Advanced Materials. 29 (2017), p. 1702181.
184. X. Wang, H. Sheng, H. Wang, Neural interfaces by hydrogels. IBRO Reports. 6 (2019), p. S394.
185. H. Yuk, T. Zhang, S. Lin, G. A. Parada, X. Zhao, Tough bonding of hydrogels to diverse non-porous surfaces. Nat. Mater. 15, 190–196 (2016).
186. M. Moretti, D. Wendt, D. Schaefer, M. Jakob, E. B. Hunziker, M. Heberer, I. Martin, Structural characterization and reliable biomechanical assessment of integrative cartilage repair. Journal of Biomechanics. 38 (2005), pp. 1846–1854.
187. D. Dendukuri, P. Panda, R. Haghgooie, J. M. Kim, T. Alan Hatton, P. S. Doyle, Modeling of Oxygen-Inhibited Free Radical Photopolymerization in a PDMS Microfluidic Device. Macromolecules. 41 (2008), pp. 8547–8556.
188. G. J. Van Amerongen, The Permeability of Different Rubbers to Gases and Its Relation to Diffusivity and Solubility. Journal of Applied Physics. 17 (1946), pp. 972–985.
189. J. Zhou, A. V. Ellis, N. H. Voelcker, Recent developments in PDMS surface modification for microfluidic devices. ELECTROPHORESIS. 31 (2010), pp. 2–16.
190. J. L. Fritz, M. J. Owen, Hydrophobic Recovery of Plasma-Treated Polydimethylsiloxane. The Journal of Adhesion. 54 (1995), pp. 33–45.
191. Y. Yu, H. Yuk, G. A. Parada, Y. Wu, X. Liu, C. S. Nabzdyk, K. Youcef-Toumi, J. Zang, X. Zhao, Multifunctional “Hydrogel Skins” on Diverse Polymers with Arbitrary Shapes. Advanced Materials. 31 (2019), p. 1807101.
192. T. Liu, M. Liu, S. Dou, J. Sun, Z. Cong, C. Jiang, C. Du, X. Pu, W. Hu, Z. L. Wang, Triboelectric-Nanogenerator-Based Soft Energy-Harvesting Skin Enabled by Toughly Bonded Elastomer/Hydrogel Hybrids. ACS Nano. 12, 2818–2826 (2018).
193. D. H. Sierra, Fibrin Sealant Adhesive Systems: A Review of Their Chemistry, Material Properties and Clinical Applications. Journal of Biomaterials Applications. 7 (1993), pp. 309–352.
194. D. G. Wallace, G. M. Cruise, W. M. Rhee, J. A. Schroeder, J. J. Prior, J. Ju, M. Maroney, J. Duronio, M. H. Ngo, T. Estridge, G. C. Coker, A tissue sealant based on reactive multifunctional polyethylene glycol. Journal of Biomedical Materials Research. 58 (2001), pp. 545–555.
195. K. A. Vakalopoulos, Z. Wu, L. Kroese, G.-J. Kleinrensink, J. Jeekel, R. Vendamme, D. Dodou, J. F. Lange, Mechanical Strength and Rheological Properties of Tissue Adhesives With Regard to Colorectal Anastomosis. Annals of Surgery. 261 (2015), pp. 323–331.

196. J. Li, A. D. Celiz, J. Yang, Q. Yang, I. Wamala, W. Whyte, B. R. Seo, N. V. Vasilyev, J. J. Vlassak, Z. Suo, D. J. Mooney, Tough adhesives for diverse wet surfaces. Science. 357, 378–381 (2017).
197. S. O. Blacklow, J. Li, B. R. Freedman, M. Zeidi, C. Chen, D. J. Mooney, Bioinspired mechanically active adhesive dressings to accelerate wound closure. Sci Adv. 5, eaaw3963 (2019).
198. H. Yuk, C. E. Varela, C. S. Nabzdyk, X. Mao, R. F. Padera, E. T. Roche, X. Zhao, Dry double-sided tape for adhesion of wet tissues and devices. Nature. 575, 169–174 (2019).
199. J. Yang, R. Bai, Z. Suo, Topological Adhesion of Wet Materials. Adv. Mater. 30, e1800671 (2018).
200. X. Chen, H. Yuk, J. Wu, C. S. Nabzdyk, X. Zhao, Instant tough bioadhesive with triggerable benign detachment. Proceedings of the National Academy of Sciences (2020), p. 202006389.
201. H. J. Kim, L. Paquin, C. W. Barney, S. So, B. Chen, Z. Suo, A. J. Crosby, R. C. Hayward, Low-Voltage Reversible Electroadhesion of Ionoelastomer Junctions. Adv. Mater., e2000600 (2020).
202. L. Pan, A. Chortos, G. Yu, Y. Wang, S. Isaacson, R. Allen, Y. Shi, R. Dauskardt, Z. Bao, An ultra-sensitive resistive pressure sensor based on hollow-sphere microstructure induced elasticity in conducting polymer film. Nature Communications. 5 (2014), , doi:10.1038/ncomms4002.
203. Z. Zhu, R. Li, T. Pan, Imperceptible Epidermal-Iontronic Interface for Wearable Sensing. Adv. Mater. 30 (2018), doi:10.1002/adma.201705122.
204. N. Bai, L. Wang, Q. Wang, J. Deng, Y. Wang, P. Lu, J. Huang, G. Li, Y. Zhang, J. Yang, K. Xie, X. Zhao, C. F. Guo, Graded intrafillable architecture-based iontronic pressure sensor with ultra-broad-range high sensitivity. Nature Communications. 11 (2020), , doi:10.1038/s41467-019-14054-9.
205. Y. Tai, M. Mulle, I. Aguilar Ventura, G. Lubineau, A highly sensitive, low-cost, wearable pressure sensor based on conductive hydrogel spheres. Nanoscale. 7, 14766–14773 (2015).
206. Y. Ko, D. Kim, G. Kwon, J. You, High-Performance Resistive Pressure Sensor Based on Elastic Composite Hydrogel of Silver Nanowires and Poly(ethylene glycol). Micromachines (Basel). 9 (2018), doi:10.3390/mi9090438.
207. M. S. Sarwar, Y. Dobashi, C. Preston, J. K. M. Wyss, S. Mirabbasi, J. D. W. Madden, Bend, stretch, and touch: Locating a finger on an actively deformed transparent sensor array. Science Advances. 3 (2017), p. e1602200.
208. D. Zhang, B. Ren, Y. Zhang, L. Xu, Q. Huang, Y. He, X. Li, J. Wu, J. Yang, Q. Chen, Y. Chang, J. Zheng, From design to applications of stimuli-responsive hydrogel strain sensors. J. Mater. Chem. B Mater. Biol. Med. 8, 3171–3191 (2020).
209. K. Tian, J. Bae, S. E. Bakarich, C. Yang, R. D. Gately, G. M. Spinks, M. In Het Panhuis, Z. Suo, J. J. Vlassak, 3D Printing of Transparent and Conductive Heterogeneous Hydrogel-Elastomer Systems. Adv. Mater. 29 (2017), doi:10.1002/adma.201604827.
210. P. Manandhar, P. D. Calvert, J. R. Buck, Elastomeric Ionic Hydrogel Sensor for Large Strains. IEEE Sens. J. 12, 2052–2061 (2012).
211. W. Fan, X. Zhang, H. Cui, C. Liu, Y. Li, Y. Xia, K. Sui, Direct Current-Powered High-Performance Ionic Hydrogel Strain Sensor Based on Electrochemical Redox Reaction. ACS Appl. Mater. Interfaces. 11, 24289–24297 (2019).

212. S. Dai, S. Wang, H. Yan, J. Xu, H. Hu, J. Ding, N. Yuan, Stretchable and self-healable hydrogel-based capacitance pressure and strain sensor for electronic skin systems. Materials Research Express. 6 (2019), p. 0850b9.
213. A. Tröls, A. Kogler, R. Baumgartner, R. Kaltseis, C. Keplinger, R. Schwödiauer, I. Graz, S. Bauer, Stretch dependence of the electrical breakdown strength and dielectric constant of dielectric elastomers. Smart Materials and Structures. 22 (2013), p. 104012.
214. Y. Hou, Y. Zhou, L. Yang, Q. Li, Y. Zhang, L. Zhu, M. A. Hickner, Q. M. Zhang, Q. Wang, Flexible Ionic Diodes for Low-Frequency Mechanical Energy Harvesting. Advanced Energy Materials. 7 (2017), p. 1601983.
215. H. Banerjee, M. Suhail, H. Ren, Hydrogel Actuators and Sensors for Biomedical Soft Robots: Brief Overview with Impending Challenges. Biomimetics. 3 (2018), doi:10.3390/biomimetics3030015.
216. H. G. Schild, Poly(N-isopropylacrylamide): experiment, theory and application. Progress in Polymer Science. 17 (1992), pp. 163–249.
217. A. Choe, J. Yeom, R. Shanker, M. P. Kim, S. Kang, H. Ko, Stretchable and wearable colorimetric patches based on thermoresponsive plasmonic microgels embedded in a hydrogel film. NPG Asia Materials. 10 (2018), pp. 912–922.
218. Y. Wang, thesis (2019).
219. Y. Li, C. Hu, J. Lan, B. Yan, Y. Zhang, L. Shi, R. Ran, Hydrogel-based temperature sensor with water retention, frost resistance and remoldability. Polymer. 186 (2020), p. 122027.
220. M. Bariya, H. Y. Y. Nyein, A. Javey, Wearable sweat sensors. Nature Electronics. 1 (2018), pp. 160–171.
221. J. Heikenfeld, A. Jajack, B. Feldman, S. W. Granger, S. Gaitonde, G. Begtrup, B. A. Katchman, Accessing analytes in biofluids for peripheral biochemical monitoring. Nat. Biotechnol. 37, 407–419 (2019).
222. J. Kim, A. S. Campbell, B. E.-F. de Ávila, J. Wang, Wearable biosensors for healthcare monitoring. Nature Biotechnology. 37 (2019), pp. 389–406.
223. H. R. Culver, J. R. Clegg, N. A. Peppas, Analyte-Responsive Hydrogels: Intelligent Materials for Biosensing and Drug Delivery. Acc. Chem. Res. 51, 2600 (2018).
224. J. Tavakoli, Y. Tang, Hydrogel Based Sensors for Biomedical Applications: An Updated Review. Polymers . 9 (2017), doi:10.3390/polym9080364.
225. E. Gianino, C. Miller, J. Gilmore, Smart Wound Dressings for Diabetic Chronic Wounds. Bioengineering. 5 (2018), p. 51.
226. H. Derakhshandeh, S. S. Kashaf, F. Aghabaglou, I. O. Ghanavati, A. Tamayol, Smart Bandages: The Future of Wound Care. Trends in Biotechnology. 36 (2018), pp. 1259–1274.
227. J. Wu, Z. Wu, H. Xu, Q. Wu, C. Liu, B.-R. Yang, X. Gui, X. Xie, K. Tao, Y. Shen, J. Miao, L. K. Norford, An intrinsically stretchable humidity sensor based on anti-drying, self-healing and transparent organohydrogels. Materials Horizons. 6 (2019), pp. 595–603.
228. O. Veiseh, B. C. Tang, K. A. Whitehead, D. G. Anderson, R. Langer, Managing diabetes with nanomedicine: challenges and opportunities. Nature Reviews Drug Discovery. 14 (2015), pp. 45–57.
229. W. Gao, S. Emaminejad, H. Y. Y. Nyein, S. Challa, K. Chen, A. Peck, H. M. Fahad, H. Ota, H. Shiraki, D. Kiriya, D.-H. Lien, G. A. Brooks, R. W. Davis, A. Javey, Fully integrated wearable sensor arrays for multiplexed in situ perspiration analysis. Nature. 529, 509–514 (2016).

230. M. Elsherif, M. U. Hassan, A. K. Yetisen, H. Butt, Wearable Contact Lens Biosensors for Continuous Glucose Monitoring Using Smartphones. ACS Nano. 12, 5452–5462 (2018).
231. J. Kim, M. Kim, M.-S. Lee, K. Kim, S. Ji, Y.-T. Kim, J. Park, K. Na, K.-H. Bae, H. Kyun Kim, F. Bien, C. Young Lee, J.-U. Park, Wearable smart sensor systems integrated on soft contact lenses for wireless ocular diagnostics. Nat. Commun. 8, 14997 (2017).
232. J. Kim, S. Imani, W. R. de Araujo, J. Warchall, G. Valdés-Ramírez, Thiago R L, P. P. Mercier, J. Wang, Wearable salivary uric acid mouthguard biosensor with integrated wireless electronics. Biosensors and Bioelectronics. 74 (2015), pp. 1061–1068.
233. P. Tseng, B. Napier, L. Garbarini, D. L. Kaplan, F. G. Omenetto, Functional, RF-Trilayer Sensors for Tooth-Mounted, Wireless Monitoring of the Oral Cavity and Food Consumption. Adv. Mater. 30, e1703257 (2018).
234. Y. Chen, S. Lu, S. Zhang, Y. Li, Z. Qu, Y. Chen, B. Lu, X. Wang, X. Feng, Skin-like biosensor system via electrochemical channels for noninvasive blood glucose monitoring. Sci Adv. 3, e1701629 (2017).
235. S. Zhang, H. Ling, Y. Chen, Q. Cui, J. Ni, X. Wang, M. C. Hartel, X. Meng, K. Lee, J. Lee, W. Sun, H. Lin, S. Emaminejad, S. Ahadian, N. Ashammakhi, M. R. Dokmeci, A. Khademhosseini, Hydrogel-Enabled Transfer-Printing of Conducting Polymer Films for Soft Organic Bioelectronics. Adv. Funct. Mater. 30, 1906016 (2020).
236. J. Wu, F. Yin, Sensitive enzymatic glucose biosensor fabricated by electrospinning composite nanofibers and electrodepositing Prussian blue film. Journal of Electroanalytical Chemistry. 694 (2013), pp. 1–5.
237. M. R. Guascito, D. Chirizzi, C. Malitesta, E. Mazzotta, Mediator-free amperometric glucose biosensor based on glucose oxidase entrapped in poly(vinyl alcohol) matrix. Analyst. 136, 164–173 (2011).
238. X. Su, J. Wei, X. Ren, L. Li, X. Meng, J. Ren, F. Tang, A new amperometric glucose biosensor based on one-step electrospun poly(vinyl alcohol)/chitosan nanofibers. J. Biomed. Nanotechnol. 9, 1776–1783 (2013).
239. G. Ren, X. Xu, Q. Liu, J. Cheng, X. Yuan, L. Wu, Y. Wan, Electrospun poly(vinyl alcohol)/glucose oxidase biocomposite membranes for biosensor applications. Reactive and Functional Polymers. 66 (2006), pp. 1559–1564.
240. S. Vaddiraju, H. Singh, D. J. Burgess, F. C. Jain, F. Papadimitrakopoulos, Enhanced Glucose Sensor Linearity Using Poly(Vinyl Alcohol) Hydrogels. Journal of Diabetes Science and Technology. 3 (2009), pp. 863–874.
241. D. Zhai, B. Liu, Y. Shi, L. Pan, Y. Wang, W. Li, R. Zhang, G. Yu, Highly sensitive glucose sensor based on pt nanoparticle/polyaniline hydrogel heterostructures. ACS Nano. 7, 3540–3546 (2013).
242. M. Mesch, C. Zhang, P. V. Braun, H. Giessen, Functionalized Hydrogel on Plasmonic Nanoantennas for Noninvasive Glucose Sensing. ACS Photonics. 2 (2015), pp. 475–480.
243. C. Zhang, G. G. Cano, P. V. Braun, Linear and fast hydrogel glucose sensor materials enabled by volume resetting agents. Adv. Mater. 26, 5678–5683 (2014).
244. B. Vilozny, A. Schiller, R. A. Wessling, B. Singaram, Multiwell plates loaded with fluorescent hydrogel sensors for measuring pH and glucose concentration. J. Mater. Chem. 21, 7589–7595 (2011).
245. J. T. Suri, D. B. Cordes, F. E. Cappuccio, R. A. Wessling, B. Singaram, Continuous Glucose Sensing with a Fluorescent Thin-Film Hydrogel. Angewandte Chemie. 115 (2003), pp. 6037–6039.

246. C. Zhang, M. D. Losego, P. V. Braun, Hydrogel-Based Glucose Sensors: Effects of Phenylboronic Acid Chemical Structure on Response. Chemistry of Materials. 25 (2013), pp. 3239–3250.

247. M. Wu, Y. Zhang, Q. Liu, H. Huang, X. Wang, Z. Shi, Y. Li, S. Liu, L. Xue, Y. Lei, A smart hydrogel system for visual detection of glucose. Biosensors and Bioelectronics. 142 (2019), p. 111547.

248. Y. Kim, H. Namgung, T. S. Lee, Synthesis of a glucose oxidase-conjugated, polyacrylamide-based, fluorescent hydrogel for a reusable, ratiometric glucose sensor. Polym. Chem. 7, 6655–6661 (2016).

249. B. Ying, S. Park, L. Chen, X. Dong, E. W. K. Young, X. Liu, NanoPADs and nanoFACEs: an optically transparent nanopaper-based device for biomedical applications. Lab Chip (2020), doi:10.1039/d0lc00226g.

250. J. N. Cambre, B. S. Sumerlin, Biomedical applications of boronic acid polymers. Polymer. 52 (2011), pp. 4631–4643.

251. S. Kitano, K. Kataoka, Y. Koyama, T. Okano, Y. Sakurai, Die Makromolekulare Chemie, Rapid Communications. 12 (1991), pp. 227–233.

252. S. Kitano, I. Hisamitsu, Y. Koyama, K. Kataoka, T. Okano, Y. Sakurai, Effect of the incorporation of amino groups in a glucose-responsive polymer complex having phenylboronic acid moieties. Polymers for Advanced Technologies. 2 (1991), pp. 261–264.

253. I. Hisamitsu, K. Kataoka, T. Okano, Y. Sakurai, Pharmaceutical Research. 14 (1997), pp. 289–293.

254. K. Kataoka, H. Miyazaki, M. Bunya, T. Okano, Y. Sakurai, Totally Synthetic Polymer Gels Responding to External Glucose Concentration: Their Preparation and Application to On−Off Regulation of Insulin Release. Journal of the American Chemical Society. 120 (1998), pp. 12694–12695.

255. J. Shang, J. Yan, Z. Zhang, X. Huang, P. Maturavongsadit, B. Song, Y. Jia, T. Ma, D. Li, K. Xu, Q. Wang, Q. Lin, A hydrogel-based glucose affinity microsensor. Sens. Actuators B Chem. 237, 992–998 (2016).

256. T. Kajisa, T. Sakata, Glucose-responsive hydrogel electrode for biocompatible glucose transistor. Sci. Technol. Adv. Mater. 18, 26–33 (2017).

257. J. Yu, J. Wang, Y. Zhang, G. Chen, W. Mao, Y. Ye, A. R. Kahkoska, J. B. Buse, R. Langer, Z. Gu, Glucose-responsive insulin patch for the regulation of blood glucose in mice and minipigs. Nat Biomed Eng. 4, 499–506 (2020).

258. J. Wang, Z. Wang, J. Yu, A. R. Kahkoska, J. B. Buse, Z. Gu, Glucose-Responsive Insulin and Delivery Systems: Innovation and Translation. Adv. Mater. 32, e1902004 (2020).

259. H. Lee, C. Song, Y. S. Hong, M. S. Kim, H. R. Cho, T. Kang, K. Shin, S. H. Choi, T. Hyeon, D.-H. Kim, Wearable/disposable sweat-based glucose monitoring device with multistage transdermal drug delivery module. Sci Adv. 3, e1601314 (2017).

260. M. T. Ghoneim, A. Nguyen, N. Dereje, J. Huang, G. C. Moore, P. J. Murzynowski, C. Dagdeviren, Recent Progress in Electrochemical pH-Sensing Materials and Configurations for Biomedical Applications. Chem. Rev. 119, 5248–5297 (2019).

261. Y. Zhao, M. Lei, S.-X. Liu, Q. Zhao, Smart hydrogel-based optical fiber SPR sensor for pH measurements. Sensors and Actuators B: Chemical. 261 (2018), pp. 226–232.

262. N. Abu-Thabit, Y. Umar, E. Ratemi, A. Ahmad, F. Ahmad Abuilaiwi, A Flexible Optical pH Sensor Based on Polysulfone Membranes Coated with pH-Responsive Polyaniline Nanofibers. Sensors . 16 (2016), doi:10.3390/s16070986.

263. Y. Zhang, H. Ji, D. Snow, R. Sterling, G. M. Brown, A pH Sensor Based on a Microcantilever Coated with Intelligent Hydrogel. Instrumentation Science & Technology. 32 (2004), pp. 361–369.
264. S. Naficy, G. M. Spinks, G. G. Wallace, Thin, tough, pH-sensitive hydrogel films with rapid load recovery. ACS Appl. Mater. Interfaces. 6, 4109–4114 (2014).
265. A. Shastri, L. M. McGregor, Y. Liu, V. Harris, H. Nan, M. Mujica, Y. Vasquez, A. Bhattacharya, Y. Ma, M. Aizenberg, O. Kuksenok, A. C. Balazs, J. Aizenberg, X. He, An aptamer-functionalized chemomechanically modulated biomolecule catch-and-release system. Nature Chemistry. 7 (2015), pp. 447–454.
266. Q. T. Trinh, G. Gerlach, J. Sorber, K.-F. Arndt, Hydrogel-based piezoresistive pH sensors: Design, simulation and output characteristics. Sensors and Actuators B: Chemical. 117 (2006), pp. 17–26.
267. A. Richter, G. Paschew, S. Klatt, J. Lienig, K.-F. Arndt, H.-J. P. Adler, Review on Hydrogel-based pH Sensors and Microsensors. Sensors . 8, 561–581 (2008).
268. M.-J. Yin, M. Yao, S. Gao, A. Ping Zhang, H.-Y. Tam, P.-K. A. Wai, Rapid 3D Patterning of Poly(acrylic acid) Ionic Hydrogel for Miniature pH Sensors. Advanced Materials. 28 (2016), pp. 1394–1399.
269. C. Ruan, K. Zeng, C. A. Grimes, A mass-sensitive pH sensor based on a stimuli-responsive polymer. Analytica Chimica Acta. 497 (2003), pp. 123–131.
270. B. Gu, M.-J. Yin, A. P. Zhang, J.-W. Qian, S. He, Low-cost high-performance fiber-optic pH sensor based on thin-core fiber modal interferometer. Opt. Express. 17, 22296–22302 (2009).
271. A. Richter, A. Bund, M. Keller, K.-F. Arndt, Characterization of a microgravimetric sensor based on pH sensitive hydrogels. Sensors and Actuators B: Chemical. 99 (2004), pp. 579–585.
272. F.-S. Wang, T.-F. Wang, H.-H. Lu, W.-S. Ao-Ieong, J. Wang, H.-L. Chen, C.-H. Peng, Highly Stretchable Free-Standing Poly(acrylic acid)-block-poly(vinyl alcohol) Films Obtained from Cobalt-Mediated Radical Polymerization. Macromolecules. 50 (2017), pp. 6054–6063.
273. J. Liu, X. Zhang, Y. Liu, M. Rodrigo, P. D. Loftus, J. Aparicio-Valenzuela, J. Zheng, T. Pong, K. J. Cyr, M. Babakhanian, J. Hasi, J. Li, Y. Jiang, C. J. Kenney, P. J. Wang, A. M. Lee, Z. Bao, Intrinsically stretchable electrode array enabled in vivo electrophysiological mapping of atrial fibrillation at cellular resolution. Proc. Natl. Acad. Sci. U. S. A. (2020), doi:10.1073/pnas.2000207117.
274. J. M. Nassar, M. D. Cordero, A. T. Kutbee, M. A. Karimi, G. A. Torres Sevilla, A. M. Hussain, A. Shamim, M. M. Hussain, Paper Skin Multisensory Platform for Simultaneous Environmental Monitoring. Advanced Materials Technologies. 1 (2016), p. 1600004.
275. D. H. Ho, Q. Sun, S. Y. Kim, J. T. Han, K. Do Hwan, J. H. Cho, Stretchable and Multimodal All Graphene Electronic Skin. Advanced Materials. 28 (2016), pp. 2601–2608.
276. M. Segev-Bar, N. Bachar, Y. Wolf, B. Ukrainsky, L. Sarraf, H. Haick, Multi-Parametric Sensing Platforms Based on Nanoparticles. Advanced Materials Technologies. 2 (2017), p. 1600206.
277. N. T. Tien, S. Jeon, D.-I. Kim, T. Q. Trung, M. Jang, B.-U. Hwang, K.-E. Byun, J. Bae, E. Lee, J. B. -H. Tok, Z. Bao, N.-E. Lee, J.-J. Park, A Flexible Bimodal Sensor Array for Simultaneous Sensing of Pressure and Temperature. Advanced Materials. 26 (2014), pp. 796–804.

278. S. Harada, W. Honda, T. Arie, S. Akita, K. Takei, Fully printed, highly sensitive multifunctional artificial electronic whisker arrays integrated with strain and temperature sensors. ACS Nano. 8, 3921–3927 (2014).
279. Z. Lei, Q. Wang, P. Wu, A multifunctional skin-like sensor based on a 3D printed thermo-responsive hydrogel. Materials Horizons. 4 (2017), pp. 694–700.
280. D. Rus, M. T. Tolley, Design, fabrication and control of soft robots. Nature. 521, 467–475 (2015).
281. S. Chen, Y. Cao, M. Sarparast, H. Yuan, L. Dong, X. Tan, C. Cao, Soft Crawling Robots: Design, Actuation, and Locomotion. Advanced Materials Technologies. 5 (2020), p. 1900837.
282. R. F. Shepherd, F. Ilievski, W. Choi, S. A. Morin, A. A. Stokes, A. D. Mazzeo, X. Chen, M. Wang, G. M. Whitesides, Multigait soft robot. Proc. Natl. Acad. Sci. U. S. A. 108, 20400–20403 (2011).
283. G. Gu, J. Zou, R. Zhao, X. Zhao, X. Zhu, Soft wall-climbing robots. Science Robotics. 3 (2018), p. eaat2874.
284. D. Chen, Q. Pei, Electronic Muscles and Skins: A Review of Soft Sensors and Actuators. Chem. Rev. 117, 11239–11268 (2017).
285. T. Li, G. Li, Y. Liang, T. Cheng, J. Dai, X. Yang, B. Liu, Z. Zeng, Z. Huang, Y. Luo, Fast-moving soft electronic fish Sci. Advocate. 3, e1602045 (2017).
286. H.-W. Huang, M. S. Sakar, A. J. Petruska, S. Pané, B. J. Nelson, Soft micromachines with programmable motility and morphology. Nat. Commun. 7, 12263 (2016).
287. X. Qian, Y. Zhao, Y. Alsaid, X. Wang, M. Hua, T. Galy, H. Gopalakrishna, Y. Yang, J. Cui, N. Liu, M. Marszewski, L. Pilon, H. Jiang, X. He, Artificial phototropism for omnidirectional tracking and harvesting of light. Nat. Nanotechnol. 14, 1048–1055 (2019).
288. Y. Zhao, C. Xuan, X. Qian, Y. Alsaid, M. Hua, L. Jin, X. He, Soft phototactic swimmer based on self-sustained hydrogel oscillator. Science Robotics. 4 (2019), p. eaax7112.
289. M. Baumgartner, F. Hartmann, M. Drack, D. Preninger, D. Wirthl, R. Gerstmayr, L. Lehner, G. Mao, R. Pruckner, S. Demchyshyn, L. Reiter, M. Strobel, T. Stockinger, D. Schiller, S. Kimeswenger, F. Greibich, G. Buchberger, E. Bradt, S. Hild, S. Bauer, M. Kaltenbrunner, Resilient yet entirely degradable gelatin-based biogels for soft robots and electronics. Nat. Mater. (2020), doi:10.1038/s41563-020-0699-3.
290. C. Yang, W. Wang, C. Yao, R. Xie, X.-J. Ju, Z. Liu, L.-Y. Chu, Hydrogel Walkers with Electro-Driven Motility for Cargo Transport. Sci. Rep. 5, 13622 (2015).
291. H. Yuk, S. Lin, C. Ma, M. Takaffoli, N. X. Fang, X. Zhao, Hydraulic hydrogel actuators and robots optically and sonically camouflaged in water. Nat. Commun. 8, 14230 (2017).
292. E. Palleau, D. Morales, M. D. Dickey, O. D. Velev, Reversible patterning and actuation of hydrogels by electrically assisted ionoprinting. Nat. Commun. 4, 2257 (2013).
293. D. J. Beebe, J. S. Moore, J. M. Bauer, Q. Yu, R. H. Liu, C. Devadoss, B. H. Jo, Functional hydrogel structures for autonomous flow control inside microfluidic channels. Nature. 404, 588–590 (2000).
294. A. S. Gladman, E. A. Matsumoto, R. G. Nuzzo, L. Mahadevan, J. A. Lewis, Biomimetic 4D printing. Nat. Mater. 15, 413–418 (2016).
295. D. Morales, E. Palleau, M. D. Dickey, O. D. Velev, Electro-actuated hydrogel walkers with dual responsive legs. Soft Matter. 10, 1337–1348 (2014).
296. O. Erol, A. Pantula, W. Liu, D. H. Gracias, Transformer Hydrogels: A Review. Advanced Materials Technologies. 4 (2019), p. 1900043.

297. M. Ding, L. Jing, H. Yang, C. E. Machnicki, X. Fu, K. Li, I. Y. Wong, P.-Y. Chen, Multifunctional soft machines based on stimuli-responsive hydrogels: from freestanding hydrogels to smart integrated systems. Materials Today Advances. 8, 100088 (2020).
298. C. H. Yang, S. Zhou, S. Shian, D. R. Clarke, Z. Suo, Organic liquid-crystal devices based on ionic conductors. Materials Horizons. 4 (2017), pp. 1102–1109.
299. C. H. Yang, B. Chen, J. Zhou, Y. M. Chen, Z. Suo, Electroluminescence of Giant Stretchability. Advanced Materials. 28 (2016), pp. 4480–4484.
300. R. L. Truby, M. Wehner, A. K. Grosskopf, D. M. Vogt, S. G. M. Uzel, R. J. Wood, J. A. Lewis, Soft Somatosensitive Actuators via Embedded 3D Printing. Adv. Mater. 30, e1706383 (2018).
301. E. Acome, S. K. Mitchell, T. G. Morrissey, M. B. Emmett, C. Benjamin, M. King, M. Radakovitz, C. Keplinger, Hydraulically amplified self-healing electrostatic actuators with muscle-like performance. Science. 359 (2018), pp. 61–65.
302. V. L. Pushparaj, M. M. Shaijumon, A. Kumar, S. Murugesan, L. Ci, R. Vajtai, R. J. Linhardt, O. Nalamasu, P. M. Ajayan, Flexible energy storage devices based on nanocomposite paper. Proceedings of the National Academy of Sciences. 104 (2007), pp. 13574–13577.
303. B. Scrosati, Paper powers battery breakthrough. Nature Nanotechnology. 2 (2007), pp. 598–599.
304. L. Hu, J. W. Choi, Y. Yang, S. Jeong, F. La Mantia, L.-F. Cui, Y. Cui, Highly conductive paper for energy-storage devices. Proceedings of the National Academy of Sciences. 106 (2009), pp. 21490–21494.
305. L. Hu, H. Wu, F. La Mantia, Y. Yang, Y. Cui, Thin, Flexible Secondary Li-Ion Paper Batteries. ACS Nano. 4 (2010), pp. 5843–5848.
306. J. Yoon, S. Jo, I. S. Chun, I. Jung, H.-S. Kim, M. Meitl, E. Menard, X. Li, J. J. Coleman, U. Paik, J. A. Rogers, GaAs photovoltaics and optoelectronics using releasable multilayer epitaxial assemblies. Nature. 465 (2010), pp. 329–333.
307. J. Peet, J. Y. Kim, N. E. Coates, W. L. Ma, D. Moses, A. J. Heeger, G. C. Bazan, Efficiency enhancement in low-bandgap polymer solar cells by processing with alkane dithiols. Nature Materials. 6 (2007), pp. 497–500.
308. S. Xu, Y. Qin, C. Xu, Y. Wei, R. Yang, Z. L. Wang, Self-powered nanowire devices. Nature Nanotechnology. 5 (2010), pp. 366–373.
309. S. Wang, L. Lin, Z. L. Wang, Nanoscale Triboelectric-Effect-Enabled Energy Conversion for Sustainably Powering Portable Electronics. Nano Letters. 12 (2012), pp. 6339–6346.
310. Z. L. Wang, J. Chen, L. Lin, Progress in triboelectric nanogenerators as a new energy technology and self-powered sensors. Energy & Environmental Science. 8 (2015), pp. 2250–2282.
311. S. Wang, L. Lin, Z. L. Wang, Triboelectric nanogenerators as self-powered active sensors. Nano Energy. 11 (2015), pp. 436–462.
312. J. Chun, B. U. Ye, J. W. Lee, D. Choi, C.-Y. Kang, S.-W. Kim, Z. L. Wang, J. M. Baik, Boosted output performance of triboelectric nanogenerator via electric double layer effect. Nature Communications. 7 (2016), , doi:10.1038/ncomms12985.
313. J. Bae, J. Lee, S. Kim, J. Ha, B.-S. Lee, Y. Park, C. Choong, J.-B. Kim, Z. L. Wang, H.-Y. Kim, J.-J. Park, U.-I. Chung, Flutter-driven triboelectrification for harvesting wind energy. Nature Communications. 5 (2014), , doi:10.1038/ncomms5929.

314. F. Yi, J. Wang, X. Wang, S. Niu, S. Li, Q. Liao, Y. Xu, Z. You, Y. Zhang, Z. L. Wang, Stretchable and Waterproof Self-Charging Power System for Harvesting Energy from Diverse Deformation and Powering Wearable Electronics. ACS Nano. 10 (2016), pp. 6519–6525.
315. Y.-C. Lai, J. Deng, S. Niu, W. Peng, C. Wu, R. Liu, Z. Wen, Z. L. Wang, Electric Eel-Skin-Inspired Mechanically Durable and Super-Stretchable Nanogenerator for Deformable Power Source and Fully Autonomous Conformable Electronic-Skin Applications. Advanced Materials. 28 (2016), pp. 10024–10032.
316. B.-U. Hwang, J.-H. Lee, T. Q. Trung, E. Roh, D.-I. Kim, S.-W. Kim, N.-E. Lee, Transparent Stretchable Self-Powered Patchable Sensor Platform with Ultrasensitive Recognition of Human Activities. ACS Nano. 9 (2015), pp. 8801–8810.
317. F. Yi, L. Lin, S. Niu, P. K. Yang, Z. Wang, J. Chen, Y. Zhou, Y. Zi, J. Wang, Q. Liao, Y. Zhang, Z. L. Wang, Stretchable-Rubber-Based Triboelectric Nanogenerator and Its Application as Self-Powered Body Motion Sensors. Advanced Functional Materials. 25 (2015), pp. 3688–3696.
318. X. Chen, X. Pu, T. Jiang, A. Yu, L. Xu, Z. L. Wang, Tunable Optical Modulator by Coupling a Triboelectric Nanogenerator and a Dielectric Elastomer. Advanced Functional Materials. 27 (2017), p. 1603788.
319. L. Sun, S. Chen, Y. Guo, J. Song, L. Zhang, L. Xiao, Q. Guan, Z. You, Ionogel-based, highly stretchable, transparent, durable triboelectric nanogenerators for energy harvesting and motion sensing over a wide temperature range. Nano Energy. 63 (2019), p. 103847.
320. B. Ying, Z. Chen, R. Zuo, J. Li, X. Liu, An anti-freezing, ambient-stable and highly stretchable ionic skin with strong surface adhesion for wearable sensing and soft robotics. In submission (2020).

Link between Chapter 2 and Chapter 3

In the previous chapter, I reviewed the recent advances of hydrogel skin-like devices for wearables and soft robotics. I briefly introduce the basic concept of hydrogels and summarize their tough and ionically conductive formats. I also reviewed the strategies to design bioinspired hydrogel matrix with enhanced merits including the ambient stability, antifreezing capability. After summarizing applications of hydrogel skin-like ionic devices for wearables, soft robotics and energy harvesting, I propose and highlight several challenges to be addressed in this thesis for the real-world applications of wearable electronics and soft robotics. Those challenges include limited functionality, low stability, high power-consumption, and poor adhesive.

Next chapter will mainly endow hydrogels with multifunctionality, capable of self-powering multimodal sensing with ambient stability. Specifically, I develop a diode-like artificial ionic skin (AIskin) that consists of a bilayer double-network hydrogel structure charged with opposite polyelectrolytes. This Aiskin exhibits high toughness, stretchability, ambient stability, transparency and controlled ion mobility and can convert mechanical strain and humidity into multiple electronic signals and sensing without external power supply.

Chapter 3

An ambient-stable and stretchable ionic skin with multimodal sensation

3. Chapter 3: An ambient-stable and stretchable ionic skin with multimodal sensation

Binbin Ying[1,2], Qiyang Wu[1,2], Jianyu Li[1,3*], Xinyu Liu[1,2,4*]

[1]Department of Mechanical Engineering, McGill University, 817 Sherbrooke Street West, Montreal, QC H3A 0C3, Canada.

[2]Department of Mechanical and Industrial Engineering, University of Toronto, 5 King's College Road, Toronto, Ontario, M5S 3G8, Canada.

[3]Department of Biomedical Engineering, McGill University, 3775 rue University, Montreal, QC H3A 2B4, Canada

[4]Institute of Biomaterials and Biomedical Engineering, University of Toronto, 164 College Street, Toronto, ON M5S 3G9, Canada

*Corresponding authors. Emails: jianyu.li@mcgill.ca; xyliu@mie.utoronto.ca.

Materials Horizons, Royal Society of Chemistry, 2020,7, 477-488

DOI: 10.1039/c9mh00715f.

Reproduced and adapted with permission from Royal Society of Chemistry

3.1. Conceptual insights

To bridge the gap between human skin and its artificial counterparts, hydrogel iontronics is emerging as a promising alternative to electronic artificial skins, as it better mimics the human skin in terms of mechanical properties and sensing principles (i.e., sensing signals are transmitted through ions rather than electrons). Here, inspired by the salient features of human skin, we report a novel design of hydrogel iontronics for developing an artificial ionic skin (AIskin) with unprecedented properties. Different from existing designs of hydrogel iontronics with only conductive ionic hydrogels, the AIskin features diode-like electrical characteristics based on controlled ionic movements, which is an analog of transmembrane ion transport of neuron sensors in human skin. It shows high stretchability and toughness, high optical transparency and ambient stability. It can sense force, strain and humidity by transducing mechanical and chemical inputs into four types of electrical signals (e.g., resistance, capacitance, open-circuit voltage and short-circuit current), among which the last two are self-generated without the need of external power supply. We demonstrate the application of the AIskin to wearable strain-humidity sensing, human-machine interaction, and energy harvesting. Thanks to the combination of its unique mechanical properties and multimodal sensation, the AIskin could enable the development of next-generation artificial skins with improved functionality and human-machine integration, and thus stimulate the further growth of hydrogel iontronics as a complementary technology to existing wearable and stretchable electronics.

3.2. Introduction

Skin is the largest organ of the human body, serving as physical and hygroscopic barriers to protect the inner body and control transepidermal water exchange, while containing signal sensors to perceive various environmental stimuli such as pressure, deformation, and temperature (*1-4*). These functions are linked with salient features of the skin: highly deformable polymer networks to resist physical damages (*5*); hygroscopic compositions (e.g., pyrrolidone carboxylic acid) to retain water (*6*); a variety of sensory neurons (e.g., mechanoreceptors, thermoreceptors, and pain receptors) powered by biological sources to transduce stimuli into controlled ion movements and propagation of action potentials (**Figure 3.1**A) (*3, 7, 8*). To recapitulate these features for wearable electronics and healthcare applications, significant efforts have been made on engineering electronic counterparts of the human skin (i.e., electronic skin), leading to various design strategies involving electronic components, elastomeric substances or a combination of thereof (*9*-*20*). Despite their remarkable functionalities and applications that have been demonstrated, existing electronic skins differ from the native skin in terms of charge carriers (electrons versus ions in native skin), the content and permeability of water, resulting in limited biocompatibility and suboptimal human-machine interfaces especially for the long-term usage (*21*, *22*).

While the gap between real and electronic skins persists, recent progress of iontronics highlights the use of hydrated and ionic materials like hydrogels for making ionic devices (i.e., pressure sensors (*23, 24*) and touchpad (*25*)), capable of transducing mechanical stimuli into electrical signals such as of capacitance or resistance. The existing ionic devices usually convert the applied touch, pressure, deformation or temperature into a change in their resistance or capacitance, the electrical readout of which requires continuous power supply with voltages typically of 1-10 V (*26*) and power consumptions of up to 0.015 mW (i.e., around 3 AA batteries per week) (*24*). Although stretchable batteries can be integrated with those ionic devices (*27*), the requirement of external or on-chip power supplies still, to some extent, compromises long-term usage. Further development is needed toward a multifunctional self-powered ionic device. First, the devices should equip with self-generated power to mitigate the need of external power supply for long-term usage. Second, they need to enable the sensing of more than one stimulus like the human skin. In addition, the devices must be physically stable (i.e., mitigating water loss) during usage and biocompatible when interfacing with the human body.

To meet the aforementioned requirements, we report a new design and method to make ionic devices, called artificial ionic skin (AIskin), capable of recapitulating the salient features of the human skin. AIskin exhibits excellent skin-like mechanical deformability and ambient stability.

It can sustain more than 400% strains without rupture and maintain its function after storage and 800 cycles of deformation. Different from the previous ionic devices consisting of homogenous hydrogels and/or elastomer, our design utilizes a heterogenous hydrogel of bilayer structure, which can realize controlled ion movements responsive to the mechanical deformation and humidity. This design resembles the conventional semiconductive diodes structurally and the sensory neurons in human skin in terms of stimuli sensing function. The AIskin converts both mechanical stimuli and humidity into four types of electrical signals: resistance, capacitance, open circuit voltage (OCV) and short circuit current (SCC), of which the latter two signals are self-generated without external power supply. These features of our AIskin potentially blur the boundary between humans and devices, and promise board use ranging from wearable and implantable devices, soft robotics to wound dressing capable of monitoring the local body motion and moisture of the wound bed (*28*-*30*).

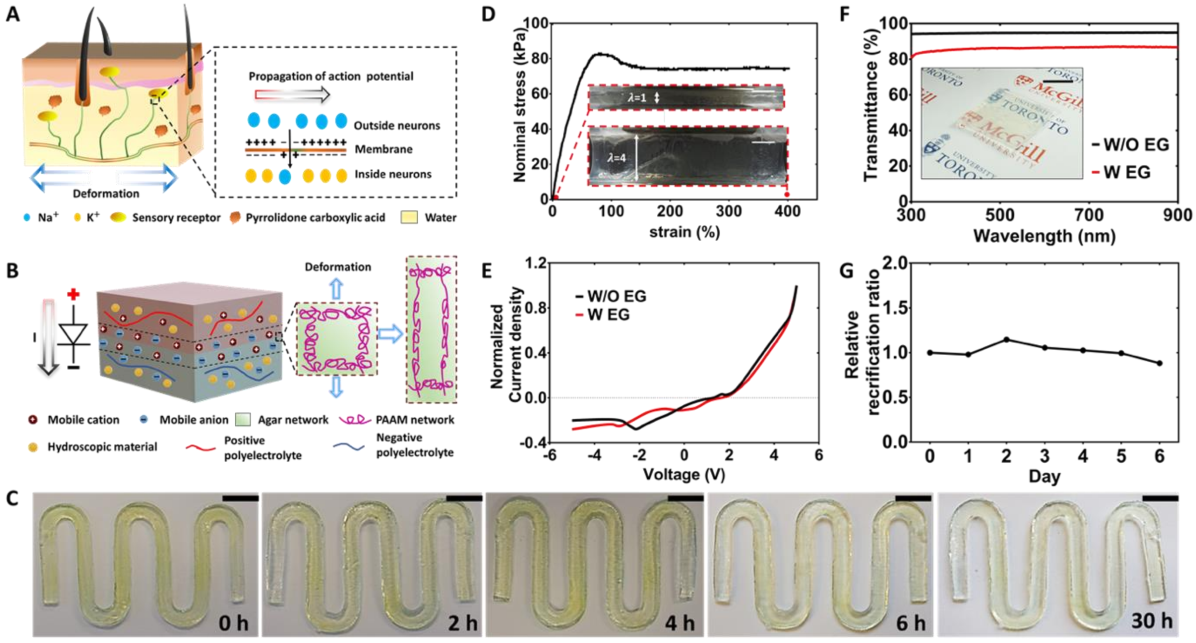

Figure 3.1. Design and characterization of an AIskin. (**A**) Schematic of the human skin that resists physical damage, holds water due to the hygroscopic substance (i.e., pyrrolidone carboxylic

acid), and transports ionic signal directionally within sensory neurons. (**B**) Schematic illustration of the AIskin. The top layer is stretchable hydrogel containing positively-charged polyelectrolyte, and the bottom layer is stretchable hydrogel with the negative polyelectrolyte. The area between two dashes indicates the depletion zone at the interface. (**C**) AIskin strips show no additional swelling after 30-hour desalination in DI water, scale bar = 1 cm. Yellow dye is added for visualization. (**D**) AIskin is stretched more than 400% (down inset) of the original length (upper inset) without fracture, scale bar in the two insets is 10 mm. (**E**) The rectifying performance of AIskin with (W, red line) and without (W/O, black line) EG. Scan rate is 179 mV s^{-1}. (**F**) Transmittance of an AIskin with and without EG right after synthesis. The thickness of the AIskin is 3 mm; the inset shows a transparent AIskin, scale bar is 20 mm. (**G**) Rectifying stability of an AIskin with EG at the RH of 65%.Results and Discussion

3.3. Results and discussion

3.3.1. Design of AIskin

The AIskin is a bilayer double-network hydrogel with hygroscopic substances and positively- and negatively-charged polyelectrolytes in its two separate layers (**Figure 3.1**B). A hygroscopic material was incorporated into the matrix to reduce the loss of water and achieve humidity sensing capability; ethylene glycol (EG) was used as it is a neutral hygroscopic reagent and expected to impact minimally on the controlled ionic movement in the AIskin. The model polyelectrolytes used here include poly (sodium 4-styrenesulfonate) (PSS) and poly (diallyl dimethylammonium chloride) (PDAC), which carry negative and positive charges fixed to their polymer chains, respectively. The hydrogel matrix is composed of an interpenetrating agarose-polyacrylamide (Agar-PAAm) network, and the selection of Agar and PAAm for constructing the double-network hydrogel was due to their confirmed biocompatibility and wide use in biomedical

(*31*). Such matrix features a unique design, where two initially separate pieces of Agar hydrogel, containing PSS and PDAC respectively, are bonded together with a single interpenetrating PAAm network into a monolithic "diode-like" device (see details in **Figure S3.1** and the **Materials and Methods** section). Compared with the previously demonstrated one-pot synthesis (*32*), this method significantly reduces additional swelling of the AIskin in aqueous environments (**Figure 3.1**C) making it possible to predefine the geometries of the Agar-PAAm hydrogel and the resulting devices. Agar, as the first network, confines the polyelectrolyte chains and only allows the movement of mobile ions; this enables the directional ion transmission. We hypothesized that this unique design could lead to diode-like electronic characteristics (i.e., unidirectional ion movements resulting in an OCV between the two hydrogel layers), as well as superior stretchability and physical integrity (particularly strong bilayer bonding) of the heterogenous device.

3.3.2. Mechanical properties of the AIskin

The mechanical performance of the AIskin was first evaluated. The pure-shear tests showed the AIskin can be stretched at more than 400% of its initial length without rupture (**Figure 3.1**D and Movie S3.1), and the measured fracture energy (i.e., toughness) was up to 1,826 Jm^{-2} (**Figure 3.1**D, **Figure S3.2**A-B). Interestingly, unlike other double-network hydrogels reported previously (*32-34*), the AIskin showed a characteristic elastic-nearly-plastic behavior, in which the stress plateau, 'yielding strength', was at 82 kPa and the critical strain was 100% (**Figure 3.1**D). The transition can be attributed to the breakage of physical cross-links of the Agar network and the effective crack-bridging effect of the PAAm network. This feature indicates a superior energy dissipating capacity, which may limit the stress transfer to the underlying tissues when interfacing with the human body (*33*). To verify this, cyclic tensile and compression tests were carried out;

the testing results revealed a large hysteresis loop in the first loading-unloading cycle (**Figure S3.2**C-D), corresponding to the breakage of physical cross-links of the Agar network. Following the first cycle, the hydrogel became elastic due to the permanent cross-links of the PAAm network. To examine the integrity of the bilayer structure, we performed standard 180-degree peeling tests (**Figure S3.2**E). The fracture appeared at one open end of the hydrogel layer with PSS without any debonding at the interface observed. In addition, no debonding of the two hydrogel layers was observed during the compression and tensile tests of the AIskin, indicating that the bilayer structure held strong structural integrity. The results confirmed that the AIskin is highly stretchable and tough, in addition to its intrinsic heterogeneity (required for the diode function) to be shown below. It will meet the mechanical requirements of wearable electronics given the maximum strain (~55%) of human motion (*35*).

3.3.3. Diode-like electrical properties of the AIskin

The electrical characteristics of the AIskin was then examined. Stainless steel electrodes (0.02 mm thick) were used in the tests. **Figure 3.1**E illustrates the representative current-voltage curves of the AIskin resembling those of conventional semiconductor diodes. The device is ON under forward bias (offset voltage: 2V, **Figure 3.1**E), and OFF under reverse bias (<2V). The results are consistent with the mechanisms proposed previously (*36, 37*): under negative potential, the current density in the backward direction is dramatically reduced compared to that in the forward direction; when the positive potential goes higher than 1.23 V to overcome barriers of electrode reaction, the redox reactions of water begins with H^+ and OH^- produced on the positive and negative electrodes, respectively; with the applied potential increased beyond >2V, more ions (e.g., H^+ and OH^-) are created and diffuse across the charged polyelectrolyte layer continuously, leading to the formation of water at the interface and the substantial increase of current density.

The critical voltage was also verified with hydrogels with single polyelectrolyte (either PSS or PDAC) in **Figure S3.3**A where the current density was raised up upon the potential greater than 2 V. The minute non-zero current at zero potential can be explained by the charging and discharging effects within the diode junction capacitance and the electrical double layer (EDL) capacitance between the electrode and hydrogel when the voltage scans from +5V to 0V (*38*, *39*). Further capacitance-voltage (C-V) testing confirmed the existence of the junction capacitance within the ionic diode, by showing an unsymmetrical C-V response of the AIskin and symmetrical C-V responses of the bilayer PSS Hydrogel and the bilayer PDAC hydrogel (**Figure S3.4**A), The AIskin also revealed a frequency-dependent C-V characteristic in the negative bias range (**Figure S3.4**B), which is typical for conventional electronic diodes (*40*).

Similar to other material matrices consisting of oppositely-charged polyelectrolytes, our AIskin functions like a diode with a rectification ratio of ~5 (**Figure 3.1**E), which is primarily attributed to the presence of a depletion zone at the interface of the oppositely-charged hydrogel bilayers. There was a reduction of the rectification ratio when the sweeping rate increased beyond 277 mV s^{-1} (**Figure S3.3**B-C). This observation confirms that the diode current was caused by unidirectional movements of the mobile ions in the AIskin, rather than by other types of charge carriers (*41*). The depletion zone is only accessible to selective ions (Na^+, H^+, OH^-, and Cl^-) under positive potentials, indicative of controlled ion movements within the AIskin. In contrast, no rectifying effect was observed on samples consisting of hydrogels with sole positively- or negatively-charged polyelectrolytes (**Figure S3.3**A). The controlled ion movement resembles the selective ionic movement in sensory neurons in natural skins.

3.3.4. Ambient stability of the AIskin

We next examined the effect of hygroscopic substance on ambient stability of the AIskin. Concentrated salts such as lithium chloride and calcium chloride, used in previous studies (*42*), are inapplicable here as they will overwhelm the desired charge distribution within the AIskin and result in loss of diode-like response. To select a suitable hygroscopic substance, we used two criteria: (i) it should have no impact on the controlled ion movements in the AIskin matrix; and (ii) it can maintain the rectifying performance of the AIskin. Two neutral hygroscopic substances, EG and glycerol, were tested. We first demonstrated that both materials did not alter the electrical characteristics of the AIskin. The AIskin exhibited a good rectifying effect right after the addition of EG (**Figure 3.1**E) or glycerol (**Figure S3.3**D). We also examined the rectification stability of our AIskin over long-term exposure in air. After three days of exposure under ambient conditions of a laboratory environment (21 °C and relative humidity of 60~65%), the AIskin with EG maintained a higher current density and a smaller reduction of the rectification ratio than the one with glycerol (**Figure S3.3**D-F). In addition, we also quantified the effect of the EG concentration for device treatment on the device rectification ratio, and found that the AIskin treated with 50% (v/v) EG maintained the highest rectification ratio after three days of exposure under the same laboratory environment (**Figure S3.3**G-I). Therefore, the 50% (v/v) EG was selected as the hygroscopic material to construct the ambient stable AIskin. The hydrogels treated with 50% (v/v) EG also maintained high transparency (**Figure 3.1**F) quantified by a transmittance of 81-87% in the range of 300-900 nm, slightly lower than that (95%) of the samples without the EG treatment (**Figure 3.1**F). Higher transparency can be realized by reduce the thickness of AIskin if necessary **(Figure S3.5).**

To further study the ambient stability of the EG-laden AIskin, the rectification ratios and mass changes of the samples stored at different moisture conditions were tested over six days. No obvious decrease of the rectification ratio was observed on the samples stored at the relative humidity (RH) of 65% over six days (**Figure 3.1**G). The corresponding sample mass dropped to 77% of its original mass in the first three days of storage, and then became relatively stable in the range of 67-73% of the original mass during day 3-6 (**Figure S3.6**). Notably, in an extremely dry environments (RH = 13%), our EG-laden AIskin still retained 50% of its original mass over six days storage (**Figure S3.6**), and showed no significant difference of the rectification ratio compared with the ones stored at higher RHs such as 65% and 85% (**Figure S3.7**A). In contrast, the devices without EG lost both the water content and rectifying effect entirely at the RH of 13% (**Figure S3.6** and **Figure S3.7**B). The stability of other electrical output signals (e.g., OCV) of the AIskin over storage will be discussed in the following section. These observations indicate that the EG-laden AIskin can preserve its electronic diode function in a wide range of RHs and could serve as a relatively ambient-stable material for many applications where the device needs to maintain its electronic functions at different moisture conditions.

3.3.5. Strain sensing capability of the AIskin based on four types of output signal

The hydrogel-based ionic diode has been applied to energy harvesting from mechanical compressions by converting its compressive deformation into the change of built-in potential and the diffusion of free ions (*37*). Therefore, we hypothesized that our AIskin can sense mechanical stimuli not only through changes of its resistance and capacitance but also through changes in its OCV and SCC. Next, we characterized the AIskin for strain sensing based on different types of output signal. After ensuring that diode-like electrical performance is repeatable for multiple current-voltage measurements on one device **(Figure S3.7**C**),** different compressive strains were applied along the thickness of the AIskin (in the range of 6-44%). The device still maintained its electrical characteristic of a diode with a slight increase of its rectification ratio (**Figure S3.7**D-E). This phenomenon can be explained by the fact that, with a compressive strain, the counterionic current carriers migrate a shorter distance to the opposite electrode with the decrease of the device thickness, leading to an increase in the conductivity of the forward-based diode in the forward direction. The conductivity of the backward-based diode is less dependent on the thickness of the AIskin due to the depletion zone with extremely low conductivity (*41*).

Next, we demonstrate that the AIskin can serve as a strain sensor. Due to its unique electronic properties, the AIskin exhibits unprecedented strain-sensing capacity, i.e., it transforms mechanical stimuli into self-generated electrical signals (i.e., OCV and SSC), besides its conventional sensing modes (e.g., resistance- and capacitance-based sensing).

The response of resistance and capacitance resembles that of ionic conductors with homogenous charge distribution (i.e., homogenous ionic conductors). **Figure 3.2**A shows a resistance-strain calibration curve of the EG-laden AIskin, which was collected under a forward-bias voltage of 3 V. As the compressive strain increased from 10% to 50%, the resistance at the RH of 65% reduced from 20.23 kΩ to 4.54 kΩ. Under compression the device thickness decreased and the device in-plane area increased due to the incompressibility of the AIskin material (*43*). For the resistance-based strain sensing, our AIskin behaves like a homogeneous ionic conductor that detects mechanical strains based on geometry-change-induced resistance change. To confirm this, we compared gauge factors of our AIskin, a bilayer of pure PSS hydrogels, and a bilayer of pure PDAC hydrogels, and found comparable gauge factor values (**Figure S3.8**). The AIskin can also sense strain based on the change in capacitance. **Figure 3.2**B shows that the device capacitance at the RH of 65% increased from 2.85 μF to 9.54 μF as the compressive strain rose from 10% to 50%.

Under compression, besides the increase of the hydrogel-electrode contact area, the effective capacitance per area increases within the hydrogel-electrode interface (**Figure S3.9**A), which is based on the redistribution of free ions and polyelectrolyte backbones within the EDL interfaces during deformation. We found no obvious difference of the capacitive gauge factor (GF_c) among the AIskin, PSS hydrogel bilayer, and PDAC hydrogel bilayer (**Figure S3.9**B-C), confirming that the capacitance change is predominantly due to the increase of capacitance in the EDL interface during compression (*38, 44*). These findings proved that our AIskin can be used for strain detection in wearable applications in the traditional resistance- and capacitance-based sensing modes.

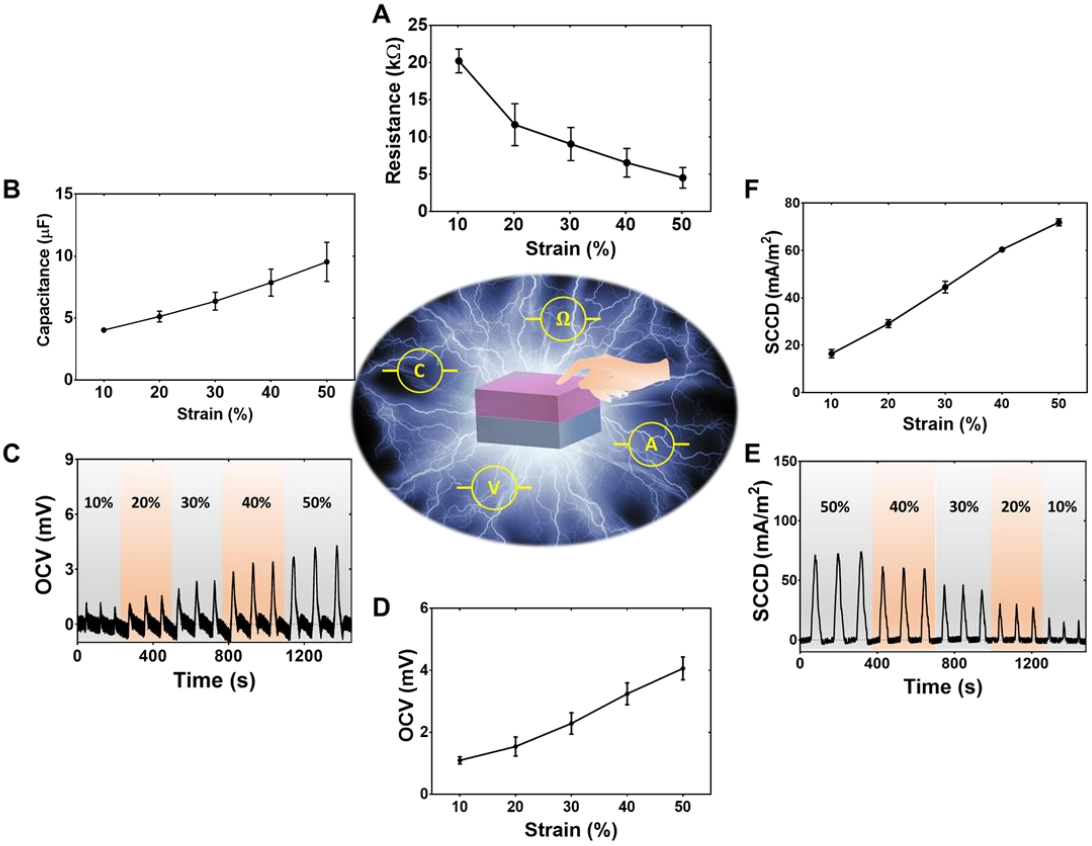

Figure 3.2. Calibration of the EG-laden AIskin for strain sensing based on different output signals. (**A**) Calibration data of device resistance vs. strain at the RH of 65% (N=3). (**B**) Calibration

data of device capacitance vs. strain at the RH of 65% (N=3). The compressive strains increase from 10% to 50%. (**C**) OCV output curves under repeated compression of different strain levels at the RH of 65%. The initial zero-strain OCV levels are adjusted to zero for comparison of the OCV peaks. The strain rising and reducing rates are 5mm min^{-1} and 2.5 mm min^{-1}, respectively. (**D**) Calibration data of OCV peak vs. strain at the RH of 65% (N=3). (**E**) SCCD output curves under repeated compression of different strain levels at the RH of 65%. The initial zero-strain SCCD levels are adjusted to zero for comparison of the SCCD peaks. The strain rising and reducing rates are 5mm min^{-1} and 2.5 mm min^{-1}, respectively. (**F**) Calibration data of SCCD peak vs. strain at the RH of 65% (N=3). Error bars, standard deviations.

In addition, our AIskin also allows for OCV- and SCC-based strain sensing without external power supply (i.e., self-generated sensing modes). Ag/AgCl electrodes were used in these tests for collecting self-generated signals. We first measured the OCV output of our EG-laden AIskin under different compressive strain levels. **Figure 3.2**C shows the measured waveforms of the device OCV with repetitive loads applied to compress the device to five different strain levels at the RH of 65%. From the curve at the strain of 50%, one can find that a potential increase followed an applied strain, and that, once the load was removed, the mobile ion concentrations (thus the build-in potential) gradually recovered to their initial equilibria because of the elastic recovery of the hydrogel matrix. This strain-induced change in OCV can be explained as follows. The concentration gradients of mobile ions in the two hydrogel layers of our AIskin cause diffusion of Na^+ into the PDAC layer and Cl^- into the PSS layer (**Figure 3.1** and **Figure S3.10**), a depletion region is formed at the interface of the two hydrogel layers. The geometry change of an AIskin under deformation can cause the re-diffusion of mobile ions and lead to a change of the device built-in potential (measured as the OCV), and larger deformation results in a larger OCV change.

As the compressive strain increased from 10% to 50%, the peak of the OCV output (the built-in potential of the ionic diode) of the device rose from 1.1 mV to 4.1 mV (**Figure 3.2**D). The OCV response to strain was much more obvious on the ionic-diode AIskin, than that on the PSS/PSS or the PDAC/PDAC hydrogel bilayers (**Figure S3.11**A), suggesting that our diode-like AIskin can better realize self-generated, OCV-based strain sensing.

We then quantified the short circuit current density (SCCD) as a function of the compression strain. **Figure 3.2**E shows the measured waveforms of the device SCCD with repetitive loads applied to compress the device to five different strain levels at the RH of 65%. Taken the data at the strain level of 50% as an example, a strengthened diffusion of ions was observed upon deformation, producing a large current pulse (average: 71.9 mA m^{-2}), which is comparable to that of an ionic system reported previously (*37*). Moreover, thanks to the excellent mechanical property, the AIskin can produce longer current response time (the time duration of half peak SCCD response on strain) than those piezoelectric and triboelectric generators (*45-48*), thus producing substantial energy with mechanical stimulus. Larger geometric deformation of an AIskin results in a larger SCCD. As the compressive strain increased from 10% to 50%, the peak value of SCCD rises from 16.5 mA m^{-2} to 71.9 mA m^{-2} (**Figure 3.2**F). Any deformation-induced redistribution of the mobile ions can lead to a change of the SCCD in the material, and this phenomenon also exists on a bilayer of pure PSS/PSS or PDAC/PDAC hydrogel (**Figure S3.11**B).

In addition, the durability and performance stability of AIskin for strain sensing using self-generated signals were also tested. After ~800 cycles of repeated compressive loading-unloading cycles (16.7 h), the OCV change showed no noticeable degradation at the RH of 13% (**Figure S3.12**A-B), indicating good retention of the strain sensing function of the AIskin over repeated loading under dry environments. Besides, after one month of storage at the RH of 65%, the OCV output of the device showed only a slight decrease comparing to that of a device after 6-day storage at the same RH value (**Figure S3.12**C).

To further test the strain sensing performance of our AIskin, we examined the robustness of AIskin by measuring the four types of device outputs at different rising speeds of the applied compressive strain. The resistance and capacitance outputs at the four deformation speeds are relatively stable [coefficient of variation (CV): 2% for resistance and 8.6% for capacitance] in the strain range of <50% (**Figure S3.13**A-B). Similarly, the OCV and SCCD outputs also remained relatively constant (CV: 2% for OCV and 13% for SCCD) at the four strain rising speeds (**Figure S3.13**C-D). These data confirmed that our AIskin has repeatable strain sensing performance under different compressive loading conditions.

3.3.6. Humidity sensing capability of the AIskin based on four types of output signal

Besides strain sensing, we hypothesized that our EG-laden AIskin can be deployed as a humidity sensor, as the hydrated network can absorb or release water based on the ambient humidity, leading to changes in the ion concentration and distribution (*49*). We conditioned the AIskin in an enclosed chamber of controllable relative humidity for 3 days to allow for sufficient water exchange, and measured the changes in its resistance and capacitance. We found that these signal outputs from the AIskin changed with the relative humidity (RH) of the environment (10-90%). As shown in **Figure 3.3**A, without any strain applied, the device resistance decreased from 327 kΩ to 23.9 kΩ as the RH rose from 13% to 85%, indicating that our AIskin can be used as a humidity sensor based its resistance readout. In a drier environment, the water content inside the AIskin decreases, leading to a lower conductivity of the polyelectrolytes (*50*). Under zero-strain condition, the device capacitance increased substantially with the humidity in the RH range of <65%, and was then saturated at a higher RH level (**Figure 3.3**B). This capacitance saturation phenomenon was further confirmed by the capacitance-RH data under different compressive strain levels (**Figure 3.3**C). It can be understood that the number of dissociated ions and the ion mobility increase with the water content and RH, causing the increase of the effective capacitance within the EDL and depletion zone, and when the system is fully hydrated, this effective capacitance gets saturated (*50*, *51*).

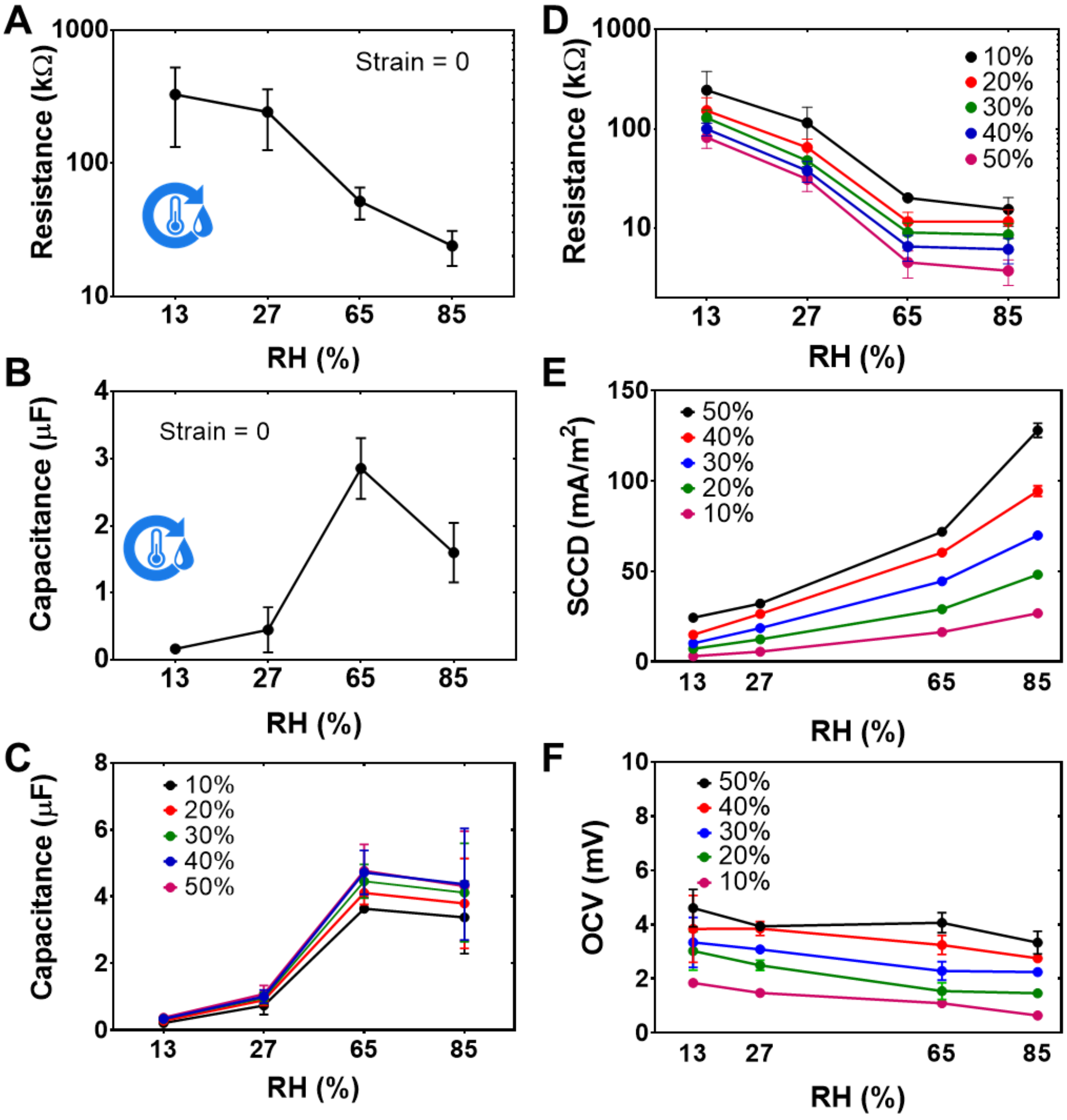

Figure 3.3. Calibration of the EG-laden AIskin for humidity sensing based on different output signals. The RH increased from 13 to 85%. (**A**) Resistance-RH curve without strain (N=3).

(**B**) Capacitance-RH curve without strain (N=3). (**C**) Capacitance-RH curves at different strain conditions (N=3). (**D**) Resistance-RH curves at different strain conditions (N=3). (**E**) SCCD-RH curves at different strain conditions (N=3). (**F**) OCV-RH curves at different strain conditions (N=3). Error bars, standard deviations.

The response of the AIskin to both mechanical strain and humidity shows the potential of simultaneous strain and humidity sensing on the same monolithic device. We measured the capacitance, resistance, OCV, and SCCD of the AIskin under different strain levels at various humidity conditions (**Figure 3.3**C-F). The results indicate that, when utilized as a humidity sensor under compressive strains, the resistance and SCCD sensing modes show more obvious changing trends with the RH change in the full RH range than the capacitance and OCV sensing modes. As the OCV outputs showed little correlation with the RH change, the SCCD mode is more suitable for humidity sensing.

3.3.7. Demonstrations of the AIskin

Thanks to the unique combination of its excellent mechanical and electronic performance, the AIskin can be used as a wearable sensor and an energy harvester. A wearable and stretchable finger joint strain sensor was constructed using the AIskin (**Figure 3.4**A). The compliant sensor conformed to the surface of a finger joint during finger bending (Movie S3.2), and detected the joint motion under different RH values of the environment. The finger's bending-straightening motions can be transduced into the change of resistance (**Figure 3.4**B), capacitance (**Figure 3.4**C), OCV and SCC (**Figure 3.4**D). At different RH levels, the resistance and capacitance outputs of the device also changed (**Figure 3.4**B-C), showing the feasibility of sensing the environmental humidity using the same sensor. In addition, the strain sensing under four sensing modes was rapid without obvious time delay in responding to the finger motion (**Figure 3.4**B-D). The response and recovery time of the RH sensing were also measured in the resistance mode. An EG-laden AIskin with a thickness of 300 μm showed a faster performance of response time = 3s and recovery time = 94s than a commercial indoor digital hygrometer (B0778C8C9L, AMIR; response time: 30s and recovery time 419s; **Figure S3.14**). Faster response time of the RH sensing can be realized by reducing the thickness of the Aiskin (*52*). We also constructed a four-button touch pad using self-generated signal (OCV-based), and employed it to play the video game, Greedy Snake, on a laptop computer (**Figure 3.4**E and Movie S3.3). This demonstration highlights the feasibility of using our AIskin as a human-machine interface.

Based on its self-generated sensing modes, the AIskin was also demonstrated for energy harvesting from human motions. We installed a piece of disk-shaped AIskin (diameter: 30 mm, and thickness: 8 mm) inside a shoe at its heel position (**Figure 3.5**A), and measure its OCV and SCC outputs (**Figure 3.5**B-C) during walking. We calculated the power and energy output levels of our AIskin energy harvester based on the device calibration data (**Figure 3.3**E-F). At a compressive strain of 50% and a RH of 85%, the peak SCCD and OCV produced by an AIskin are 128 mA m^{-2} (**Figure 3.3**E) and 3.33 mV (**Figure 3.3**F), respectively; hence, its maximum power output and average energy output were calculated to be 426.7 μW m^{-2} and 3200 μJ per mechanical stimulus, respectively. The average energy output of our device is larger than those reported previously (**Table 3.1**), showing effectiveness of our AIskin material for low-frequency energy harvesting. The device power output can be further improved by assembling multiple thin layers of AIskin. The presented demonstrations show the great potential of our AIskin as a strain and humidity sensor using self-generated signals and/or a wearable low-frequency energy harvester, for applications such as human-machine interaction, wearable electronics, personal healthcare and beyond.

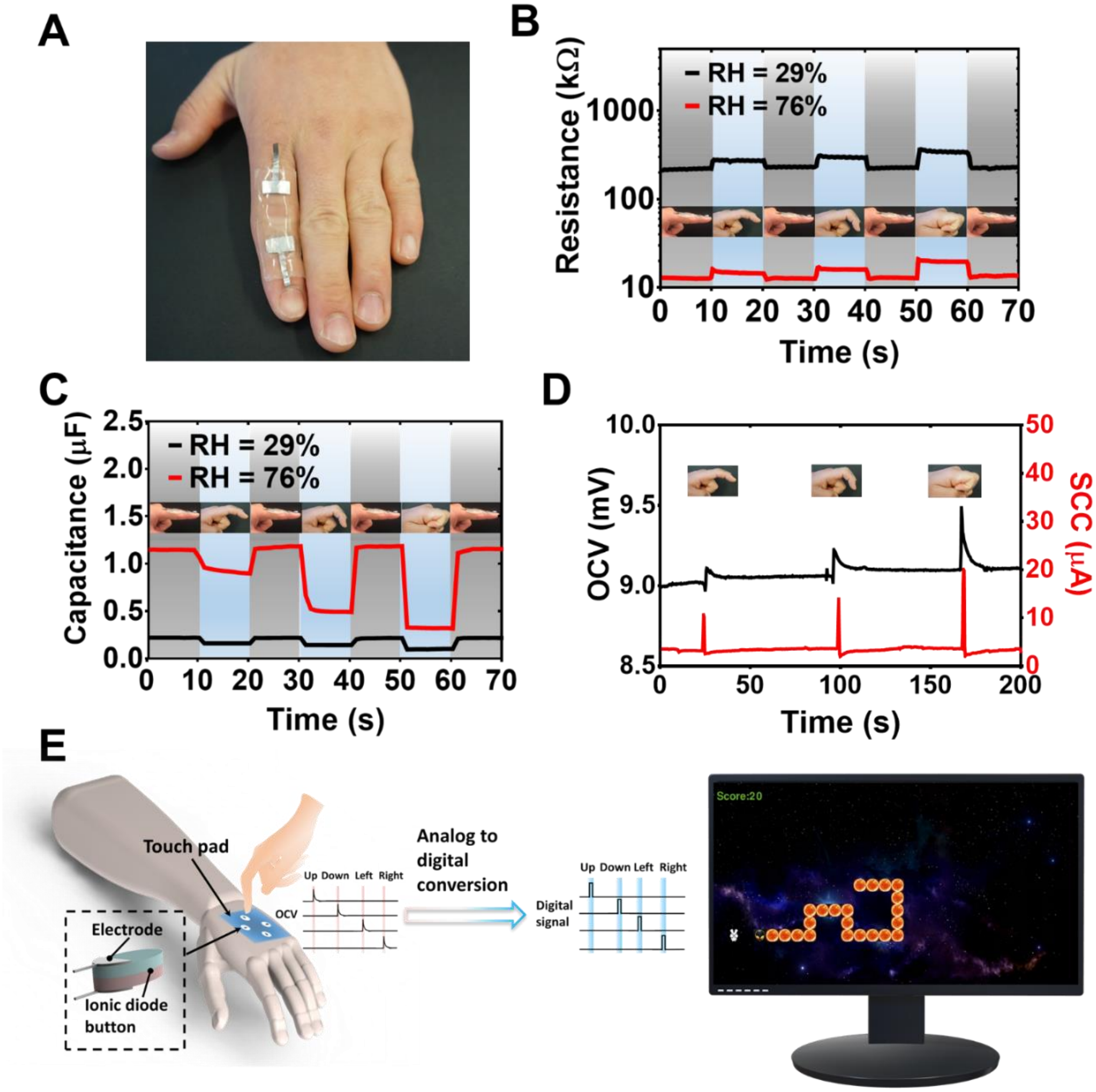

Figure 3.4. Demonstrations of the AIskin as a wearable strain/humidity sensor and four-button artificial skin using self-generated signals for human-machine interaction. (**A**) An AIskin sensor mounted on an index finger for strain and humidity sensing. (**B**) Resistance and (**C**) Capacitance outputs of the sensor at three different bending angles and two RH conditions. (**D**). SCC and OCV outputs at RH = 76 %. (**E**) Schematic illustration of a four-button touch pad mounted on human hand using self-generated signals to control the movement of a greedy snake by pressing the ionic diode buttons.

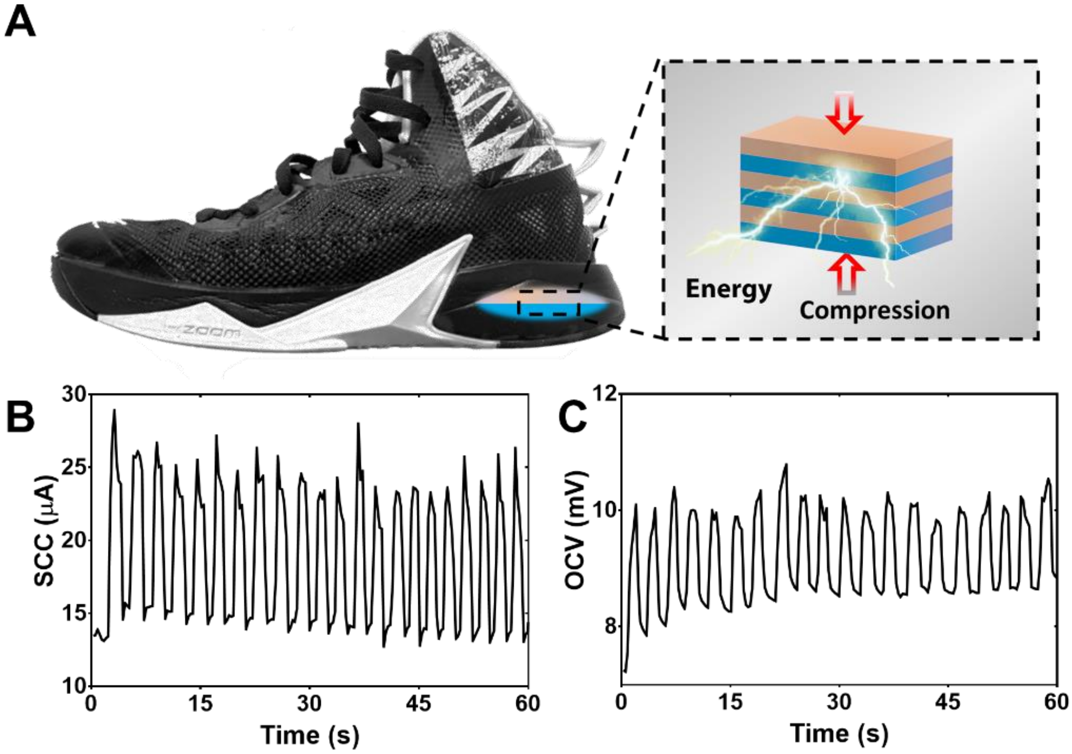

Figure 3.5. Demonstration of the AIskin as a shoe walking energy harvester. (**A**) Schematic illustration of the mechanical walking energy harvesting. (**B**) SCC and (**C**) OCV outputs from an energy harvester inside a shoe heel, the step frequency is around 0.4 Hz.

3.4. Conclusions

In this study, we report a new design and method to fabricate diode-like bilayered DN hydrogels for ionic hydrogel devices (AIskin). The devices recapitulate the salient features of human skin by combining stretchability, ambient stability and sensing properties. Our results have demonstrated that AIskin can sustain more than 400% strains without rupture, which is attributed to the double network design of the material, namely the synergistic effect of physically cross-linked agarose and covalently cross-linked PAAm networks. Importantly, the PAAm network enables seamless integration/adhesion of the two layers of preformed dissimilar hydrogels. The inclusion of neutral hygroscopic substance EG maintains the electrical characteristics of AIskin and substantially improve its stability in ambient environment. Our results have also confirmed that AIskin is an ionic analog of the diode based on controlled movements of oppositely-charged ions at the interface of its bilayer structure. Compared to previously reported diode-like hydrogels made of brittle hydrogels, AIskin provides higher stretchability and toughness as well as ambient stability to resist water loss.

Thanks to the unique combination of mechanical, physical and electrical properties, the AIskin enables numerous applications such as strain/humidity sensing, human-machine interaction, and energy harvesting. We experimentally confirm that the AIskin converts humidity and mechanical stimuli into changes in resistance, capacitance, OCV, and SCCD, and show that the OCV- and SCCD-based sensing modes are self-generated due to the presence of ionic diode structure, different from the widely used resistance- and capacitance-based sensing modes. In addition, we could also apply our AIskin design to ion sensing as external ionic stimuli have been proved to induce an amplified ionic current change within the ionic diode system (*53*). In our current demonstrations, strain/humidity sensing are mainly conducted in the environment that does not induce obvious variations of the ion concentrations of the AIskin. Therefore, only mechanical and humidity stimuli need to be considered here. The AIskin can be calibrated for strain and humidity sensing in the four types of sensing modes. For proof-of-demonstration, a wearable finger joint sensor, a four-button touch pad using self-generated signals, and a shoe walking energy harvester were demonstrated for strain-humidity sensing, human-machine interface, and walking energy harvesting, respectively. Notably, the energy output of our device is larger than some of piezoelectric or triboelectric devices and non-stretchable ionic diodes (**Table 3.1**) (*45-48, 54, 55*). The power output can be further improved by assembling multiple layers of AIskin.

While this work is focused on the design, fabrication and characterization of AIskin, further development is needed to increase the integration level and improve the performance of the AIskin. For instance, microfabrication methods for constructing micrometer-sized DN-hydrogel ionic diodes need to be developed to realize more complex AIskin systems such as wearable, self-powered micro-sensor arrays (*56*, *57*) and stretchable ionic logic circuits (*21*, *58*). The resulting microscale ionic diode might have better electrical characteristics than the macroscopic counterparts because the scale-down of depletion zone could enhance the rectifying performance of the Aiskin (*41*). Besides, microfabrication technology could enable a multifunctional sensor by integrating multiple pieces of AIskin on a single chip to decouple the AIskin's simultaneous response to both strain and humidity. For example, to monitor humidity and strain simultaneously, one can fabricate a monolithic AIskin device with one humidity sensor arranged on a body part without obvious deformation and another strain sensor on the body part with the maximum strains generated during operation. In this way, the strain sensor output can be compensated based on the environment humidity. One can also seal the strain sensor by a thin layer of elastomer (*59*) to reduce the coupling effect with humidity. To this end, one can resort to the existing manufacturing techniques such as soft lithography and 3D printing, which have been applied to fabrication of stretchable electronics (*60*-*62*). In addition, refining the electrical properties of the AIskin could improve the performance to meet the practical needs. For instance, the power output of AIskin against deformation can be improved by increasing concentrations of the polyelectrolytes or doping the AIskin with high-conductivity material (e.g., CNTs) (*37*, *41*).

In summary, we develop an ambient-stable and stretchable ionic skin inspired by the salient features of human skin. They are skin-like sensors with high stretchability and multifunctional sensing capability, and can serve as an alternative technology to current stretchable sensing and energy harvesting devices. The presented design and fabrication approach to construct mechanically-robust dissimilar hydrogel assemblies are applicable to other hydrogel systems. Given the diversity of polyelectrolytes and hydrogels, the repertoire of ionic devices could be expanded to achieve different functionalities, for instance, sensing of pH (*63*), gas (*64*), ion strengths (*65*) and glucose (*44, 66*). We envision that the design and method presented here will lead to the development of next-generation wearable and implantable devices with improved human-machine interfaces.

Table 3.1. Comparison of energy harvesting performance between the AIskin and other devices reported previously.

Peak SCCD (mA m^{-2})	**Maximum strain**	**Energy output per stimulus (μJ m^{-2}) (*)**	**Frequency (Hz)**	**Working mechanism**
128	Above 50%	3200	0.02-0.5(†)	Ionic diode (this work)
7	0.03%	60	0.1(†)	Ionic diode (*54*)
0.5	0.19%	0.12	11.2(‡)	Piezoelectric (*55*)
1.2	N/A	875	10-20(‡)	Triboelectric (*46*)
0.009	N/A	0.065	10-20(‡)	Triboelectric (*45*)
1.3	0.13%	585	10-20(‡)	Triboelectric (*48*)
14	N/A	703	10-20(‡)	Triboelectric (*47*)

(*) Calculated as the product of half peak SCCD, half peak OCV and the time duration of half peak SCCD.

(†) Calculated as strain rate divided by maximum strain**.**

(‡) Derived from the OCV-time curve.

3.5. Materials and Methods

3.5.1. Materials

Poly (sodium 4-styrenesulfonate) solution (PSS, M$_w$ = 70 kDa, 30 wt. %), Poly (diallyldimethylammonium chloride) solution (PDAC, M$_w$ = 400-500 kDa, 20 wt. %), Agarose (biochemistry research grade), acrylamide (AAm), covalent cross-linker N,N'-methylenebis(acrylamide) (MBAA), photoinitiator IRGACURE 2959 (I2959), hygroscopic substances Ethylene glycol (EG), Glycerol and humidity control reagent Lithium chloride (LiCl) were purchased from Sigma. Ag/AgCl ink were purchase from Ercon Inc. to fabricate a thin layer of electrodes (0.02 mm thick) on PET film. 3M Very-High-Bond (VHB) foam tape (0.05 mm thick) were purchased from McMaster-Carr. Milli-Q (18.3 MΩ) water was used in all experiments.

3.5.2. Fabrication of artificial ionic skin (AIskin)

A facile two-step polymerization method was used to fabricate the AIskin (Figure S1**)**. In the first step, the first network hydrogel with polyelectrolyte was synthesized following a previously reported protocol (*41*). In brief, Agarose (2.0 wt. %) was added to PSS solutions (7.0 wt. %) and PDAC solutions (5.0 wt. %), respectively. The mixtures were heated at 100 °C for 20 min under continuous stirring to obtain a transparent pre-hydrogel solution. For gelation of the solutions, the hot mixtures were poured into glass molds and then cooled to room temperature for 20 min. In the second step, the PSS and PDAC gel were immersed in the degassed AAm precursor solution (17 wt. %), containing 1 mM MBAA and 0.4 wt. % I2959, for at least 12 h in the dark environment. Then, two layers of oppositely charged hydrogel containing AAm monomers were stacked together and clamped tightly in a glass mold. After that, the whole device was irradiated with 254 nm UV (28 ~ 32 mW/cm^2, UVO-Cleaner 42A, Jelight Company, Inc.) for 2 hours to cross-link the AAm monomers to form the second network. The obtained hydrogels were desalinated to remove residual ions (the desalination time is 4 hours unless indicating elsewhere) and then sealed in a Ziploc bag before tests. As a control, two layers of only positive or negative charged DN hydrogel were synthesized respectively by the abovementioned method.

3.5.3. Fabrication and test of ambient stable AIskin

Hygroscopic reagents were added into the hydrogel devices to increase their ambient stability. The obtained DN hydrogel was immersed in the EG [25, 50 and 75% (v/v)] at least 1 hour to reach the equilibrium state. 400 mL LiCl solution (19M, 15 M, 8 M and 6 M) was stored in airtight plastic storage containers (86 oz.) to maintain a certain relative humidity (13%, 27%, 65%, and 85%, respectively). After the placement of EG processed devices, their mass and electric performance were monitored continuously for 1 week to evaluate the ambient stability. To compare the water retention capability of different hygroscopic reagents, Glycerol solution (50 vol%) was also used in this test.

3.5.4. Mechanical Characterization

Uniaxial compression tests were carried out with a rheometer (TA instruments). Cylindrical AIskin with a thickness of ~4 mm and a diameter of ~12 mm was utilized for compression tests. The compressive strain was estimated as t/t_0, where t is the displacement of the platen and t_0 is the original thickness of a device. The compressive strain speed was set at 0.35 % s^{-1}. The compressive stress was calculated as F/A_0, where F is the force applied to the device and A_0 is the original area of the sample. Pure shear tests were conducted to determine the matrix toughness with a universal testing machine (MTESTQuattro, ADMET, the loading cell is 150 LB). A rectangular strip of gel ($80 \times 25 \times 4$ mm^3) was glued to two rigid acrylate clamps ($80 \times 10 \times 1.5$ mm^3). Both unnotched and notched samples were prepared for pure shear tests. For notched samples, an edge crack with a length of 30 mm was cut using a razor blade in the middle section of the sample. The tensile strain rate was fixed at 200% min^{-1}. The tensile strain (ε) was defined as the length change (Δl) divided by the original length (l_0) of the sample. The toughness was defined by integrating the area under a stress-strain curve of the unnotched sample, where strain used the range from 0% to the fractured value of a notched sample (*67*). Junction adhesion energy, namely the energy required to increase a unit area of the p-n junction crack, was measured with 180-degree peel tests by the same tensile testing machine. A rectangular strip of DN hydrogel devices ($80 \times 20 \times 4$ mm^3) with one end open as an edge crack was used in this peeling test. Both surfaces of a device were bonded to a rigid polyethylene terephthalate (PET) film with super glue, to limit deformation to the crack tip. Two free ends of the device were attached to the machine grips. The loading rate was set constant at 100 mm min^{-1}. The adhesion energy was two times the plateau value of the ratio of the force and width (*68*). Mineral oil was used to seal around the whole device to avoid water evaporation during all mechanical tests. Both force and displacement were recorded continuously throughout the experiment.

3.5.5. Optical Characterization

The transmittance of AIskin with different thicknesses was measured with a UV-vis spectrometer (SpectraMax M5, Molecular Devices, Sunnyvale, CA) under the different humidity conditions.

3.5.6. Electrical characterization

Electrical characterization was conducted both under compressive and tensile modes. The current-voltage characteristics, resistance, open circuit potential, and short circuit current of the as-prepared device were measured by using a source meter (Keithley 2602, Keithley Instrument Inc.) controlled through LabTracer software. The sweep voltage (sweep scan rate = 179 mV s^{-1}) was set at the range from +5 V to -5 V when measuring the rectifying performance. The sweep voltage was set at a constant value of + 3 V when measuring the resistance. The sweep current was set at zero when measuring the open circuit voltage. The sweep voltage was set at zero when measuring the short circuit current. Each compressive /tensile cycle occurred with a 70s rest during open circuit voltage and short circuit current measurement. The capacitance was measured by using an LCR Meter (Agilent, E4980A) controlled through a LabVIEW interface. In the LCR meter, the test frequency was set at 1 kHz. The resistance and capacitance under various strain rate (2.5% s^{-1}, 5% s^{-1}, 10% s^{-1} and 20% s^{-1}) were studied under compressive mode. Capacitance-voltage (C-V) measurements were performed using an LCR meter under its C_p-R_p mode. The C-V sweeps of devices were performed between -5 V and 5 V with an AC signal with a peak-to-peak magnitude of 100 mV. In all tests, electrodes were mounted on both the bottom and top of devices.

3.5.7. Human-machine interface

The four-button touch pad was fabricated by placing 4 pairs of AIskin (12 mm in diameter and 2 mm in thickness) into the VHB spacer with 4 holes. Then the AIskin area was sandwiched between 2 Ag/AgCl electrodes before sealed by a 3M transparent tape and another VHB layer. The acquisition of OCV signal from artificial skin to the laptop was realized by an Arduino UNO control board equipped with 10-bit analog-to-digital converters. Python 3.0 was used to analyzed data and program the interface of greedy snake game.

3.5.8. Statistical analysis

Statistical analyses were performed on GraphPad Prism software (GraphPad Software, Inc.). Results are depicted as mean ± standard deviation (SD), we conducted unpaired Student's t test to analyze the statistical differences of experiment results. We used parametric test and assumed any experimental groups are normally distributed with the same SD. Differences were considered statistically significant if $P < 0.05$.

3.5.9. Testing of the AIskin on human hands

Informed consent was obtained from the human participant for the experiments.

Notes

3.6. Conflicts of interest

The authors have no conflict to declare.

3.7. Acknowledgments

The authors acknowledge Prof. Francois Barthelat for the access to a tensile tester, and also thank the technical assistance from Zhen Yin, Hang Xu, Lu Liu, Chuan Qiao and Guoying Dong on mechanical testing, the technical assistance from Dr. Pelayo Garcia de Arquer on capacitance-voltage test. This work was supported by the Natural Sciences and Engineering Research Council of Canada (RGPIN-2017-06374, RGPAS 507980-17, and RGPIN-2018-04146), the Canada Foundation for Innovation (#37719), and the University of Toronto.

3.8. References

1. J. Dargahi, S. Najarian, Human tactile perception as a standard for artificial tactile sensing-a review. *Int. J. Med. Rob. Comput. Assisted Surg.* **1**, 23-35 (2004).
2. M. L. Hammock, A. Chortos, B. C. K. Tee, J. B. H. Tok, Z. Bao, 25th anniversary article: the evolution of electronic skin (e‐skin): a brief history, design considerations, and recent progress. *Adv. Mater.* **25**, 5997-6038 (2013).
3. A. Chortos, J. Liu, Z. Bao, Pursuing prosthetic electronic skin. *Nat. Mater.* **15**, 937-950 (2016).
4. M. Boer, E. Duchnik, R. Maleszka, M. Marchlewicz, Structural and biophysical characteristics of human skin in maintaining proper epidermal barrier function. *Adv. Dermatol. Allergol.* **33**, 1-5 (2016).
5. W. Yang *et al.*, On the tear resistance of skin. *Nat. Commun.* **6**, 6649 (2015).
6. K. Laden, R. Spitzer, Moisturizing agent in skin. *J. Soc. Cosmet. Chem.* **18**, 351-360 (1967).
7. Y. Lee, C.-H. Lee, U. Oh, Painful channels in sensory neurons. *Mol. Cells* **20**, 315-324 (2005).
8. Y. Roudaut *et al.*, Touch sense: functional organization and molecular determinants of mechanosensitive receptors. *Channels* **6**, 234-245 (2012).
9. Y. Sun, W. M. Choi, H. Jiang, Y. Y. Huang, J. A. Rogers, Controlled buckling of semiconductor nanoribbons for stretchable electronics. *Nat. Nanotechnol.* **1**, 201-207 (2006).
10. D.-H. Kim *et al.*, Epidermal electronics. *Science* **333**, 838-843 (2011).
11. D.-H. Kim *et al.*, Materials for multifunctional balloon catheters with capabilities in cardiac electrophysiological mapping and ablation therapy. *Nat. Mater.* **10**, 316-324 (2011).
12. D.-H. Kim *et al.*, Materials and noncoplanar mesh designs for integrated circuits with linear elastic responses to extreme mechanical deformations. *Proc. Natl. Acad. Sci. U.S.A.* **105**, 18675-18680 (2008).
13. T. Sekitani *et al.*, Stretchable active-matrix organic light-emitting diode display using printable elastic conductors. *Nat. Mater.* **8**, 494–499 (2009).

14. T. Sekitani *et al.*, A rubberlike stretchable active matrix using elastic conductors. *Science* **321**, 1468-1472 (2008).
15. S. J. Benight, C. Wang, J. B. Tok, Z. Bao, Stretchable and self-healing polymers and devices for electronic skin. *Prog. Polym. Sci.* **38**, 1961-1977 (2013).
16. J. Y. Oh *et al.*, Intrinsically stretchable and healable semiconducting polymer for organic transistors. *Nature* **539**, 411-415 (2016).
17. R. Pelrine, R. Kornbluh, Q. Pei, J. Joseph, High-speed electrically actuated elastomers with strain greater than 100%. *Science* **287**, 836-839 (2000).
18. J. Zang *et al.*, Multifunctionality and control of the crumpling and unfolding of large-area graphene. *Nat. Mater.* **12**, 321-325 (2013).
19. D. J. Lipomi *et al.*, Skin-like pressure and strain sensors based on transparent elastic films of carbon nanotubes. *Nat. Nanotechnol.* **6**, 788-792 (2011).
20. J. Liang, L. Li, X. Niu, Z. Yu, Q. Pei, Elastomeric polymer light-emitting devices and displays. *Nat. Photonics* **7**, 817-824 (2013).
21. H. R. Lee, C. C. Kim, J. Y. Sun, Stretchable ionics-a promising candidate for upcoming wearable devices. *Adv. Mater.* **30**, 1704403 (2018).
22. C. Yang, Z. Suo, Hydrogel ionotronics. *Nat. Rev. Mater.* **3**, 125-142 (2018).
23. J. Y. Sun, C. Keplinger, G. M. Whitesides, Z. Suo, Ionic skin. *Adv. Mater.* **26**, 7608-7614 (2014).
24. Z. Lei, P. Wu, A supramolecular biomimetic skin combining a wide spectrum of mechanical properties and multiple sensory capabilities. *Nat. Commun.* **9**, 1134 (2018).
25. C.-C. Kim, H.-H. Lee, K. H. Oh, J.-Y. Sun, Highly stretchable, transparent ionic touch panel. *Science* **353**, 682-687 (2016).
26. Y. C. Lai *et al.*, Actively perceiving and responsive soft robots enabled by self‐powered, highly extensible, and highly sensitive triboelectric proximity‐ and pressure‐sensing skins. *Adv. Mater.* **30**, 1801114 (2018).
27. P. Rewatkar, S. Goel, Based membraneless co-laminar microfluidic glucose biofuel cell With MWCNT-fed bucky paper bioelectrodes. *IEEE Trans. Nanobiosci.* **17**, 374-379 (2018).
28. N. Mehmood, A. Hariz, S. Templeton, N. H. Voelcker, A flexible and low power telemetric sensing and monitoring system for chronic wound diagnostics. *Biomed. Eng. Online* **14**, 17 (2015).
29. E. Gianino, C. Miller, J. Gilmore, Smart wound dressings for diabetic chronic wounds. *Bioengineering* **5**, 51 (2018).
30. H. Derakhshandeh, S. S. Kashaf, F. Aghabaglou, I. O. Ghanavati, A. Tamayol, Smart bandages: the future of wound care. *Trends Biotechnol.* **30**, 1259-1274 (2018).
31. K. Y. Lee, D. J. Mooney, Hydrogels for tissue engineering. *Chem. Rev.* **101**, 1869-1880 (2001).
32. Q. Chen, L. Zhu, C. Zhao, Q. Wang, J. Zheng, A robust, one‐pot synthesis of highly mechanical and recoverable double network hydrogels using thermoreversible sol‐gel polysaccharide. *Adv. Mater.* **25**, 4171-4176 (2013).
33. J. P. Gong, Why are double network hydrogels so tough? *Soft Matter* **6**, 2583-2590 (2010).
34. J.-Y. Sun *et al.*, Highly stretchable and tough hydrogels. *Nature* **489**, 133-136 (2012).
35. T. Yamada *et al.*, A stretchable carbon nanotube strain sensor for human-motion detection. *Nat. Nanotechnol.* **6**, 296-301 (2011).

36. W. Zhang, X. Zhang, C. Lu, Y. Wang, Y. Deng, Flexible and transparent paper-based ionic diode fabricated from oppositely charged microfibrillated cellulose. *J. Phys. Chem. C* **116**, 9227-9234 (2012).
37. Y. Zhou *et al.*, Biocompatible and flexible hydrogel diode‐based mechanical energy harvesting. *Adv. Mater. Technol.* **2**, 1700118 (2017).
38. S. Z. Bisri, S. Shimizu, M. Nakano, Y. Iwasa, Endeavor of iontronics: from fundamentals to applications of ion‐controlled electronics. *Adv. Mater.* **29**, 1607054 (2017).
39. M. Lucia, J. Hernandez-Rojas, C. Leon, I. Martil, Capacitance measurements of pn junctions: depletion layer and diffusion capacitance contributions. *Eur. J. Phys.* **14**, 86-89 (1993).
40. D. S. Cabral, R. L. Moreno, T. C. Pimenta, L. B. Zoccal, P. C. Crepaldi, *Implementation of Schottky barrier diodes (SBD) in standard CMOS process for biomedical applications*. Biomedical Engineering-Technical Applications in Medicine (InTech, Croatia, 2012).
41. O. J. Cayre, S. T. Chang, O. D. Velev, Polyelectrolyte diode: nonlinear current response of a junction between aqueous ionic gels. *J. Am. Chem. Soc.* **129**, 10801-10806 (2007).
42. Y. Bai *et al.*, Transparent hydrogel with enhanced water retention capacity by introducing highly hydratable salt. *Appl. Phys. Lett.* **105**, 151903 (2014).
43. Y.-H. Na *et al.*, Necking phenomenon of double-network gels. *Macromolecules* **39**, 4641-4645 (2006).
44. J. Heikenfeld *et al.*, Wearable sensors: modalities, challenges, and prospects. *Lab Chip* **18**, 217-248 (2018).
45. G. Zhao *et al.*, Transparent and stretchable triboelectric nanogenerator for self-powered tactile sensing. *Nano Energy* **59**, 302-310 (2019).
46. X. Pu *et al.*, Ultrastretchable, transparent triboelectric nanogenerator as electronic skin for biomechanical energy harvesting and tactile sensing. *Sci. Adv.* **3**, e1700015 (2017).
47. W. Xu *et al.*, Environmentally friendly hydrogel‐based triboelectric nanogenerators for versatile energy harvesting and self‐powered sensors. *Adv. Energy Mater.* **7**, 1601529 (2017).
48. F.-R. Fan *et al.*, Transparent triboelectric nanogenerators and self-powered pressure sensors based on micropatterned plastic films. *Nano letters* **12**, 3109-3114 (2012).
49. N. Yamazoe, Y. Shimizu, Humidity sensors: principles and applications. *Sens. Actuators* **10**, 379-398 (1986).
50. G. Wee *et al.*, Effect of the ionic conductivity on the performance of polyelectrolyte‐based supercapacitors. *Adv. Funct. Mater.* **20**, 4344-4350 (2010).
51. O. Larsson, E. Said, M. Berggren, X. Crispin, Insulator polarization mechanisms in polyelectrolyte‐gated organic field‐effect transistors. *Adv. Funct. Mater.* **19**, 3334-3341 (2009).
52. M. Ahmadipour, M. F. Ain, Z. A. Ahmad, Effect of thickness on humidity sensing properties of RF magnetron sputtered CaCu 3 Ti 4 O 12 thin films on alumina substrate. *IEEE Sensors Journal* **17**, 3224-3230 (2017).
53. S.-M. Lim *et al.*, Ion-to-ion amplification through an open-junction ionic diode. *Proc. Natl. Acad. Sci. U. S. A.*, 201903900 (2019).
54. Y. Hou *et al.*, Flexible ionic diodes for low‐frequency mechanical energy harvesting. *Adv. Energy Mater.* **7**, 1601983 (2017).
55. S. Xu *et al.*, Self-powered nanowire devices. *Nat. Nanotechnol.* **5**, 366-373 (2010).

56. K. Dong *et al.*, A highly stretchable and washable all-yarn-based self-charging knitting power textile composed of fiber triboelectric nanogenerators and supercapacitors. *ACS Nano* **11**, 9490-9499 (2017).
57. S. Park *et al.*, Stretchable energy‐harvesting tactile electronic skin capable of differentiating multiple mechanical stimuli modes. *Adv. Mater.* **26**, 7324-7332 (2014).
58. Y. Wang, Z. Wang, Z. Su, S. Cai, Stretchable and transparent ionic diode and logic gates. *Extreme Mech. Lett.* **28**, 81-86 (2019).
59. H. Yuk, T. Zhang, G. A. Parada, X. Liu, X. Zhao, Skin-inspired hydrogel–elastomer hybrids with robust interfaces and functional microstructures. *Nat. Commun.* **7**, 12028 (2016).
60. Z. Guo, U. Aboudi, P. Peumans, R. T. Howe, F.-K. Chang, A super stretchable organic thin-film diodes network that can be embedded into carbon fiber composite materials for sensor network applications. *J. Microelectromech. Syst.* **25**, 524-532 (2016).
61. S. Wang *et al.*, Skin electronics from scalable fabrication of an intrinsically stretchable transistor array. *Nature* **555**, 83-88 (2018).
62. Q. Hua *et al.*, Skin-inspired highly stretchable and conformable matrix networks for multifunctional sensing. *Nat. Commun.* **9**, 244 (2018).
63. Q. Xu, L. An, M. Yu, S. Wang, Design and synthesis of a new conjugated polyelectrolyte as a reversible ph sensor. *Macromol. Rapid. Commun.* **29**, 390-395 (2008).
64. J. Wu *et al.*, Extremely deformable, transparent, and high-performance gas sensor based on ionic conductive hydrogel. *ACS Appl. Mater. Interfaces* **11**, 2364-2373 (2018).
65. M. Sun *et al.*, Hydrogel interferometry for ultrasensitive and highly selective chemical detection. *Adv. Mater.* **30**, 1804916 (2018).
66. J. Kim *et al.*, Simultaneous monitoring of sweat and interstitial fluid using a single wearable biosensor platform. *Adv. Sci.* **5**, 1800880 (2018).
67. J. Li, W. R. Illeperuma, Z. Suo, J. J. Vlassak, Hybrid hydrogels with extremely high stiffness and toughness. *ACS Macro Lett.* **3**, 520-523 (2014).
68. R. Rivlin, A. G. Thomas, Rupture of rubber. I. Characteristic energy for tearing. *J. Polym. Sci.* **10**, 291-318 (1953).

3.9. Supplementary Materials

An ambient-stable, stretchable and self-powered ionic skin with multimodal sensation

Figure S3.1. Two-step synthesis of AIskin.

Figure S3.2. Mechanical performance of the AIskin.

Figure S3.3. Rectification effect of an AIskin at different conditions.

Figure S3.4. Capacitance-voltage (C-V) response of different types of biolayer hydrogels.

Figure S3.5. Transmittance of EG-laden AIskin at the wavelength of 700 nm with different experimental conditions.

Figure S3.6. Measurement of water loss as a function of RHs.

Figure S3.7. Rectifying effect of AIskin at different RHs and strains.

Figure S3.8. Resistance-strain relations of the AIskin, PSS hydrogel and PDAC hydrogel.

Figure S3.9. Capacitance-strain relations of the AIskin, PSS hydrogel, and PDAC hydrogel.

Figure S3.10. Schematic mechanism of OCV change with applied deformation on an AIskin.

Figure S3.11. Self-generating capability of the AIskin, PSS hydrogel, and PDAC hydrogel.

Figure S3.12. Durability and stability of the AIskin for the use of strain sensor.

Figure S3.13. Sensing robustness of AIskin under different strain rates.

Figure S3.14. Comparison of the response and recovery time between our AIskin and a commercial hygrometer (B0778C8C9L, AMIR).

Movie S3.1. Pure shear test to show the stretchability and toughness of the AIskin.

Movie S3.2. AIskin sandwiched between VHB films mounted on a finger joint to show high transparency and stretchability.

Movie S3.3. Human-machine interaction by using a four-button touch pad with self-generated signals to control the movement of a greedy snake.

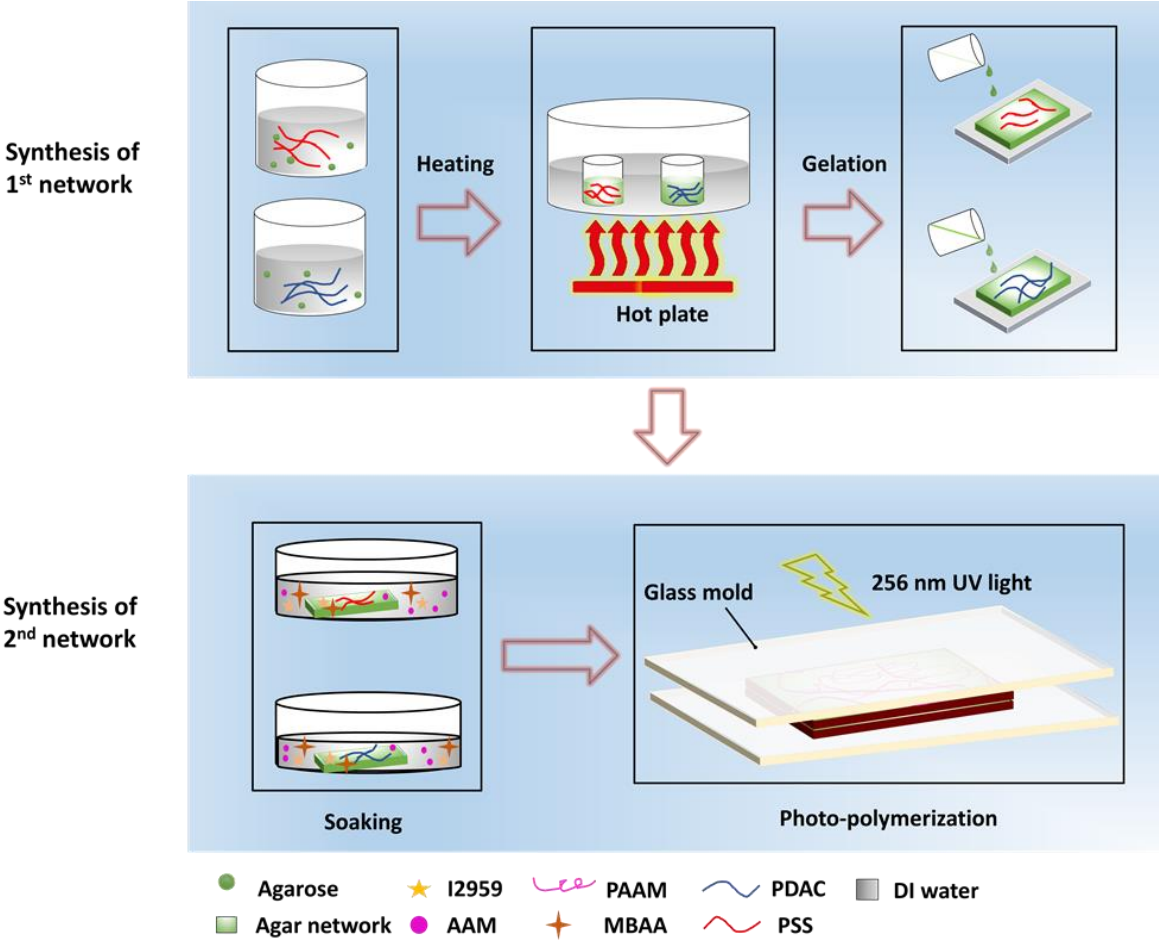

Figure S3.1. Two-step synthesis of AIskin.

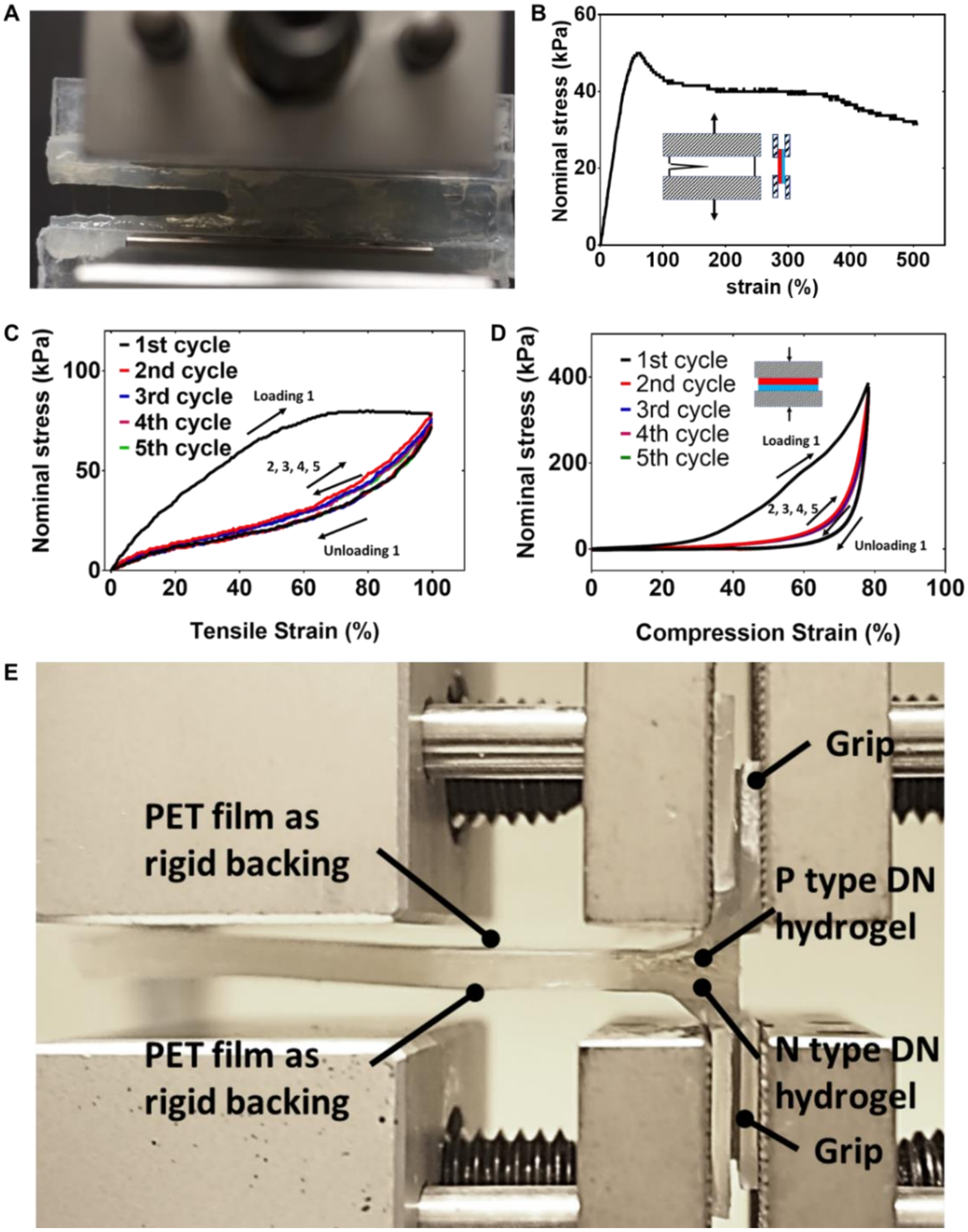

Figure S3.2. Mechanical performance of the AIskin. (**A**) Pure-shear test for measuring the toughness of an AIskin. A piece of hydrogel with a notch was stretched until the crack propagates. (**B**) Stress-strain curve of the AIskin. (**C**) Five successive tensile loading-unloading cycles of an AIskin at the maximum strain of 100%. **(D)** Five successive compression loading-unloading cycles of an AIskin at a maximum strain of 80%. **(E)** Peeling adhesion test. Digital photo showing the AIskin under 180-degree peeling test, in which two surfaces of hydrogel were glued to a PET film to eliminate energy dissipation in regions away from the crack tip. Two open ends of hydrogel with grip were stretched with a universal testing machine.

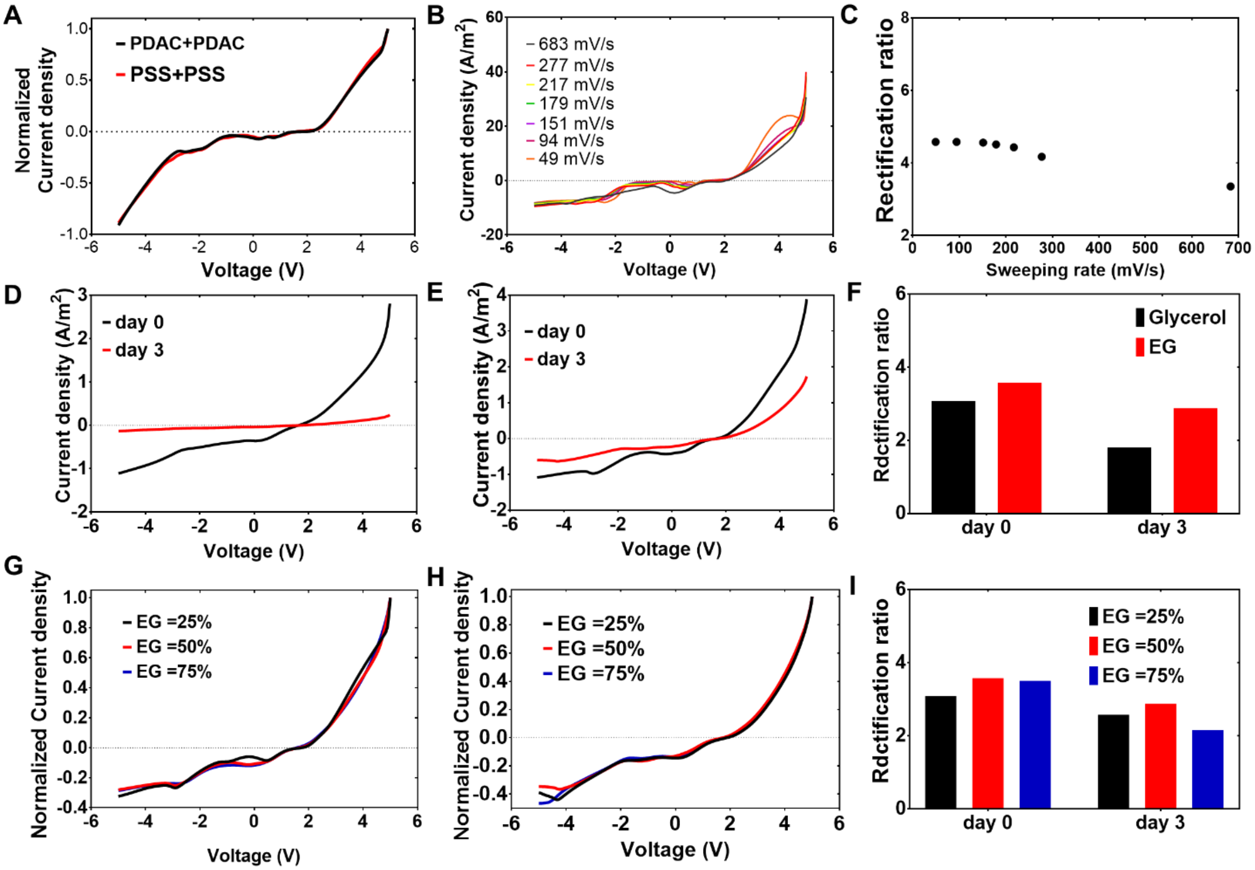

Figure S3.3. Rectification effect of an AIskin at different conditions. (A) Voltage-current curves for the hydrogel skin with the same charge density. (**B**) Voltage-current curves and (**C**) Rectification ratio of an AIskin at different sweeping rates. **(D)** Voltage-current curves for an ambient stable AIskin with 50 v/v % glycerol on day 0 and day 3. (**E**) Voltage-current curves for an ambient stable AIskin with 50 v/v % EG on day 0 and day 3. (**F**) Rectification ratio is compared between two hygroscopic materials on day 0 and day 3. (**G**) Voltage-current curves for ambient stable AIskin with different EG concentrations on day 0. (**H**) Voltage-current curves for ambient stable AIskin with different EG concentrations on day 4. (**I**) Rectification ratio is compared between ambient stable AIskin with different concentrations of EG on day 0 and day 3.

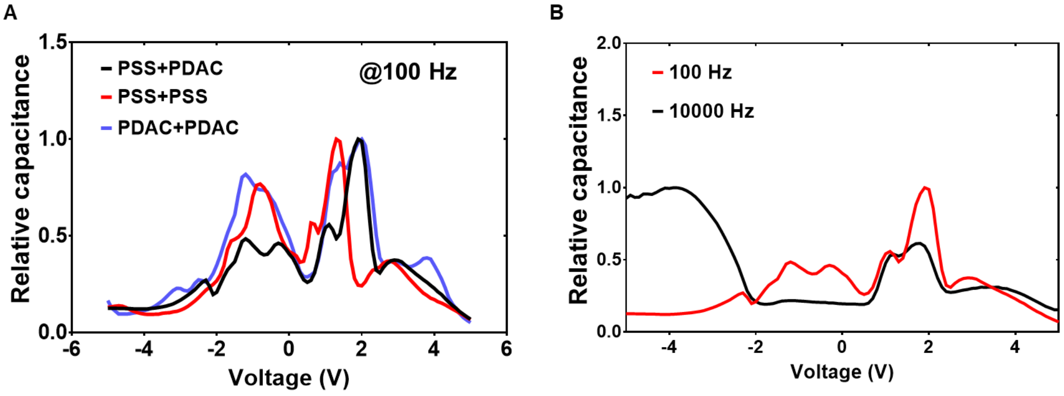

Figure S3.4. Capacitance-voltage (C-V) response of different types of biolayer hydrogels. (A) Comparison between AIskin, bilayer PSS hydrogel and bilayer PDAC hydrogel when the scan frequency is 100 Hz. (**B**) Comparison of the C-V responses of the same AIskin under low (100 Hz) and high (10000 Hz) scan frequencies. All the devices were washed for 4 h before tests.

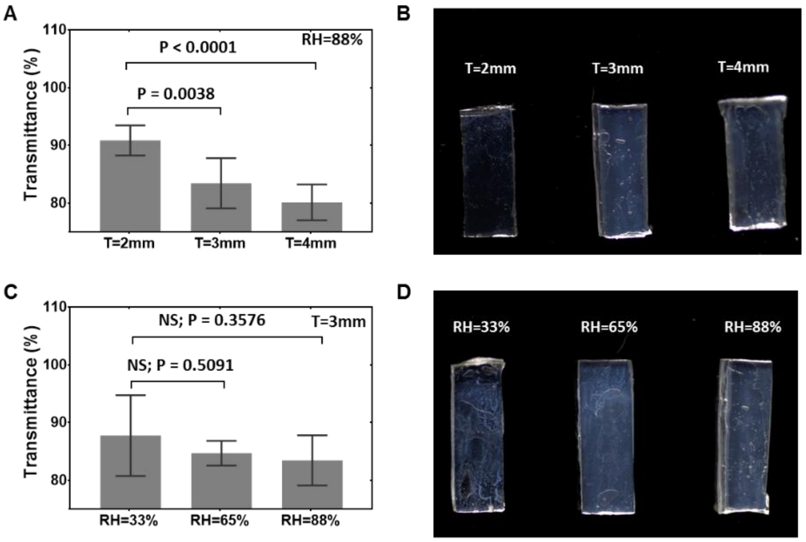

Figure S3.5. Transmittance of EG-laden AIskin at the wavelength of 700 nm with different experimental conditions. (**A**) RH = 88%, and thickness varies from 2 mm to 4 mm. (**B**) Optical photographs showing the transparency of samples with different thicknesses. (**C**) Thickness =

3mm, RH varies from 33% to 88%. (**D**) Optical photographs showing the transparency of samples under different RH values. All the samples were stored in humidity chambers for at least 3 days before transmittance measurement.

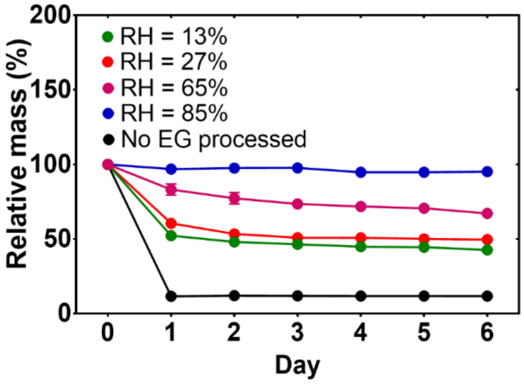

Figure S3.6. Measurement of water loss as a function of RHs. The mass of AIskin is normalized with its initial mass (N = 3).

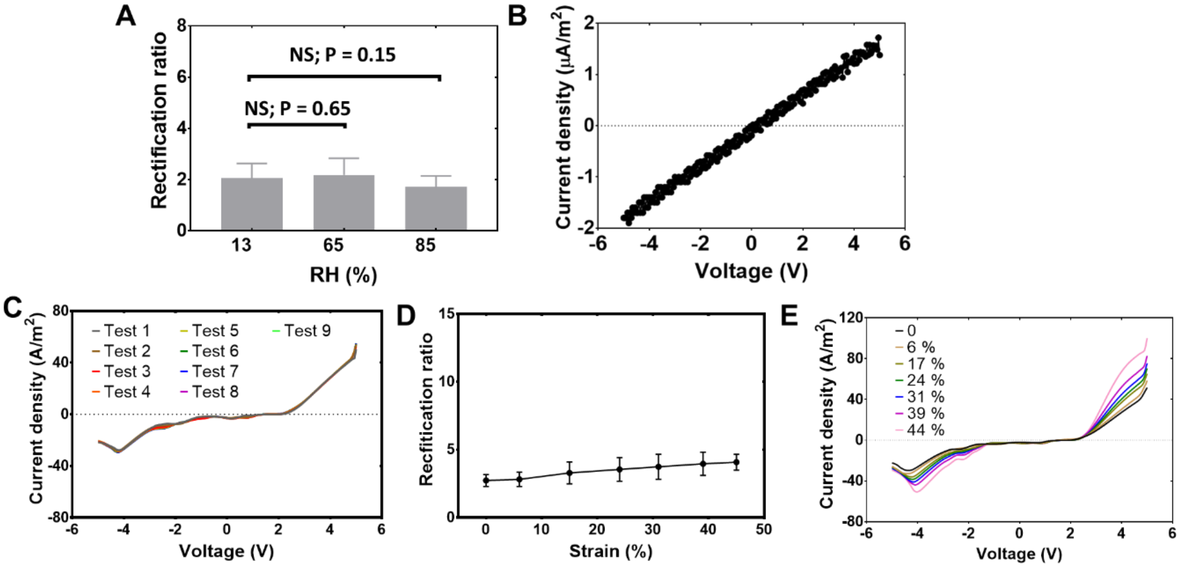

Figure S3.7. Rectifying effect of AIskin at different RHs and strains. (**A**) Rectification ratios of AIskin at different RHs after storage for 3 days (N=9). NS: not significant. (**B**) Voltage-current curves of an AIskin without EG after 3-day storage at RH 13%. (**C**) Repeated I-V testing results of an AIskin under the laboratory environment (21 °C and relative humidity of 60~65%). Between each measurement, the device was electrically shorted for 60 s. (**D**) Rectification ratio of an AIskin under different strains (N=3). (**E**) Voltage-current curves of an AIskin under different strains. The AI skin used in **Figure S3.7**C-D was washed for 2 h.

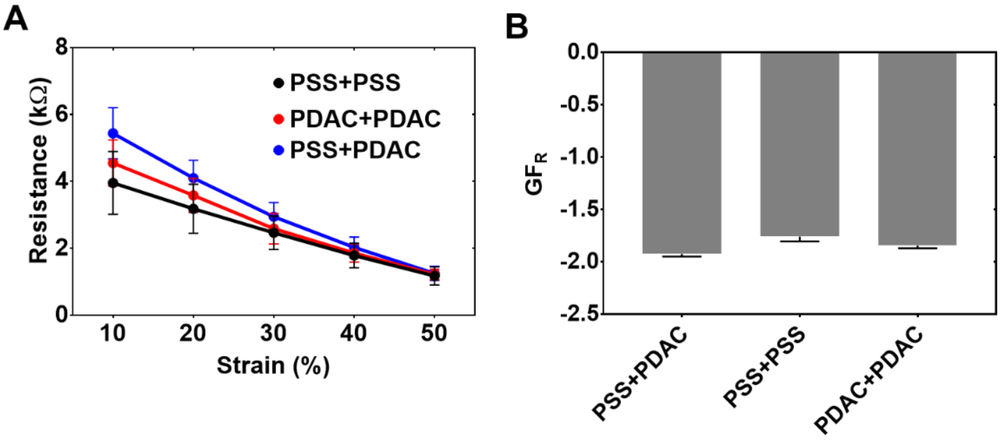

Figure S3.8. Resistance-strain relations of the AIskin, PSS hydrogel and PDAC hydrogel. (**A**) Resistance-strain curves of the AIskin, PSS and PDAC DN hydrogels (N=3-4). The compressive strains vary from 10% to 50%. (**B**) Resistive gauge factors (GF_R) among the AIskin, bilayered PSS and bilayered PDAC hydrogels.

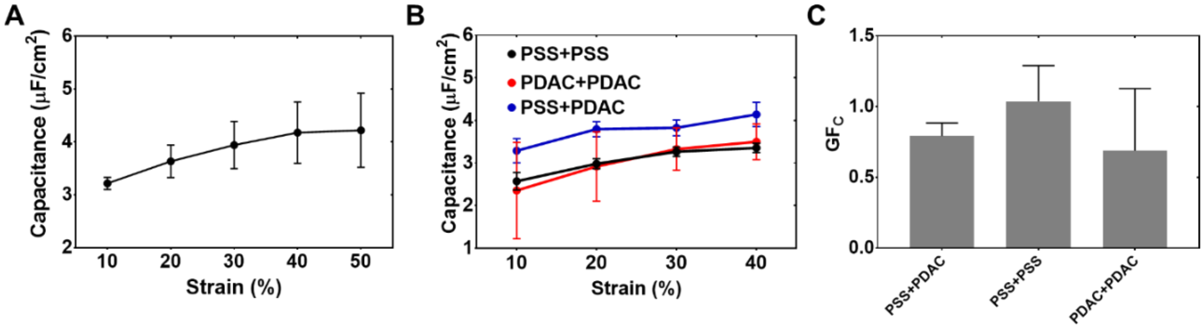

Figure S3.9. Capacitance-strain relations of the AIskin, PSS hydrogel, and PDAC hydrogel. (**A**) Capacitance-strain curves of the ambient stable AIskin at the RH of 65% (N=3). The compressive strains vary from 10% to 50%. The capacitance is normalized by the area of electrode-hydrogel contact. (B) Capacitance-strain curves of the AIskin, PSS and PDAC DN hydrogel (N=3-4). The compressive strains vary from 10% to 40%. (**C**) Capacitive gauge factors (GF_C) among the AIskin, bilayered PSS and bilayered PDAC hydrogels.

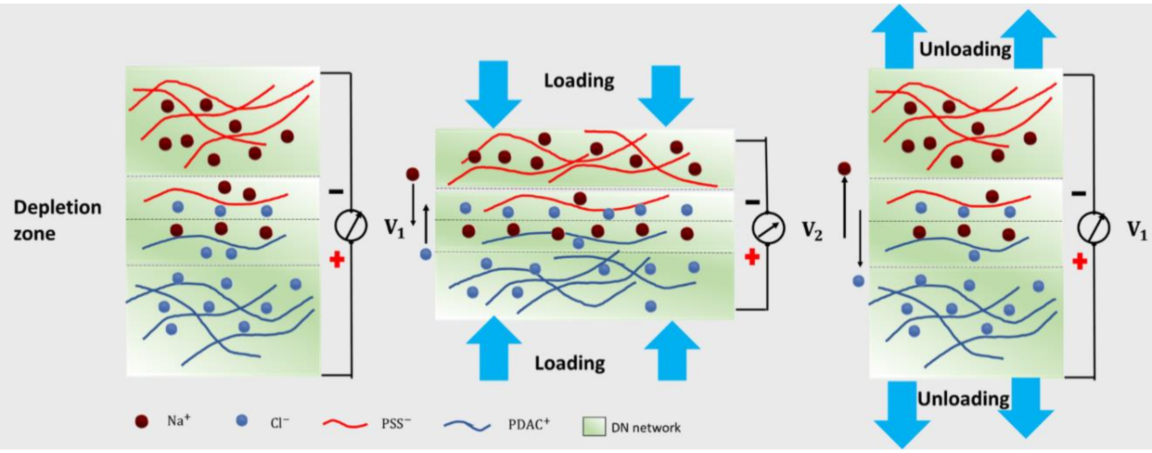

Figure S3.10. Schematic mechanism of OCV change with applied deformation on an AIskin.

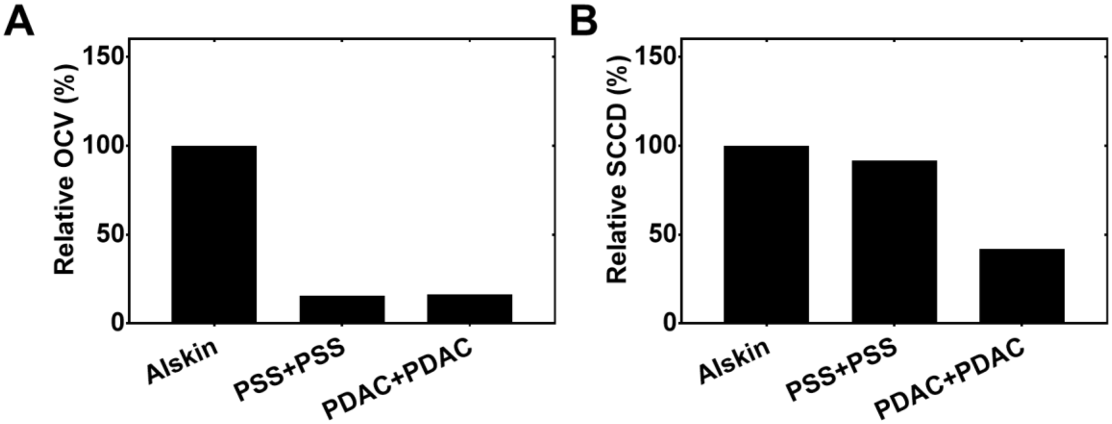

Figure S3.11. Self-powering capability of the AIskin, PSS hydrogel, and PDAC hydrogel. (**A**) Relative OCV of the AIskin, bilayered PSS and bilayered PDAC hydrogels. **(B)** Relative SCCD of the AIskin, bilayered PSS and bilayered PDAC hydrogels. The compressive strain is 50% and the strain speed is 10% s^{-1} for all three devices.

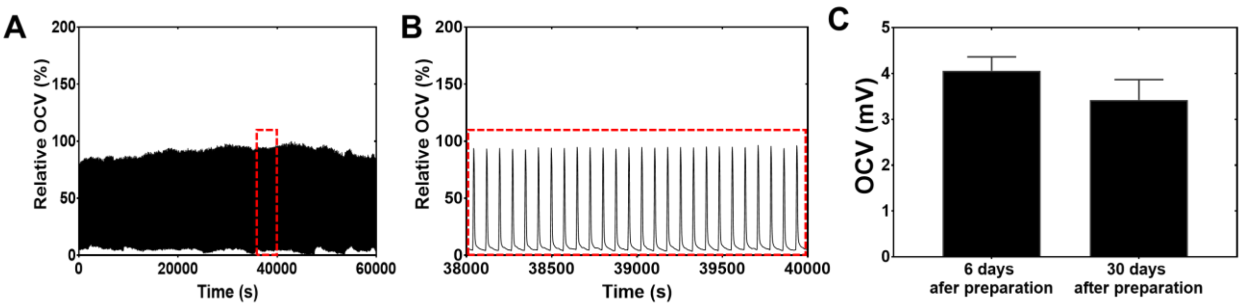

Figure S3.12. Durability and stability of the AIskin for the use of strain sensor. OCV is measured as a representative signal in this study. (**A**) Durability of OCV signals after ~1000 cycles of repeated loading-unloading steps at the RH of 13%. The strain is 50%. (**B**). Zoom-in plot of **Figure S3.12**A. (**C**) Stability of OCV signals over one-month storage at the RH of 65% (N=3).

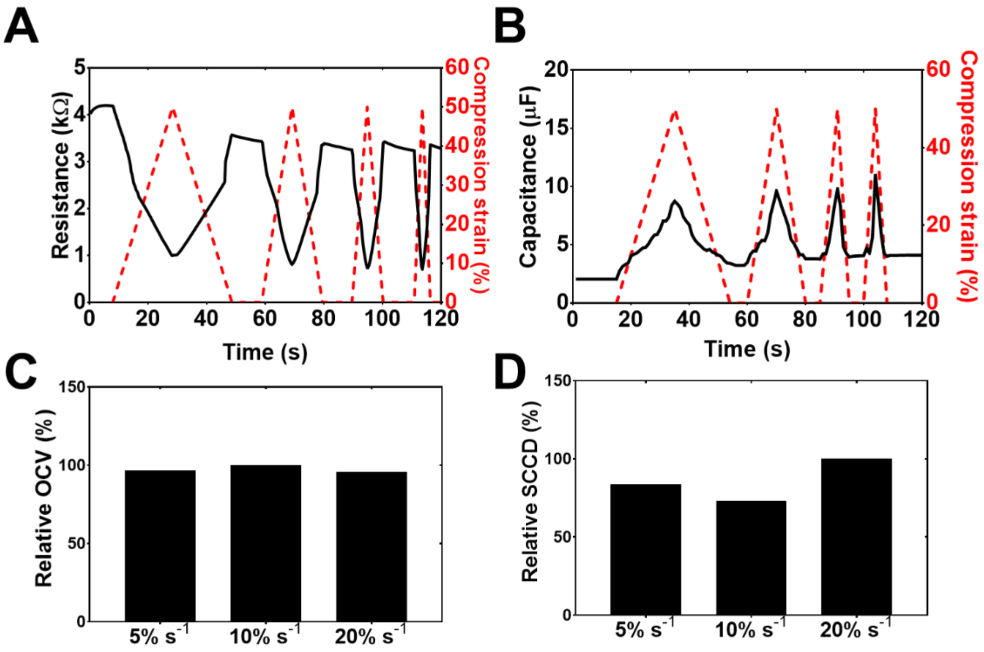

Figure S3.13. Sensing robustness of AIskin under different strain rates. (**A**) Resistance curve at specific strain rates (2.5% s^{-1},5% s^{-1}, 10% s^{-1} and 20% s^{-1}). (**B**) Capacitance curve at specific strain rates (2.5% s^{-1},5% s^{-1}, 10% s^{-1} and 20% s^{-1}). (**C**) Relative OCV at specific strain rates (5%

s^{-1}, 10% s^{-1} and 20% s^{-1}). (**D**) Relative SCCD at specific strain rates (5% s^{-1}, 10% s^{-1} and 20% s^{-1}). The compressive strain is set at 50%.

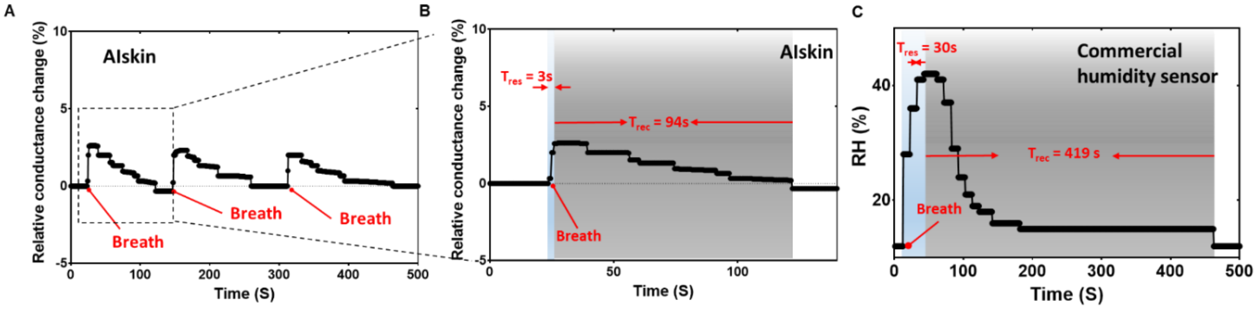

Figure S3.14. Comparison of the response and recovery time between our AIskin and a commercial hygrometer (B0778C8C9L, AMIR). (**A**) Relative conductance changes of an EG-laden AIskin with a thickness of 300 μm with repeated human breath applied. (**B**) Zoomed-in view of one response cycle (response time: 3s, and recovery time: 94s) in **Figure S3.14**A. (**C**) The response (response time: 30s, and recovery time: 419s) of the commercial hygrometer to one human breath.

Movie S3.1. Pure shear test to show the stretchability and toughness of the AIskin.

Movie S3.2. AIskin sandwiched between VHB films mounted on a finger joint to show high transparency and stretchability.

Movie S3.3. Human-machine interaction by using a self-powered four-button artificial skin to control the movement of a greedy snake.

Link between Chapter 3 and Chapter 4

In the previous chapter, I developed a diode-like artificial ionic skin (AIskin) that consists of a bilayer double-network hydrogel structure charged with opposite polyelectrolytes. This Aiskin exhibits high toughness, stretchability, ambient stability, transparency and controlled ion mobility and can convert mechanical strain and humidity into multiple electronic signals and sensing without external power supply.

However, like most other hydrogel ionic devices, this AIskin does not consist strong surface adhesive and its mechanical and electrical performance at the subzero temperature has not been studied. Therefore, in the next chapter, I selected one of the most popular used tough hydrogels, i.e., Alg-PAAm tough DN hydrogel, and empowered this hydrogel with high toughness and stretchability, high ionic conductivity, excellent ambient stability, superior anti-freezing capability and strong adhesion for diverse surfaces simultaneously. With high integration flexibility for different wearable and soft robotic designs with different materials, this hydrogel system is demonstrated for wearable strain sensing (on human body and fibric), human-machine interaction, and motion/deformation sensing on soft robotic systems under various environmental conditions.

Chapter 4

An anti-freezing, ambient-stable and highly stretchable ionic skin with strong surface adhesion for wearable sensing and soft robotics

4. Chapter 4. An anti-freezing, ambient-stable and highly stretchable ionic skin with strong surface adhesion for wearable sensing and soft robotics

Binbin Ying[1,2], Zeyuan Chen[2#], Runze Zuo[2#], Jianyu Li[1,3], Xinyu Liu[1,4*]

[1]Department of Mechanical Engineering, McGill University, 817 Sherbrooke Street West, Montreal, QC H3A 0C3, Canada.

[2]Department of Mechanical and Industrial Engineering, University of Toronto, 5 King's College Road, Toronto, Ontario, M5S 3G8, Canada.

[3]Department of Biomedical Engineering, McGill University, 3775 rue University, Montreal, QC H3A 2B4, Canada.

[4]Institute of Biomedical Engineering, University of Toronto, 164 College Street, Toronto, ON M5S 3G9, Canada.

[#] These authors contributed equally.

* Corresponding author: xyliu@mie.toronto.ca.

In submission

4.1. Introduction

Natural living systems display complex structures to survive in complicated and diverse environments. For example, properties such as freeze tolerance, dehydration resistance, and self-adaptation are commonly found in certain mammals, fishes, frogs, insects and bacteria. For human, skin is the largest organ of the body, serving as the first physical, thermal and hygroscopic barrier to protect the inner body, maintain the body temperature and control transepidermal water exchange. The skin also contains the largest sensor network to perceive various environmental stimuli that humans encounter, such as pressure, strain, deformation, humidity, temperature and pain. These functions are linked with salient features of the skin: highly deformable polymer networks (collagen and elastic fiber) to resist physical damage (*1*); hygroscopic compositions (e.g., pyrrolidone carboxylic acid) to retain water (*2*); fat cells to tolerate freeze; a variety of sensory neurons (e.g., mechanoreceptors, thermoreceptors, and pain receptors) to transduce stimuli based on the controlled movements of inorganic ions (**Figure 4.1**A) (*3-5*).

Many features of the human skin have inspired researchers to develop its electronic counterpart (i.e., artificial skins) (*6-10*), leading to a variety of promising applications such as wearable electronics, wearable robots and soft robotics (*11*). Noticeably, because of the inherent material match and functional complementarity between artificial skins and soft robotics, there has been significant research efforts spent on developing skin-like stretchable and wearable sensors for integration with various soft robotic systems (*12-17*). This rapid development would enable soft robots to interact with their users and environments more intelligently. Among different types of sensing materials used in artificial skins, hydrated and ionic materials such as deformable and tough ionic hydrogels are one of the most suitable sensor candidates to mimic the multiple functions of biological systems. Ionic hydrogels contain mobile ionic charge carriers replicating ion transport in the natural skin, excellent material biocompatibility (*18-20*), and tunable mechanical properties with on-demand design of toughness, stretchability and elasticity to accommodate the diverse mechanical properties of surfaces the artificial skin will be mounted on (*21, 22*). Recently, a variety of ionic hydrogel-based skin-like devices (also called hydrogel-based iontronic devices) have been developed, including pressure sensors (*8, 23*) and touchpads (*10, 24*), strain sensors (*10*), and robotic skins (*12*). These devices are capable of transducing applied touch, pressure, deformation, humidity or temperature into changes of electrical signals (e.g., capacitance or resistance), and mimicking the sensing functions of natural skin.

Despite the recent advances, researchers still need to address several important challenges to further broaden the practical applications of hydrogel-based iontronics. For instance, ionic hydrogel-based devices must possess long-term stability (i.e., mitigating water loss) during open-air operation, and simultaneously maintain mechanical deformability and electrical conductivity in cold environments (i.e., anti-freezing characteristics). Without special material design, water evaporation and freezing significantly weaken the mechanical and electrical properties of hydrogels. Thus, the real-world sensing application of ionic hydrogels is still limited by their poor ambient stability. In addition, for many applications such as wearable sensing and soft robotics, ionic hydrogel-based devices should firmly adhere to substrates of different materials (e.g., human skins, fabric clothes, and elastomers) under various conditions (e.g., dry and wet surfaces, sweaty skin, subzero temperature, and dynamic deformation and movement) to enhance the fidelity of signals acquisition, and show good biocompatibility when interfacing with human body. Conventional hydrogel devices and most electronic skins usually do not have good self-adhesion and therefore can only adhere to substrates with assistance of additional adhesives such as bandages, scotch tapes, or 3M adhesives (*25-27*). However, these adhesives can easily debond when adhering to substrates under certain conditions such as wet, cold, and continuously deformed surfaces; they are not suitable for use under subzero temperatures due to the hardening of adhesive matrix; the limited biocompatibility of some of these adhesives could be another issue when used for wearable devices on human body. To date, there is no existing hydrogel-based devices that can satisfy the aforementioned requirements simultaneously (previous reports summarized in **Table 4.1).**

To address these challenges, we report a new design of hydrogel-based ionic skin (iSkin) recapitulating the salient features of human skin, which possesses high stretchability, high toughness, good long-term ambient stability, superior anti-freezing property, and strong surface adhesion to different types of surfaces. The unique combination of these properties enables a variety of applications of the iSkin to wearable sensing and soft robotics. The experimental results demonstrate that the iSkin has a rupture toughness of 11.41 $kJ\cdot m^{-2}$, sustains more than 1975% strains without rupture, and maintains its electrical function after 1300 cycles of stretching deformation. As a sensor, the iSkin shows a comparable conductivity (0.904 $S\cdot m^{-1}$) to similar ionic conductive hydrogels under ambient conditions of a laboratory environment (21°C and relative humidity of 60~65%). In addition, it can maintain its conductive property for at least one month in the laboratory environment. With extreme low temperature tolerance (down to −95°C), iSkin shows an acceptable level of conductivity (1.96×10^{-5} $S\cdot m^{-1}$) for sensing even at −70°C. As a promising sensor candidate for smart clothes, wearables and soft robotics at various extreme environment conditions, iSkin can strongly adhere to different substrate surfaces (i.e., elastomer, cloth fabric with an adhesion energy of 398 $J\cdot m^{-2}$, dry and sweaty skin surfaces with an adhesion energy of 649 $J\cdot m^{-2}$) to ensure secured attachment and sensing signal fidelity. In addition, the adhesion of the iSkin on various surfaces show excellent long-term stability both in water environment and at sub-zero temperatures (tested at −30°C). These merits of the iSkin could potentially blur the boundary between humans and machines, and promise broad applications such as strain-sensing smart clothes in wet, underwater and/or extremely cold conditions, fabric-hydrogel hybrid robotic exosuits for the operation in harsh environments, smart sensing gloves for human-machine interaction, deformation/force-feedback soft robots for interactive manipulation and navigation.

4.2. Results

4.2.1. Design of iSkin

The iSkin consists of two layers: (i) a bulk dissipative hydrogel matrix containing hygroscopic/cryoprotective substances and inorganic ions; (ii) an adhesive thin layer of an interpenetrating positively charged bridging polymer coated on the hydrogel surface (**Figure 4.1**B). The dissipative hydrogel matrix is composed of a tough double-network (DN) hydrogel containing hybrid cross-linked and interpenetrating alginate-polyacrylamide (Alg-PAAm) networks, and the selection of Alg and PAAm for constructing the tough hydrogel was due to their excellent mechanical performance capable of effectively dissipating energy under deformation (*28*), confirmed biocompatibility and wide use in biomedical devices (*29*). Cryoprotective solutions have been widely applied to prevent various biological samples from icing damage at sub-zero temperatures, owing to their inhibition behaviors of hindering the ice crystallization of water molecules (*30*). Here, we incorporated glycerol, as a hygroscopic and cryoprotective material, into the tough hydrogel matrix to reduce the loss of water and lower the ice crystallization temperature of the hydrogel. We selected glycerol for this purpose because it is well accepted as a nontoxic anti-freezing, hygroscopic agent and a nonionic kosmotrope (*31*), which brings minimal impact to the mechanical performance of tough hydrogel as well as to the adhesive layer. The model inorganic ions used here are sodium (Na^+) and chorolide (Cl^-) ions since sodium chorolide (NaCl) is the most common electrolyte salt and shows low biotoxicity and good electrical conductivity. After the tough hydrogel fully cross-linked (overnight at the room temperature), we incorporated the glycerol-water binary solvent (glycerol: 66.6 wt%) with saturatedly dissolved NaCl into the

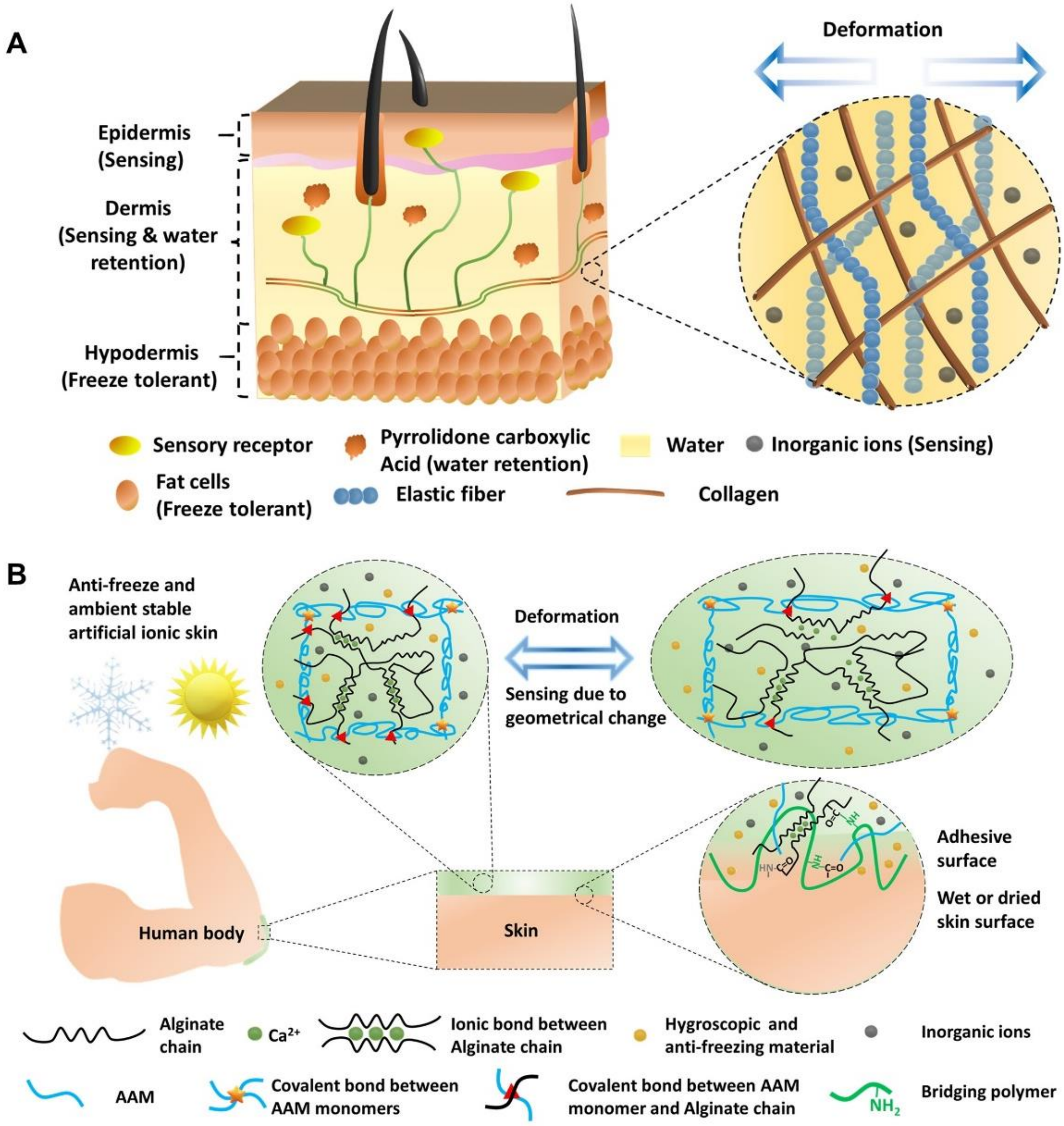

Figure 4.1. Design of a highly stretchable, anti-freezing and ambient-stable, artificial ionic skin (iSkin) with diverse strong adhesive capability. (**A**) Schematic of the human skin that resists physical deformation due to the elastin fiber and collagen in the dermis layer, maintains the body temperature due to the fat cells in hypodermis layer, holds water due to the hygroscopic substance (i.e., pyrrolidone carboxylic acid), and transduces stimuli due to the controlled movements of inorganic ions. (**B**) Schematic illustration of an iSkin adhered to diverse substrates

(the human skin is used here as an example). The iSkin is made from a hydrogel dissipative matrix (light green square) containing both ionically (calcium; green circles) cross-linked and covalently cross-linked polymers (black and light blue lines) and is laden with hygroscopic and anti-freezing reagents (yellow circles) and inorganic ions (gray circles). The iSkin surface consists a layer of bridging polymer with plenty of primary amines (green lines), which can penetrate the iSkin and the target substrate.

pre-fabricated tough hydrogel matrix by a facile method called solvent exchange for 2.5 h to ensure the fully equilibrium state (*30*), in which the solvent solution volume is 20 times the volume of the hydrogel (see details in **Figure S4.1**A and B**,** and the **Materials and Methods** section). During the solvent exchange process, the water molecules in the hydrogel were exchanged with the hygroscopic/cryoprotective molecules and the electrolyte ions. This process maintained the high transparency of the tough hydrogel (iSkin in **Figure S4.5**C). Compared with the previously demonstrated one-pot synthesis that introduces the binary solvent and electrolyte into the monomer solution during polymerization (ionic cross-linking of alginate network and covalent cross-linking of PAAm network) (*32*), this two-step solvent exchange method avoids the complicated optimization process during synthesis. In addition, this method can be conveniently expanded to fabricate tough hydrogels incorporating a variety of cryoprotectant and electrolyte solutions at different concentrations facilely tuning the anti-freezing property, conductivity, and mechanical properties (e.g., toughness and stretchability) of the material as needed.

We rendered the tough hydrogel surface highly adhesive by employing a bridging polymer that bears positively charged primary amine groups. Here, chitosan was selected as the bridging polymer because of its high concentration of primary amine groups and the resultant strong adhesion energy (*29*). Such a bridging polymer can be absorbed to a surface through both electrostatic attraction and covalent bonding. In terms of covalent bonding, the amide bond (−CO−NH−) can be formed between primary amine groups (−NH_2) on the bridging polymer and carboxylic groups (−COO^-) on both the tough hydrogel matrix (mainly the alginate network) and the to-be-adhered substrate (e.g., skin, carboxylated elastomer, and carboxylated cloth fabrics) (**Figure 4.1B**) in the presence of two common coupling reagents [1-ethyl-3-(3-dimethylaminopropyl)carbodiimide (EDC) and N-hydroxysulfosuccinimide (NHS). In addition, carboxylic acid groups on the alginate network and primary amine groups on the to-be-adhered substrate (e.g., skin, aminated elastomer) can form the amide bond directly in the presence of EDC and NHS. (**Figure 4.1B**). If the to-be-adhered substrate is permeable, the bridging polymer can penetrate into the target surface (e.g., skin), forming physical entanglements and chemical anchors (**Figure 4.1B**) (*29*). Our ready-to-use iSkin with adhesive was then applied on the to-be-adhered substrate with compression. We hypothesized that this unique material design converts the original water-based tough hydrogel into a cryoprotectant-based organohydrogel with increased freezing tolerance (*30*), high stretchability, high ambient stability, good conductivity, and strong adhesion on surfaces under diverse conditions (e.g., wet, cold, and dynamically deformed surfaces), making it feasible to construct the adhesive iSkin for use in various environments.

4.2.2. Mechanical and electrical testing of iSkin

The mechanical performance of iSkin was first tested at room temperature (21ºC). The pure-shear testing showed that iSkin can be stretched to 1975% of its initial length without rupture (**Figure 4.2**A, B and **Movie S4.1**), and the fracture energy (i.e., fracture toughness) was determined to be 11.4 $kJ \cdot m^{-2}$ (**Figure 4.2**B and C, **Figure S4.2**A and B). Adding glycerol and NaCl into the original tough hydrogel during iSkin preparation altered its mechanical properties. While exhibiting similar stretchability [1975% vs. 2200% for the original one (**Figure S4.3**A and **Movie**

S4.2)], our iSkin displayed a slightly higher fracture toughness (11.4 kJ·m$^{-2,}$) and higher Young's modulus (53.6 kPa**, Figure 4.2**B) compared with the original tough hydrogel [fracture toughness: 9.3 kJ·m^{-2} **(Figure 4.2**C**, Figure S4.2**C and D) and Young's modulus: 26.2 kPa (**Figure S4.3**A)]. The original Alg-PAAm tough hydrogel was formed by covalently and ionically cross-linked polymers. The electrostatic interactions between alginate chains and calcium ions formed ionic cross-links that unzip and can dissipate energy under deformation (*33*). Surprisingly, we found the monovalent ions (Na^+ and Cl^-) within iSkin matrix did not impair the mechanical performance of the tough hydrogel, which is different from the results of a previous report (*34*, *35*). The maintenance of mechanical property after solvent exchange is possibly due to the incorporation of the glycerol-water binary solvent system. Glycerol introduced noncovalent interactions within the hydrogel polymer chains (*32*) and increased the polymer network density (*30*), which was evidenced by the shrinkage of the hydrogel length measured by 6.2±2.5% (n =3) during solvent exchange. In addition, the incorporation of glycerol could possibly reduce the competition of the Na^+ and Cl^- ions for binding sites on the alginate chains, thus protecting the ionic cross-links.

To further verify this speculation, cyclic tensile testing of hydrogels with different synthesis conditions was carried out; all the testing results of the original tough hydrogel, glycerol-laden tough hydrogel, and iSkin revealed a large hysteresis loop in the first loading-unloading cycle (**Figure S4.3B**, **C** and **F**), corresponding to the breakage of ionic cross-linking of the alginate network. Following the first cycle, these hydrogels became elastic due to the permanent cross-linking of the PAAm network (**Figure S4.3B**, **C** and **F**). In contrast, both the glycerol-laden Alg-PAAm hydrogel without Ca^{2+} cross-linking and the iSkin without Ca^{2+} cross-linking showed no obvious hysteresis loop during five continuous loading-unloading cycles (**Figure S4.3D** and **E**). The disappearance of hysteresis loop in testing results of the Ca^{2+} cross-linking-free hydrogel matrices further proved that the ionic cross-linking on the alginate chains is critical for the mechanical properties of tough hydrogel, and that monovalent ions (Na^+ and Cl^-) within the iSkin hydrogel matrix have negligible effect on the ionically cross-linked alginate chains due to the incorporation of glycerol. Furthermore, both the iSkin (with glycerol and NaCl electrolyte) and the glycerol-laden tough hydrogel (without NaCl electrolyte) showed higher elastic moduli [53.6 kPa for iSkin and 58.8 kPa for glycerol-laden tough hydrogel (**Figure S4.3**C)] than that (26.2 kPa) of the original tough hydrogel. The increase in hydrogel Young's modulus after glycerol incorporation could be due to the reinforcement effect of the hydrogel matrix caused by noncovalent interactions (hydrogen bonds) between hydroxyl groups on the glycerol chains and carboxyl groups and amino groups on the alginate and PAAm chains (*32*). Consequently, iSkin also showed an increased fracture toughness compared with the original tough hydrogel. Moreover, it is worth noting that there is a smoother elastic-to-plastic transition on the characteristic curve of the iSkin (**Figure 4.2**B) than that of the original tough hydrogel (**Figure S4.3**A), which could be due to the large amount of noncovalent interactions between glycerol chains and alginate and PAAm chains (e.g., hydrogen bonds). The high stretchability (≤1975%) of iSkin can meet the mechanical requirements of wearable sensing and soft robotics given the typical strain levels of human skin during movements [≤~55% (*10*)] and most soft robots [≤100%~150% (*36*)]. The comparable mechanical performance (e.g., Young's module, toughness or stretchability) of the iSkin to that of other substrates (e.g., skin and elastomers) will make it a suitable material candidate for constructing sensors for wearables and soft robots (*22, 37*).

The electrical characteristics of the iSkin were then examined at room temperature (21ºC). Stainless steel electrodes (0.02mm thick) were used to establish electrical contacts on the hydrogel. Although the incorporation of glycerol enhanced the mechanical performance of tough hydrogel and its anti-freezing properties (to be discussed below), the addition of the organic solvent glycerol (66.6 wt%) significantly reduced the ionic hydrogel's conductivity (**Figure S4.4**A). With the addition of NaCl, the conductivity of the glycerol-laden hydrogel was recovered and reached its maximum of 0.904±0.302 S·m^{-1} (n = 4) at NaCl's saturation concentration (5.4M), more than twice the conductivity of original tough hydrogel (**Figure S4.4**A). Further addition of NaCl into the solvent exchange solution for treating the hydrogel does not help because no more NaCl can be dissolved (**Figure S4.4**B and C). We adopted this glycerol-water binary system with saturated NaCl for solvent exchange treatment of the hydrogel to achieve the highest conductivity, which is desired in sensing applications. The conductivity of the iSkin (0.904 S·m^{-1}) is comparable to those of previously reported conductive ionic hydrogels (**Table 4.1**).

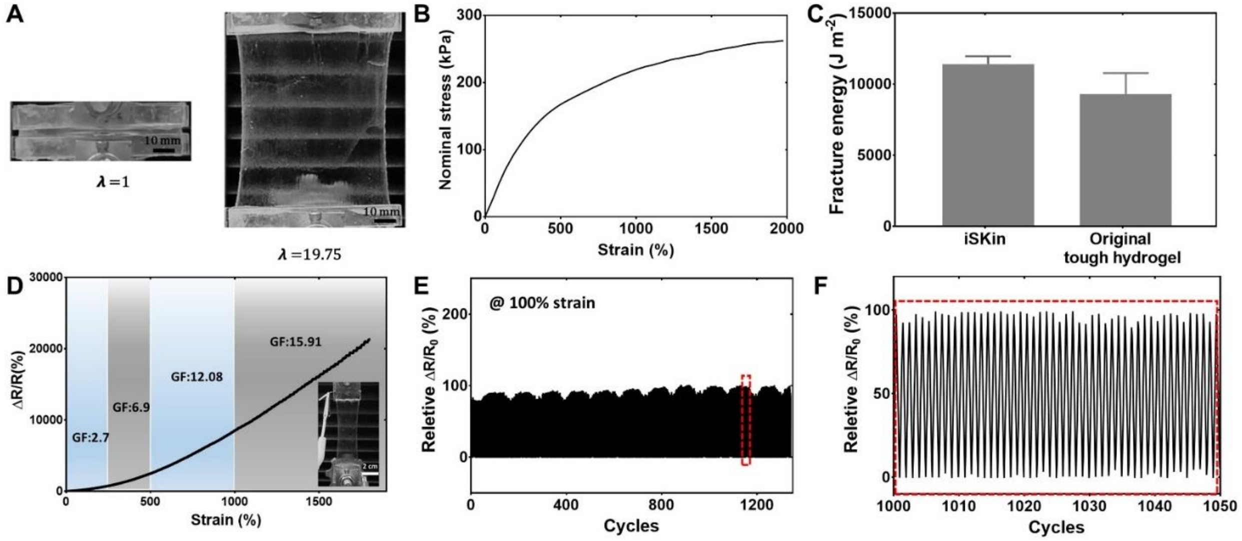

Figure 4.2. Mechanical and electrical testing of iSkin. (A) iSkin was stretched more than 1975% (right figure) of the original length (left figure) without fracture. (**B**) Strain-stress curve of iSkin under stretch. (**C**) The comparison of fracture toughness between iSkin and original Alg-PAAm tough hydrogel (N=4 for iSkin and N=3 for original tough hydrogel). **(D**) Relative resistance

change as a function of strain and its gauge factor (GF) at different strain ranges. The inset figure shows the resistance measurement setup during the tensile testing. (**E**) Stability of relative resistance changes of iSkin at 100% strain for 1300 cycles. (**F**) Zoom-in view of data in (E) from cycle 1000 to 1050. R_0 is the initial resistance value of each cycle. The overall time for the stability test is 7.5 h at the relative humidity (RH) of 25% under room temperature.

Taking advantage of its high stretchability and good conductivity, the iSkin can serve as a highly deformable and stretchable strain sensor. A representative plot of the relative resistance change ($\Delta R/R$) as a function of tensile strain of an iSkin sample (L×W×T: $5 \times 28 \times 1.4$ mm^3, tensile direction: 5 mm edge) is presented in **Figure 4.2**D. It is observed that the resistance of iSkin proportionally increase with the applied stain up to 1800%. To evaluate the strain sensitivity of iSkin-based sensors, gauge factor (GF) was further calculated from the slope of the relative resistance change ($\Delta R/R$) versus strain at different slope ranges. As shown in **Figure 4.2**D, the GF was found to increase with the strain. The GF can reach to 6.9 once the strain range is from 250% to 500% and 15.91 from 1000% and 1800%, respectively. The maximum strain level and GF of the iSkin is comparable to those of previous reported organohydrogel or hydrogel-based strain sensors (*38, 39*). In addition, the durability of iSkin for strain sensing was also tested. After 1300 cycles of repeated tensile loading-unloading cycles, the relative resistance change was maintained well even at a dried laboratory condition (RH = 25%, **Figure 4.2**E and F), indicating its good retention of strain sensing function. The conductive durability and the comparable strain sensitivity of the iSkin will make it a suitable sensing component for long-term wearables and soft robotics applications.

4.2.3. Ambient stability and anti-freezing testing of iSkin

We next examined the effect of hygroscopic/cryoprotective substance on ambient stability and anti-freezing capability of the iSkin. Compared with other bio-inspired neutral substances (e.g., ethylene glycol and dimethyl sulfoxide) and pure concentrated salts especially in high concentration (e.g., lithium chloride, sodium chloride and calcium chloride) (*40*), glycerol was selected here as the hygroscopic/cryoprotective candidate because of its low biotoxicity during on-skin wearable sensing, its little damaging to ionic cross-linking network and charging groups within the adhesive layer due to the neutrally charged property of glycerol, and its effective anti-dehydration and freezing inhibiting effects by disrupting the hydrogen bonds between H_2O molecules (*30*) and by forming strong hydrogen bonds with water molecules (*41*).

First, the changes in mass and resistance of iSkin samples (L×W×T: 40×10×1.4 mm^3) were characterized to measure its ambient stability at room temperature under different humidity conditions. No mass decrease was observed on samples stored at the relative humidity (RH) of 63% over 30 days (**Figure 4.3**A). Interestingly, the iSkin stored in the high RH environment (RH=88%) experienced a slight mass increase due to the large amounts of hydroxyl groups on the glycerol chains that led to a lower vapour pressure of water in the iSkin hydrogel matrix than the environment. In contrast, the mass of the original tough hydrogel rapidly decreased to 20% of the original mass, even in the extremely wet environment (RH = 88%) after only 3 days storage (**Figure 4.3**A and **Figure S4.5**A). This large mass reduction is due to the fact that the original hydrogel matrix without glycerol has a higher internal vapour pressure of water than that of the environment (*42*). Noticeably, in an extremely dry environment (e.g., RH = 15%), our iSkin can still maintain 75% of its original mass even after 30 days (**Figure 4.3**A), validating the strong water-retaining capability of glycerol. Similarly, the electrical resistance (measured along its length direction) of iSkin shows a good long-term ambient stability. For instance, there is no obvious resistance fluctuation observed on the iSkin device in the first five days while the resistance of the original tough hydrogel increased significantly even at the high RH conditions (RH = 63% and 88%, **Figure 4.3**B). On the other hand, although the resistance of iSkin in an extremely dry environment (e.g., RH=15%) experienced certain increase because of its mass decrease, the resistance level of ~100 kΩ after 30 days storage can still meet the requirement of strain sensing (*43*). In addition, we also studied the ambient stability of pure NaCl-laden hydrogel. The hydrogels treated with pure saturated NaCl solution (5.4M) showed relatively good stability in a humid environment (RH = 88%) but experienced an obvious mass decrease (33.2% and 57.1% after 30 days) when the RH was 63% and 38%, respectively (**Figure S4.5**B). In addition, the NaCl-laden hydrogel easily lost its high transparency for long-term storage even at RH = 63% because of salt precipitation as the evaporation of water from hydrogels (**Figure S4.5**C). These findings further proved that pure salts (e.g., NaCl) are not sufficient to maintain the water content in the hydrogel and to enhance its ambient stability. In contrast, the iSkin maintained its optical transmittance and its shape at RH = 63% after 30 days, while the original hydrogel shrunk obviously (**Figure S4.5**C). These observations indicate that the iSkin can preserve its optical transparency, shape and electronic function and could serve as a good ambient-stable material for many potential applications, particularly for wearables and soft robotics during the open-air usage.

As a promising sensing unit for wearables and robotics, we then examined the anti-freezing performance of the iSkin in subzero temperature environments. There are three different states of water in a hydrogel system, namely “free water” (fast exchange), “intermediate water” (slow exchange), and “unfrozen bound water” (*42*). Here, glycerol (66.6 wt%) solution dissolved with saturated NaCl content was used to treat tough hydrogel to optimize its amount of unfrozen bound water and enhance its anti-freezing property (*44*). Indeed, the as-synthesized iSkin showed excellent freezing tolerance with good transparency, mechanical flexibility and stretchability (twisting, bending, stretching and knotting) at extremely cold conditions (−30 °C for 24 h, **Figure 4.3**C and **Movie S4.3**) due to the large amount of unfrozen bound water. In contrast, the original tough hydrogels turned into an ice-like solid and was fragile when bending at −30 °C (**Figure S4.6**A and **Movie S4.3**) owing to their large amount of "free water" stored in the hydrogel. The iSkin remained unfrozen even at −70 °C for at least 1 h (**Figure S4.6**B). In addition, iSkin also remained high conductivity under extremely cold environment (5.34×10^{-2} $S \cdot m^{-1}$ @−25 °C and 8.7×10^{-3} $S \cdot m^{-1}$ @ −40 °C), which was superior to the original hydrogel (**Figure 4.3**D). The conductivity of iSkin was maintained even at −70 °C (1.96×10^{-5} $S \cdot m^{-1}$), while the conductivity of original hydrogel decreased to an unmeasurable level once below −25 °C (**Figure 4.3**D).

Besides the expected contribution from glycerol, the excellent anti-freezing property of iSkin may also partially stem from the ice-inhibiting effect of the hydrogel networks (*30*) and the electrolyte salts (*45*). To accurately determine the origin of the anti-freezing characteristic as well as the anti-freezing limits of the iSkin, we used differential scanning calorimetry (DSC) to test different treated hydrogels and their exchanged solvents from −120 °C to 15 °C. During heating, the original (water-based) hydrogel began to melt from −6.5 °C and revealed a sharp melting peak occurred at −1 °C (labelled on the yellow curve in **Figure 4.3**E), which is consistent with the results from a previous report (*45*). The DSC testing result of the original hydrogel also shows a peak shift compared to that of the pure water (yellow curve at **Figure S4.7**A). This slight peak shift can be attributed to the ice-inhibiting effect of Alg-PAAm polymer networks. We also found that pure electrolyte salt (NaCl) has a further ice-inhibiting effect on hydrogel as the melting point shifts from −6.5 °C to −24 °C (labelled on the green curve in **Figure 4.3**E). The melting point of

NaCl-laden tough hydrogel shifts more than that of pure saturated NaCl solution at 5.4M (−22 °C, labelled on the green curve in **Figure S4.7**A), further confirming the ice-inhibiting effect of the Alg-PAAm networks. Notably, both the glycerol-laden hydrogel and iSkin did not show any melting peak in the whole endo/heating thermogram because these two types of hydrogel did not frozen and showed no cold-crystallization peak on the Exo/cooling thermogram (**Figure S4.8**), which is consistent with the previous reported observation (*30*). During heating, the glycerol-laden hydrogel and iSkin only showed a peak similar to a glass transition at −97 °C and −95 °C, respectively (zoomed-in insets of blue and red curves in **Figure 4.3**E), indicating no observable icing of the hydrogels. This anti-freezing performance is better than most of the previously reported ionic hydrogels (**Table 4.1**).

In addition, we found that the presence of other components (e.g., NaCl and Alg-PAAm polymer networks) increased the glass transition point of glycerol-water system (66.6 wt%) to a higher temperature (blue and red curves in **Figure 4.3**E and red curve in **Figure S4.7**A), which is due to the components' disturbance to the strong supercooling phenomenon in the glycerol-water system. In fact, the anti-freezing and supercooling properties of the glycerol and the glycerol-laden hydrogel mainly depend on the glycerol-water ratio, as shown in **Figure S4.7** (blue lines) and **Figure S4.9**; a lower glycerol concentration (e.g. 30 wt%**, Figure S4.9**A) showed both crystallization and melting peaks on the DSC thermogram while a higher ones (e.g. 66.6 wt%, blue curve in **Figure S4.7;** and 85 wt%, **Figure S4.9**B) have neither of peaks due to the strong supercooling effect. As a result, the freezing tolerance of tough hydrogel can be enhanced accordingly and such a simple solvent exchanging method is effective to enhance the freezing tolerance of hydrogels. These observations indicate that the iSkin could serve as a good anti-freezing stretchable sensing component for use on wearables and soft robots in extremely cold environments.

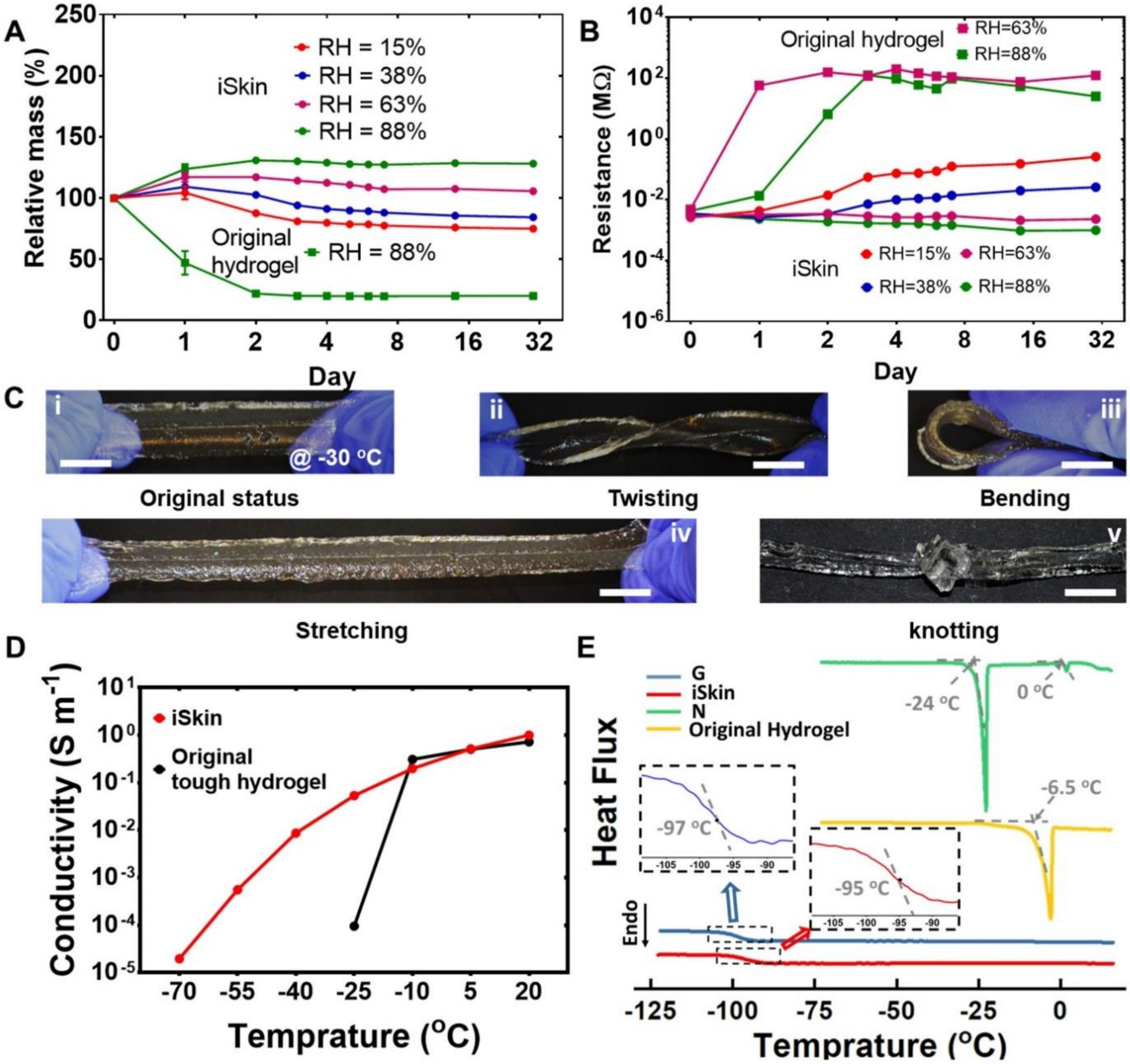

Figure 4.3. Ambient stability and anti-freezing capability of iSkin. (A) Mass change as a function of RHs (15%, 38%, 63%, 88%) for iSkin within 30 days. Original Alg-PAAm tough hydrogel at the RH=88% was used as control. The mass of hydrogel is normalized with its initial mass (N = 4). (**B**) The resistance changes of iSkin and original Alg-PAAm tough hydrogel under different humidity conditions within 30 days. (C) Photographs of iSkin without freezing and can

twist, bend, stretch and knot at −30 °C. Scale bar is 2 cm. (**D**) Temperature-dependent ionic conductivity investigation of iSkin and the original tough hydrogel. **(E)** Dynamic scanning calorimetry (DSC) results at the endo direction of iSkin, NaCl-laden tough hydrogel (N), glycerol-laden tough hydrogel (G), and the original tough hydrogel in the temperature range from −120 °C to 15 °C. The small gray arrows highlight the melting points of NaCl-laden tough hydrogel and the original tough hydrogel.

4.2.4. Surface adhesion testing of the iSkin

The strong adhesion of hydrogel to surfaces is a favorable feature for applications in wearable sensing and soft robotics. For on-skin wearable sensing, the iSkin should adhere tightly to the human skin to enhance the fidelity of signal acquisition and eliminate motion-induced signal artifacts. The self-adhesion of our pristine iSkin (**Figure S4.10**) is not strong enough to withstand a heavy weight and rigorous deformation. In order to satisfy the adhesion requirement of various applications (e.g., smart clothes for underwater and/or extremely cold environments, wearables for sweaty and dynamically deformed human skin during sports, and smart wound dressing for wet organ surfaces during recovery monitoring), our iSkin should adhere to various surfaces firmly during wearing. The adhesion property of the iSkin for different substrates with different surface conditions was investigated. The adhesion energy was quantified by T-peeling tests (setup shown in **Figure S4.11**).

First, we chose porcine skin (L×W: 80mm×15mm) as the model for iSkin-skin bonding testing as it closely resembles the surface property of human skin and is robust and tough enough to ensure that the ultimate adhesion failure occurs at the iSkin-skin interface. Due to the bridge polymer interpenetration and the covalent bonding between amino and carboxyl groups on skin and hydrogel surfaces, the adhesion energy of iSkin to the regular porcine skin was 537.4 $J{\cdot}m^{-2}$

(pink curve in **Figure 4.4**A and B, **Movie S4.4**), which indicates strong adhesion (*29*). External ions may hamper the adhesion capability by disturbing the positively charged primary amine groups of bridge polymer and thus the formation of both imine and ionic bonds (*46*). However, we found that the interfacial adhesion energy of the iSkin-skin bonding has no significant difference with that of hydrogel-skin bilayer bonded with the same bridge polymer layer (**Figure S4.12**), proving the presence of neutrally charged glycerol can suppress the side effect of pure ions to the adhesion performance.

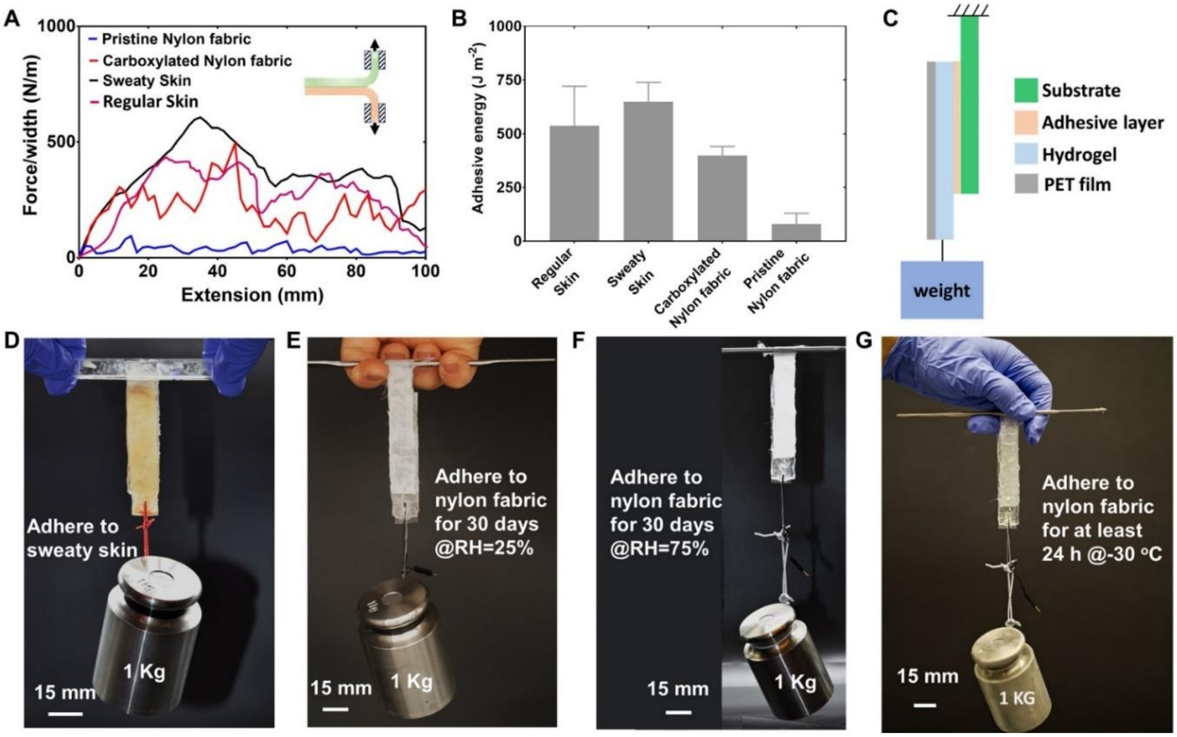

Figure 4.4. Surface Adhesion Property of iSkin. (A) Force/width curve for adhesion between iSkin and different substrate surfaces. (**B**) Comparison of the adhesive energy between different substrate surfaces. (**C**) Schematic setup of the adhesion test between iSkin and diverse substrate surfaces (**D**) The adhesion stability of iSkin adhered to sweaty porcine skin. (**E**) The long-term adhesion capability of iSkin adhered to carboxylated nylon fabric at relatively dry environment (RH=25%) (**F**) The long-term adhesion capability of iSkin adhered to carboxylated nylon fabric

at relatively wet environment (RH=75%) (**G**) The anti-freezing adhesion capability of iSkin adhered to carboxylated nylon fabric. Subzero temperature is −30 °C.

In addition, most ionic hydrogel devices do not have strong adhesion capability to wet surfaces (**Table S4.1**). The adhesion formation of a hydrogel device with skin is often complicated because of the sweating and the dynamic movements of skin. Sweating is inevitable in real life especially during long-term wearable sensing (e.g., during sport and exercise). To simulate the sweating condition on skin, the porcine skin was first covered with artificial sweat (**Figure S4.13**B) before the attachment of an iSkin. The adhesion energy of sweaty iSkin-skin bonding was found to be 649.3 $J \cdot m^{-2}$ (black curve in **Figure 4.4**A, B, and D, **Movie** S4**.**4), which shows a slightly higher adhesion performance than that (537.4 $J \cdot m^{-2}$) without sweat exposure, confirming strong wet adhesion capability. Similarly, we chose nylon fabric (the out-layer of most winter coats such as Canada Goose®) as the model substrate to mimic the adhesion between iSkin and the winter coat. We found that the iSkin can adhere strongly to the carboxylated nylon fabric with an adhesion energy 398.4 $J \cdot m^{-2}$ (red curve in **Figure 4.4**A and B, **Movie S4.4**), while the bonding between iSkin and the pristine nylon fabric is weak (79.7 $J \cdot m^{-2}$) due to the non-existence of carboxyl groups. This strong bonding is mainly because primary amine groups within the bridging polymer covalently bind with the carboxyl groups from the carboxylated nylon fabric and the iSkin matrix.

Furthermore, we studied its anti-freezing and long-term adhesion capability to different substrates. As shown in **Figure 4.4**C, the adhesion between iSkin and substrates (adhesion area: $1.3 \times 5.5\ cm^2$) securely held a 1kg weight (14.0 kPa) in both dried and humid environments for more than 30 days (**Figure 4.4**E and F). In addition, the adhesion between the iSkin and nylon fabric at underwater or subzero temperature environment was comparable to that of the original one; that is, the iSkin-nylon fabric adhesion held a 500 g weight (7.0 kPa) at the underwater environment for more than 20 h (**Figure S4.13**A, **Movie** S4.5**)** and held a 1kg weight (14.0 kPa) at −30 °C for more than 24 h (**Figure 4.4**G, **Movie** S4.5). The adhesion maintenance of iSkin at low temperature could be attributed to the diffusion of glycerol into the thin adhesion layer and the inhibition of ice formation in this layer. This strong surface adhesion under diverse conditions ensures the fidelity of signal acquisition from the iSkin device as a sensing component on wearables and soft robots in diverse environments.

To our best knowledge, this is the firstly reported conductive ionic hydrogel with high stretchability, high toughness, long-term stability, superior diverse adhesion capability, and anti-freezing behavior, making it particularly useful for the construction of adhesive ionic skins for applications in various extreme environments. Note that both ionic-related mechanical and adhesive properties were either enhanced or maintained due to the presence of glycerol, despite of the disturbance from monoions.

4.2.5. Adhesive iSkin for wearable sensing and human-machine interaction

Thanks to the unique combination of mechanical, electrical, anti-freezing and surface adhesion properties, our iSkin can serve as wearable strain sensors for joint gait measurement and human-machine interaction. Here, an iSkin strain sensor of $80\times25\times1.4\text{mm}^3$ was attached to the arm joint position of a winter coat. Our iSkin can firmly adhere to the winter coat surface during arm bending at subzero temperature (−10.6 °C in **Figure 4.5**A and **Figure S4.14**). Due to its good conductivity, high stretchability and freezing-tolerant adhesion capability at low temperature, the iSkin strain sensor can monitor the bending-release motions of an arm at −10.6 °C without debonding from the winter coat (**Figure 4.5**B). This capability can be utilized to design smart winter cloth with iSkin strain sensors for extreme environment applications.

We also demonstrated on-skin strain sensing during user exercise. In this application, the iSkin should always adhere strongly to the human skin whether the skin is dry, wet (e.g., with sweat), and/or in dynamic movement condition. By applying a thin layer of adhesive bridge polymer, a piece of iSkin (80×25×1.4 mm^3) was attached to the knee of a volunteer for gait measurement (**Figure 4.5**C**).** Compared with the pristine iSkin, the adhesive iSkin can firmly adhere to the knee after multiple vigorous jumps (**Figure S4.15**, **Movie S4.6**). Furthermore, we found this strong adhesion can endure a long-term vigorous workout (e.g. 30-min step-up) without debonding from the sweaty and dynamically stretched skin surface (**Figure 4.5**C, **Figure S4.16**C and D, **Movie** S4**.**6). As expected, our iSkin has no observable adverse effect on the skin once detached (**Figure S4.16**A and B), thanks to the excellent biocompatibility of the iSkin material system. In addition, the resistance output of iSkin for walking gait measurement is highly repeatable before and after this 30-min vigorous workout (**Figure 4.5**D**)**, further proving the strong and robust on-skin adhesion and reliable strain sensing capability of the iSkin.

The wearable iSkin strain sensor can also be used for constructing a gesture-based interface for human-machine interaction. We constructed a strain-sensing glove by pieces of iSkin (30×10×1.4 mm^3) array on the five finger joints (**Figure 4.5**E) of a surface-functionalized Ecoflex glove (glove fabrication and preparation described in **Materials and methods**). The resistance of each iSkin changed proportionally with the bending angle of its corresponding finger joint (**Figure 4.5**I). The resistance change was converted into a voltage change through a voltage divider circuit and read by an Arduino UNO board. Due to the strong bonding between Ecoflex and iSkin (to be further discussed in the next section), a user wearing the glove can reliably control the gesture of a robotic hand due to the high signal fidelity of the iSkin strain sensors **(Movie S4.7**). As a demonstration, the robotic hand was controlled by the glove to expressed the message of ‘I love you’ with three sequential hand gestures (**Figure 4.5**F-H and **Movie S4.7**). This demonstration highlights the feasibility of using our iSkin for human-machine interaction.

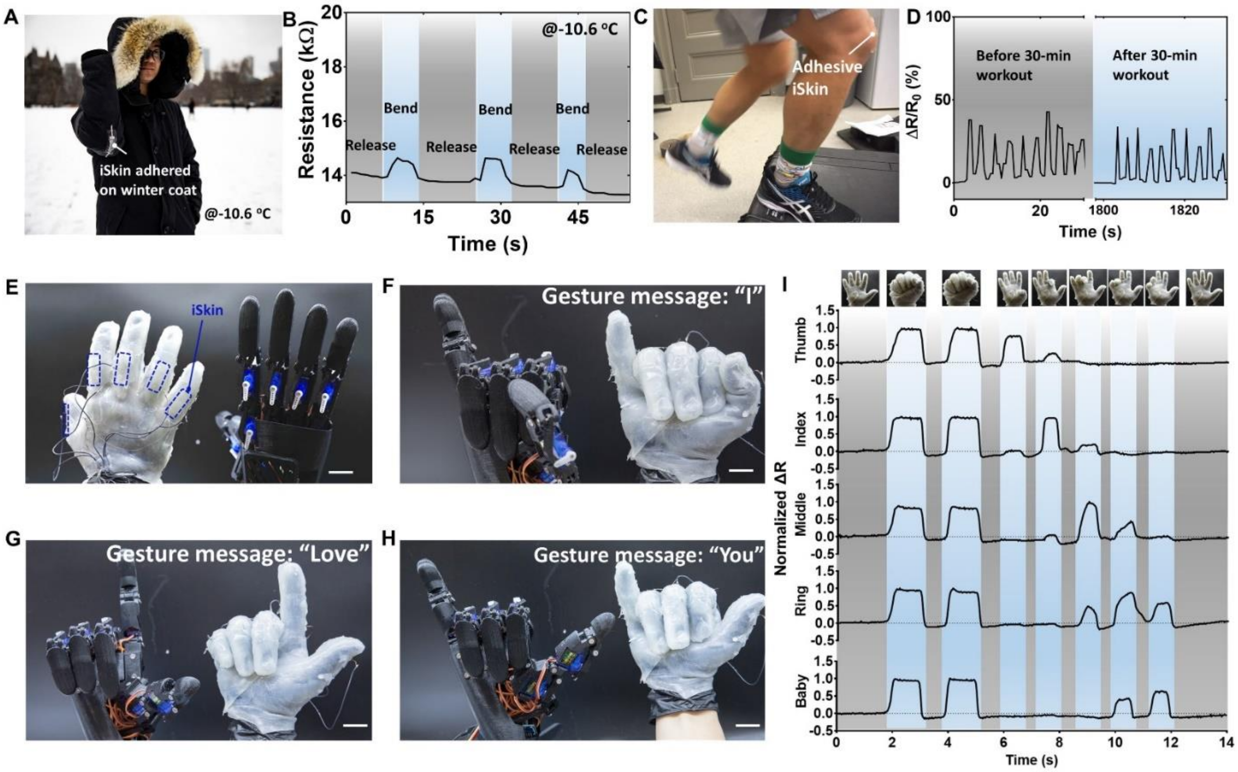

Figure 4.5. Adhesive iSkin for wearable demonstrations and human-machine interaction. (A) Anti-freezing iSkin adhered to a winter coat for strain sening at −10.6 °C. (**B**) Repeatable resistance outputs of the wearable iSkin on the winter coat for arm motion monitoring at −10.6 °C. (**C**) Schematic setup of iSkin adhered to the knee for gait measurement, showing good adhesion capability when adhered to a dynamic and sweaty skin surface during long-term vigorous workout (e.g. step-up). (**D**) Relative resistance outputs of the iSkin adhered to the knee for walking gait measurement. (**E**) Schematic setup of iSkin (denoted within purple dash rectangle) adhered homemade glove (00-35 Ecoflex) for human-machine interaction. (**F-H**) Demonstrations of the

robotic hands controlled by human hand gestures to show “I”, “Love”, “ You”. Scale bar: 2 cm. (**I**) Normalized resistance change (ΔR) of iSkins is plotted as a function of time during a sequence of finger gestures, in which the iSkins were adhered on each finger joint of the glove.

4.2.6. Adhesive iSkin for strain sensing on soft grippers and locomotive soft robots

The large-strain sensing capability of the highly stretchable iSkin would also be highly useful for strain sensing on soft robots. Recently, soft robotic systems have been developed to bridge the gap between machines and people due to their unprecedented adaptability (*47*). Constructed from intrinsically soft and/or stretchable materials, soft robots hold great potential for many applications, including manipulation of fragile objects, navigation in space-restricted and/or harsh environments, and human rehabilitation and assistance. For strain/deformation measurement on soft robots, it is highly desired to develop stretchable strain sensors that are made from materials compatible with soft robot materials and can be readily integrated into existing soft robot designs (*11, 12, 47*). With comparable mechanical properties to Ecoflex and other commonly used elastomers in soft robots, our iSkin is mechanically compatible with typical soft robot designs. The strong surface adhesion capability of iSkin on elastomers will also enable flexible integration of strain sensors during or after soft robot fabrication. In this section, we demonstrate the facile integration of iSkin strain sensors onto two typical soft robotic systems—a soft gripper and a quadruped soft robot—to endow them with reliable deformation feedback under both normal and extreme conditions. Importantly, different from other hydrogel-based ionic sensors (*12, 48*), the unique combination of high ambient stability, excellent anti-freezing property, and strong adhesion capability (for diverse material surfaces) of the iSkin could further expand the scope of its applications in soft robotics.

We first demonstrated the strong bonding between iSkin and Ecoflex on a bilayer of 1.4-mm-thick iSkin on the 100-μm-thick Ecoflex (Ecoflex 00-50, Smooth-On Inc.). Instead of using the bridge polymer adhesive layer, here the iSkin was bonded to the Ecoflex using an alternative strategy that has revealed the largest hydrogel-elastomer adhesion energy reported ever (*49, 50*). This strong iSkin-Ecoflex adhesion stems from *in-situ* chemical grafting of methacrylate groups on the surface of the chemisorbed Ecoflex to the PAAm network during curing (*49*). Nevertheless, the bridge polymer adhesive layer we demonstrated in previous sections is still effective to create strong bonding between iSkin and Ecoflex or other elastomers through surface functionalization of the elastomer surface with amine (*51*) and/or carboxyl (*46*) groups. The strong hydrogel-Ecoflex bonding was maintained after adding anti-freezing and electrolyte compounds into the hydrogel matrix of iSkin, and this adhesion can endure large stretching [>150, beyond the strain limit (100%~150%) of most soft robots (*36*)] without debonding (**Figure 4.6**A, **Movie S4.8**).

We then characterized the performance of an iSkin-equipped soft bending actuator (**Figure 4.6**B). A piece of iSkin (50×18×1.4 mm^3) was attached to the top surface of the bending actuator for bending angle measurement. Cyclic inflation-deflation tests were conducted, during which the actuator was repeatedly inflated (with a constant pressure for 2.5 s) and deflated (with zero input pressure for 2.5 s) with the inflation pressure increasing cycle by cycle from 6.8 kPa to 25.5 kPa (**Figure 4.6**C and **Movie S4.9**). The iSkin firmly adhered to the actuator surface during repeated bending of an bending angle θ from 0° to 90°, and no debonding occured during the entire test (**Figure 4.6**C and **Movie S4.9**). The attachment of the iSkin layer with mechanical properties comparable to Ecoflex had no obvious impact on operation of the actuator (**Movie S4.9**). The resistance change ΔR of the iSkin (**Figure 4.6**D and E) increased with the actuator bending angle θ faithfully and in real time during the entire inflation-deflation period. In contrast, the inner pressure of the actutor, monitored by a pressure sensor, only dramatically increased at the beginning of the inflation peirod then rapidly dropped and stablized at a much lower level (blue curve in **Figure 4.6**D) because of the air leakage through Ecoflex; both the initial peak value or the stabalized value of the actuator inner pressure did not correlate with the actuator bending angle. This result proved that the iSkin can provide more reliable deformation/postion feedback for a soft actuator than their innner pressure. In addition, we repeatly exerted an upward force to the free end of the inflated bending actuator with an intial angle of 60° (insets in **Figure 4.6**F and **Movie S4.10**), and found that the iSkin resistance decreased upon force application and alway recovered to its initial value after force removal (red curve in **Figure 4.6**F, and **Movie S4.10**), while the actuator inner pressure did not change noticeably with the force applied and removed (blue line in **Figure 4.6**F and **Movie S4.10**). This observation further illustrates that the iSkin integrated on a soft robotic system could provide human-like sensing feedback indicating robot-environment interaction. The adhesion-enabled integration of pre-fabricated iSkin sensors onto soft robots provides a general and facile strategy for developing position- and force-feedback soft robots.

To further demonstrate the utility of iSkin sensing feedback, we integrated three iSkin sensors ($50\times18\times1.4$ mm^3) on a soft gripper for object grasping (**Figure 4.6**G). The soft gripper was inflated continuously to grasp an object (potato or peach in our experiments) until a secured grabbing was achieved and then deflated to it is natural initial shape, during which the resistance values of the three iSkin sensors were continuously monitored. It was found that the slope of the measured resistance curve decrease obviously upon contact between the gripper arm and the object (**Figure 4.6**H and **Movie S4.11**). Resistance curves of the same iSkin sensor from repeated grasping of the same potato are highly consistent, which proves the high repeatability and robustness of the iSkin sensor. No obvious difference was observed in resistance curves of the three iSkin sensors during the same grasping process. The slope-changing portion of the resistance curve measured during object grasping (labelled with dashed ovals in **Figure 4.6**H) could be potentially utilized, together with other feedback modalities (e.g., contact forces and curvature distributions of the gripper arms), for shape classification and object recognition during grasping, through learning-based algorithms (*11, 52*). Equipped with the anti-freezing iSkin sensors, such a soft gripper could be used for robotic manipulation tasks in extreme cold environments (e.g., pick and place of frozen food items in cold storage rooms).

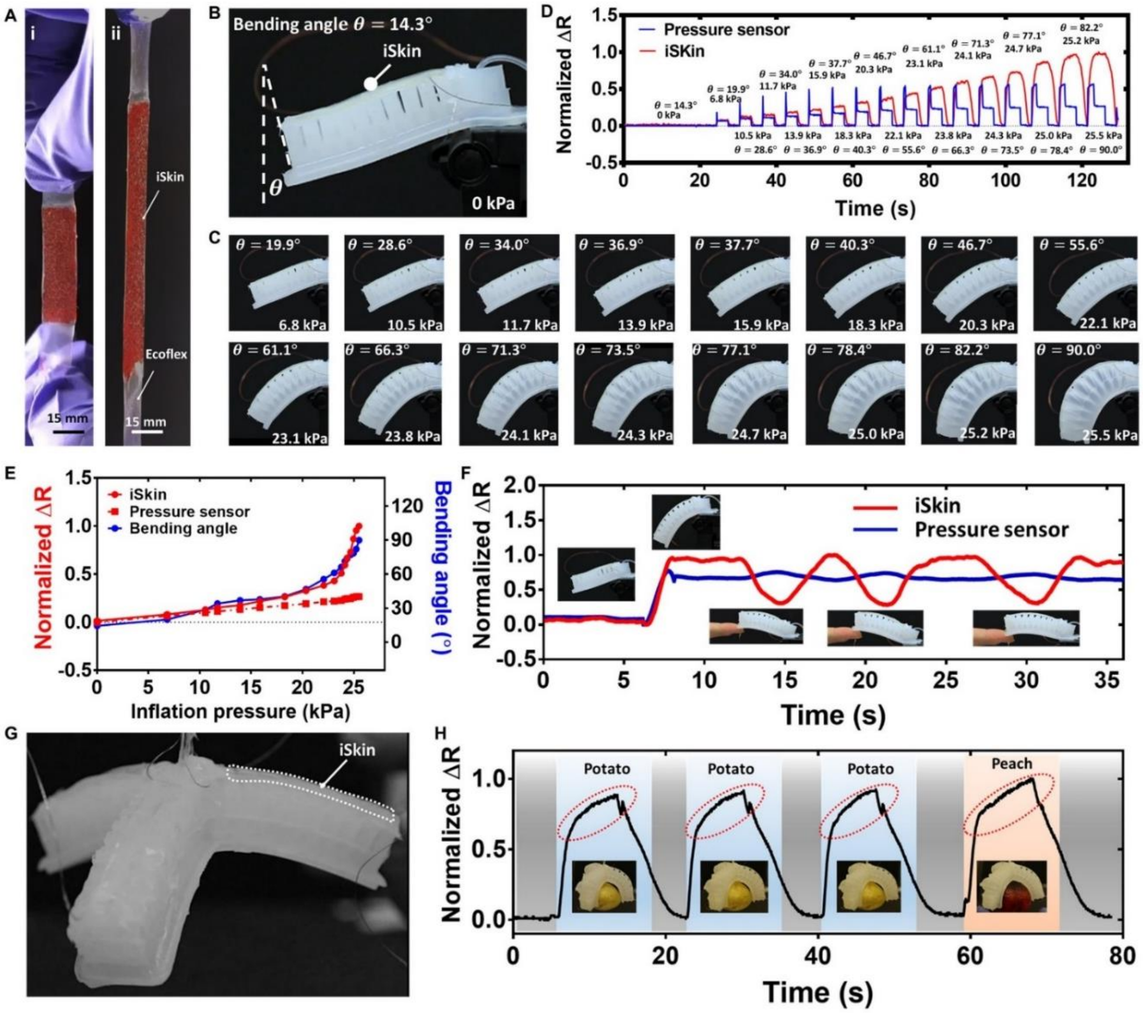

Figure 4.6. Performance of iSkin-equipped smart soft actuators. (A) the strong adhesion between iSkin and Ecoflex can endure large stretch (at least 150%). Note that red food dyes are

stained on iSkin to enhance the contrast between iSkin and elastomers. Images of an iSkin-equipped smart soft actuator at **(B)** 0 kPa and **(C)** during a dynamic free displacement test, in which the actuator experiences periods of deflation (0 kPa) to increasing inflation pressure (held for 2.5 s) in increments of 6.8~25.5 kPa. **(D)** iSkins endow soft actuators with the ability to sense their actuated state**.** Resistance change (ΔR) of iSkin and a commercial inflation pressure sensor after normalization is plotted as a function of time during inflation. (**E**) Normalized ΔR for iSkin and the commercial inflation pressure sensor, and bending angle θ, as a function of inflation pressure read from a pressure meter during free displacement. (**F**) Normalized ΔR for iSkin and the commercial inflation pressure sensor is plotted as a function of time when an iSkin-equipped smart soft actuators was undergoing three times hand bending, in which the actuator is in inflation status. Inset figures show the soft actuators under different status. (**G**) Optical photo of an iSkin-equipped smart soft robotic gripper. (**H**) Normalized ΔR of an iSkin is plotted as a function of time during fruits and vegetable grabbing. The curve shape difference within the red dash circle during grabbing procedure can differentiate varies kinds of fruits and vegetable. Inset figures show the soft robotic gripper grabbing a potato and a peach.

Most of the previous studies focused on developing sensing technologies for soft robots in the normal temperature range (*12, 16, 47, 48, 53, 54*), there is little research on the performance of soft robotic sensors under extremely cold conditions. In addition, strong adhesion between hydrogel-based ionic sensors and soft robots under the subzero temperature has not been reported. Here we first studied the bonding between iSkin and soft robots under the subzero environment. The bonded iSkin-Ecoflex bilayer presented in **Figure 4.6**A was stored at −30 °C for overnight before testing. The strong adhesion between the iSkin and Ecoflex was maintained well in a such cold temperature, and the anti-freezing adhesion can still endure large stretching (>110%) without any debonding (**Figure S4.17A, Movie S4.12**). This meets the requirement of soft/stretchable sensors for many soft robotic applications in extremely cold environment. In contrast, a bonded bilayer of original tough hydrogel and Ecoflex layer cannot be stretched anymore after overnight storage at −30 °C, due to the freezing of the original hydrogel (**Figure S4.17B, Movie S4.12).**

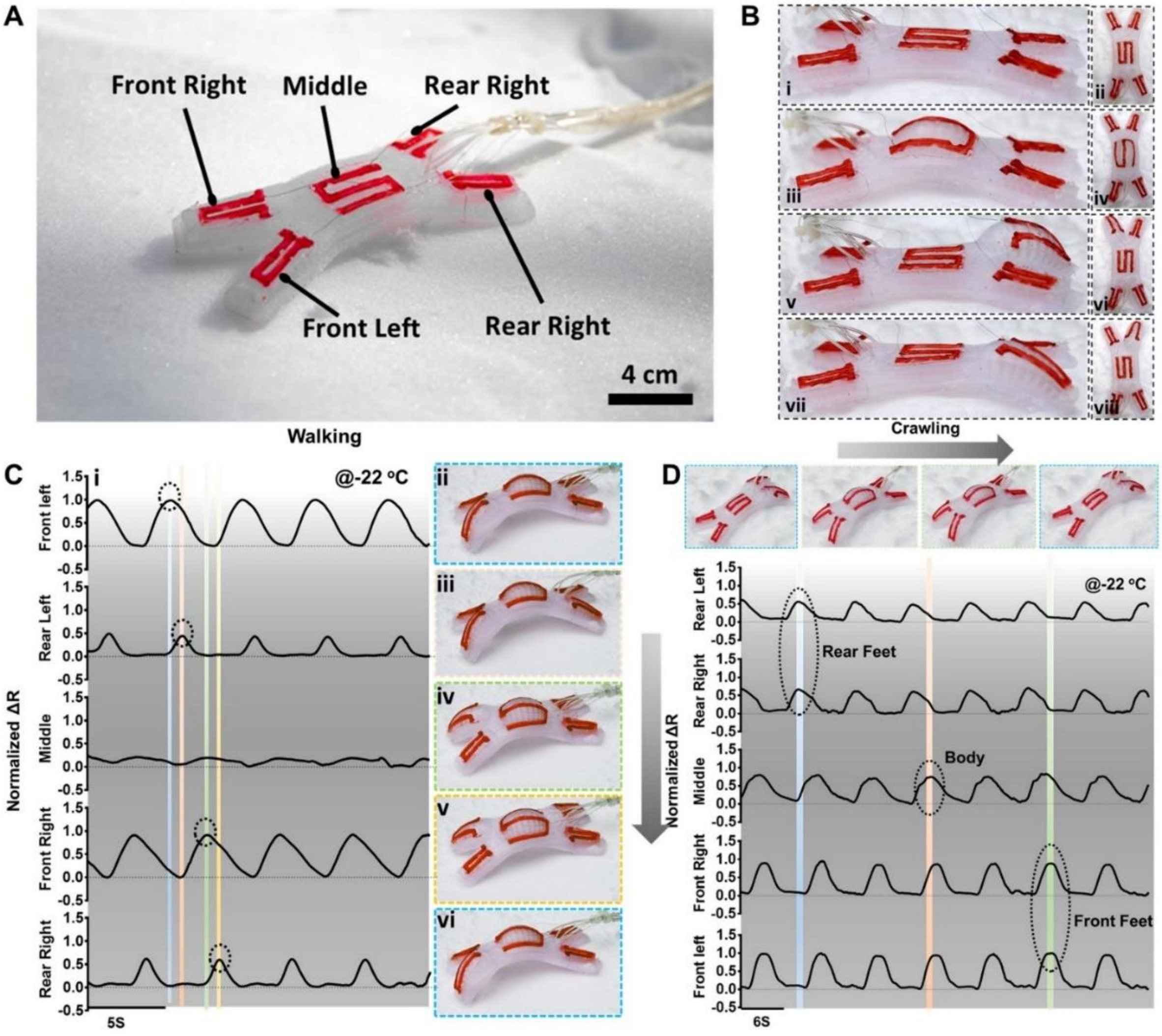

Figure 4.7. Performance of iSkin-equipped intelligent soft robots at the subzero environment. (A) An optical photo of an iSkin-equipped pneumatic intelligent soft robot. The U-shape iSkins were bonded on the front right, front left, rear right and rear left feet/ pneumatic chamber, and Z-shape iSkin bonded on the body (middle).Note that red food dyes are stained on iSkin to enhance

the contrast between iSkin and elastomers. (**B**) Optical photos of an iSkin-equipped pneumatic intelligent soft robot under different inflation stages: (i, iii, v, vii) side view and (ii, iv, vi, viii) top view of the robot under depressurization, body (middle), left and right foot under inflaction sequentially. There is no debonding happening beween iSkin and Ecoflex robots during cyclic inflation-deflation from the side view figures. (**C**) iSkins endow soft robot with the ability to sense their actuated state and gait patterns even at the extremely cold enviroment. Normalized ΔR of five iSkins is plotted as a function of time when soft robot is under walking gait at −22 °C (**i**) and optical photos of the soft robot during a sequence of dynamic walking on the snow (**ii-vi**). (**D**) Optical photos of the soft robot during a sequence of dynamic crawling on the snow (**i-iv**) and normalized ΔR of five iSkins is plotted as a function of time when soft robot is under crawling gait at −22 °C (**v**).

Then, we integrated iSkin sensors (colored by red dye) onto a classical quadruped soft robot to provide motion feedback of the five pneumatic actuators on the robot (**Figure 4.7**A). Four U-shaped iSkin sensors were individually adhered on four legs of the robot, and one S-shaped iSkin sensor on the middle body part. Because of its excellent anti-freezing property, the iSkin is still highly stretchable at subzero temperature and thus does not add obvious restriction to the compliance of the soft robot. **Figure 4.7**B shows the locomotion sequence of the soft robot operating on outdoor snow at −5.3 °C **(Movie S4.13),** during which the five iSkin sensors strongly adhered to the robot body and provided reliable motion feedback signals. This excellent adhesion and anti-freezing performance are essential for demonstrating a motion-feedback soft robot operating in extremely cold conditions. **Movie S4.13** presented the two locomotion modes (walking and crawling) of the iSkin-equipped quadruped soft robot on the snow. One can see that the iSkin have little compliance restriction on the locomotion of the soft robot at low temperature due to the unique shape design and the mechanical stretchability of iSkin in a such harsh environment. Under walking gait, current pressurizing patterns can produce forward locomotion at a speed of 0.56 m·hour^{-1} (4 body lengths hour^{-1}) on the snow (**Figure S4.18, Movie S4.13**).

To further testing the robot in a colder environment, we operate the robot in a freezer chamber (−22 °C, **Figure S4.19A**) and measured the feedback signals from the five iSkin sensors. During the entire testing of 500 locomotion cycles of the robot, there was no debonding of the iSkin observed **(Movie S4.14** and **Movie S4.15**), confirming the feasibility of long-term use of the iSkin at freezing temperature. At −22 °C, the robot can produce forward walking locomotion at a speed of 1.2 m·hour^{-1} (8.5 body lengths·hour^{-1}**, Figure S4.19**, **Movie S4.14**) and forward crawling locomotion at a speed of 1 m·hour^{-1} (7 body lengths·hour^{-1}, **Figure S4.20, Movie S4.15**). During the testing, the iSkin sensors provided real-time motion feedback of the locomotive gaits of the five pneumatic actuators (walking gait feedback shown in **Figure 4.7**C and **Movie S4.14**; crawling gait feedback shown in **Figure 4.7**D and **Movie S4.15**). These results show that iSkin strain sensor possesses high material compatibility, easy-to-attach surface adhesion capability, and excellent anti-freezing property suitable for sensing applications on soft robots operating in extremely cold environments.

4.3. Conclusions and Discussion

In this study, we reported the design, fabrication and characterization of a novel adhesive hydrogel-based ionic skin (iSkin), and demonstated its applications in wearable sensing and soft robotics. The iSkin recapitulates the salient features of human skin by combining high toughness and stretchability, ambient stability, anti-freezing property and strain sensing capability. Our results have demonstrated that the iSkin has a toughness of 11.41 kJ·m^{-2} and can sustain more than 1975% strain without rupture, which is mainly attributed to the hybrid cross-linked network design of the material, namely the synergistic effect of ionic cross-linked alginate and covalently cross-linked PAAm networks. Importantly, we found, for the first time, that the inclusion of monovalent ions into the hydrogel networks did not unzip the calcium-alginate ionic bonds and maintained the mechanical property of original tough hydrogel due to the incorparation of the neutral hygroscopic substance glycerol. In addition, due the to unique chemical structure of tough hydrogel and negaligible electrical effect of neutral hygroscopic/cryoprotective substance, the positively charged bridge polymer within the adhesive layer of the iSkin can penetrate into both the tough hydrogel and the target surface (e.g., skin), forming strong adhesion by electrostatic interactions, physical entanglement, and chemically anchoring.

The iSkin showed both strong dry and wet adhesion capability to different substrate surfaces including skin and cloth fabric with the adhesion energy of 398 $J\cdot m^{-2}$ and 649 $J\cdot m^{-2}$, respectively. Moreover, the inclusion of the neutral hygroscopic substance glycerol and the electrolyte NaCl maintains the electrical conductivity of iSkin, and substantially improves the stability of its conductivity, physical and adhesive properties both in ambient and extremely cold environments. Our iSkin showed an ambient conductivity of 0.904 $S\cdot m^{-1}$ comparable to similar conductive ionic hydrogels and can maintain its electrical property after 1300 cycles stretching and one-month storage in the ambient environment. With an extremely low temperature tolerance (−95 °C), our iSkin show measurable conductivity of 1.96×10^{-5} $S\cdot m^{-1}$ even at −70 °C. In addition, the strong iSkin-substrate bonding revealed long-term stability both in dry/wet environments and at extremely low temperature (at least −30 °C). Thanks to the unique combination of mechanical, physical and electrical properties, the iSkin can find numerous applications such as smart winter coat with strain sensing capability, wearable exosuit for gait measurement, stretchable electronic glove for human-machine interaction, motion-feedback soft robots operating in cold environments.

While this work was focused on the design, characterization and proof-of-concept demonstration of the iSkin, further research is needed to increase the integration level and improve the performance of the iSkin. For instance, microfabrication and 3D printing methods need to be developed for constructing micrometer-sized iSkin components and realizing more complex designs such as micro-sensor arrays for enhanced spatial sensing resolution (*43, 55, 56*). In addition, similar to other types of stretchable hydrogel sensor, the repertoire of ionic devices could be expanded to achieve other functionalities, for instance, sensing of humidity (*10*), temperature, pH (*57*), glucose (*58*), and other biomolecules and chemicals (*17*). Such multi-modality sensing capabilities of the iSkin can potentially empower wearables and soft robots with higher level of intelligence for more sophisticated tasks. Moreover, the iSkin is potentially an excellent conductive material to fabricate ultrastretchable triboelectric nanogenerator, which can serve as stretchable and portable power sources for seamlessly integration with untethered wearables and soft robots (*47, 59*). Last but not least, the adhesion method based on the bridging polymer adhesive needs to be further improved to shorten the relative long time to form strong adhesion (5-30 min) (*29, 50*), which may be solved by the recent developed dry double-sided adhesive tape working for a variety of material surfaces (*51*).

In summary, we developed a highly stretchable, anti-freezing, ambient-stable ionic skin inspired by the salient features of human skin. With strong surface adhesion capability, the iSkin is highly suitable for wearable sensing and soft robotics. The presented design and fabrication approach to construct mechanically and electrically robust hydrogel is also applicable to constructing other hydrogel systems. We envision that the results presented here will lead to the development of next-generation wearable devices and soft robotic systems with human-like sensation.

4.4. Materials and methods

4.4.1. Materials

Ionic cross-linker calcium sulfate ($CaSO_2$, 255548), Alginate (A2033), acrylamide (AAm, A8887), covalent cross-linker N,N'-methylenebis(acrylamide) (MBAA, M7279), free-radical initiator ammonium persulfate (APS, A3678), polymerization accelerator tetramethyl-ethylenediamine (TEMED, T7024), photoinitiator IRGACURE 2959 (I2959), acetic acid (695092), sodium chrolide, bridging polymer chitosan of medium molecular (448877), the coupling reagents, 1-ethyl-3-(3-dimethylaminopropyl) carbodiimide hydrochloride (EDC, E1769) and nhydroxysulfosuccinimide (sulfo-NHS, 56485), hygroscopic substance glycerol (G9012) and humidity control reagent Lithium chloride (LiCl, 793620) were purchased from Sigma. Hydrochloric acid (HCl, 9H61734) was purchased from Bioshop. Artificial sweat with PH = 5.5 was purchased from Taobao. Milli-Q (18.3 MΩ) water was used in all experiments. Porcine skin was purchased from a local grocery store. Pure nylon fabric was purchased from Amazon.

4.4.2. Fabrication of iSkin

The fabrication of iSkin consists of three steps: i) the synthesis of dissipative matrix alginate-polyacrylamide (Alg-PAAm) tough hydrogel; ii) solvent exchange; and iii) adhesive layer coating. The Alg-PAAm tough hydrogel was prepared following a modified protocol based on a previously reported protocol (*29*). In brief, shown in **Figure S4.1**, sodium alginate powder and acrylamide were first dissolved in distilled water at 2 wt. % and 12 wt. % respectively, and stirred overnight until a clean solution was obtained. After degassing, this prepared pregel solution of 10mL was then mixed with 36μL of 2 wt. % MBAA, 8μL of TEMED in one syringe (syringe A, BD, 20mL); 226μL of 0.27M APS and 191μL of 0.75M $CaSO_4$ slurries were injected into another syringe (syringe B, BD, 20mL). All bubbles should be removed before further cross-linking. After connecting by a female luer x female luer adapter (Cole-Parmer), solutions in two syringes were mixed by push the syringe pistons forward and back for 10 times. The mixture was stored inside a closed glass mold at room temperature overnight to allow complete polymerization.

After that, hygroscopic reagents and electrolyte salt were added into the hydrogel devices to increase their ambient stability, anti-freezing capability and ionic conductivity. Unless noted elsewhere, the conductive hygroscopic solvent for exchanging was prepared by adding glycerol to the saturated NaCl aqueous solution (5.4 M) and the weight ratio of glycerol to distilled water is 2:1 due to the fact that at around 66.6 wt% of glycerol in a glycerol-water mixture the lowest freezing temperature is achieved (*44*). To ensure that the concentration of NaCl and glycerol in the external solution remained nearly constant before and after soaking the hydrogel, we prepared the solvent solution with a volume 20 times the volume of the hydrogel. The obtained tough hydrogels were taken out of the molds and were either directly used for testing as the control group or immersed in the conductive hygroscopic solvent for 2.5-h exchanging to reach the equilibrium state as reported before (*30*).

Before surface adhesive layer development, all the visible liquid should be removed from the hydrogel. The surface was treated with the bridging polymer and coupling agents for carbodiimide coupling reaction. The bridging polymer chitosan was dissolved into distilled water at 2.0 wt. % and the pH was adjusted to 5.5~6 by acetic acid. EDC and NHS were used as the coupling reagents. The final concentrations of EDC and NHS in the solution of the bridging polymer were both 12mg/mL. The mixture of the bridging polymer and coupling reagents was applied to the surface of the dissipative matrix and then sticked on the porcine skin or nylon fabric surface.

The iSkin was adhered to the elastomers using the modified method reported previously (*49*). Briefly, the surfaces of elastomers (e.g., 00-50 Ecoflex, Smooth On) were thoroughly cleaned with methanol and deionized water, and completely dried with nitrogen gas before the benzophenone treatment. Thereafter, benzophenone solution (10 wt.% in ethanol) was applied onto the elastomer to evenly cover the entire elastomer surface for 15 min at room temperature. Then, the elastomer was washed with methanol three times and completely dried with nitrogen gas before use. Hydrogel was prepared by mixing 10 ml of a carefully degassed aqueous pregel solution (12.wt.% AAm, 2 wt.% sodium alginate and 36μL of 2 wt. % MBAA) with ionic cross-linkers (191μL of 0.75M $CaSO_4$ slurries) and Irgacure 2959 (0.2 wt.%). The mixture was then mixed quickly, poured onto the freshly treated elastomer film supported by a glass mold, and then covered by glass plate with hydrophobic coating. The whole assembled mold followed by ultraviolet irradiation in a 254 nm ultraviolet chamber (28–32 $mWcm^{-2}$, UVO-Cleaner 42A, Jelight Company, Inc.) for an hour, during which the PAAm network was covalently cross-linked and bonded onto elastomer surface. Thereafter, the whole hydrogel-elastomer film was peeled off from the glass mold and soaked in the conductive hygroscopic solvent for 2.5 h exchanging. Then, the iSkin-elastomer film was fabricated successfully and put in a Ziploc bag at 4 °C.

4.4.3. Mechanical Characterization

Pure shear tests were conducted to determine the matrix toughness with a universal testing machine (Instron, Model 5543, the loading cell is 250N). A rectangular strip of tough hydrogel ($75 \times 24 \times 1.4\ mm^3$) was glued to two rigid acrylate clamps ($80 \times 10 \times 1.5\ mm^3$). Both unnotched and notched samples were prepared for pure shear tests. For notched samples, an edge crack with a length of 30 mm was cut using a razor blade in the middle section of the sample. The tensile strain rate was fixed at 200% min^{-1}. The tensile strain (ε) was defined as the length change (Δl) divided by the original length (l_0) of the sample. The toughness was defined by integrating the area under a stress-strain curve of the unnotched sample, where strain used the range from 0% to the fractured value of a notched sample (*33*).

Adhesion energy, namely the energy required to increase a unit area of the iSkin-substrate interfacial crack, was measured with T-peel tests by the same tensile testing machine. A ribbon of the iSkin (80 × 15 × 1.4 mm^3) was adhered to a natural porcine skin substrate, skin with artificial sweat treated, or a carboxylated nylon strip (treated by 1M HCl for 3 h) with one end open, forming a bilayer with an edge crack. Overnight compression was applied between the iSkin-substrate bilayer before mechanical peeling testing. During the waiting time, the specimens were sealed in a Ziploc bag before tests. The surfaces of an iSkin were bonded to a rigid polyethylene terephthalate (PET) film with super glue, to limit deformation to the crack tip. The free ends of iSkin and the substrate were attached to plastic sheets, to which the machine grips were attached. The loading rate was set constant at 100 mm min^{-1}. The adhesion energy was two times the plateau value of the ratio of the force and width. Both force and displacement were recorded continuously throughout the experiment. An iSkin was adhered to the pristine nylon strip substrate with the same protocol as the control group. A minimum of three specimens were used for all mechanical test conditions.

4.4.4. Resistance and Conductivity Measurement

Unless mentioned elsewhere, all the hydrogel samples for electrical characterization were in the size of 5×28×1.4 mm^3. The resistance of as-prepared iSkin were measured by using a portable LCR Meter (LCR-916, GWINSTEK) at 1 kHz. The conductivity of the sample was deduced from recorded resistance and dimension for the resistance-strain test, the tensile strain rate was fixed at 100% min^{-1}. Both resistance and displacement were recorded continuously throughout the experiment.

4.4.5. Ambient Stability Characterization

400 mL LiCl solution with different concentrations was stored in airtight plastic storage containers (86 oz.) to construct certain environment chambers with varies relative humidity (15%, 38%, 63%, and 88%, respectively). After the placement of processed devices into the environment chambers, the mass and resistance of iSkin ($40\times 10 \times 1.4$ mm^3) were monitored continuously for one month to evaluate the ambient stability. As control, the features of NaCl-laden and original Alg-PAAm hydrogel were also measured here.

4.4.6. Anti-freezing Characterization

The freezing point of samples were characterized using a differential scanning calorimeter (TA Instruments, DSC 2920) with a mechanical cooling system. Samples (5-10 mg) were contained in hermetically sealed aluminum pans (TA Instruments, Tzero Aluminum Hermetic Pan) for testing, with an empty pan used as the reference. The DSC was operated under a 35 µL min^{-1} nitrogen flow rate and data were captured at a rate of 5 Hz. Samples were cooled at a rate of 2 °C min^{-1} to −120 °C. After an isothermal period of 30 min, samples were heated up at 2 °C min^{-1} to the initial equilibration temperature (15°C). The conductivity of as-prepared iSkin at different temperatures was measured in the DMA chamber from room temperature to −70 °C.

4.4.7. Fabrication of strain-sensing glove, soft gripper, and quadruped soft robot

The smart glove for human-machine interaction was fabricated as followed: The pre-cured Ecoflex A and B (00-35 fast, Smooth-On Inc.) were mixed quickly and our human-like model hand was dipped into the mixture entirely and then cured in the open air for 5 min. Flesh bonded elastomer-iSkin was then adhered to the finger joint of the glove with coating a thin layer of pre-cured Ecoflex as glue. Metal wires were used for connecting iSkin to control a robotic hand to make gestures accordingly. Robotic hand (Youbionic Robot Right Hand 2019) was purchase on Robotshop. The fabrication of soft robots and grippers has been reported previously (*14, 60, 61*), and here we will only introduce the adherence process of iSkin to soft robots and grippers. Similarly, flesh bonded Ecoflex-iSkin was adhered to the soft robots and grippers with coating a thin layer of pre-cured Ecoflex on Ecoflex side as glue. Once cured, the metal wires were used for connecting iSkin to Arduino boards for electrical data acquisition and gait pattern control.

4.4.8. Statistical analysis

Statistical analyses were performed on GraphPad Prism software (GraphPad Software, Inc.). Results are depicted as mean ± standard deviation (SD), we conducted unpaired Student's t test to analyze the statistical differences of experiment results. We used parametric test and assumed any experimental groups are normally distributed with the same SD. Differences were considered statistically significant if $P < 0.05$.

4.4.9. Testing of iSkin on human knees

The tests of the devices on human body described here do not need Institutional Review Board (IRB) approval, because our experiments do not affect living people physically or physiologically, and we have not sought or received identifiable private information. The hand and knees shown in **Figure S4.10, S4.15 and S4.16** are those of B. Ying, who has given his consent to publish these images.

4.5. References

1. W. Yang *et al.*, On the tear resistance of skin. *Nat. Commun.* **6**, 6649 (2015).
2. K. Laden, R. Spitzer, Moisturizing agent in skin. *J. Soc. Cosmet. Chem.* **18**, 351-360 (1967).

3. Y. Lee, C.-H. Lee, U. Oh, Painful channels in sensory neurons. *Mol. Cells* **20**, 315-324 (2005).
4. Y. Roudaut *et al.*, Touch sense: functional organization and molecular determinants of mechanosensitive receptors. *Channels* **6**, 234-245 (2012).
5. A. Chortos, J. Liu, Z. Bao, Pursuing prosthetic electronic skin. *Nat. Mater.* **15**, 937-950 (2016).
6. Y. Sun, W. M. Choi, H. Jiang, Y. Y. Huang, J. A. Rogers, Controlled buckling of semiconductor nanoribbons for stretchable electronics. *Nat. Nanotechnol.* **1**, 201-207 (2006).
7. D.-H. Kim *et al.*, Materials for multifunctional balloon catheters with capabilities in cardiac electrophysiological mapping and ablation therapy. *Nat. Mater.* **10**, 316-324 (2011).
8. J. Y. Sun, C. Keplinger, G. M. Whitesides, Z. Suo, Ionic skin. *Advanced Materials* **26**, 7608-7614 (2014).
9. W. B. Ying *et al.*, Water Proof, Highly Tough and Fast Self-healing Polyurethane for Durable Electronic Skin. *ACS Applied Materials & Interfaces* **12**, 11072−11083 (2020).
10. B. Ying, Q. Wu, J. Li, X. Liu, An ambient-stable and stretchable ionic skin with multimodal sensation. *Materials Horizons* **7**, 477-488 (2020).
11. B. Shih *et al.*, Electronic skins and machine learning for intelligent soft robots. *Science Robotics* **5**, eaaz9239 (2020).
12. C. Larson *et al.*, Highly stretchable electroluminescent skin for optical signaling and tactile sensing. *science* **351**, 1071-1074 (2016).
13. J. W. Booth *et al.*, OmniSkins: Robotic skins that turn inanimate objects into multifunctional robots. *Science Robotics* **3**, eaat1853 (2018).
14. S. Y. Kim *et al.*, Sustainable manufacturing of sensors onto soft systems using self-coagulating conductive Pickering emulsions. *Science Robotics* **5**, eaay3604 (2020).
15. T. G. Thuruthel, B. Shih, C. Laschi, M. T. Tolley, Soft robot perception using embedded soft sensors and recurrent neural networks. *Science Robotics* **4**, eaav1488 (2019).
16. H. Zhao, K. O'Brien, S. Li, R. F. Shepherd, Optoelectronically innervated soft prosthetic hand via stretchable optical waveguides. *Science Robotics* **1**, eaai7529 (2016).
17. K. B. Justus *et al.*, A biosensing soft robot: Autonomous parsing of chemical signals through integrated organic and inorganic interfaces. *Science Robotics* **4**, eaax0765 (2019).
18. H. Sheng *et al.*, Neural interfaces by hydrogels. *Extreme Mechanics Letters* **30**, 100510 (2019).
19. H. R. Lee, C. C. Kim, J. Y. Sun, Stretchable ionics-a promising candidate for upcoming wearable devices. *Adv. Mater.* **30**, 1704403 (2018).
20. C. Yang, Z. Suo, Hydrogel ionotronics. *Nat. Rev. Mater.* **3**, 125-142 (2018).
21. M. Zhu *et al.*, Antifreezing Hydrogel with High Zinc Reversibility for Flexible and Durable Aqueous Batteries by Cooperative Hydrated Cations. *Advanced Functional Materials* **30**, 201907218 (2019).
22. X. Liu, J. Liu, S. Lin, X. Zhao, Hydrogel machines. *Materials Today* **36**, 102-124 (2020).
23. Z. Lei, P. Wu, A supramolecular biomimetic skin combining a wide spectrum of mechanical properties and multiple sensory capabilities. *Nature communications* **9**, 1-7 (2018).

24. C.-C. Kim, H.-H. Lee, K. H. Oh, J.-Y. Sun, Highly stretchable, transparent ionic touch panel. *Science* **353**, 682-687 (2016).
25. J. Ge *et al.*, A stretchable electronic fabric artificial skin with pressure‐, lateral strain‐, and flexion‐sensitive properties. *Advanced Materials* **28**, 722-728 (2016).
26. H. Yuk, T. Zhang, S. Lin, G. A. Parada, X. Zhao, Tough bonding of hydrogels to diverse non-porous surfaces. *Nature materials* **15**, 190-196 (2016).
27. T. Yamada *et al.*, A stretchable carbon nanotube strain sensor for human-motion detection. *Nature nanotechnology* **6**, 296-301 (2011).
28. J.-Y. Sun *et al.*, Highly stretchable and tough hydrogels. *Nature* **489**, 133-136 (2012).
29. J. Li *et al.*, Tough adhesives for diverse wet surfaces. *Science* **357**, 378-381 (2017).
30. F. Chen *et al.*, Rational Fabrication of Anti-Freezing, Non-Drying Tough Organohydrogels by One-Pot Solvent Displacement. *Angew Chem Int Ed Engl* **57**, 6568-6571 (2018).
31. W. P. Williams, P. J. Quinn, L. I. Tsonev, R. D. Koynova, The effects of glycerol on the phase behaviour of hydrated distearoylphosphatidylethanolamine and its possible relation to the mode of action of cryoprotectants. *Biochimica et Biophysica Acta (BBA)-Biomembranes* **1062**, 123-132 (1991).
32. L. Han *et al.*, Mussel-Inspired Adhesive and Conductive Hydrogel with Long-Lasting Moisture and Extreme Temperature Tolerance. *Advanced Functional Materials* **28**, 1704195 (2018).
33. J. Li, W. R. Illeperuma, Z. Suo, J. J. Vlassak, Hybrid hydrogels with extremely high stiffness and toughness. *ACS Macro Letters* **3**, 520-523 (2014).
34. J. Li, Z. Suo, J. J. Vlassak, Stiff, strong, and tough hydrogels with good chemical stability. *Journal of Materials Chemistry B* **2**, 6708-6713 (2014).
35. C. H. Yang *et al.*, Strengthening alginate/polyacrylamide hydrogels using various multivalent cations. *ACS applied materials & interfaces* **5**, 10418-10422 (2013).
36. A. Miriyev, K. Stack, H. Lipson, Soft material for soft actuators. *Nature communications* **8**, 1-8 (2017).
37. H. Yang *et al.*, Adhesive Bio-composite Electrodes on Sweaty Skin for Long-term Continuous Electrophysiological Monitoring. *ACS Materials Letters* **2**, 478-484 (2020).
38. H. Liao, X. Guo, P. Wan, G. Yu, Conductive MXene Nanocomposite Organohydrogel for Flexible, Healable, Low‐Temperature Tolerant Strain Sensors. *Advanced Functional Materials* **29**, 1904507 (2019).
39. H. Qiao *et al.*, Multiple Weak H-Bonds Lead to Highly Sensitive, Stretchable, Self-Adhesive, and Self-Healing Ionic Sensors. *ACS Appl Mater Interfaces* **11**, 7755-7763 (2019).
40. Y. Bai *et al.*, Transparent hydrogel with enhanced water retention capacity by introducing highly hydratable salt. *Applied Physics Letters* **105**, 151903 (2014).
41. J. L. Dashnau, N. V. Nucci, K. A. Sharp, J. M. Vanderkooi, Hydrogen bonding and the cryoprotective properties of glycerol/water mixtures. *The Journal of Physical Chemistry B* **110**, 13670-13677 (2006).
42. S. Cerveny, J. Colmenero, A. Alegria, Dielectric investigation of the low-temperature water dynamics in the poly (vinyl methyl ether)/H2O system. *Macromolecules* **38**, 7056-7063 (2005).
43. H. Yuk *et al.*, 3D printing of conducting polymers. *Nature Communications* **11**, 1-8 (2020).

44. L. B. Lane, Freezing Points of Glycerol and Its Aqueous Solutions. *Industrial & Engineering Chemistry* **17**, 924-924 (1925).
45. X. P. Morelle *et al.*, Highly Stretchable and Tough Hydrogels below Water Freezing Temperature. *Adv Mater* **30**, e1801541 (2018).
46. J. Yang *et al.*, Design Molecular Topology for Wet–Dry Adhesion. *ACS applied materials & interfaces* **11**, 24802-24811 (2019).
47. D. Rus, M. T. Tolley, Design, fabrication and control of soft robots. *Nature* **521**, 467-475 (2015).
48. S. Cheng, Y. S. Narang, C. Yang, Z. Suo, R. D. Howe, Stick‐On Large‐Strain Sensors for Soft Robots. *Advanced Materials Interfaces* **6**, 1900985 (2019).
49. H. Yuk, T. Zhang, G. A. Parada, X. Liu, X. Zhao, Skin-inspired hydrogel–elastomer hybrids with robust interfaces and functional microstructures. *Nature communications* **7**, 1-11 (2016).
50. J. Yang, R. Bai, B. Chen, Z. Suo, Hydrogel adhesion: A supramolecular synergy of chemistry, topology, and mechanics. *Advanced Functional Materials* **30**, 1901693 (2020).
51. H. Yuk *et al.*, Dry double-sided tape for adhesion of wet tissues and devices. *Nature* **575**, 169-174 (2019).
52. K. Chin, T. Hellebrekers, C. Majidi, Machine learning for soft robotic sensing and control. *Advanced Intelligent Systems* **2**, 1900171 (2020).
53. R. L. Truby *et al.*, Soft somatosensitive actuators via embedded 3D printing. *Advanced Materials* **30**, 1706383 (2018).
54. T. Yamaguchi, T. Kashiwagi, T. Arie, S. Akita, K. Takei, Human‐Like Electronic Skin‐Integrated Soft Robotic Hand. *Advanced Intelligent Systems* **1**, 1900018 (2019).
55. S. Wang *et al.*, Skin electronics from scalable fabrication of an intrinsically stretchable transistor array. *Nature* **555**, 83-88 (2018).
56. Q. Hua *et al.*, Skin-inspired highly stretchable and conformable matrix networks for multifunctional sensing. *Nature communications* **9**, 1-11 (2018).
57. Q. Xu, L. An, M. Yu, S. Wang, Design and synthesis of a new conjugated polyelectrolyte as a reversible ph sensor. *Macromolecular rapid communications* **29**, 390-395 (2008).
58. J. Kim *et al.*, Simultaneous monitoring of sweat and interstitial fluid using a single wearable biosensor platform. *Advanced Science* **5**, 1800880 (2018).
59. X. Pu *et al.*, Ultrastretchable, transparent triboelectric nanogenerator as electronic skin for biomechanical energy harvesting and tactile sensing. *Science advances* **3**, e1700015 (2017).
60. F. Ilievski, A. D. Mazzeo, R. F. Shepherd, X. Chen, G. M. Whitesides, Soft robotics for chemists. *Angewandte Chemie International Edition* **50**, 1890-1895 (2011).
61. R. F. Shepherd *et al.*, Multigait soft robot. *Proceedings of the national academy of sciences* **108**, 20400-20403 (2011).
62. W. Xie *et al.*, Ultra-stretchable, bio-inspired ionic skins that work stably in various harsh environments. *Journal of Materials Chemistry A* **6**, 24114-24119 (2018).
63. Q. Rong, W. Lei, J. Huang, M. Liu, Low Temperature Tolerant Organohydrogel Electrolytes for Flexible Solid-State Supercapacitors. *Advanced Energy Materials* **8**, 1801967 (2018).
64. Y. Ren *et al.*, Ionic liquid–based click-ionogels. *Science advances* **5**, eaax0648 (2019).

65. J. Xu, G. Wang, Y. Wu, X. Ren, G. Gao, Ultrastretchable Wearable Strain and Pressure Sensors Based on Adhesive, Tough, and Self-healing Hydrogels for Human Motion Monitoring. *ACS Appl Mater Interfaces* **11**, 25613-25623 (2019).
66. Y. Yang *et al.*, Conductive Organohydrogels with Ultrastretchability, Antifreezing, Self-Healing, and Adhesive Properties for Motion Detection and Signal Transmission. *ACS Appl Mater Interfaces* **11**, 3428-3437 (2019).
67. Q. Rong *et al.*, Anti-freezing, Conductive Self-healing Organohydrogels with Stable Strain-Sensitivity at Subzero Temperatures. *Angew Chem Int Ed Engl* **56**, 14159-14163 (2017).
68. Z. Qin *et al.*, Freezing-Tolerant Supramolecular Organohydrogel with High Toughness, Thermoplasticity, and Healable and Adhesive Properties. *ACS Appl Mater Interfaces* **11**, 21184-21193 (2019).
69. S. Li, H. Pan, Y. Wang, J. Sun, Polyelectrolyte complex-based self-healing, fatigue-resistant and anti-freezing hydrogels as highly sensitive ionic skins. *Journal of Materials Chemistry A* **8**, 3667-3675 (2020).
70. J. Song *et al.*, Mechanically and Electronically Robust Transparent Organohydrogel Fibers. *Advanced Materials* **32**, 1906994 (2020).
71. Z. Liu *et al.*, Poly (ionic liquid) hydrogel-based anti-freezing ionic skin for a soft robotic gripper. *Materials Horizons* **7**, 919-927 (2020).
72. H. Chen, X. Ren, G. Gao, Skin-Inspired Gels with Toughness, Antifreezing, Conductivity, and Remoldability. *ACS Appl Mater Interfaces* **11**, 28336-28344 (2019).

4.6. Acknowledgments:

Funding: This work was supported by the Natural Sciences and Engineering Research Council of Canada (RGPIN-2017-06374, RGPAS 507980-17, and RGPIN-2018-04146), the Canada Foundation for Innovation (#37719), and the University of Toronto. The authors acknowledge Prof. Mitchell Winnik for the access to a tensile tester and DSC, and Dr. Yang Liu, Dr. Hang Zhou and Prof. Mitchell Winnik for the technical assistance on usage of the DSC. We also thank the technical advices about bioadhesives from Guangyu Bao and Zhenwei Ma. **Author contributions:** B.Y., J.Y., and X.L. conceived the idea and designed experiments. B.Y., and Z.C. carried out material preparation and characterization. B.Y., Z.C. and R.Z. carried out the experiments of strain sensing, human machine interaction and soft robotics. B.Y., Z.C., R.Z. and X.L. performed data analysis. B.Y. and X.L. wrote the manuscript with input from all the other authors. All authors contributed to, and agree with, the content of the final version of the manuscript. **Competing interests**: The

authors declare that they have no competing financial interest. **Data and materials availability**: All data needed to evaluate the conclusions in the paper are present in the paper or the Supplementary Materials.

Table 4.1. Comparison between iSkin and other similar hydrogel devices reported previously

Strain$_{max}$ (RT)	**Toughness$_{Fracture}$ (J·m^{-2}, RT)**	**Reported Anti-freezing capability (°C)**	**Conductivity (RT, S·m^{-1})**	**Ambient stability**	**Adhesion capability**	**Solvent**	**Electrolyte salt/ Conductor**	**Bio-toxicity**	**Ref**
1973%	11410	−95	0.9	≥30 d	649 J·m^{-2} (Both wet and dry)	H_2O, G	NaCl	Low	This work
700%	2000	−57	8	N/A	No	H_2O	$CaCl_2$	N/A	(45)
620%	2300	−20	8.2	≥ 30 d	60 kPa (Dry)	H_2O, G	CNT	High	(32)
1700%	N/A	−40	1.928×10^{-4}	≥ 2 d	No	H_2O, EG	NaCl	High	(62)
300%	N/A	−40	1.6	N/A	No	H_2O, EG	LiCl	High	(63)
1390%	N/A	−75	0.83	N/A	No	H_2O	ILs	High	(64)
2100%	N/A	N/A	0.35	No	250 J·m^{-2} (Wet)	H_2O	SC	Low	(65)
2000%	N/A	−20	1.5	No	40 J·m^{-2} † (Dry)	H_2O, G	MAANa	N/A	(66)
960%	N/A	−55	N/A	N/A	No	H_2O, EG	PEDOT: PSS	N/A	(67)
960%	N/A	−80	N/A	≥7 d	~100 kPa (Dry)	H_2O, G	Na_3Cit	N/A	(68)
~600%	N/A	−24.7	0.72	N/A	No	H_2O	NaCl	Low	(69)
400%	N/A	−80	0.765	>30 d	No	H_2O, G	KCl	Low	(70)
900%	N/A	−20	1.1	N/A	No	H_2O	ILs	High	(71)
715%	N/A	−20	0.4	N/A	No	H_2O, G	NaCl	Low	(72)

(†) Calculated as Force/width curve in the paper

RT: Room Temperature

PEDOT:PSS: Poly(3,4-ethylenedioxythiophene) polystyrene sulfonate

ILs: Ionic Liquids

G: Glycerol

MAANa: Sodium Methacrylate

SC: Sodium Casein

4.7. Supplementary Materials

An anti-freezing, ambient-stable and highly stretchable ionic skin with strong surface adhesion for wearable sensing and soft robotics

Figure S4.1. iSkin synthesis.

Figure S4.2. Mechanical pure-shear tests for measuring the toughness of iSkin and original hydrogel..

Figure S4.3. Mechanical properties of hydrogels treated by different strategies.

Figure S4.4. Electrical property of iSkin and optical photos of glycerol-water binary solvent for exchange..

Figure S4.5. Water loss measurement of different processed hydrogels as a function of RHs within 30 days.

Figure S4.6. Anti-freezing property of different processed hydrogels.

Figure S4.7. Anti-freezing property of different exchanging solvents.

Figure S4.8. DSC results of different processed hydrogels at the Exo direction.

Figure S4.9. Anti-freezing property of glycerol acqueous solution with different concentrations.

Figure S4.10. iSkin adhered to different material (self-adhesive).

Figure S4.11. Setup photos of iSkin under T-peel test when adhered to substrates.

Figure S4.12. Adhesion property of two types of hydrogel-skin bonding.

Figure S4.13. Setups of wet adhesion test.

Figure S4.14. Anti-freezing wearable sensor demonstration.

Figure S4.15. Comparision of adhesion capability between adhesive iSkin and regular iSkin withour adhesvie layer once adhering to the knee.

Figure S4.16. The adhesion performance of adhesive iSkins on the knee.

Figure S4.17. The bonding and stretchability of different hydrogel-Ecoflex combinations at −30 °C.

Figure S4.18. Optical photos of the iSkin-equipped intelligent soft robot during a sequence of dynamic walkin on the snow.

Figure S4.19. Optical photos of the iSkin-equipped intelligent soft robot during a sequence of dynamic walking at −22 ^{o}C

Figure S4.20. Optical photos of the iSkin-equipped intelligent soft robot during a sequence of dynamic crawling at −22 ^{o}C.

Movie S4.1: Mechanical pure shear test to show the stretchability and toughness of iSkin

Movie S4.2: Mechanical pure shear test to show the stretchability of the original tough hydrogel

Movie S4.3: Anti-freezing capability of iSkin and original tough hydrogel at −30 °C

Movie S4.4: Adhesion property between iSkin and diverse substrates

Movie S4.5: The anti-freezing and long-term underwater adhesive capability between iSkin and diverse substrates Movie S6: Adhesive capability of iSkin when utilized as a wearable stretchable senor adhered on the knee during workout

Movie S4.7: iSkin adhered on Ecoflex glove for human machine interaction

Movie S4.8: iSKin-Ecoflex bonding and its stretchability

Movie S4.9: Free displacement of an iSkin-equipped smart soft actuator alternating between inflated and deflated states

Movie S4.10: External manipulation an iSkin-equipped smart soft actuator inflated at 22 kPa

Movie S4.11: Grabbing and differentiating fruits and vegetables possessing different spherical shapes with the iSkin-equipped smart soft bending gripper

Movie S4.12: iSkin-Ecoflex bonding capability @ −30 °C

Movie S4.13: The locomotion of iSkin-equipped intelligent soft robot on the snow

Movie S4.14: The locomotive walking of an iSkin-equipped intelligent soft robot at −22 °C

Movie S4.15: The locomotive crawling of an iSkin-equipped intelligent soft robot at −22 °C

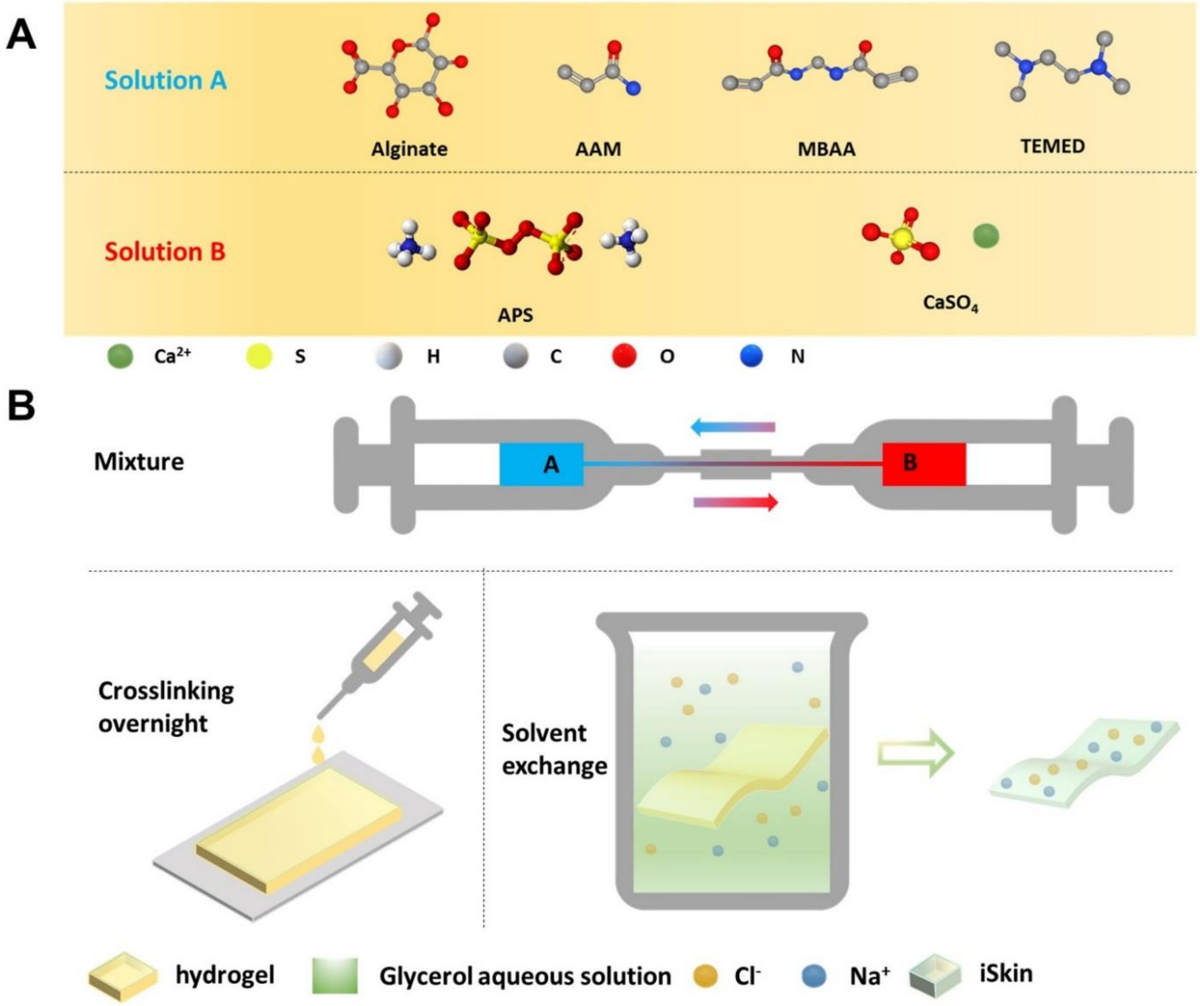

Figure S4.1. iSkin synthesis. (**A**) Composition of solution A and B. (**B**) Preparation process of iSkin.

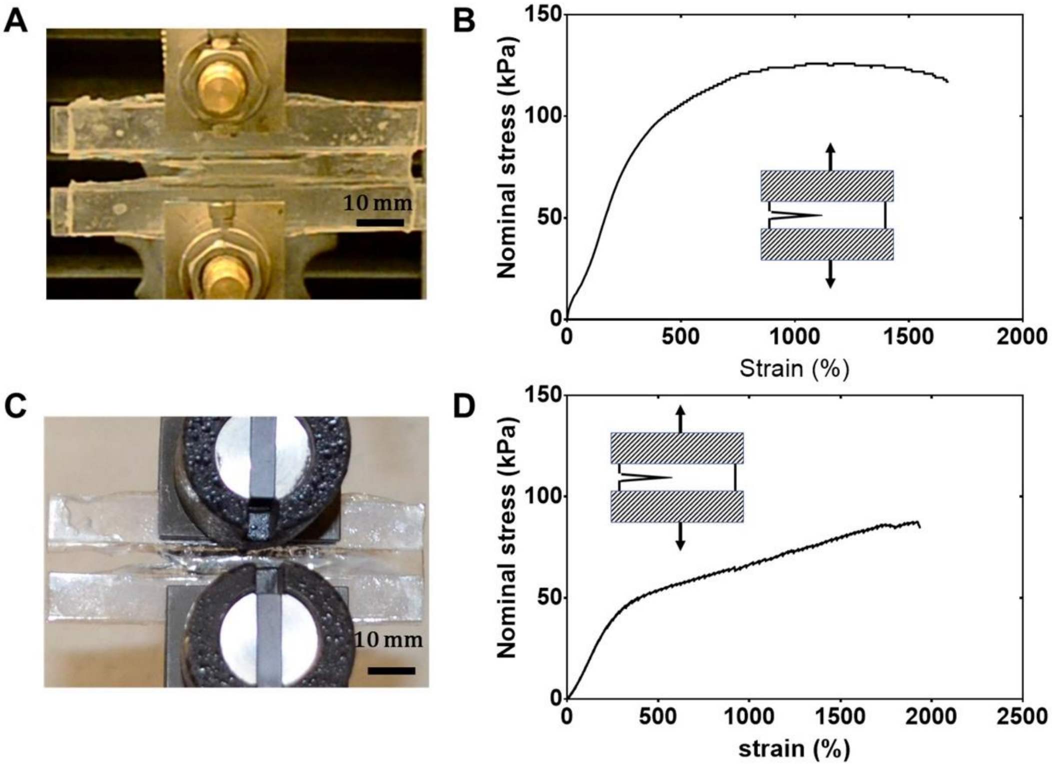

Figure S4.2. Mechanical pure-shear tests for measuring the toughness of iSkin and original hydrogel. A piece of hydrogel with a notch was stretched until the crack propagates. (**A**) Photo of a piece of iSkin with a notch stretched until the crack propagates. (**B**) Stress-strain curve of iSkin. (**C**) Photo of a piece of the original Alg-PAAm tough hydrogel with a notch stretched until the crack propagates (**D**) Stress-strain curve of the original Alg-PAAm tough hydrogel.

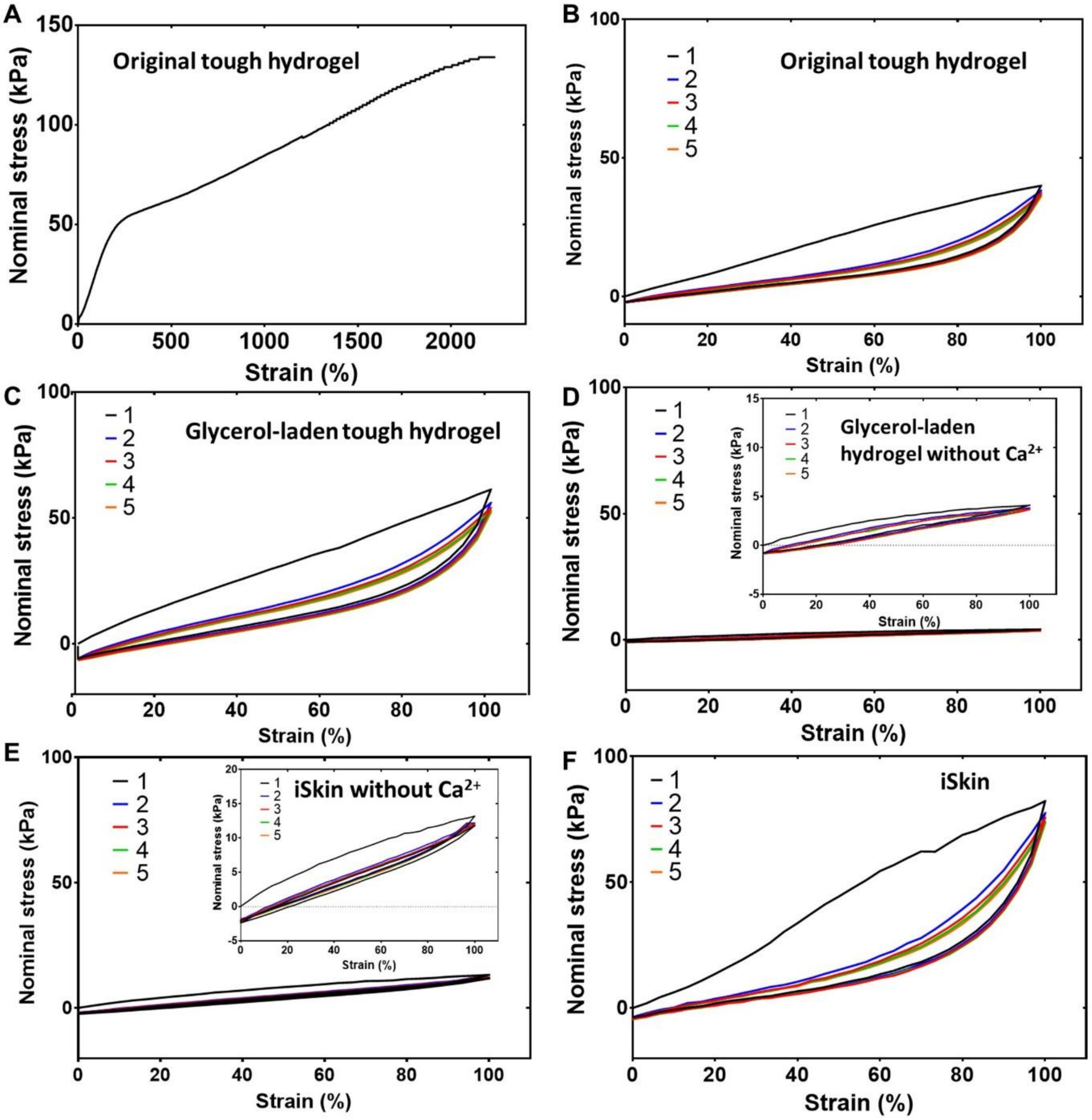

Figure S4.3. Mechanical properties of hydrogels treated by different strategies. (A) Strain-stress curve of an original Alg-PAAm tough hydrogel. Five successive tensile loading-unloading cycles of (**B**) an original Alg-PAAm tough hydrogel, (**C**) a glycerol-laden tough hydrogel, (**D**) a glycerol-laden hydrogel without Ca^{2+} cross-linking, (**E**) an iSkin without Ca^{2+} cross-linking, and (**F**) an iSkin at the maximum strain of 100%.

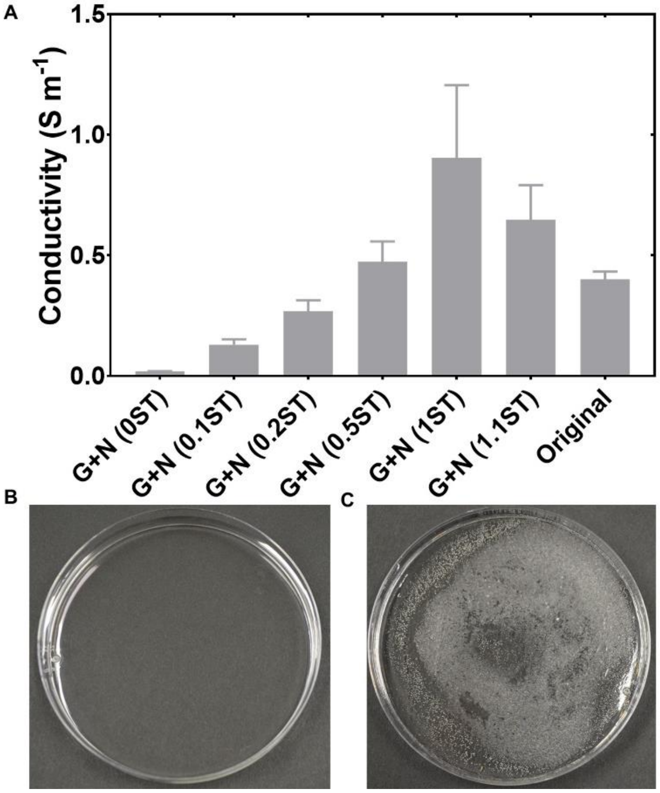

Figure S4.4. Electrical property of iSkin and optical photos of glycerol-water binary solvent for exchange.(**A**) The electrical conductivity of iSkin with varied NaCl contents dissolved in the 66.6 wt.% glycerol aqueous solution [G+N (0ST), G+N (0.1ST), G+N (0.2ST), G+N (0.5ST), G+N (1ST) and G+N (1.1ST)]. Note that G+N is the short term of iSkin laden with glycerol-NaCl aqueous solution; ST means the dissolving NaCl content is saturated (5.4M); 0ST means no NaCl dissolved; 0.1ST means the 0.1 time of saturated NaCl content dissolved; So are 0.2ST, 0.5ST, 1ST and 1.1ST, respectively. Optical photo of glycerol-water binary solvent with (**B)** NaCl (1ST) and **(C)** NaCl (1.1ST) within the 66.6 wt. % glycerol aqueous solution. NaCl powder was visible after three-day dissolving when the NaCl content was beyond the saturated level.

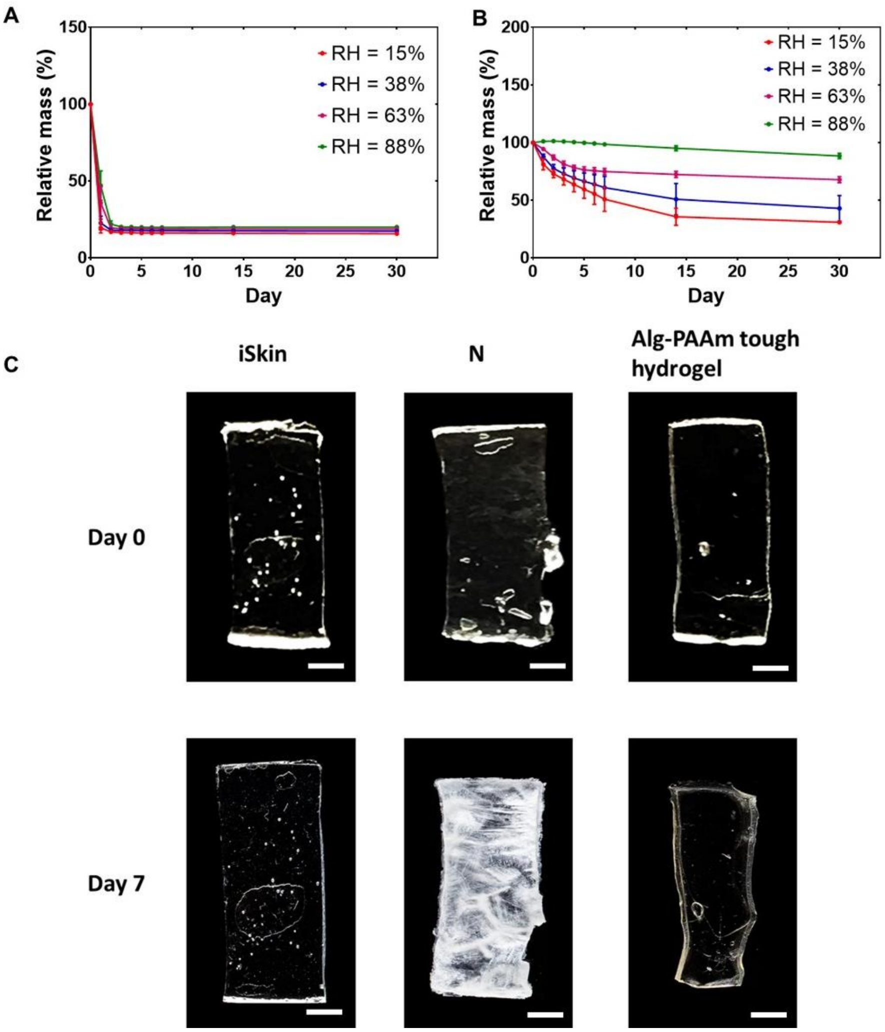

Figure S4.5. Water loss measurement of different processed hydrogels as a function of RHs within 30 days for (**A**) NaCl-laden Alg-PAAm hydrogel and (**B**) original Alg-PAAm tough hydrogel. The mass of hydrogel is normalized with its initial mass (N = 3-4). (**C**) Optical photos of 3 different hydrogels at day 0 and day 7 to show the appearance and transparency change at RH=63%. These appearances maintained unchanged since day 7 as well. Scale bar: 10 mm.

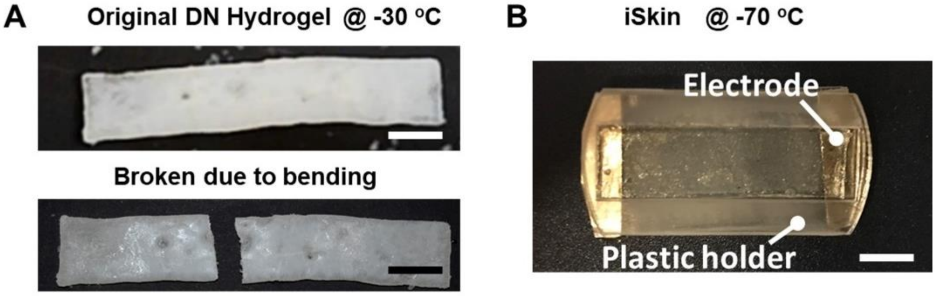

Figure S4.6. Anti-freezing property of different processed hydrogels. (**A**) Original Alg-PAAm tough hydrogel froze at −30 °C and broke due to bend. Scale bar is 15 mm. (**B**) Optical photo of iSkin at −70 °C. The gel showed no freezing phenomenon after placed in the −70 °C for 1 h. Note the stainless film is for conductivity measurement.

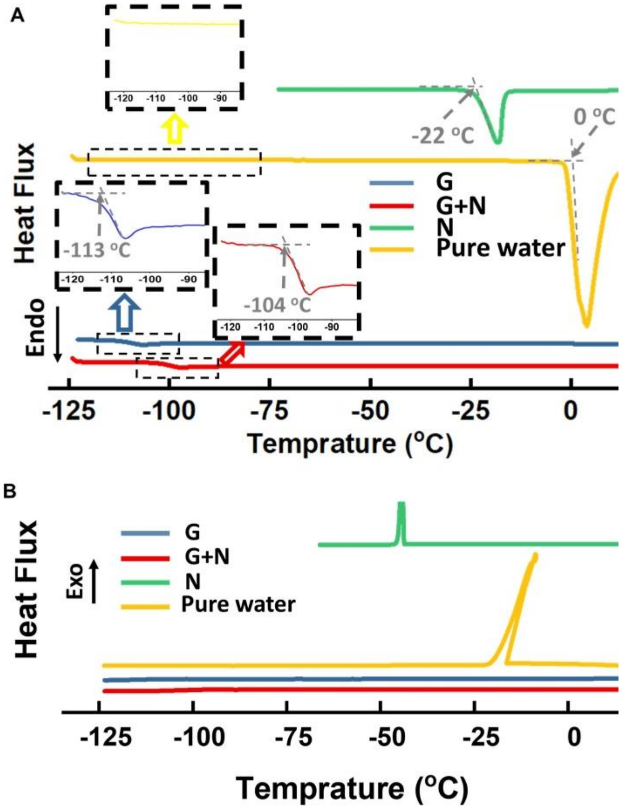

Figure S4.7. Anti-freezing property of different exchanging solvents. DSC results at the (**A**) Exo direction and (**B**) Endo direction of 66.6 wt. % glycerol aqueous solution with saturated NaCl contents dissolved (labelled as G+N), 66.6 wt. % glycerol aqueous solution (labelled as G), saturated NaCl aqueous solution at 5.4M concentration (labelled as N) and pure water between −120 °C and 15 °C. The small gray arrows highlight the melting points of solutions. It can be seen from the above figure that the melting point of pure water is 0 °C, and the melting point of NaCl aqueous solution at max solubility is about −22 °C, consistent with the theoretical data.

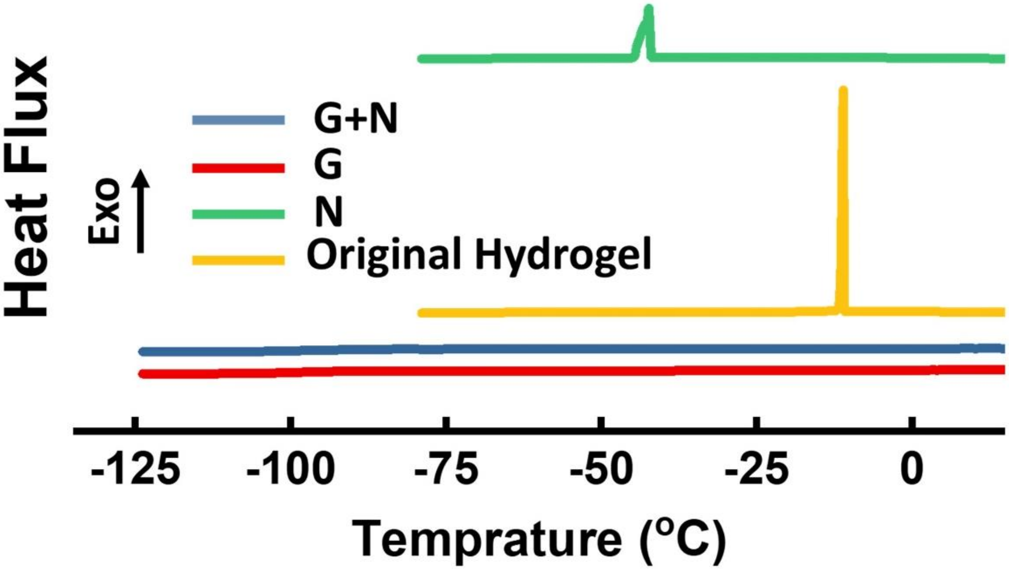

Figure S4.8. DSC results of different processed hydrogels at the Exo direction. NaCl-laden hydrogel (labelled as N), glycerol-laden hydrogel (labelled as G), iSkin, and original hydrogel was tested between −120 °C and 15 °C .

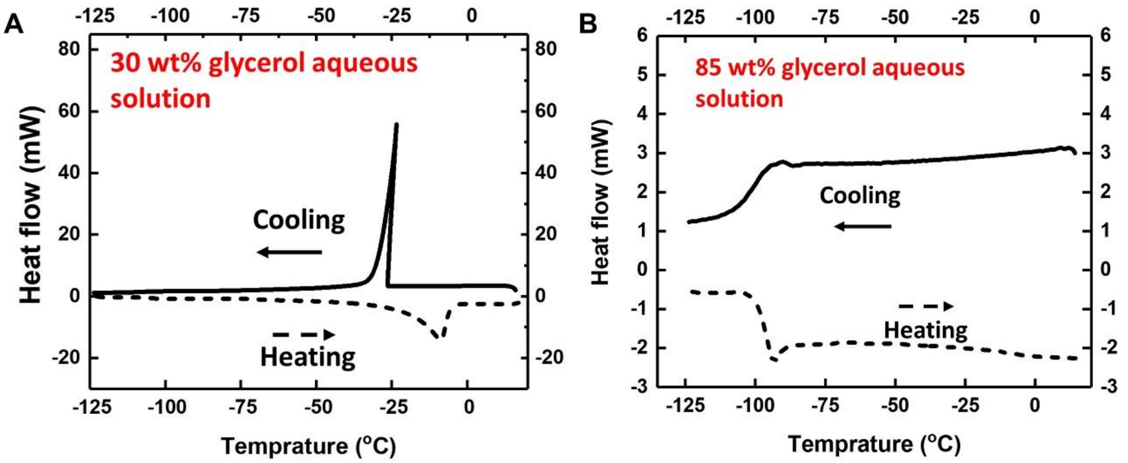

Figure S4.9. Anti-freezing property of glycerol aqueous solution with different concentrations. DSC results of (**A**) 30 wt% glycerol aqueous solution, and (**B**) 85 wt% glycerol aqueous solution.

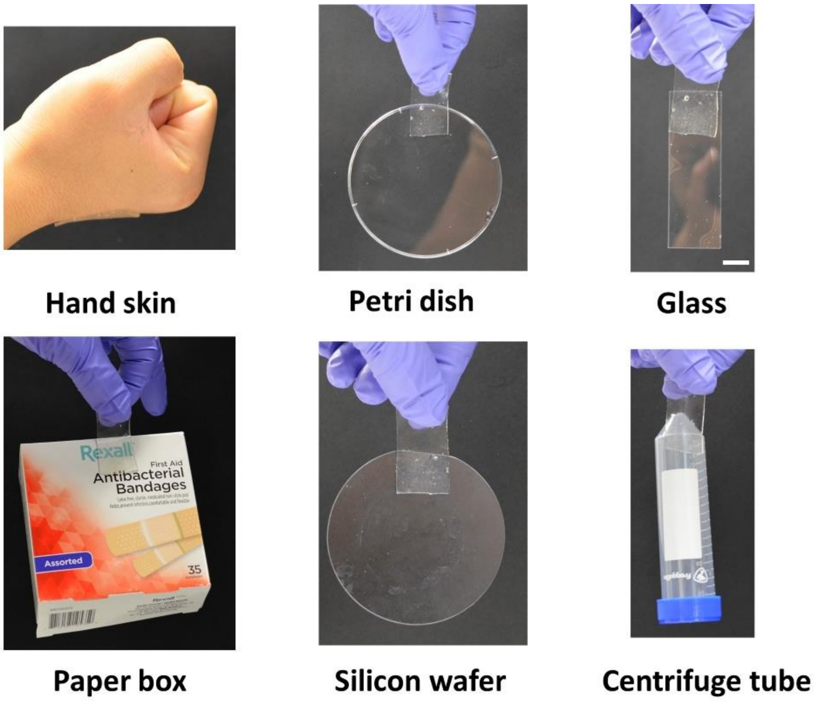

Figure S4.10. iSkin adhered to different material (self-adhesive).

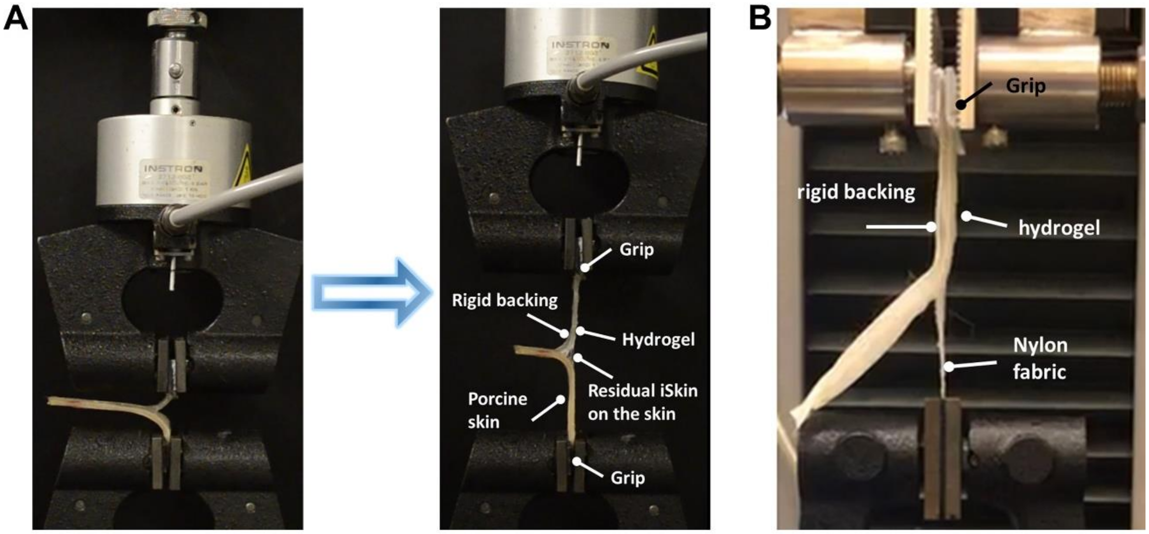

Figure S4.11. Setup photos of iSkin under T-peel test when adhered to substrates: (**A**) porcine skin and (**B**) nylon fabric.

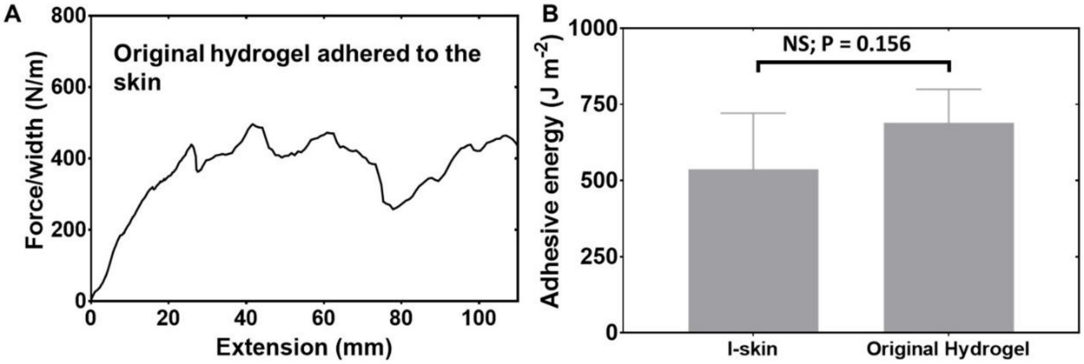

Figure S4.12. Adhesion property of two types of hydrogel-skin bonding. (A) Force/width curve for the adhesion between original hydrogel and porcine skin surface. **(B)** Comparison of adhesive energy between iSkin-skin bonding and original-hydrogel-skin bonding. (N≥3)

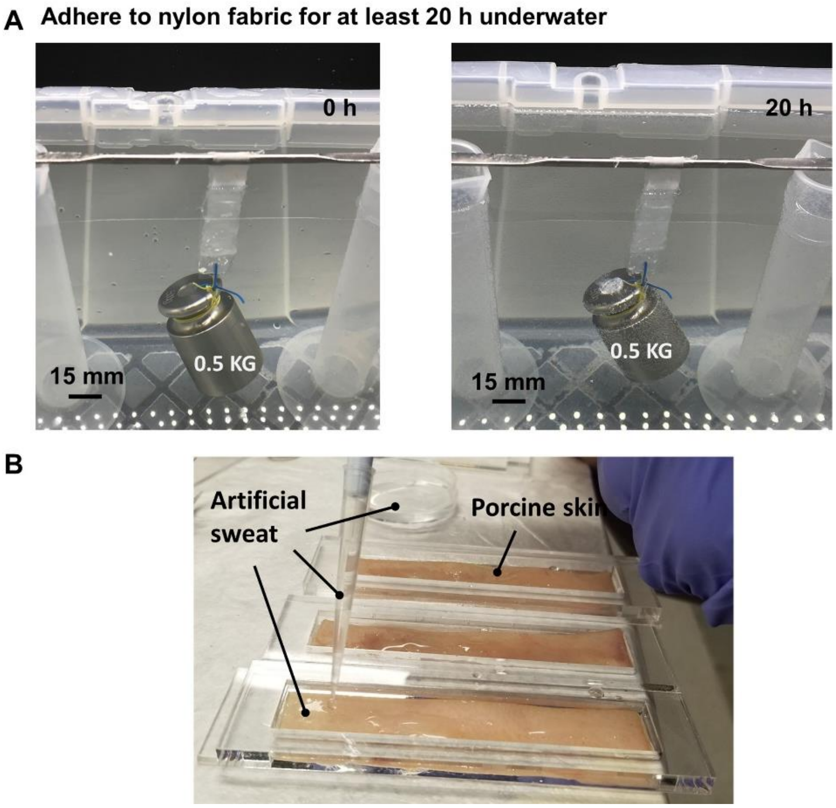

Figure S4.13. Setups of wet adhesion tests. (A) The long-term underwater adhesion capability of iSkin to the carboxylated nylon fabric. (**B**) Porcine skin surface treated by the artificial sweat for wet skin adhesion test.

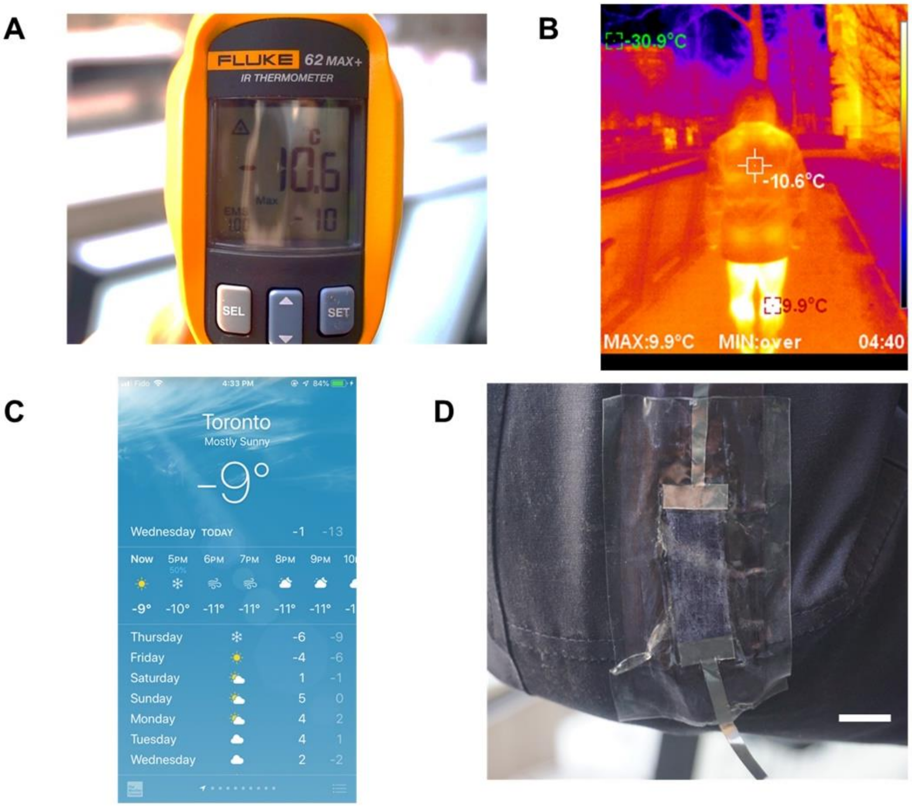

Figure S4.14. Anti-freezing wearable sensor demonstration. (A) The environment temperature (−10.6 °C) measured by a thermometer (Fluke 62 MAX+). (**B)** The outlayer temperature (−10.6 °C, measured by a thermal imaging camera, HT-19) of winter coat where iSkin was adhered to. **(C)** The local temperature in Toronto read from a cellphone (**D**) Zoom-in image of an iSkin adhered to Canada Goose winter coat. The VHB was used to attach electrode to iSkin.

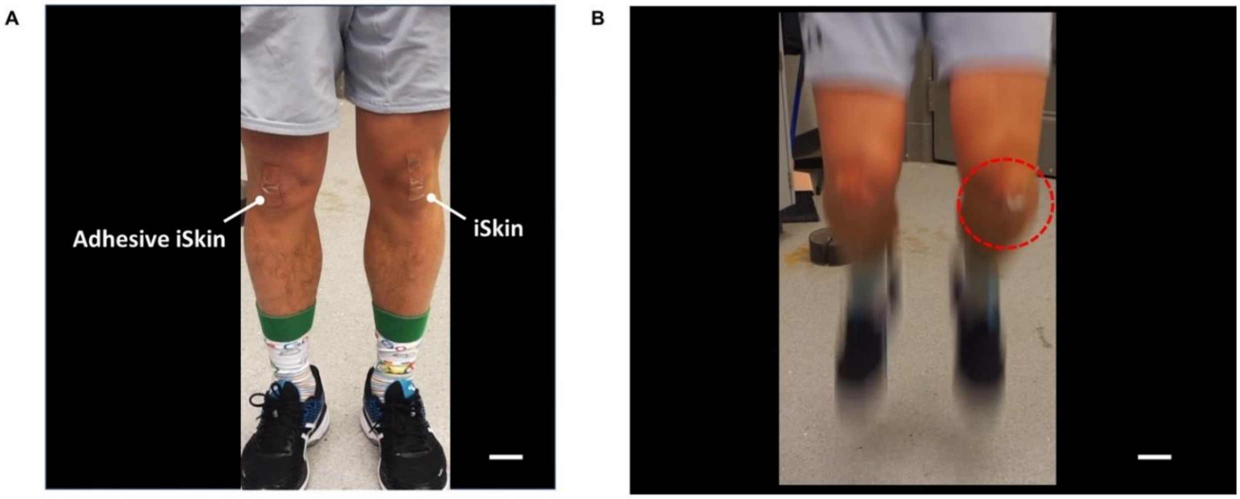

Figure S4.15. Comparison of adhesion capability between adhesive iSkin and regular iSkin without adhesive layer once adhering to the knees: (**A**) before and **(B**) during vigorous jump**.**

Figure S4.16. The adhesion performance of adhesive iSkins on the knees. The skin condition (**A**) before and (**B**) after applying adhesive iSkin. The bonding between the iSkin and knees (**C**) before and (**D**) after 30-min step-up workout. Scale bar: 25 mm.

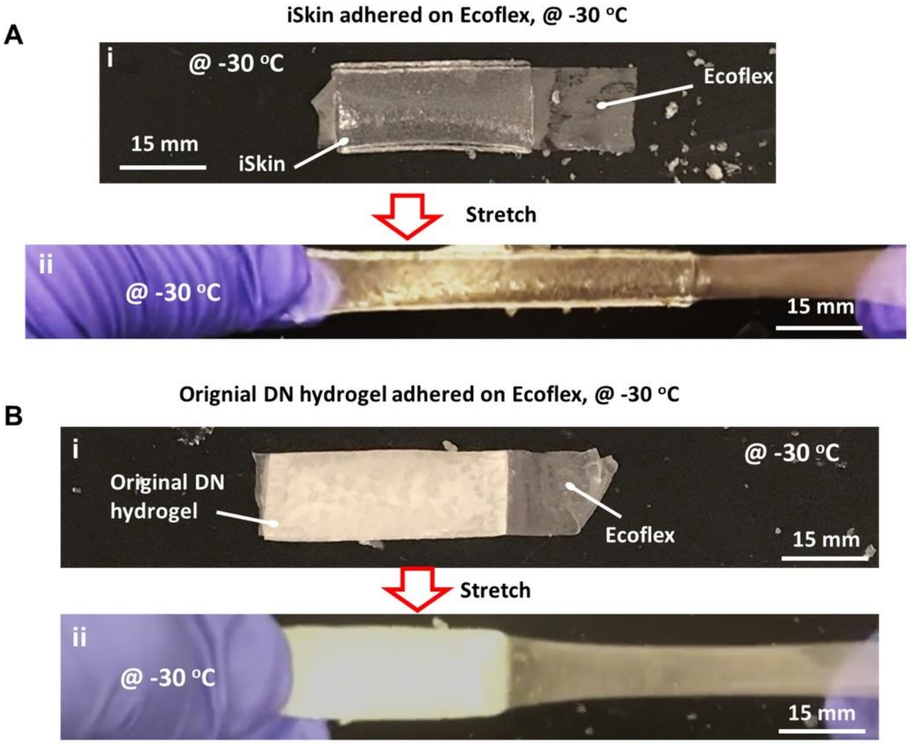

Figure S4.17. The bonding and stretchability of different hydrogel-Ecoflex combinations at −30 °C: (**A**) iSkin-Ecoflex bilayer and (**B**) original-hydrogel-Ecoflex bilayer.

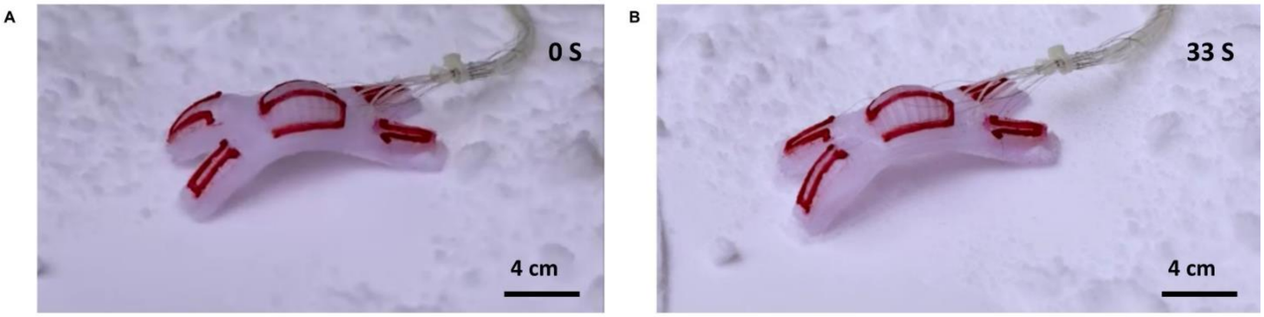

Figure S4.18. Optical photos of the iSkin-equipped intelligent soft robot during a sequence of dynamic walking on the snow: (A) at time= 0 s and (**B**) at time =33 s.

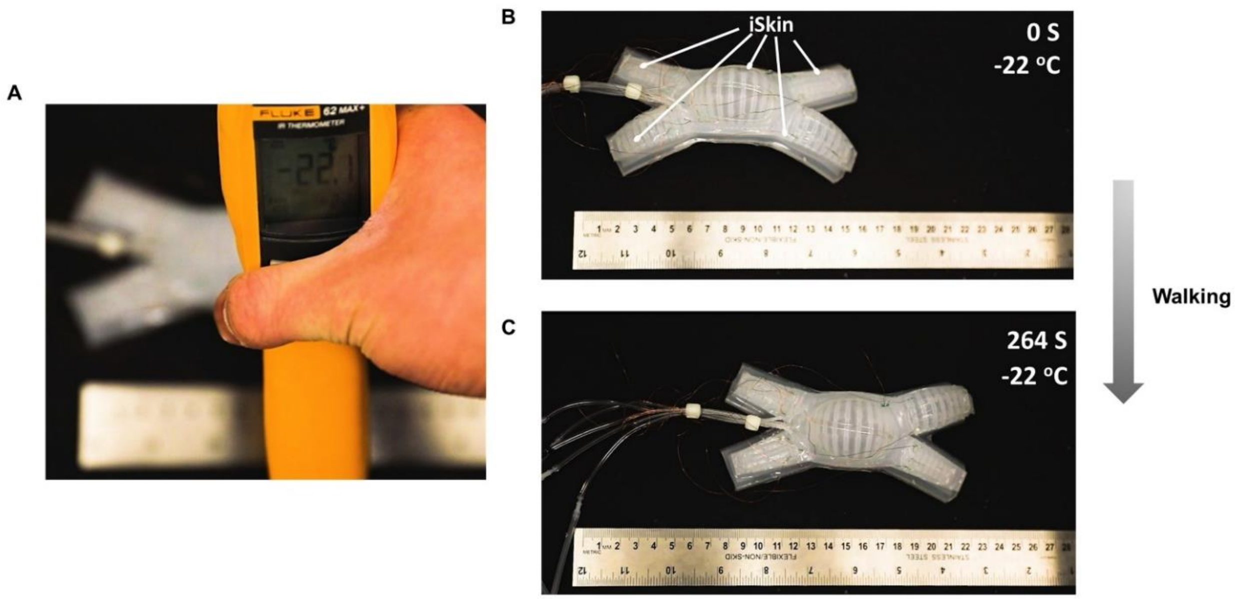

Figure S4.19. Optical photos of the iSkin-equipped intelligent soft robot during a sequence of dynamic walking at −22 °C: (A) temperature read from a thermal meter.(**B**) photo at time= 0 s and (**C**) at time =264 s.

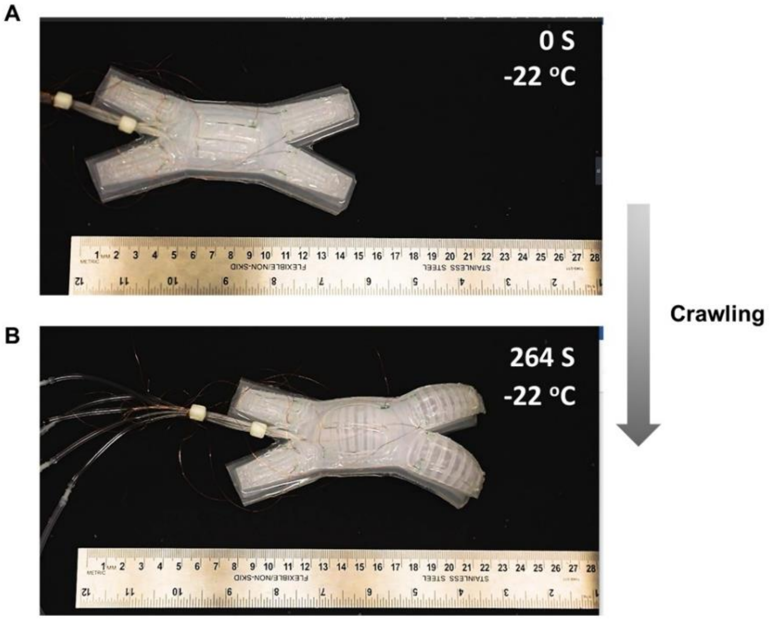

Figure S4.20. Optical photos of the iSkin-equipped intelligent soft robot during a sequence of dynamic crawling at −22 °C: (A) photo at time= 0 s and (**B**) at time =264 s.

Link between Chapter 4 and Chapter 5

In the previous chapter, I empowered one of the most popular used tough hydrogels, i.e., Alg-PAAm tough DN hydrogel, with anti-freezing capability, good conductivity, ambient-stability and strong surface adhesion capability simultaneously. This kind of combination will make hydrogel ionic devices highly suitable for wearable sensing and soft robotics.

However, like most stretchable electronics, hydrogel ionic devices require continuous and large power supply during long-term usage. To provide a compatible and sustainable power source and reduce the power consumption, in the next chapter I present an anti-freezing, highly stretchable ionic triboelectric nanogenerator (iTENG) for mechanical energy harvesting and self-powering sensing. The iTENG could broaden the applications of hydrogel-based sensors, soft robotics and stretchable power units in the extreme environment.

5. Chapter 5. An anti-freezing, and stretchable ionic triboelectric nanogenerator for mechanical energy harvesting and self-powering sensing

Binbin Ying[1,2], Yilun Wan[2], Runze Zuo[2], Xinyu Liu[2, 3*]

[1]Department of Mechanical Engineering, McGill University, 817 Sherbrooke Street West, Montreal, QC H3A 0C3, Canada.

[2]Department of Mechanical and Industrial Engineering, University of Toronto, 5 King's College Road, Toronto, Ontario, M5S 3G8, Canada.

[3]Institute of Biomedical Engineering, University of Toronto, 164 College Street, Toronto, ON M5S 3G9, Canada

To be submit

5.1. Introduction

The rapid growth of wearable electronics and soft robotics relies on power sources that are mechanically flexible, stretchable and even biocompatible. So far, flexible energy storage devices [e.g., supercapacitors (*1-3*) and batteries (*4*)] have been developed to reduce the constraint on our human body and the soft robotic body. However, most of these sources lack the self-powering capability. On the other hand, flexible energy harvesting devices such as solar cells and nanogenerators have been developed in the past decade to realize a fully sustainable power source (*5-8*). For example, triboelectric nanogenerators (TENGs) can convert any mechanical energy into electricity based on the coupling effect of contact electrification and electrostatic induction. Recently, TENGs have attracted tremendous attention as promising next-generation mechanical energy-harvesting devices due to advantages such as a high degree of freedom for material selection, high voltage output, simple structure, easy fabrication and availability, environmental friendliness, and low cost (*9-12*). Today, conductive materials such as carbon nanotubes, graphene, carbon paste, silver nanowires (*13-16*) have been utilized for the construction of stretchable TENGs to meet the requirement of rapid development of stretchable electronics. Nevertheless, the sheet resistance increased remarkedly at large strain (e.g. >100%) because the percolated networks of those conductive fillers are easily broken (*17*), limiting their application for large strain scenarios. Alternatively, TENGs with ultrahigh stretchability have been reported by using ionogels (*18-21*). Those as-fabricated devices consist practically useful features such as ambient stability and anti-freezing capability due to the intrinsically non-volatile performance of ionic liquids. Therefore, ionogels-based TENGs can realize mechanical energy harvesting over a wide temperature range. However, the broader application of ionogels for TENGs and other stretchable electronics is still limited by their high cost, difficulty of accessibility, relatively low conductivity, and the potential toxic of ionic liquids.

On the other hand, hydrated and ionic materials such as deformable and tough ionic hydrogels are one of the most ideal stretchable candidates because of their excellent biocompatibility (*22-24*), large stretchability with relatively small conductivity changing (*25*), and tunable mechanical properties (e.g., toughness, stretchability and elasticity) (*26, 27*). Thus, ionic hydrogels have been developed for various wearable and robotic applications, including pressure sensors (*28, 29*), strain sensor (*30*), touchpad (*30, 31*), robotic skin (*32*) and TENG (*25*). Due to the water-based yet solid, soft, highly stretchable, transparent and biocompatible features of hydrogels, ionic hydrogel-based TENGs show the huge potential as the power source for wearable electronics and soft robotics. However, hydrogel-based TENGs still suffer from several emergent issues that need to be addressed. Although there have been many efforts made to endow hydrogel-TENGs with practical features such as self-healing (*33*), anti-contamination (*34*) as well as better mechanical reliability (e.g., enhancing the bonding between the conductive hydrogel and electrification elastomer) (*35*), current hydrogel-based TENGs still suffer from the freezing issue under low temperature usage. Regular hydrogel ionic devices cannot maintain mechanical deformability and electrical conductivity under extremely cold environments.

To address this challenge, herein we report a novel and low-cost anti-freezing and highly stretchable ionic hydrogel-based triboelectric nanogenerator (iTENG). This iTENG is capable of both biomechanical energy harvesting and self-powering sensing by using dielectric elastomer as the electrification layer and freeze-tolerate ionic hydrogel as the electrode. Features such as robust hydrogel-elastomer bonding, high stretchability (300%) and extremely anti-freezing capability (e.g., −53 ^{o}C) have never been achieved simultaneously elsewhere but realized successfully here. The soft skin-like nanogenerator can generate an open circuit voltage of up to 380 V and an instantaneous areal power density of 5.7 mW m^{-2} with good durability. The iTENG can harvest mechanical energy from various human motions and serve as a self-powered wearable sensor in both regular environment and the extremely cold temperature. This work provides a feasible technology to design stretchable and sustainable power sources, which could potentially solve the energy issues of the next-generation stretchable electronics and soft robotics in the harsh environment.

5.2. Results

5.2.1. Design of iTENG

The iTENG consists of a sandwich-like architecture with the antifreezing hydrogel sealed between two elastomer (Ecoflex) films (**Figure 5.1**A), and a metal belt or wire was attached to the ionic hydrogel for the electrical connection. The thicknesses of anti-freezing hydrogel and PDMS films were controlled to be approximately 1.6 mm and 150 μm, respectively. The final devices could be tailored into arbitrary two-dimensional shapes. The anti-freezing hydrogel is made of a bulk dissipative hydrogel matrix [tough double-network (DN) hydrogel] containing hygroscopic/cryoprotective substances and inorganic ions. Specifically, hybrid cross-linked alginate-polyacrylamide (Alg-PAAm) networks were selected here due to their excellent and tunable mechanical performance (e.g., toughness and young's module) (*36*), confirmed biocompatibility for healthcare usage (*37*). Cryoprotective solutions have been widely applied to prevent various biological samples from icing damage at sub-zero temperatures, owing to their inhibition behaviors of hindering the ice crystallization of water molecules (*38*). Here, glycerol as a hygroscopic and cryoprotective material was incorporated into the tough hydrogel matrix because it is well accepted as a nontoxic agent. In addition, the nonionic kosmotrope feature of glycerol brings minimal impact to the mechanical performance of tough hydrogel with ionical cross-links (*39*). The model inorganic ions used here are sodium (Na^+) and chorolide (Cl^-) monoions since sodium chorolide (NaCl) shows low biotoxicity and good electrical conductivity. As been proved by our group's previous study, the presence of electrolyte salt contributed to the high ionic conductivity at room temperature ($0.904\ S\cdot m^{-1}$), regardless the negative effect from glycerol (*40*). In addition, the resistance of this conductive antifreezing hydrogel steadily increases with the tensile strain (*40*), but the increase rate in the strain range of 0-300% is much slower than that of other traditionally stretchable electronic conductors (*15*). Moreover, this resistance increase is much smaller than the inherent impedance of a TENG at the scale of MΩ and thus has little negative impact on the TENG's performance (*41*).

On the other hand, the interfacial bonding strength between the Alg-PAAm hydrogel (hydrophilic) and the elastomer films (typically hydrophobic) is naturally weak, reducing the mechanical reliability and ambient stability of hydrogel-based TENG (*35*). Inspired by the structures and functions of mammalian skins, here the Alg-PAAm hydrogel was bonded to the Ecoflex using an alternative strategy that has revealed the largest hydrogel-elastomer adhesion energy reported ever (*42*, *43*). By treating the elastomer surfaces with 10 wt.% benzophenone (BP, a ultraviolet-assisted grafting agent) in ethanol solution, the PAAm pre-hydrogel polymers can *in-situ* chemically graft methacrylate groups on the surface of the chemisorbed Ecoflex during hydrogel covalently cross-linking (**Figure 5.1**C) (*42*). Before bonding the two hydrogel-elastomer hybrid layers into an iTENG devices, we conducted a 2.5-h solvent exchange process to partially replace the water molecules in the hydrogel with glycerol and incorporate the electrolyte ions. The detail fabrication procedure can be found in **Figure S5.1**A and B and the **Materials and Methods** section. As a result, this robust bonding interface can withstand at least 300% strain with no visible delamination occurring (**Figure 5.1**D), beyond the maximum strain range of human motion and most soft robotic movement (*40*, *44*).

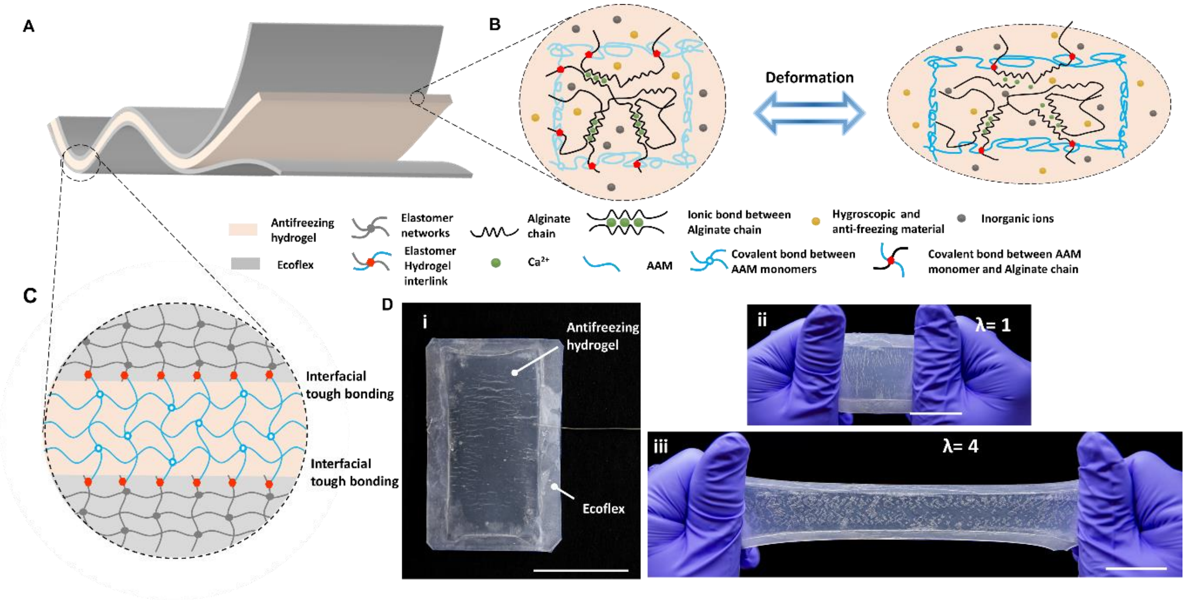

Figure 5.1. The design of anti-freezing, and stretchable iTENG with robust interfacial bonding. (A) Scheme of the iTENG with a sandwich structure. (B) Schematic illustration of the antifreezing hydrogel under deformation. The antifreezing hydrogel is made from a hydrogel

dissipative matrix (light pink square) containing both ionically (calcium; green circles) cross-linked and covalently cross-linked polymers (light blue circles and lines) and is laden with hygroscopic and anti-freezing reagents (yellow balls) and inorganic ions (gray balls). (C) Schematic illustration of the tough interfacial bonding between the elastomer layer (Ecoflex) and anti-freezing hydrogel, due to the covalently anchored hydrogel polymer network on elastomer surface. (D) An iTENG with a metal wire connected to the hydrogel electrode (i); an iTENG at the initial state (stretch λ = 1, ii) and stretched state (λ= 4, iii). The scale bar is 3 cm.

5.2.2. Electrical properties of the iTENG

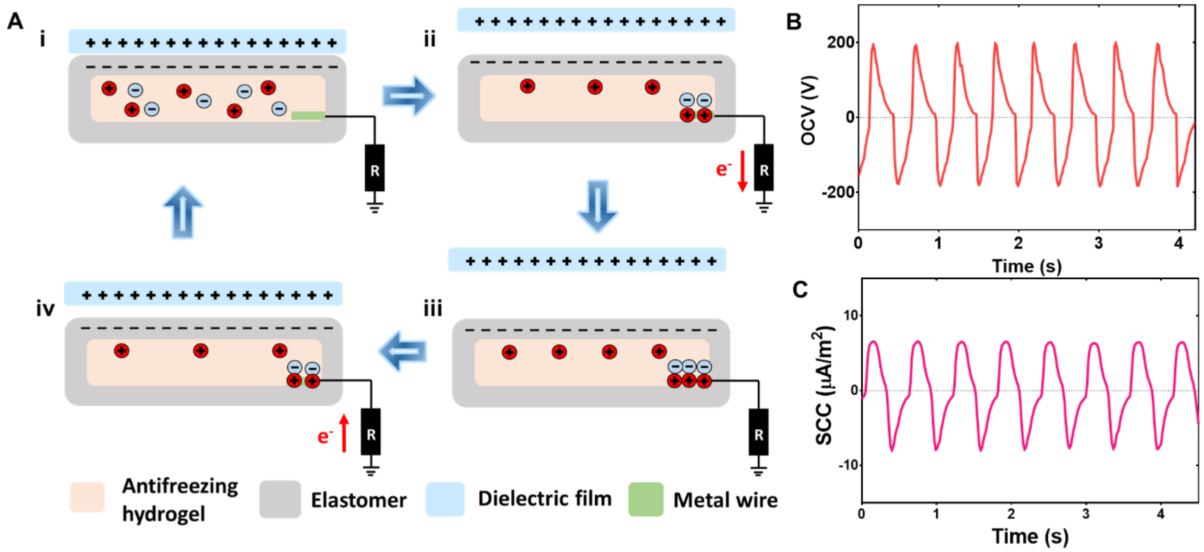

Figure 5.2. The working principle and output characteristics of the iTENG at single-electrode mode. (A) Scheme of the working mechanism of the iTENG. (B) Open circuit voltage (OCV) and (C) Short circuit current (SCC) of an iTENG across the resistor (3000 MΩ). the applied pressure is 6.7 kPa.

As potential utilized for wearable and stretchable electronics, we characterized the iTENG in the single-electrode mode by simply connecting the antifreezing ionic hydrogel to the ground by a metal wire through the external load (**Figure 5.2**A). Dielectric films (e.g., skin, nylon, and stainless steel) and elastomer (e.g., Ecoflex and PDMS) served as the positive and negative triboelectric layers (*45*), respectively (**Figure 5.2**A). The energy harvesting is based on the contact electrification and electrostatic induction. Before mechanical force is applied, there is no contact between elastomer and dielectric film. Therefore, no surface charges are generated on two films. As a result, the positive (Na^+) and negative (Cl^-) ions of the ionic hydrogel remains randomly distributed across the whole matrix. Once dielectric materials contact with the elastomer film of the iTENG upon the application of mechanical force, electrification occurs at the interface. Specifically, charges transfer from the dielectric film to the elastomer due to their different extent of electronegativity, leading to the same amount of charges generating at the surface of the dielectric film (positive) and the elastomer (negative), respectively (**Figure 5.2**A, i) (*16*). Because the two opposite charges coincide at almost the same plane, there is practically no electrical potential difference between those two surfaces (*25*). When the dielectric film moves away from the elastomer, those two oppositely charged surfaces become separated in space, resulting in a potential difference. The unscreened negative charges on the elastomer surface will induce the movement of the positive ions (Na^+) in the ionic hydrogel to accumulate at the hydrogel-elastomer interface, balancing the static charges (**Figure 5.2**A, ii). Meanwhile, negative ions (Cl^-) move and accumulate at the hydrogel-metal interface, leading to the formation of electrical double layer; a transient charge flows from the metal wires to the ground through the external load, generating a voltage output simultaneously (**Figure 5.2**A, ii). This electrostatic induction reaches the equilibrium until the separation distance between the two charged surfaces reached a maximum (**Figure 5.2**A, iii). Upon moving the dielectric film back to the elastomer, the whole process reverses, resulting in an electron flux with the opposite direction flow from the ground to the metal/hydrogel interface through the external load (**Figure 5.2**A, iv). By repeating the contact-separation movement between the dielectric object and the iTENG, multiple alternative current and voltage can be generated.

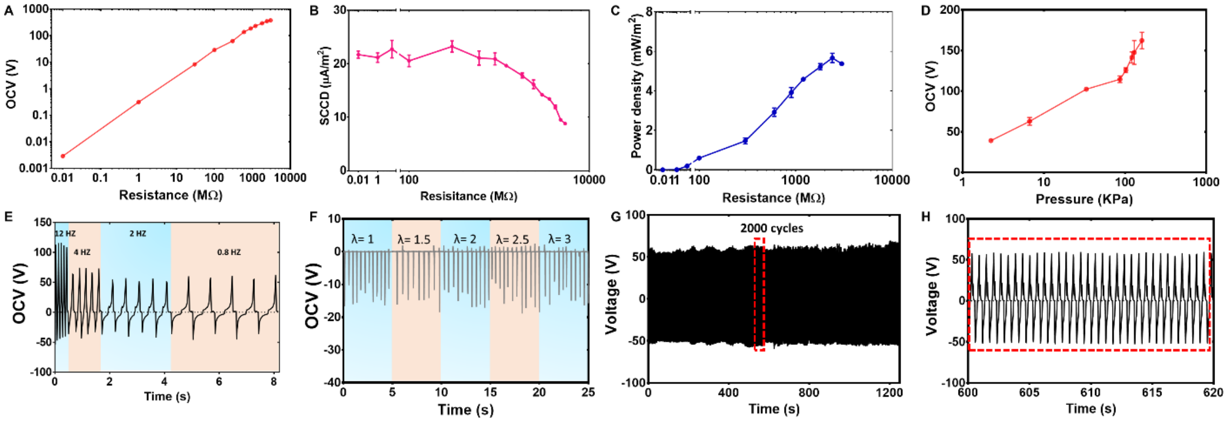

Figure 5.3.**The electrical properties of the iTENG under different conditions**. Variation of the output (**A**) voltage, (**B**) current density, and (**C**) power density with the external loading resistance. N=5. Variation of peak amplitudes of the output voltage across the resistor (300 MΩ) for different contact (**D**) pressure and (**E**) frequency. (**F**) Variation of the output voltage across the resistor (600 MΩ) at different stretched length upon one finger tapping exerted at a force of 10 N and a frequency of 2 Hz. Output voltage stability of the iTENG when subjected to (**G**) 2000 cycles of contact separation motions and its (**H**) zoom-in view.

The electrical performance of the iTENG was evaluated by measuring the open circuit voltage (OCV) and short circuit current (SCC). A pork skin or stainless-steel film was used to have the continuous contact-separation movement to an iTENG (3 × 3 cm^2). Unless mentioned elsewhere, the frequency (2 Hz) of the contact-separation motion and the pressure (6.7 kPa) between the two contacting films were all controlled to be the same by a linear motor for all following tests. **Figure 5.2**B and C show representative OCV and SCC curves via the stainless-steel contact. With the external load of 3000 MΩ, the iTENG generates the peak-peak OCV and peak-peak areal SCC of 380 V (**Figure 5.2**B) and 14.5 uA m^{-2} (**Figure 5.2**C), respectively. As the impedance of the external load affects the energy-harvesting performance of TENGs, herein, the OCV and areal SCC of the iTENG were evaluated across various load resistances. **Figure 5.3**A and B show the variations of output voltage and current density with different load resistances: the output voltage increases, and the current density decreases with an increase of external load resistance. **Figure 5.3**C shows that the maximum output areal power density is 5.7 mW m^{-2} at an external load resistance of 2400 MΩ. In the future, antifreezing hydrogel with higher conductivity and elastomer films with unique structure can be designed to further enhance the generating power density (*25*). Potentially applied for the self-powering mechanical sensing, we then characterized the electrical responses of the iTENG under mechanical deformation (e.g., applied pressure). **Figure 5.3**D shows then peak-peak OCV value across the resistor (300 MΩ) increases as the magnitude of applied pressure at 2 Hz. The growing pressure can increase the effective contact area between the dielectric film and the elastomer thus enhancing the energy-harvesting performance (*33*). In addition, potentially utilized for a sustainable wearable energy harvester in our daily life (e.g., breath, heartbeat, walk and running) for wearable electronic devices, we evaluated the energy harvesting performance of the iTENG over the range of daily mechanical frequencies (1-10 Hz). As shown in **Figure 5.3**E, the peak amplitudes of OCV increases as the frequency increases from 0.8 to 12 Hz and reaches a maximum value of 150 V under an applied pressure of 45 kPa across the resistor (300 MΩ). We also studied the electrical performance of iTENG upon large strain. By controlling the contact area constant by simple finger tapping exerted at a force of 10 N and a frequency of 2 Hz, the iTENG is able to maintain a stable performance with a peak voltage of around 15 V across the external resistor (600 MΩ) over the strain range from 0 to 200% (larger than the maximum value of human motion) (**Figure 5.3**F). The durability of the produced iTENG was evaluated by measuring the voltage output for 2000 continuous cycles of contact-separation motion (pork skin was uses as the dielectric film to mimic human skin in wearable scenarios). The device shows a stable OCV performance across the external resistor (300 MΩ) under the applied pressure of 8.7 kPa (**Figure 5.3**G and H), indicating the suitability as a wearable device for long-term usage.

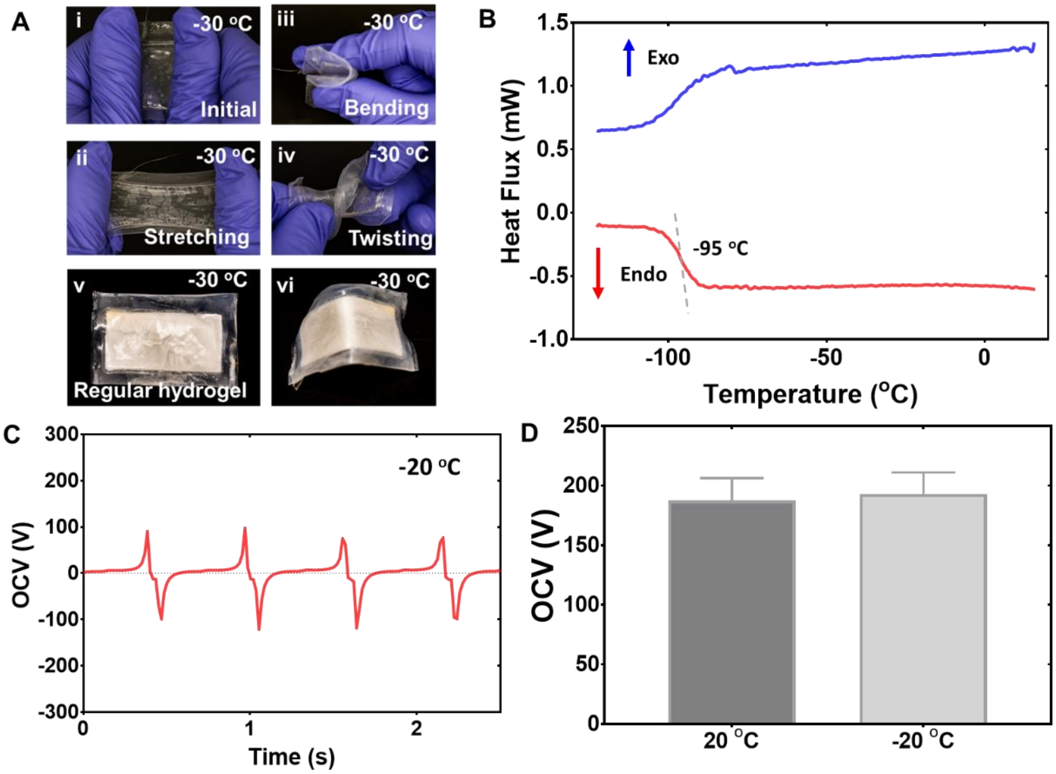

Figure 5.4. Antifreezing properties of the iTENG. (**A**) Photographs of an anti-freezing iTENG that can twist, bend and stretch (i-iv) and a regular iTENG is entirely frozen after 3 h (v-vi) at −30 °C. **(B)** Dynamic scanning calorimetry (DSC) results of an iTENG (antifreezing hydrogel) in the temperature range from −120 °C to 15 °C. Reproduced from Ref. *(40)* (**C**) The open-circuit voltage of an iTENG at −20 °C. (**D**) Comparison of the peak-peak OCV value at 20 °C and -20 °C. N=4.

5.2.3. Anti-freezing properties of the iTENG

One major concern about regular hydrogels is freezing at the subzero temperature, which makes them mechanically rigid and electrically non-conductive (*40*). As a promising sensing and energy harvesting unit for wearable electronics, we then examined the anti-freezing performance of the iTENG in low temperature environments. Here, glycerol (66.6 wt%) solution dissolved with saturated NaCl content was used to treat tough hydrogel to optimize its amount of unfrozen bound water and enhance its anti-freezing property (*46*). Indeed, the as-fabricated iTENG shows excellent freezing tolerance with good mechanical flexibility and stretchability (twisting, bending and stretching) at extremely cold conditions [−30 °C for 24 h, Figure 5.4A (i-iv)] due to the large amount of unfrozen bound water. In contrast, the regular hydrogel iTENG becomes entirely frozen and cannot be stretchable at −30 °C after 1 h (Figure 5.4A (v-vi)) due to the large amount of free water. We further accurately determined the anti-freezing limits of the iTENG by differential scanning calorimetry (DSC) from −120 °C to 15 °C. Notably, the anti-freezing hydrogel does not show any cold-crystallization peak in the whole exo/cooling thermogram or any melting peak in the whole endo/heating thermogram (Figure 5.4B) because this hydrogel does not freeze, which is consistent with the previous reported observation (*38*). During heating, the anti-freezing hydrogel only shows a peak similar to a glass transition at −95 °C (Figure 5.4B), indicating no observable icing of the hydrogels. This anti-freezing performance is better than most of the previously reported ionic hydrogels (*40*). In addition, Ecoflex has been known to have an extremely low freezing limit of -53.8 °C (*47*). Moreover, our previous work has reported that the anti-freezing hydrogel shows high conductivity under extremely cold environment (5.34×10^{-2} $S \cdot m^{-1}$ @−25 °C, 8.7×10^{-3} $S \cdot m^{-1}$ @ −40 °C and 1.96×10^{-5} $S \cdot m^{-1}$ @−70 °C) (*40*). The good conductivity plus the mechanical deformability of both hydrogel and Ecoflex at low temperature are essential to realize stretchable self-powering sensors and energy harvesters at subzero temperature (e.g., -50 ^{o}C). To further verify the self-powering efficiency of the iTENG at low temperature, here we evaluated its electrical output performance at −20 °C (Figure 5.4C). The output voltage of the iTENG at −20 °C is similar to that at 20 °C with other conditions constant (the external load is 300MΩ, applied force is 35 kg, contact-separation frequency is 2 Hz) (Figure 5.4D). These observations indicate that the iTENG has good low-temperature tolerance and could serve as stretchable and self-powering sensing component and energy harvester for wearable use in extremely cold environments.

5.2.4. Demonstration

The superior energy-harvesting performance along with being extremely stretchable and anti-freezing makes iTENG an ideal sustainable power source for the realization of self-powered electronics. The iTENG can be used to directly drive external electronics for real-time applications by scavenging biomechanical energy, especially the energy of human motions. A pack of 30 blue light-emitting diodes (LEDs) connected in series were driven to send the warn signal of *“SOS”* by tapping an iTENG on the human hand (3 ×3 cm^2, human body as the reference electrode/ ground, **Figure 5.5**A and B, and **Movie** S5.1, Supporting Information). The tapping frequency was approximately 2 Hz.

Furthermore, the energy-harvesting ability of an iTENG under extremely cold environment was explored by charging energy storage devices (e.g., capacitors) to power electronics, as shown in **Figure 5.5**C. The detailed circuit diagram is illustrated in **Figure 5.5**D. For demonstration, an iTENG was firstly stored in a fridge (-20 ^{o}C) for at least 3 h to fully reach the equilibrium and then tapped by the hand to charge a 10 μF capacitor through a bridge rectifier and then to power an digital clock (**Figure 5.5**C, **Movie** S5.2). The tapping frequency was about 2 Hz and the representative current after rectifying is shown in **Figure S5.3**. In ~3.4 min, the voltage of the capacitor could be charged and increased linearly to 3 V, which can later power the clock (**Figure 5.5**C and E, **Movie** S5.2). Subsequently, the capacitor can be charged back to 3 V in about 4 min, powering the clock repeatedly (**Figure 5.5**E). These demonstrations indicate that our iTENG could act as stretchable and wearable self-powered electronics as well as sustainable power sources in both regular and extreme living conditions.

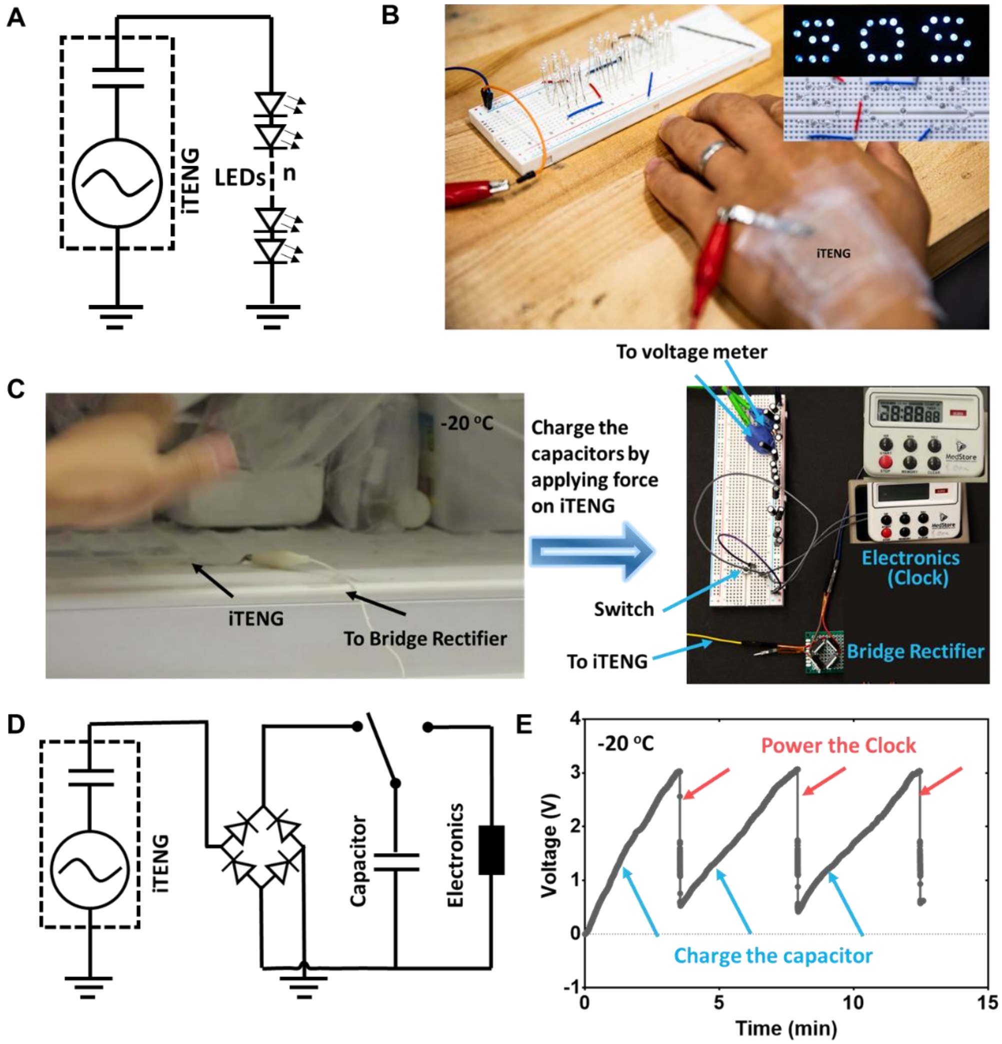

Figure 5.5. Biomechanical energy harvesting by the iTENG in the room temperature and subzero temperature. (A) The equivalent circuit to light the multiple LEDs connected in series

by tapping the iTENG at single-electrode mode. (**B**) An image of 30 blue LEDs lightened by tapping the iTENG on a hand to send the warn signal of "*SOS*". (**C**) Image of an antifreezing iTENG in the fridge (-20 ^{o}C), and the image and (**D**) the equivalent circuit of a self-charging system that uses the energy harvested from the iTENG to power electronics (for example, an electronic clock). (**E**) Voltage profile of a 10 µF capacitor being charged by tapping the iTENG and then used to power the electronic clock at -20 ^{o}C.

5.3. Conclusion

In summary, we designed a novel but low-cost ionic TENG based on an anti-freezing ionic hydrogel. The resultant iTENG shows high stretchability (at least 300%), high conductivity, durability (2000 times), and stable electrical performance in both regular environment and the extremely cold temperature (e.g., −53 ^{o}C), which are all highly desirable properties for the next-generation mechanical energy harvesters but have previously been barely achieved. For proof-of-demonstration, iTENG was designed as a sustainable and effective energy source/ biomechanical energy harvester for self-powered electronics, including powering commercial LEDs and a digital clock. We envision that the iTENG and its self-powering sensing and mechanical energy harvesting capabilities in both room and cold temperature will have great potential for use in the next-generation wearable electronics and soft robotics.

5.4. Materials and methods

5.4.1. Materials

Ionic cross-linker calcium sulfate ($CaSO_2$, 255548), Alginate (A2033), acrylamide (AAm, A8887), covalent cross-linker N,N'-methylenebis(acrylamide) (MBAA, M7279), photoinitiator IRGACURE 2959 (I2959), acetic acid (695092), sodium chrolide, bridging polymer chitosan of medium molecular (448877), the coupling reagents, 1-ethyl-3-(3-dimethylaminopropyl) carbodiimide hydrochloride (EDC, E1769) and nhydroxysulfosuccinimide (sulfo-NHS, 56485), hygroscopic substance glycerol (G9012) were purchased from Sigma. Milli-Q (18.3 MΩ) water was used in all experiments. Porcine skin was purchased from a local grocery store.

5.4.2. Fabrication of iTENG

The fabrication of iTENG consists of three steps: i) the fabrication of alginate-polyacrylamide (Alg-PAAm) tough hydrogel-elastomer hybrid structure; ii) solvent exchange; and iii) the bonding of two hydrogel- elastomer bilayers.

The hydrogel-elastomer bilayer structure was prepared based on the modified method reported previously (*17*, *40*). In brief, the pre-cured Ecoflex A and B (00-30, Smooth-On Inc.) were mixed quickly and spin-coated on a hydrophobic glass slide. After curing on the hot plate (80 ^{o}C) for 40 min, the surfaces of Ecoflex were thoroughly cleaned with methanol and deionized water, and completely dried with nitrogen gas before the benzophenone treatment. Thereafter, benzophenone solution (10 wt.% in ethanol) was applied onto the elastomer to evenly cover the entire elastomer surface for 15 min at room temperature. Then, the elastomer was washed with methanol three times and completely dried with nitrogen gas before use. Hydrogel was prepared by mixing 10 ml of a carefully degassed aqueous pregel solution (12.wt.% AAm, 2 wt.% sodium alginate and 36μL of 2 wt. % MBAA) with ionic cross-linkers (191μL of 0.75M $CaSO_4$ slurries) and Irgacure 2959 (0.2 wt.%). The mixture was then mixed quickly, poured onto the freshly treated elastomer film and then covered by glass plate with hydrophobic coating. The whole assembled mold followed by ultraviolet irradiation in a 254 nm ultraviolet chamber (28–32 $mWcm^{-2}$, UVO-Cleaner 42A, Jelight Company, Inc.) for an hour, during which the PAAm network was covalently cross-linked and bonded onto elastomer surface.

After that, hygroscopic reagents and electrolyte salt were added into the hydrogel layer of the bilayer structure to increase their ambient stability, anti-freezing capability and ionic conductivity. Generally, hydrogel can reach the equilibrium state once immersed in the conductive hygroscopic solvent for 2.5-h exchanging as reported before (*38*). Unless noted elsewhere, the conductive hygroscopic solvent for exchanging was prepared by adding glycerol to the saturated NaCl aqueous solution (5.4 M) and the weight ratio of glycerol to distilled water is 2:1 due to the fact that at around 66.6 wt% of glycerol in a glycerol-water mixture the lowest freezing temperature is achieved (*46*). To ensure that the concentration of NaCl and glycerol in the external solution remained nearly constant before and after soaking the hydrogel, we prepared the solvent solution with a volume 20 times the volume of the hydrogel.

Before bonding, all visible liquid should be removed from the hydrogel surface. The bridging polymer chitosan was dissolved into distilled water at 2.0 wt. % and the pH was adjusted to 5.5~6 by acetic acid. EDC and NHS were used as the coupling reagents. The final concentrations of EDC and NHS in the solution of the bridging polymer were both 12mg/mL. The mixture of the bridging polymer and coupling reagents was applied on one hydrogel surface of the hybrid structure and then pressed on another hybrid structure for at least 1 h for carbodiimide coupling reaction. After that, the surrounding Ecoflex edge was sealed by the degassed pre-cured Ecoflex.

5.4.3. Characterization and measurements

A linear motor was used to provide the input of mechanical motions (**Figure S5.2**). For all the tests of energy generation of the iTENG, the voltage and current were recorded by a Keithley 2614B source meter. The force applied by the motor was detected by a force sensor. For the measurement of the output performances of the iTENG at subzero temperatures, the iTENG along with the linear motor was kept inside a fridge (-20 ^{o}C).

5.4.4. Anti-freezing Characterization

The freezing point of samples were characterized using a differential scanning calorimeter (TA Instruments, DSC 2920) with a mechanical cooling system. Samples (5-10 mg) were contained in hermetically sealed aluminum pans (TA Instruments, Tzero Aluminum Hermetic Pan) for testing, with an empty pan used as the reference. The DSC was operated under a 35 μL min^{-1} nitrogen flow rate and data were captured at a rate of 5 Hz. Samples were cooled at a rate of 2 °C min^{-1} to −120 °C. After an isothermal period of 30 min, samples were heated up at 2 °C min^{-1} to the initial equilibration temperature (15°C).

5.4.5. Statistical analysis

Statistical analyses were performed on GraphPad Prism software (GraphPad Software, Inc.). Results are depicted as mean ± standard deviation (SD), we conducted unpaired Student's t test to analyze the statistical differences of experiment results. We used parametric test and assumed any experimental groups are normally distributed with the same SD. Differences were considered statistically significant if $P < 0.05$.

5.5. References

1. L. Hu *et al.*, Highly conductive paper for energy-storage devices. *Proceedings of the National Academy of Sciences* **106**, 21490-21494 (2009).
2. V. L. Pushparaj *et al.*, Flexible energy storage devices based on nanocomposite paper. *Proceedings of the National Academy of Sciences* **104**, 13574-13577 (2007).
3. B. Scrosati, Paper powers battery breakthrough. *Nature nanotechnology* **2**, 598-599 (2007).
4. L. Hu, H. Wu, F. La Mantia, Y. Yang, Y. Cui, Thin, flexible secondary Li-ion paper batteries. *ACS nano* **4**, 5843-5848 (2010).
5. J. Yoon *et al.*, GaAs photovoltaics and optoelectronics using releasable multilayer epitaxial assemblies. *Nature* **465**, 329-333 (2010).
6. J. Peet *et al.*, Efficiency enhancement in low-bandgap polymer solar cells by processing with alkane dithiols. *Nature materials* **6**, 497-500 (2007).
7. S. Xu *et al.*, Self-powered nanowire devices. *Nature nanotechnology* **5**, 366-373 (2010).
8. S. Wang, L. Lin, Z. L. Wang, Nanoscale triboelectric-effect-enabled energy conversion for sustainably powering portable electronics. *Nano letters* **12**, 6339-6346 (2012).

9. J. Bae *et al.*, Flutter-driven triboelectrification for harvesting wind energy. *Nature communications* **5**, 1-9 (2014).
10. J. Chun *et al.*, Boosted output performance of triboelectric nanogenerator via electric double layer effect. *Nature communications* **7**, 1-9 (2016).
11. S. Wang, L. Lin, Z. L. Wang, Triboelectric nanogenerators as self-powered active sensors. *Nano Energy* **11**, 436-462 (2015).
12. Z. L. Wang, J. Chen, L. Lin, Progress in triboelectric nanogenerators as a new energy technology and self-powered sensors. *Energy & Environmental Science* **8**, 2250-2282 (2015).
13. X. Chen *et al.*, Tunable optical modulator by coupling a triboelectric nanogenerator and a dielectric elastomer. *Advanced Functional Materials* **27**, 1603788 (2017).
14. F. Yi *et al.*, Stretchable-rubber-based triboelectric nanogenerator and its application as self-powered body motion sensors. *Advanced Functional Materials* **25**, 3688-3696 (2015).
15. B.-U. Hwang *et al.*, Transparent stretchable self-powered patchable sensor platform with ultrasensitive recognition of human activities. *ACS nano* **9**, 8801-8810 (2015).
16. Y. C. Lai *et al.*, Electric eel - skin - inspired mechanically durable and super - stretchable nanogenerator for deformable power source and fully autonomous conformable electronic - skin applications. *Advanced Materials* **28**, 10024-10032 (2016).
17. F. Yi *et al.*, A highly shape-adaptive, stretchable design based on conductive liquid for energy harvesting and self-powered biomechanical monitoring. *Science advances* **2**, e1501624 (2016).
18. P. Zhang *et al.*, Stretchable, Transparent, and Thermally Stable Triboelectric Nanogenerators Based on Solvent - Free Ion - Conducting Elastomer Electrodes. *Advanced Functional Materials* **30**, 1909252 (2020).
19. Z. Liu *et al.*, Poly (ionic liquid) hydrogel-based anti-freezing ionic skin for a soft robotic gripper. *Materials Horizons* **7**, 919-927 (2020).
20. L. Sun *et al.*, Ionogel-based, highly stretchable, transparent, durable triboelectric nanogenerators for energy harvesting and motion sensing over a wide temperature range. *Nano Energy* **63**, 103847 (2019).
21. Y. Ren *et al.*, Ionic liquid–based click-ionogels. *Science advances* **5**, eaax0648 (2019).
22. C. Yang, Z. Suo, Hydrogel ionotronics. *Nature Reviews Materials* **3**, 125 (2018).
23. H. R. Lee, C. C. Kim, J. Y. Sun, Stretchable ionics–a promising candidate for upcoming wearable devices. *Advanced Materials* **30**, 1704403 (2018).
24. H. Sheng *et al.*, Neural interfaces by hydrogels. *Extreme Mechanics Letters* **30**, 100510 (2019).
25. X. Pu *et al.*, Ultrastretchable, transparent triboelectric nanogenerator as electronic skin for biomechanical energy harvesting and tactile sensing. *Science advances* **3**, e1700015 (2017).
26. X. Liu, J. Liu, S. Lin, X. Zhao, Hydrogel machines. *Materials Today,* (2020).
27. M. Zhu *et al.*, Antifreezing hydrogel with high zinc reversibility for flexible and durable aqueous batteries by cooperative hydrated cations. *Advanced Functional Materials* **30**, 1907218 (2020).
28. J. Y. Sun, C. Keplinger, G. M. Whitesides, Z. Suo, Ionic skin. *Advanced Materials* **26**, 7608-7614 (2014).
29. Z. Lei, P. Wu, A supramolecular biomimetic skin combining a wide spectrum of mechanical properties and multiple sensory capabilities. *Nature communications* **9**, 1134 (2018).
30. B. Ying, Q. Wu, J. Li, X. Liu, An ambient-stable and stretchable ionic skin with multimodal sensation. *Materials Horizons,* (2020).

31. C.-C. Kim, H.-H. Lee, K. H. Oh, J.-Y. Sun, Highly stretchable, transparent ionic touch panel. *Science* **353**, 682-687 (2016).
32. C. Larson *et al.*, Highly stretchable electroluminescent skin for optical signaling and tactile sensing. *science* **351**, 1071-1074 (2016).
33. K. Parida *et al.*, Highly transparent, stretchable, and self‐healing ionic‐skin triboelectric nanogenerators for energy harvesting and touch applications. *Advanced Materials* **29**, 1702181 (2017).
34. Y. Lee, S. H. Cha, Y.-W. Kim, D. Choi, J.-Y. Sun, Transparent and attachable ionic communicators based on self-cleanable triboelectric nanogenerators. *Nature communications* **9**, 1-8 (2018).
35. T. Liu *et al.*, Triboelectric-nanogenerator-based soft energy-harvesting skin enabled by toughly bonded elastomer/hydrogel hybrids. *ACS nano* **12**, 2818-2826 (2018).
36. J.-Y. Sun *et al.*, Highly stretchable and tough hydrogels. *Nature* **489**, 133-136 (2012).
37. J. Li *et al.*, Tough adhesives for diverse wet surfaces. *Science* **357**, 378-381 (2017).
38. F. Chen *et al.*, Rational Fabrication of Anti‐Freezing, Non‐Drying Tough Organohydrogels by One‐Pot Solvent Displacement. *Angewandte Chemie* **130**, 6678-6681 (2018).
39. W. P. Williams, P. J. Quinn, L. I. Tsonev, R. D. Koynova, The effects of glycerol on the phase behaviour of hydrated distearoylphosphatidylethanolamine and its possible relation to the mode of action of cryoprotectants. *Biochimica et Biophysica Acta (BBA)-Biomembranes* **1062**, 123-132 (1991).
40. B. Ying, Z. Chen, R. Zuo, J. Li, X. Liu, An anti-freezing, ambient-stable and highly stretchable ionic skin with strong surface adhesion for wearable sensing and soft robotics. *In Submission,* (2020).
41. X. Chen *et al.*, Waterproof and stretchable triboelectric nanogenerator for biomechanical energy harvesting and self-powered sensing. *Applied Physics Letters* **112**, 203902 (2018).
42. H. Yuk, T. Zhang, G. A. Parada, X. Liu, X. Zhao, Skin-inspired hydrogel–elastomer hybrids with robust interfaces and functional microstructures. *Nature communications* **7**, 1-11 (2016).
43. J. Yang, R. Bai, B. Chen, Z. Suo, Hydrogel adhesion: A supramolecular synergy of chemistry, topology, and mechanics. *Advanced Functional Materials* **30**, 1901693 (2020).
44. B. Ying, Q. Wu, J. Li, X. Liu, An ambient-stable and stretchable ionic skin with multimodal sensation. *Materials Horizons* **7**, 477-488 (2020).
45. Z. L. Wang, Triboelectric nanogenerators as new energy technology for self-powered systems and as active mechanical and chemical sensors. *ACS nano* **7**, 9533-9557 (2013).
46. L. B. Lane, Freezing Points of Glycerol and Its Aqueous Solutions. *Industrial & Engineering Chemistry* **17**, 924-924 (1925).
47. *https://www.smooth-on.com/products/ecoflex-00-30/*. accessed on Augest, 2020.

5.6. Supplementary Materials

An anti-freezing, and stretchable ionic hydrogel triboelectric nanogenerator for mechanical energy harvesting and self-powering sensing

Figure S5.1. The fabrication of iTENG.

Figure S5.2. Characterization setup**.**

Figure S5.3. Rectified current output of the iTENG by hand tapping at low temperature.

Movie S5.1. An iTENG was tapping by hand to drive 30 blue light-emitting diodes (LEDs) connected in series to send the warn signal of "*SOS*".

Moive S5.2. An iTENG stored at -20 ^{o}C was tapping by hand to charge a 10 μF capacitor to power an digital clock for muiltiple times.

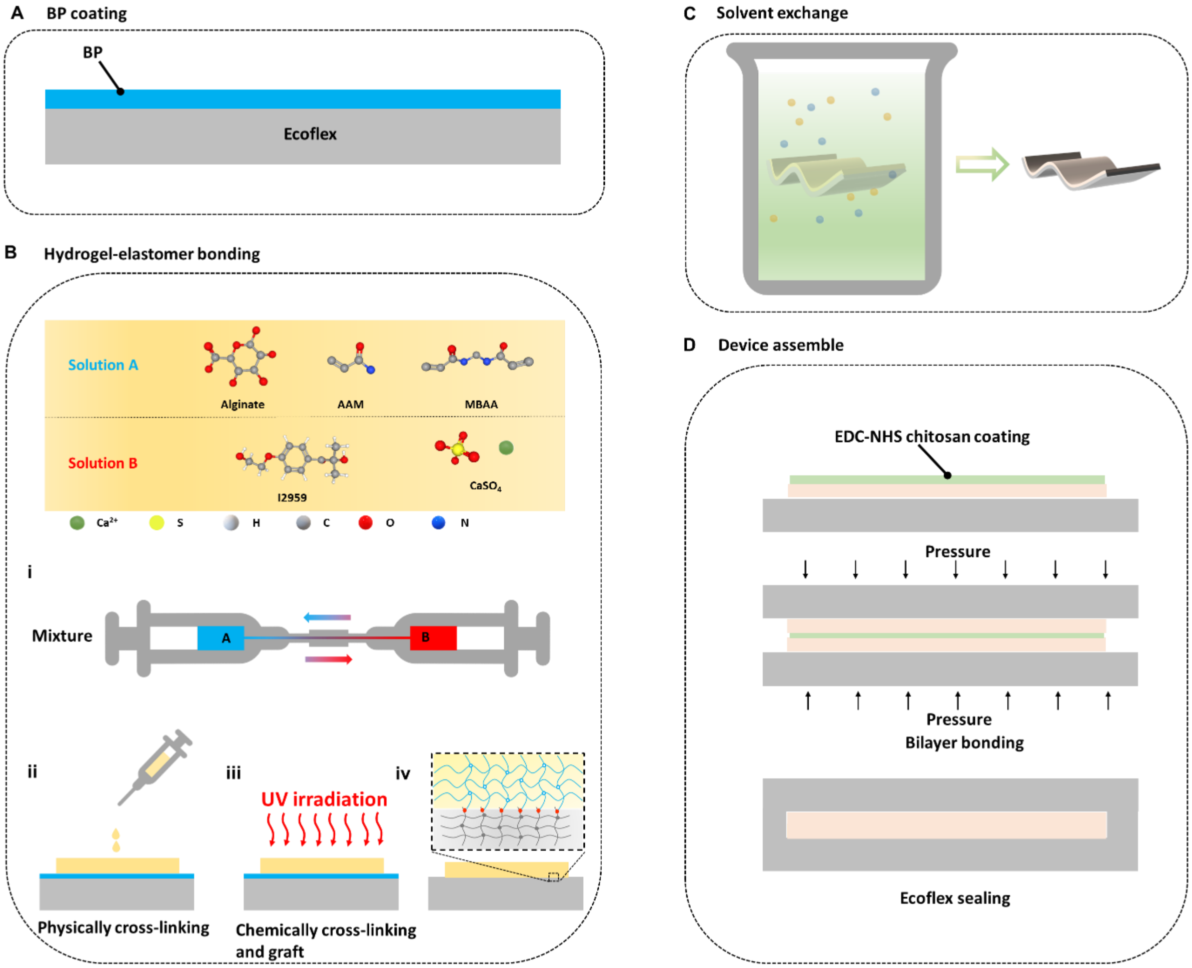

Figure S5.1. iTENG fabrication. (**A**) BP coating on Ecoflex film. (**B**) hydrogel-elastomer bonding.(**C**) Solvent enchange to endow the hydrogel with anti-freezing and conductive capability. (**D**) Device assambly.

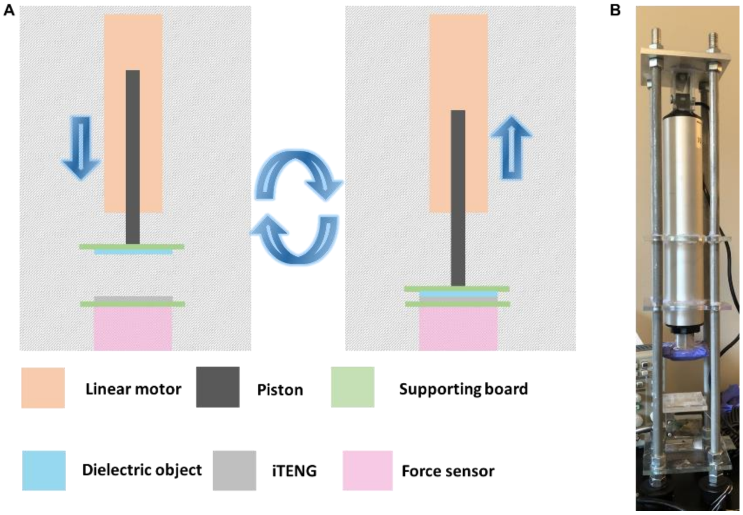

Figure S5.2. Characterization setup. (**A**) The structural diagrams and (**B**) optical photo of a home-made device for evaluating the electrical output performance of the iTENG.

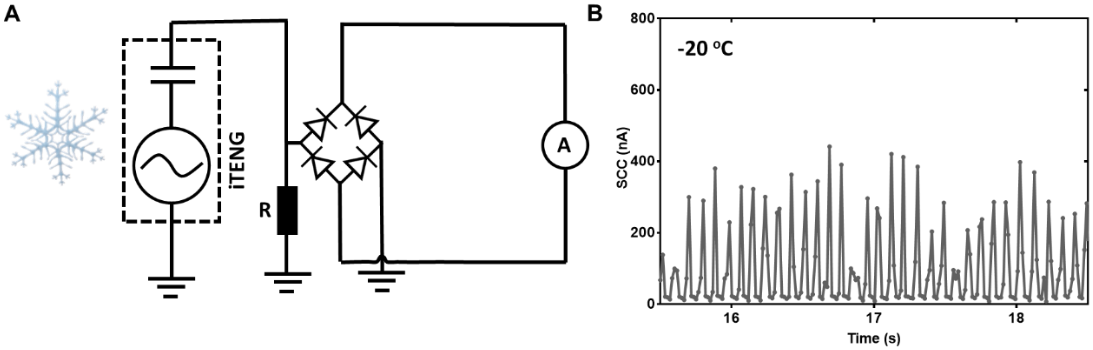

Figure S5.3. Rectified current output of the iTENG by hand tapping at low temperature. (**A**) The equivalent circuit measuring the rectified short-circuit current of the iTENG at single-electrode mode. (**B**) The output current of an iTENG at single-electrode mode tapped by a bare hand. the external resistance is 150 MΩ.

6. Chapter 6. Conclusion

6.1. Summary of accomplishments and contributions

The emerging field of hydrogel skin-like ionic devices promises to enable next generation of wearable devices and soft robotics. Before such devices come to life, there are several challenges to overcome: hydrogels need to be ionically conductive to transmit electrical signals, mechanically robust to sustain large deformation, multifunctional and multimodal to better mimic human skin, ambient stable and anti-freezing to sustain various practically environmental conditions, and capable of self-powering sensing to reduce power consumption; and should have strong adhesion to attach to various target surfaces. This thesis contributes to this field by devoting efforts to several important aspects, as summarized below:

1. Established a facile yet robust approach to fabricate a hydrogel ionic diode with superior mechanical properties, highly optical transparency and ambient stability.

2. Developed the first design of ionic diode-based artificial skin that is capable to sense the change of deformation, force and humidity with multimodal signals.

3. Demonstrated the first ionic diode-based wearable strain-humidity sensing, self-powering human-machine interaction, and energy harvesting.

4. Established a facile yet robust approach to fabricate an ionic hydrogel with superior mechanical properties, excellent ionic conductivity, ambient stability, wide working temperature range, and strong surface adhesion capability to a variety of substrate surfaces.

5. Demonstrated the first ionic hydrogel device for multiple applications including low-temperature wearable sensing, human-machine interaction, motion/deformation sensing on a soft gripper and a quadruped soft robot under extremely cold conditions

6. Demonstrated the first ionic hydrogel-based triboelectric nanogenerators with low cost, superior mechanical properties, excellent anti-freezing capability for applications, including low-temperature biomechanical energy harvesting and self-powering sensing.

6.2. Future work

This thesis has developed approaches to empower hydrogel materials with enhanced merits (e.g., high stretchability, toughness, self-powering, anti-dehydration, anti-freezing and bio-adhesive) for better real-world practical usage. Despite the promising progress of the applications for wearables, soft robotics and beyond, the development of hydrogel skin-like ionic devices is still in its infancy, there remain ample of research opportunities. Here, I present some prospective directions:

1. Currently, skin-inspired hydrogel ionic sensors are mainly designed with single or dual sensing modality. Rather, human skin consists a multimodal sensation capability. Therefore, new designs of hydrogel material and structure are worth exploring to realize multiple responsive hydrogel ionic sensors. For example, in biological systems, Na^+ or K^+ channels can efficiently discriminate Na^+ or K^+ from other alkali cations and even from each other, while traditional hydrogel ionic sensors have never been able to sense those differences. Current stretchable hydrogel sensors are focusing on biophysical signals, therefore, multimodally biophysical and biochemical sensing would increase knowledge of wearables and robotics. Sensing of pressure, strain and even detecting the presence of chemical and biological markers in the environment would be useful for a wide range of applications, including enhanced human-machine interaction, smart wound healing and in-situ micro-robotic controlled drug deliver (*1-4*). For biosensing, 2D materials could be incorporated to enable sophisticated applications in chemical/gas sensing (*5*).

2. Currently, skin-inspired hydrogel ionic devices are usually in bulky type and their fabrication mainly relies on manual assembly. Miniaturization and scalable fabrication of hydrogel devices will improve the user’s wearability, increase the functionality of hydrogel devices yet reduce the device-to-device variation. Most proof-of-concept ionic hydrogel devices featured thickness of ~1 mm (*6*). Careful production of thinner hydrogel film with breathability, durability, stretchability, and biocompatibility will be helpful in improving the wearers’ comfort, such as avoiding irritation events over long-term use. For example, hydrogel 3D printing has been able to extrude strain sensors (*7*), and highly conductive and soft hydrogel microstructure with high resolution (~30 μm) for bioelectronic neural recording (*8*). 3D printing is promising to highly integrate multimodal sensation into a single soft robotics as well (*9*). In addition, existing microfabrication techniques such as soft lithography could be possible for constructing micrometer-sized hydrogel arrays for multifunctional sensors with multimodality for biomedical applications such as smart organ-on-a-chip.

   On the other side, the massive dataset would be collected during the long-term wearing of highly integrated hydrogel sensors for personalized healthcare. Machine learning and AI can be integrated to enhance the data process and analyses for personalized health monitoring and disease prediction/prognosis. Full automation is another challenge and opportunity for soft robotics to adapt to complex environments. Machine learning based control could increase the possibility to realize better closed-loop operations by real-time processing and analyzing the sensed signals from the highly integrated and distributed soft hydrogel sensors (*10, 11*).

3. The ultimate goal of iontronic is to develop a human-like closed-loop system, in which it consists of ionic sensing, ionic wiring, ionic memory/computing, and ionic decision/ actuation

components. Today, stretchable hydrogel ionic sensing, wiring and actuating has been realized (*6*) while the stretchable hydrogel ionic computing has rarely been reported to realize seamless signal transduction from input end to output end within the closed-loop. The gap of stretchable hydrogel memory/computing units could be solved in the near future due to the recently developed stretchable ionic diode (*12-15*). Stretchable hydrogel ionic diode, as the counterpart of electrical diode for the traditional logic circuit in the computer, will be a basic component to construct the soft and stretchable microprocessor.

4. The development of stretchable energy supply systems is another challenge for achieving more stable and longer lasting ionic hydrogel systems for wearables and soft robotics. The trend to integrate multiple hydrogel sensor arrays into wearable/robotic platforms will increase the power consumption during continuous monitoring as well as large existing actuation power consumption. Even though fabrication of self-powered devices (e.g., integration of stretchable solar cells (*16*), stretchable TEN-based sensing and energy harvesting (*17*), stretchable ionic diode-based sensing and energy harvesting (*14*, *15*) and biofuel-powered e-skin (*18*) suggests promising ways to solve this issue by effectively reducing the power consumption, the power generation efficiency of this kind of devices remains questionable. Therefore, the development of wearable and stretchable power-storage devices with a large capacity remains potential for future wearable and soft robotic research.

5. Last but not the least, while the majority of studies on hydrogel ionic devices over-focused on the property's enhancement of hydrogel materials such as their maximum stretchability while most practical and real-world applications do not need such high performance. Future challenges remain for the translation of hydrogel ionic devices from proof-of-concept level demonstrations in laboratories to products on the market.

6.3. Publications

6.3.1. Refereed journal papers

1. **Binbin Ying,** Ryan Chen, Runze Zuo, Jianyu Li, Xinyu Liu*. An anti-freezing, ambient-stable and highly stretchable ionic skin with strong surface adhesion for wearable sensing and soft robotics. in submission, 2020.

2. **Binbin Ying**, Siwan Park, Longyan Chen, Xianke Dong, Edmond W. K. Young, and Xinyu Liu*. NanoPADs and NanoFACEs: an optically transparent nanopaper-based device for biomedical applications, ***Lab on a Chip,*** 2020

3. Alexander Winkler-Schwartz, Recai Yilmaz, Dan Huy Tran, Houssem-Eddine Gueziri, **Binbin Ying**, Marius Tuznik, Vladimir Fonov, Louis Collins, David A Rudko, Jianyu Li, Patricia Debergue, Valerie Pazos, Rolando Del Maestro, Creating a comprehensive research platform for surgical technique and operative outcome in primary brain tumor neurosurgery, ***World Neurosurgery***, 2020.

4. Longyan Chen†, **Binbin Ying†,** Pengfei Song, and Xinyu Liu*. A Nanocellulose-Paper-Based SERS Multiwell Plate with High Sensitivity and High Signal Homogeneity, ***Advanced Materials Interfaces***, (*highlighted as the Back-Cover article and selected into Hot Topic sessio*n), 2019. (**†Co-first author**)

5. **Binbin Ying,** Qiyang Wu, Jianyu Li*, Xinyu Liu*, An ambient-stable and stretchable ionic skin with multimodal sensation, ***Materials Horizons***, 2019.

6. **Binbin Ying**, Qing Zhu, Aili Zhang*. Study of Specific Absorption Rate of Radiofrequency in Frozen Tissue. ***Progress in Biomedical Engineering***, 2015.

6.3.2. Refereed journal papers (in preparation)

1. **Binbin Ying**, Xinyu Liu*. Recent Advances of Hydrogel Skin-like Devices for Wearable Biomedicals and Soft Robotics and Beyond. To be submitted (Review),2020

2. Longyan Chen, **Binbin Ying**, Xinyu Liu*. Super-Strong, Self-Healable and Conductive Nanocellulose Threads for Wearable Electronics. To be submitted, 2020

3. **Binbin Ying**, Yilun Wan, Runze Zuo and Xinyu Liu*, An anti-freezing, and stretchable ionic triboelectric nanogenerator for mechanical energy harvesting and self-powering sensing. To be submitted, 2020

4. Yueyue Pan, Sina Kheiri, Zhen Qin, **Binbin Ying**, Peng Pan, Ran Peng, Xinyu Liu*, Optical Growth and Patterning of Highly Conductive Silver on Ultrasmooth Nanocellulose Paper. To be submitted, 2020

5. Junyu Chen, **Binbin Ying**, Yichao Shi, Xinyu Liu, Wearable heater based on laser induced graphene and kirigami structure. To be submitted, 2020

6. Xian Wang, **Binbin Ying**, Xinyu Liu, Yu Sun, Magnetic microrobots for cancer treatment. In preparation, 2020

6.3.3. Full-text conference papers

1. Siwan Park†, **Binbin Ying†**, Edmond W. K. Young*, and Xinyu Liu*. NanoFACEs: an optically transparent nanopaper-based device for cell culture. The International Conference on Miniaturized Systems for Chemistry and Life Sciences (*MicroTAS*), 2020.

2. Yueyue Pan, Sina, Zhen Qin**, Binbin Ying,** Xinyu Liu*, Optical Growth and Patterning of Highly Conductive Silver on Ultrasmooth Nanocellulose Paper. The International Conference on Miniaturized Systems for Chemistry and Life Sciences (*MicroTAS*), 2020,

3. Binbin Ying, Jianyu Li and Xinyu Liu, An ambient-stable and stretchable ionic skin with multimodal sensation. *2020 MRS Fall & Spring Meeting*, 2020, Boston, USA

4. Binbin Ying, Xinyu Liu. A Highly-Transparent Nanocellulose-Paper-Based Microfluidic Device. The International Conference on Miniaturized Systems for Chemistry and Life Sciences (MicroTAS), 2018, Kaohsiung, Taiwan.

5. Longyan Chen†,**Binbin Ying†**, Pengfei Song, Xinyu Liu. A Nanopaper Device for Highly Sensitive and Homogeneous SERS Sensing. The International Conference on Miniaturized Systems for Chemistry and Life Sciences (MicroTAS), 2017, Savannah, USA.

6. **Binbin Ying**, Qing Zhu, Aili Zhang and Lisa X. Xu. Study of Specific Absorption Rate of Radiofrequency in Frozen Tissue. The 7th World Congress of Biomechanics, 2014, Boston, USA.

7. Qing Zhu, **Binbin Ying**, Aili Zhang and Lisa X.Xu. Numerical Study of the Influence of Water Evaporation on Radiofrequency Ablation.The American Society of Mechanical Engineers Summer Bioengineering Conference (ASME), 2013, Oregon, USA.

8. **Binbin Ying**, Qing Zhu and Aili Zhang. Study of Temperature's impact on Specific Absorption Rate of Radiofrequency in Tissue. Chinese Biomedical Engineering (CBME), 2013, Chengdu, China.

9. Ping Liu, Xiaomin Ren, Jinqiu Liu, Qing Zhu, Xianjing Zou, **Binbin Ying** and Lisa X.Xu. A novel effective thermal treatment system against metastatic breast cancer using animal model. IEEE 34th Annual International Conference of the IEEE Engineering in Medicine and Biology Society (EMBC), 2012, San Diego, USA.

6.4. Reference

1. J. Li, D. J. Mooney, Designing hydrogels for controlled drug delivery. *Nature Reviews Materials* **1**, 1-17 (2016).
2. P. Mostafalu *et al.*, Smart bandage for monitoring and treatment of chronic wounds. *Small* **14**, 1703509 (2018).
3. S. Trombino, R. Cassano. (Multidisciplinary Digital Publishing Institute, 2020).
4. J. Wang, M.-F. Lin, S. Park, P. S. Lee, Deformable conductors for human–machine interface. *Materials Today* **21**, 508-526 (2018).
5. L. Jing, K. Li, H. Yang, P.-Y. Chen, Recent advances in integration of 2D materials with soft matter for multifunctional robotic materials. *Materials Horizons* **7**, 54-70 (2020).
6. C. Yang, Z. Suo, Hydrogel ionotronics. *Nature Reviews Materials* **3**, 125 (2018).
7. K. Tian *et al.*, 3D printing of transparent and conductive heterogeneous hydrogel–elastomer systems. *Advanced Materials* **29**, 1604827 (2017).
8. H. Yuk *et al.*, 3D printing of conducting polymers. *Nature communications* **11**, 1-8 (2020).
9. R. L. Truby *et al.*, Soft somatosensitive actuators via embedded 3D printing. *Advanced Materials* **30**, 1706383 (2018).
10. M. Wang *et al.*, Gesture recognition using a bioinspired learning architecture that integrates visual data with somatosensory data from stretchable sensors. *Nature Electronics*, 1-8 (2020).
11. X. Liu, J. Liu, S. Lin, X. Zhao, Hydrogel machines. *Materials Today*, (2020).
12. Y. Wang, Z. Wang, Z. Su, S. Cai, Stretchable and transparent ionic diode and logic gates. *Extreme Mechanics Letters* **28**, 81-86 (2019).
13. H. R. Lee *et al.*, A Stretchable Ionic Diode from Copolyelectrolyte Hydrogels with Methacrylated Polysaccharides. *Advanced Functional Materials* **29**, 1806909 (2019).
14. H. J. Kim, B. Chen, Z. Suo, R. C. Hayward, Ionoelastomer junctions between polymer networks of fixed anions and cations. *Science* **367**, 773-776 (2020).
15. B. Ying, Q. Wu, J. Li, X. Liu, An ambient-stable and stretchable ionic skin with multimodal sensation. *Materials Horizons* **7**, 477-488 (2020).
16. N. El‐Atab, N. Qaiser, R. Bahabry, M. M. Hussain, Corrugation Enabled Asymmetrically Ultrastretchable (95%) Monocrystalline Silicon Solar Cells with High Efficiency (19%). *Advanced Energy Materials* **9**, 1902883 (2019).
17. X. Pu *et al.*, Ultrastretchable, transparent triboelectric nanogenerator as electronic skin for biomechanical energy harvesting and tactile sensing. *Science advances* **3**, e1700015 (2017).
18. Y. Yu *et al.*, Biofuel-powered soft electronic skin with multiplexed and wireless sensing for human-machine interfaces. *Science Robotics* **5**, (2020).